Thermal behaviour of a novel cellular beam structural system in fire

by

Hendrig Marx

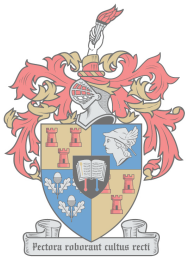

Thesis presented in partial fulfilment of the requirements for the degree of Master of Engineering in Structural Engineering in the Faculty of Engineering at Stellenbosch University

Supervisor: Dr. R.S. Walls

March 2018

The financial assistance of the National Research Foundation (NRF), Thuthuka Grant (99304), towards this research is hereby acknowledged. Opinions expressed and conclusions arrived at, are those of the author and are not necessarily to be attributed to the NRF.

Declaration

By submitting this thesis electronically, I declare that the entirety of the work contained therein is my own, original work, that I am the sole author thereof (save to the extent explicitly otherwise stated), that reproduction and publication thereof by Stellenbosch University will not infringe any third party rights and that I have not previously in its entirety or in part submitted it for obtaining any qualification.

Date: March 2018

Abstract

Thermal behaviour of a novel cellular beam structural system in fire

H. Marx

Department of Civil Engineering,
University of Stellenbosch,
Private Bag X1, Matieland 7602, South Africa.

Thesis: MEng (Structural Engineering)

March 2018

The Southern African Institute of Steel Construction (SAISC) has developed a modular steel frame structure that consists of cellular beams. The cellular beam structure (CBS) contains no concrete, which allows for a shorter construction duration, thereby significantly reducing costs. The fabricated steel members are assembled to form panels which are relatively lightweight, and which can be easily transported to site where they can be configured in various ways. The panels can easily be re-used in the future and additions to existing buildings can be made. Therefore, more economical steel buildings can be built in a shorter duration. However, as for all structures, the CBS requires a fire resistance rating. Due to the unique and complex configuration of the CBS, standard prescriptive fire design methods may lead to over-conservative and uneconomical designs, in terms of passive fire protective measures. Hence, a more advanced performance-based method has been used in this thesis, which incorporates finite element (FE) analyses and experimental testing to determine the behaviour of the CBS in fire.

This thesis, which forms part of a larger research project, has investigated the thermal behaviour of the CBS. Thermal heat transfer analyses have been performed in ABAQUS to determine the steel beam temperatures and the interior floor temperatures. The FE models have been validated based on an experimental study, in which a total of four small-scale standard fire tests were conducted. Experimental and numerical results generally show good correlation, with variations in results within the bounds of that expected in experimental fire research. Preliminary validation studies from the literature have also been performed, from which good correlations were obtained. This validated the suitability of the heat transfer modelling procedures in ABAQUS, and included the modelling of cavity radiation.

The sandwich floor system of the CBS, which includes large beams not included in the small-scale experimental tests, has been investigated by developing FE models for each of the beam sections within the floor, which included the floor boards and steel sheeting. An additional FE model was developed for each of the steel floor beams, for which

the ceiling board was neglected, thus leaving the steel sheeting directly exposed to the fire. This represented a worst-case scenario, in which the integrity of the ceiling board failed completely and detaches during a fire. The temperature distribution through the beam cross-sections is predicted to be highly non-uniform, with the bottom flange and top flange temperatures ranging between $220°C$ and $48°C$ for the primary and secondary cellular beams and between $176°C$ and $95°C$ for the channels that support the flooring system. Without the ceiling board, a higher temperature increase of $300°C$ to $500°C$ is expected, when compared to the ceiling board models. This emphasises the importance of the ceiling board and the influence it has on the steel beam temperatures.

It was found that the floor system failed, as currently specified, with regards to the insulation criteria, in which the temperature increase in the interior floor board exceeded the allowable temperature by approximately $60°C$. Therefore, a parametric investigation has been performed to determine alternative solutions that will provide sufficient insulation to the floor system. Various board materials and thicknesses were modelled, as well as different steel decking systems. A parametric fire was also investigated to determine the effect of the cooling phase on the steel members. It was found that the thickness of the ceiling-board and the interior insulation board have the most significant influence on the temperature increase within the floor system. By using a thicker ceiling board, the temperature increase on the unexposed surfaces satisfy the insulation criteria for a 20 mm gypsum type X ceiling board, as well as for a Promatect-H Calcium-Silicate (CaSi) board, while assuming that the integrity of the boards are maintained. It was noted that the CaSi-board may perform better than the gypsum board in terms of integrity, due to the higher moisture content present in the gypsum board, which can lead to shrinkage cracks. The fixities of the ceiling board should be able to accommodate the deflections which may be experienced by the CBS, in order to maintain integrity.

The findings in this thesis can be used as a foundation for further research, and the planning and execution of a full-scale fire test on the CBS. Ultimately, it was found that the CBS has the potential to provide sufficient fire resistance, based on the assumption that the integrity is maintained, thus reducing the possibility of structural failure.

Uittreksel

Termiese gedrag van 'n sellulêre balkstruktuurstelsel in vuur

H. Marx

Departement Siviele-ingenieurswese,
Universiteit Stellenbosch,
Privaatsak X1, Matieland 7602, Suid Afrika.

Tesis: MIng (Struktuuringenieurswese)

Maart 2018

Die Suider-Afrikaanse Instituut vir Staalkonstruksie (SAISC) het 'n modulêre staalraamstruktuur ontwikkel wat bestaan uit sellulêre balke. Die selulêre balkstruktuur (SBS) bevat geen beton nie, wat vinniger oprigting moontlik maak en dus die konstruksiekoste aansienlik verminder. Die vervaardigde staal elemente word saamgestel om panele te vorm wat relatief liggewig is, en wat maklik na die bouperseel vervoer kan word, waar hulle op verskillende maniere opgestel kan word. Die panele kan maklik in die toekoms hergebruik word en byvoegings aan bestaande geboue kan gemaak word. Dus kan meer ekonomiese staalgeboue in 'n korter tydperk gebou word. Soos vir alle strukture, vereis die SBS egter 'n brandweerstandsgradering. As gevolg van die unieke en komplekse opset van die SBS, sal standaard-voorgeskrewe brandontwerpmetodes tot konserwatiewe en onekonomiese ontwerpe lei, in terme van passiewe brandbeveiligingsmaatreëls. Dus is 'n meer gevorderde prestasie-gebaseerde metode gebruik in hierdie projek, wat van eindige element (EE) ontledings gebruik maak om die gedrag van die SBS in 'n brand te bepaal.

Hierdie tesis, wat deel uitmaak van 'n groter navorsingsprojek, het die termiese gedrag van die SBS ondersoek. Termiese hitte-oordragontledings is in ABAQUS uitgevoer om die staalbalke en die binne-vloer se temperature te bepaal. Die EE-modelle is bevestig op grond van 'n eksperimentele studie, waarin vier kleinskaalse standaard-vuurtoetse uitgevoer is. Die eksperimentele en numeriese resultate toon oor die algemeen goeie korrelasie, met variasies in resultate binne die grense van wat verwag word in eksperimentele brandnavorsing. Voorlopige valideringstudies vanuit die literatuur is ook uitgevoer, waaruit goeie korrelasies behaal is. Dit het die toepaslikheid van die hitte-oordrag modelleringsprosedures in ABAQUS bevestig en sluit die modellering van gaping-bestraling in.

Die vloerstelsel van die SBS, wat groot balke bevat wat nie by die kleinskaalse eksperimentele toetse ingesluit is nie, is ondersoek deur EE-modelle te ontwikkel vir elk van die balk elemente in die vloer, wat die vloerborde en staalplate insluit. 'n Addisionele EE-model is ontwikkel vir elk van die balkmodelle, waarvoor die plafonbord weggelaat is, wat veroorsaak dat die staalplaat direk aan die vuur blootgestel word. Dit verteenwoordig 'n mees ongewenste geval waarin die integriteit van die plafonbord heeltemal misluk

en af val tydens 'n brand. Dit word voorspel dat die temperatuurverspreiding deur die dwarssnitte oneweredig is, met die onderste flens- en boonste flenstemperature wat wissel tussen 220°C en 48°C vir die primêre and sekondêre sellulêre balke, en tussen 176°C en 95°C vir die kanaalbalke, wat die vloerstelsel ondersteun. Sonder die plafonbord word 'n verskil in temperatuur-toename van 300°C tot 500°C verwag, in vergelyking met die plafonbordmodelle. Dit beklemtoon die belangrikheid van die plafonbord en die invloed wat dit op die staalbalk-temperature het.

Daar is gevind dat die vloerstelsel, soos tans gespesifiseer is, misluk het met betrekking tot die isolasiekriteria, waarin die temperatuurstyging in die binne-vloerbord die toelaatbare temperatuur met ongeveer 60°C oorskry. 'n Parametriese ondersoek is dus uitgevoer om alternatiewe oplossings te bepaal wat voldoende isolasie vir die vloerstelsel sal bied. Verskeie bordmateriale en -diktes is gemodelleer, sowel as verskillende staalplaatstelsels. 'n Parametriese vuur is ook ondersoek om die effek van die verkoelingsfase op die staal elemente te bepaal. Daar is gevind dat die dikte van die plafonbord en die binne-isolasiebord die belangrikste invloed op die temperatuurstyging binne die vloerstelsel het. Deur 'n dikker plafonbord te gebruik, voldoen die temperatuurstyging op die bedekte oppervlakke aan die isolasie kriteria vir 'n 20 mm gips tipe X plafonbord, asook vir 'n 25 mm Promatect-H Kalsiumsilikaat- (CaSi) bord, mits die integriteit van die borde behoue bly. Daar is opgemerk dat die CaSi-bord moontlik beter kan presteer as die gipsbord in terme van integriteit, as gevolg van die hoër voginhoud teenwoordig in die gipsbord, wat tot krimpingskrake kan lei. Die konneksiepunte van die plafonbord moet die verplasings wat deur die SBS ondervind kan word, akkommodeer om die integriteit te behou.

Die bevindings in hierdie tesis kan gebruik word as grondslag vir verdere navorsing en die beplanning en uitvoering van 'n volskaalse brandtoets op die SBS. Daar is gevind dat die SBS die potensiaal het om voldoende brandweerstand te bied, mits die integriteit behou word, en sodoende die moontlikheid van strukturele faling verlaag.

Acknowledgements

I would like to express my sincere gratitude to the following people and organisations.

- My supervisor, Dr Richard Walls, for introducing me to the interesting field of structural fire engineering and for his guidance throughout the execution of this project.
- Amanuel Gebremeskel of the Southern African Institute of Steel Construction (SAISC), for his valuable input with regards to the cellular beam structure (CBS).
- The National Research Foundation (NRF), for their financial assistance over the past two years.
- Dirk Oosthuizen of NES Consult, for his help with the fire testing and the use of his facilities.
- Andries Botha of Voidcon, for providing the Voidcon VP50 steel decking samples.
- Gerhard Swart and Corne' White of Marley Building Systems, for providing the Promatect-H board samples.
- Mr Johan van der Merwe, for his assistance in the structures laboratory workshop during the construction of the test samples.
- My fellow students in the structures department at Stellenbosch University, for their friendliness and support around the office.
- Tarina Luddick, for her unmatched support, patience and motivation that carried me through late nights during the completion of this project.
- Finally, to my parents for their unending support in every aspect of my life, and to my friends for their support throughout my years at university.

Most importantly, all the glory be to God!
"I can do all things through Christ who strengthens me."
- (Philippians 4:13)

Contents

List of Figures

List of Tables

Nomenclature

Latin variables

A	Cross-sectional area of a steel member $[m^2]$
A_f	Compartment floor surface area $[m^2]$
A_i	Area of facet i seeing all facets in the cavity (j) $[m^2]$
A_m	Exposed surface area of a member $[m^2]$
A_t	Total enclosure area $[m^2]$
A_v	Area of vertical openings $[m^2]$
A_m/V	Section factor of unprotected steel members $[m^{-1}]$
$[A_m/V]_b$	Box section factor of the member $[m^{-1}]$
A_p/V	Section factor of protected steel members $[m^{-1}]$
b	Thermal inertia $[J/m^2s^{0.5}K]$
C_{ij}	Reflection matrix
c	Specific heat $[J/kgK]$
c_a	Specific heat of steel $[J/kgK]$
c_p	Specific heat of the insulation material$[J/kgK]$
d_p	Thickness of the insulation material$[J/kgK]$
E	Total radiative energy emitted $[W/m^2]$
F	View factor
F_{ij}	Geometrical view factor matrix
H_p/A	Section factor, based on heated perimeter of steel sections $[m^{-1}]$
h	Convective heat transfer coefficient $[W/m^2K]$
h_{eq}	Weighted average window height $[m]$
$\dot{h}_{net,c}$	Convective heat flux component $[W/m^2]$
$\dot{h}_{net,d}$	Design heat flux per unit area $[W/m^2]$
$\dot{h}_{net,r}$	Radiative heat flux component $[W/m^2]$
k	Multiplication factor in the parametric fire model

k	Thermal conductivity $[W/mK]$
k_{sh}	Shadow effect correction factor
l	Length [mm or m]
m	Combustion factor
O	Opening factor
$q_{f,d}$	Design fire load density, based on the compartment floor area $[MJ/m^2]$
$q_{f,k}$	Characteristic fire load density per unit floor area $[MJ/m^2]$
q_i^c	Radiative heat flux per unit area into a facet $[W/m^2]$
$q_{t,d}$	Design fire load density, based on the total compartment area $[MJ/m^2]$
$\dot{q}"_x$	Heat flux in one dimension $[W/m^2]$
T	Temperature $[°C$ or $K]$
t	Time [h, min or s]
t^*	Expanded time in the parametric fire model [h, min or s]
t_{lim}	Limiting time to maximum temperature for a fuel-controlled fire [h, min or s]
t_{max}	Time at which maximum temperature in heating phase is reached [h, min or s]
V	Volume of a steel section $[m^3]$

Greek variables

α_c	Convective heat transfer coefficient $[W/m^2K]$
Γ	Expansion coefficient in the parametric fire model
γ_n	Differentiation factor considering various active fire fighting measures
γ_{q1}	Partial factor considering the fire activation risk due to compartment size
γ_{q2}	Partial factor considering fire activation risk due to occupancy type
$\Delta\theta_{a,t}$	Change in steel temperature during time interval Δt $[°C$ or $K]$
$\Delta\theta_{g,t}$	Change in ambient gas temperature during time interval Δt $[°C$ or $K]$
Δl	Thermal elongation [mm or m]
$\Delta l/l$	Thermal expansion
ΔT	Change in temperature $[°C$ or $K]$
Δt	Time interval [h, min or s]
Δx	Change in distance, thickness of material $[m]$
ϵ	Emissivity
ϵ_i	Emissivity of facet i
ϵ_j	Emissivity of facet j

ϵ_m	Surface emissivity of the member
θ	Temperature [$^\circ C$ or K]
θ_a	Steel temperature [$^\circ C$ or K]
$\theta_{a,t}$	Steel temperature at time t [$^\circ C$ or K]
θ_g	Gas temperature [$^\circ C$ or K]
$\theta_{g,t}$	Ambient gas temperature at time t [$^\circ C$ or K]
θ_i	Temperature of facet i [$^\circ C$ or K]
θ_j	Temperature of facet j [$^\circ C$ or K]
θ_m	Surface temperature of the member [$^\circ C$ or K]
θ_r	Effective radiation temperature of the fire compartment [$^\circ C$ or K]
θ_{max}	Maximum gas temperature [$^\circ C$ or K]
θ^z	Absolute zero temperature [$-273.15^\circ C$ or $0K$]
λ	Thermal conductivity [W/mK]
λ_a	Thermal conductivity of steel [W/mK]
λ_p	Thermal conductivity of the insulation material [W/mK]
ρ	Density [kg/m^3]
ρ_a	Density of steel [kg/m^3]
ρ_p	Density of the insulation material [kg/m^3]
σ	Stephan Boltzmann constant, equal to 5.67×10^{-8} W/m^2K^4
ϕ	Configuration factor
ϕ	Amount of heat stored in the protection

Abbreviations

ASFP	Association for Specialist Fire Protection
BC	Boundary Condition
BD	Bond-Dek
BF	Bottom flange
BS	British Standard
BSI	British Standards Institution
C	Referring to FE models with a fire-rated ceiling-board intact
C-beam	Steel channel section
CaSi	Calcium Silicate
CB	Cellular Beam

CBS	Cellular beam structure
CEC	Commission of the European Communities
CEN	European Committee for Standardization
CF	Cold face
CFD	Computational Fluid Dynamics
CR	Cavity radiation
CSA	Canadian Standards Association
ECCS	European Convention for Constructional Steelwork
EN	European Standard (Eurocode documents)
EMF	Electromotive force
exp	Exponent
FCB	Fibre-cement board
FE	Finite Element
FEA	Finite Element Analysis
FEM	Finite Element Method
FRR	Fire resistance rating
inFCB	Inner fibre-cement board
ISO	International Standards Organisation
J-beam	Secondary cellular beam with a cross-section resembling the letter "J"
LSF	Light gauge steel frame
LW	Lower web
MgO	Magnesium Oxide
NFPA	National Fire Protection Association
noC	Referring to FE models without a fire-rated ceiling-board
P-beam	Primary cellular beam
parF	Parametric fire
REI	Fire resistance criteria: load bearing capacity (R), integrity (E) and insulation (I)
R&D	Research and development
SAISC	Southern African Institute of Steel Construction
SABS	South African Bureau of Standards
SANS	South African National Standard
SFE	Structural Fire Engineering

SFPE	Society for Fire Protection Engineers
stdF	Standard fire
TC	Thermocouple
TC3	Technical Committee 3
TF	Top flange
UW	Upper web
VP	Voidcon Profile
W	Web

Chapter 1

Introduction

1.1 Project overview

1.1.1 Problem Statement

Numerous building fires have occurred internationally, such as the recent Grenfell Tower incident in the UK (Ruddy, 2017). This has led to a growing interest in designing structures against fire. Various solutions exist to protect structures from the disastrous effects of a fire, such as passive fire protection measures, which include intumescent paints, vermiculite and fibre-cement boards, and active protection measures, which include sprinklers, fire brigades and alarm systems. However, the cost of these fire protection measures can be high. In some cases they can be more expensive than the steel that requires protection, especially when using intumescent coatings. It is therefore necessary to design steel structures in such a way that the total passive fire protection required is minimized, in order to keep the structure economical while being safe.

Designers seek to ensure the safety of a building and its occupants by satisfying the required fire resistance rating. Numerous methods exist for determining the fire resistance of a structure, such as prescriptive design methods, rational design methods and physical fire testing. Some methods incorporate over-simplified design considerations, such as deriving the fire resistance rating of a structure based on a single element, as is typically the case for most beams or columns.

Global structural modelling is crucial for designing structures for the event of a fire. The importance of analysing structures as a whole is emphasised by various authors in the literature, such as Bisby *et al.* (2013), Nadjai *et al.* (2011) and Gales *et al.* (2012). They discuss the limitations of isolated standard fire tests and the need to consider the interaction between the various building elements within the whole structure. However, before one can analyse the global behaviour of a structure, it is necessary to investigate various parts of the structure to determine the local parameters, which in turn are used as input parameters for the global analyses.

The main focus of this thesis is the thermal behaviour of a novel structural system, discussed further below, for which steel beam temperatures are determined by analysing the heat transfer through a floor system. Insufficient research is currently available to easily determine the temperature of elements in the structural system investigated in this work due to its unusual configuration. Hence, physical fire testing and numerical modelling is

required. The steel beam temperatures obtained from the thermal analyses in this work can be used to determine the mechanical response of the structure.

The following section introduces the structural system, which will be investigated in terms of structural fire resistance requirements. Thereafter, the research objectives, project scope and limitations, and the methodology will be discussed.

1.1.2 Introducing the modular structural system

The Southern African Institute of Steel Construction (SAISC) has developed a new, innovative modular steel frame structural system, which is illustrated in Figure 1.1. The structure consists of cellular beams, which are similar to castellated beams, but have circular holes in the web. Cellular beams allow for longer spans due to the higher bending resistance relative to the mass of the structure. The holes in the web also allow services, such as ducts, to pass through the beams instead of above or below, which ultimately results in lower floor heights, thereby reducing the overall cost of structures. More information regarding cellular steel beams is provided in Section 2.8.1. The structure consists of a sandwich floor system, which contains the cellular beams enclosed by a specific setup of insulation boards and a profiled steel deck, situated below the beam, and a fibre-cement board (FCB) on top of the beam. The entire sandwich floor system is supported by four columns, situated as indicated in Figure 1.1, all of which makes up a single module with dimensions of 12.75 x 8.5 x 2.56 m. The single modules are then assembled to form larger structures, as shown in Figure 1.2.

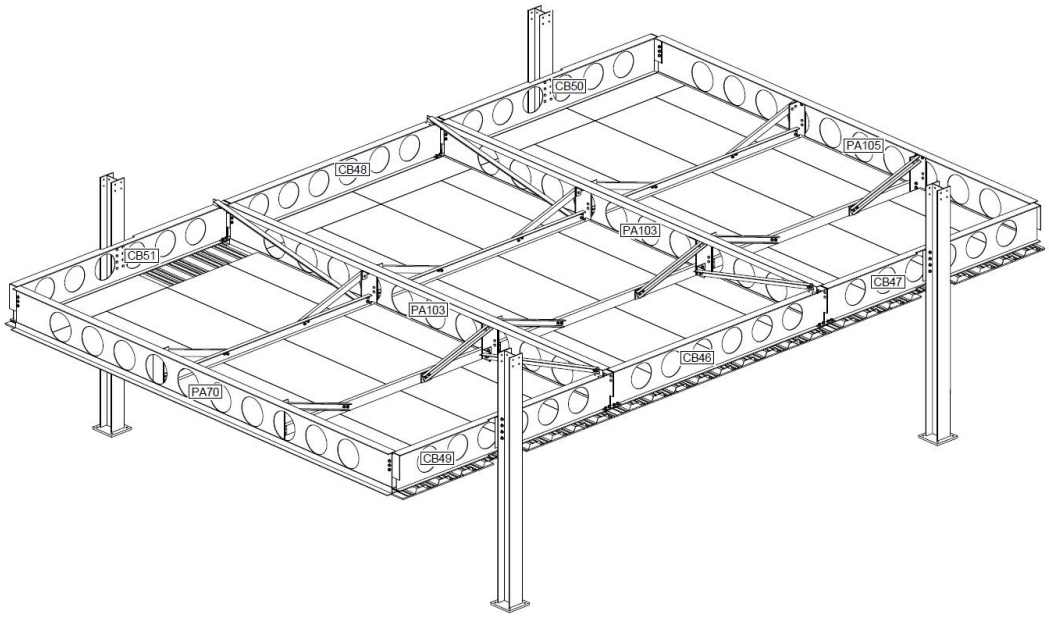

Figure 1.1: SAISC cellular beam structure (CBS) (Image used courtesy of the SAISC)

The structural system is devoid of concrete, which allows for reduced construction periods and lightweight structures. This allows for a more economical steel building with lightweight panels that could easily be transported. Another major advantage of the modular structure is that it can be configured in numerous ways, allowing for various building shapes, size and design. One example configuration is shown in Figure 1.2(b), which is a

standard office building layout.

As for all structures, the cellular beam structure (CBS) requires a fire resistance rating. A major concern of this specific structural system, however, is that it consists mainly of steel and insulation board, as discussed above. Due to the unique and complex geometry of the CBS, it is difficult to predict the fire resistance from prescriptive methods, such as design tables, etc. A more detailed approach is therefore required, in the form of numerical analyses, in order to determine whether the CBS satisfies fire resistance criteria. More details on the above-mentioned topics are discussed in the literature review.

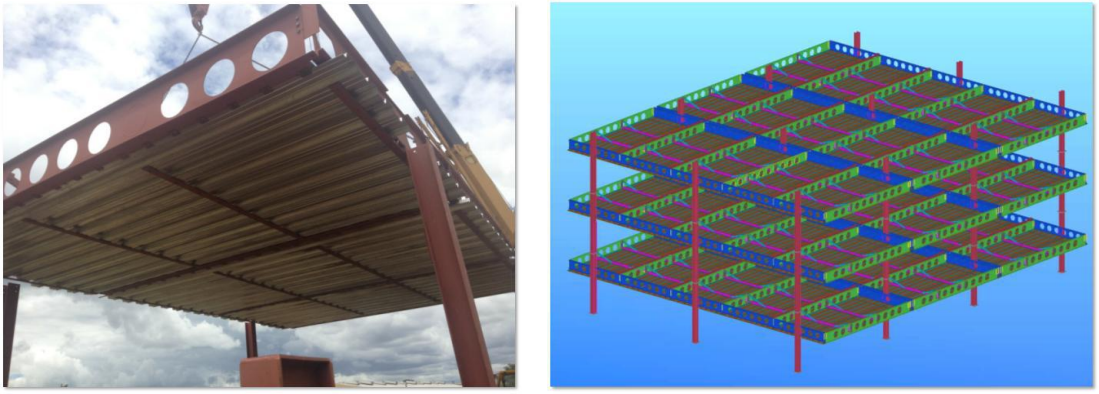

(a) Photo of a single bay (b) Example module configuration

Figure 1.2: SAISC modular structural system (Image used courtesy of the SAISC)

1.1.3 Sandwich floor system

Figures 1.3 and 1.4 present an elevation and a side elevation view on the sandwich floor system, respectively. The first figure shows a cellular steel beam on top of the bottom floor layers. The second figure depicts the internal access flooring pedestals, which are situated in the ceiling void between the cellular beams.

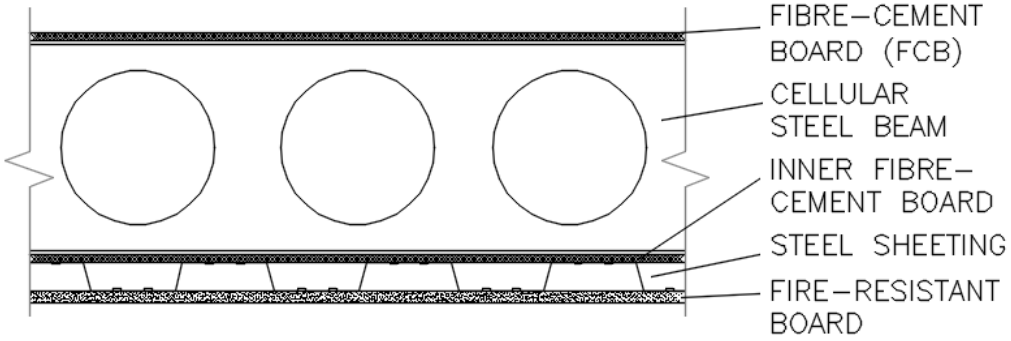

Figure 1.3: Elevation view of the sandwich floor configuration with a cellular beam section and the bottom floor layers

In the case of a typical fire, the heat transfer from the flames, which includes radiation and convection, heat up the compartment and its boundaries, such as the ceiling. Heat is then conducted through the ceiling board, which is then emitted from the unexposed side

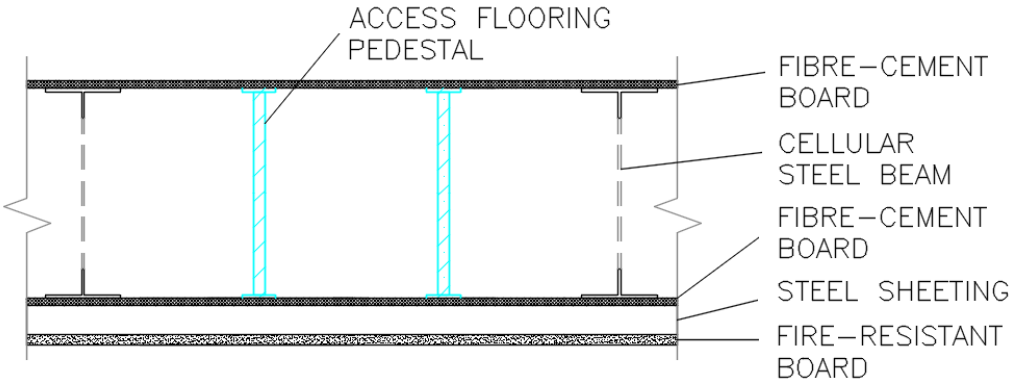

Figure 1.4: Side elevation view of the sandwich floor system showing pedestals for access flooring between the cellular beams

to the surrounding surfaces, in this case the steel decking. The heat continues to travel in this manner through the respective material layers, each with its respective thermal properties, such as emissivity and conductivity. As the temperature in the floor system increases, the conduction, radiation and relatively small amount of convection occurring within the void heats up the cellular steel beams.

Another critical aspect of the sandwich floor system is the temperature rise of the inner fibre-cement board, which will form the base on which services such as cables and ducts are located. High temperatures in this section of the floor could potentially ignite some of the services, which could cause rapid fire to spread through the floor and into adjacent compartments. The insulation criteria should therefore also be satisfied at this level within the floor system (i.e. at the top of both the bottom FCB, and not only the top FCB).

1.2 Research objectives

The primary goal of the research project is to determine the fire resistance of the modular structural system that was described in Section 1.1.2, with the focus being specifically on the thermal behaviour of the sandwich floor system within the structure. The specific objectives required to attain the goal of this research project are summarised below.

- Perform an extensive literature study to gain an understanding of heat transfer mechanisms, fire protection measures and how steel structures generally behave in fire.
- Investigate current calculation models for determining fire and steel element temperatures.
- Develop an experimental setup for the fire testing of small-scale sandwich floor samples, which will be used for validating numerical finite element models.
- Develop Finite Element (FE) models to simulate the heat transfer in the small-scale fire test models.
- Perform validation studies from the literature and verify the FE fire test models by comparing the numerical results to those obtained from the experiments. The aim

is to determine the suitability of the procedures employed using ABAQUS (Dassault Systémes, 2015) to model heat transfer through the sandwich floor system.

- Develop FE models of the real full-scale sandwich floor system in the CBS to determine the thermal response of the structure. Firstly, it is important to determine the inner floor layer temperatures in ABAQUS and to provide possible practical solutions that will meet the insulation criteria. Secondly, the work will focus on determining the steel beam temperatures that will serve as input parameters for the analysis of the structural behaviour, as performed by Kloos (2017).

- Perform a parametric study on the sandwich floor system by conducting numerical heat transfer analyses on various material and geometric parameters, as well as the consideration of a worst-case parametric fire scenario. These analyses will provide possible alternative solutions to improve the structural integrity and thermal insulation of the ceiling boards, which will ultimately improve the fire safety of the cellular beam structure.

1.2.1 Project Scope & Limitations

The modular structural system introduced in Section 1.1.2 consists of a complex geometry and configuration, which makes it difficult to analyse every aspect that needs to be considered when designing it against fire. A significant amount of research with regards to fire behaviour, thermal response and mechanical behaviour is required to gain a thorough understanding of how the structure behaves in a fire. Hence, the work performed in this thesis forms part of a decoupled thermo-mechanical analysis, which comprises a detailed thermal and mechanical analysis.

This project will focus on the thermal behaviour of the sandwich floor system described in Section 1.1.3, while the structural analyses discussed in the work have been performed by Kloos (2017). This thesis, therefore, investigates the heat transfer through the floor system to ultimately determine the temperatures of the steel beams and unexposed surfaces within the floor system.

Fire testing is an important part of structural fire engineering research and the demand for full-scale fire tests has increased significantly over the past decades, as discussed by Bisby *et al.* (2013) and various other authors. A full-scale fire test of the structure presented in Section 1.1.2 is especially necessary, due to the unique section geometries, structure configuration and material layers within the floor system. The execution of a full-scale fire test is not included in the present thesis. However, the work performed contributes to the development of a full-scale test that will be conducted in the near future.

Despite its unrealistic representation of real fire behaviour, the standard fire provides valuable information regarding fire resistance, which could easily be used as a benchmark for comparison purposes. This thesis describes four small-scale furnace tests, which will be used for validating Finite Element (FE) models, that in turn, will predict the thermal behaviour of the larger structure.

1.3 Methodology

The following section describes the procedures to be followed in this research to achieve the objectives outlined above. The project consists of theoretical calculation models, physical experimental investigations and FE analyses, all of which are used to determine element temperatures within the sandwich floor system. The following seven-step approach will be followed to obtain the objectives listed above:

1. A literature review is presented to provide in-depth understanding in the field of structural fire engineering with a focus on thermal analyses and behaviour of steel in fire. Important concepts such as fire safety, fire dynamics and heat transfer will be reviewed, along with cellular steel beam behaviour in fire, testing of structures in fire and protecting steel against fire.

2. Experimental fire-test models will be developed, from which the real thermal behaviour through a small-scale sandwich floor system will be investigated by:

   a) Measuring the temperatures at various points within the sample by using thermocouples.

   b) Analyse the results obtained from the tests.

3. FE models will be validated with experimental results from fire tests. Preliminary validation studies from literature will also be done to:

   a) Investigate the effects of radiative heat transfer within the air cavities.

   b) Simulate the fire behaviour of the test samples as accurately as possible.

   c) Determine the fire resistance of the insulation materials.

4. Compare results of physical fire tests and FE models and determine the suitability of ABAQUS, as well as the suitable parameters for the heat transfer analyses.

5. FE models will be developed further to simulate the full-scale structural floor system to:

   a) Predict the steel beam temperatures within the void of the sandwich floor system.

   b) Investigate solutions to overcome potential shortcomings.

6. A parametric study will be conducted on the configurations of the sandwich floor system to:

   a) Investigate different steel decking profiles and depths.

   b) Investigate different insulation board materials and thickness.

   c) Perform a parametric fire analysis on the sandwich floor FE models.

1.4 Thesis Structure

Chapter 2: A background on structural fire engineering
Similar research projects and experiments are investigated, from which potential challenges with regards to fire testing and the use of Finite Element Analyses (FEA) are discussed. Theoretical calculation methods from various codes are also discussed in this chapter, which includes SANS 101400-T and Eurocode documents.

Chapter 3: Experimental setup
The experimental setup of the small-scale fire-test models are presented in this chapter. The preparation of the samples, testing procedures and collection of data is also discussed.

Chapter 4: Discussion of experimental results
The observations and the results obtained from the fire tests that are described in Chapter 3 are discussed in this chapter.

Chapter 5: Validation studies and verification of small-scale tests
This chapter consists of the validation of the small-scale fire-test models with Finite Element heat transfer analyses performed in ABAQUS. Preliminary validation of the FE models using previous FE analyses obtained in the literature are also included in this chapter.

Chapter 6: Thermal Finite Element analysis of sandwich floor system
The development of the FE beam models is presented in this chapter, from which the steel beam and inner floor layer temperatures within the sandwich floor system are predicted.

Chapter 7: Parametric investigation
Various parametric studies are discussed in this chapter, where FE analyses for a variety of configurations and parameters are performed. These studies will investigate various alternative solutions for the sandwich floor system that could satisfy the fire resistance criteria.

Chapter 8: Conclusions & recommendations
An overview of the project findings are presented, along with some recommendations for future research.

Chapter 2

Literature review

2.1 Introduction

This chapter presents a brief overview to structural fire safety and a background to the approaches for structural fire engineering design. An overview of structural fire resistance, calculation models, as well as rational design methods, is also included. The aim of this section is to provide a background on the specific fire resistance requirements that need to be satisfied by the SAISC structure, which was introduced in Chapter 1.

To determine the thermal behaviour of a sandwich floor structural system, it is necessary to develop an adequate understanding of heat transfer principles and how steel and the insulation materials behave when exposed to elevated temperatures. Hence, this section presents an overview of the different modes of heat transfer and the relevant material thermal properties. Two design fires are also discussed, namely the standard fire curve and a parametric fire curve based on the Eurocode calculations. The standard fire curve was incorporated during the experimental and numerical beam analyses, which will be discussed in the following chapters, while the parametric fire is used in Chapter 7.

2.2 Structural fire safety

Fires are one of the most destructive forces in nature that lead to a large amount of financial loss due to the loss of property and agricultural areas, as well as the loss of many lives each year. A sequence of catastrophic urban fire events in the past have contributed to the increasing interest in the field of structural fire safety and protecting structures against fires. An extensive list of these fire events is available in the literature and include events, such as the great fire in London (1666) and more recent events, such as the collapse of the World Trade Centre buildings WTC 1, 2 & 7 in New York (2001). These catastrophic events changed the understanding of fire resistance design in buildings and the need to consider all aspects of the structure. In his article, "Structures in Fire, Yesterday, Today and Tomorrow", Franssen (2005) presents the evolution of structural fire safety engineering during the last decades. He discusses how the focus on the behaviour of structures in fire has shifted from only considering the fire resistance of individual structural elements to considering global structural behaviour, which takes the level of loading and mechanical boundary conditions into account.

The safety of the occupants and property within and outside the building depends on numerous factors. These factors range from the smoke caused by the fire, which could lead to asphyxiation of building occupants, the potential failure of certain elements in the building or even total structural collapse. Probably the most crucial factor when it comes to fire safety is the possibility of fire spread, which is where compartmentation should be considered (Buchanan and Abu, 2017).

2.3 Structural fire engineering

The design of structures in fire has become a major part in the design of buildings, especially when designing steel structures. Structural fire engineering consists of a combination of three main disciplines, namely: structural design, fire science and the study of heat transfer, as depicted in Figure 2.1. Over the past couple of decades, the overlapping interest between the respective disciplines has become more integrated. Structural engineers in the past had very little knowledge and experience in the field of fire science and heat transfer, and the same situation was experienced from the other disciplines towards structural design (Rein, 2012).

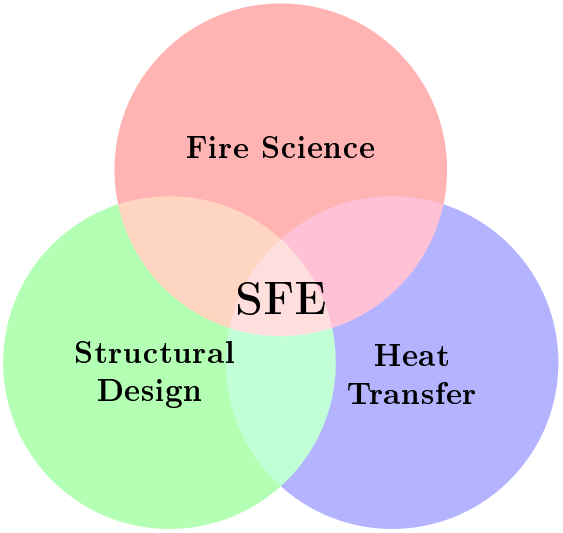

Figure 2.1: Integration of SFE disciplines, adapted from (Rein, 2012)

When it comes to designing structures in fire, there are three main components. First, a fire analysis should be performed to determine the appropriate design fire, which is the time-temperature relationship for the specific compartment. Various fire scenarios could exist for a certain compartment or building. The fire scenario usually depends on factors such as the geometry of the fire compartment, type of occupancy, ventilation conditions and nature of the fuel load. When designing the structural members within the compartment, an assumed worst-case fire scenario is used (Lennon, 2011).

After the analysis of the fire behaviour within the particular compartment, a thermal response analysis should be performed. At this point, a heat transfer analysis should be performed to determine the temperatures of the structural elements and within the system. Once the temperatures of the structural elements are known, the structural response to the exposed time-temperature relationship can be determined. The mechanical

behaviour of the structure is determined and should be designed to resist all mechanical and thermal loads for any specified fire scenario. Figure 2.2 presents the fire design procedure along with the corresponding Eurocode documents (Zaharia, 2014), although any suitable codes may be used.

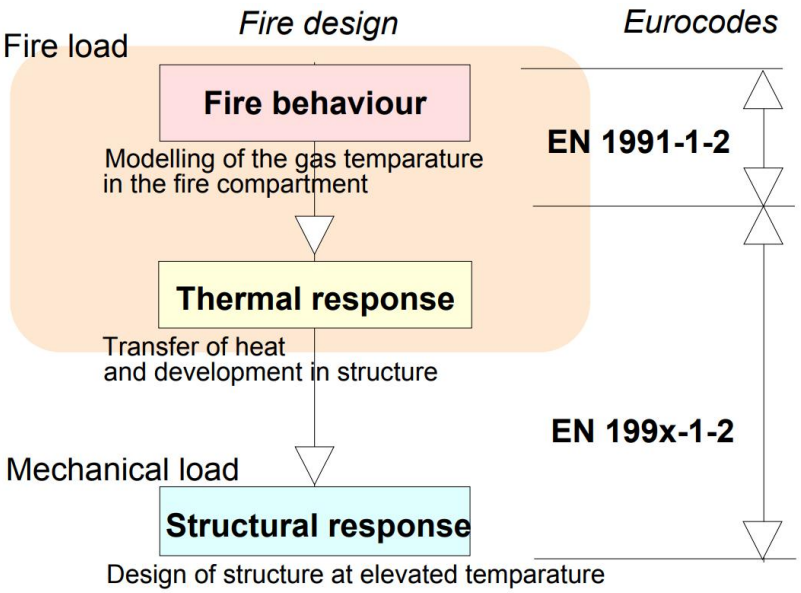

Figure 2.2: Fire design according to Eurocodes (Zaharia, 2014)

2.3.1 Structural fire engineering design approaches

There are two distinct approaches with regards to designing structures in fire, namely the prescriptive design approach and the performance based approach that incorporates rational design methods. The prescriptive design approach makes use of simple calculation methods and tabulated data which are based on simplified assumptions, such as uniform temperature distributions through steel sections. Popular prescriptive approaches include the use of tables and guidelines provided in the Yellow Book (ASFP, 2014) and the Euro-Nomogram (ECCS, 1999), which are focussed on passive fire protection and determining the thickness of insulation materials.

Until recently, various technical disciplines used prescriptive design methods for designing structures against fire. However, most prescriptive methods are based on standard fire tests of isolated elements that do not represent real fire behaviour. Bailey (2009) notes that designers and manufacturers tend to ignore the actual behaviour in structures and rather focus on satisfying the standard fire test requirements to obtain approval.

Bailey (2009) discusses the various approaches to structural fire engineering and the different levels of complexity that accompany each approach. Figure 2.3 presents the three main components of structural fire engineering and the available approaches for each.

The level of complexity ranges between simple models that incorporate numerous simplified assumptions, to advanced analysis techniques, which includes Computational Fluid

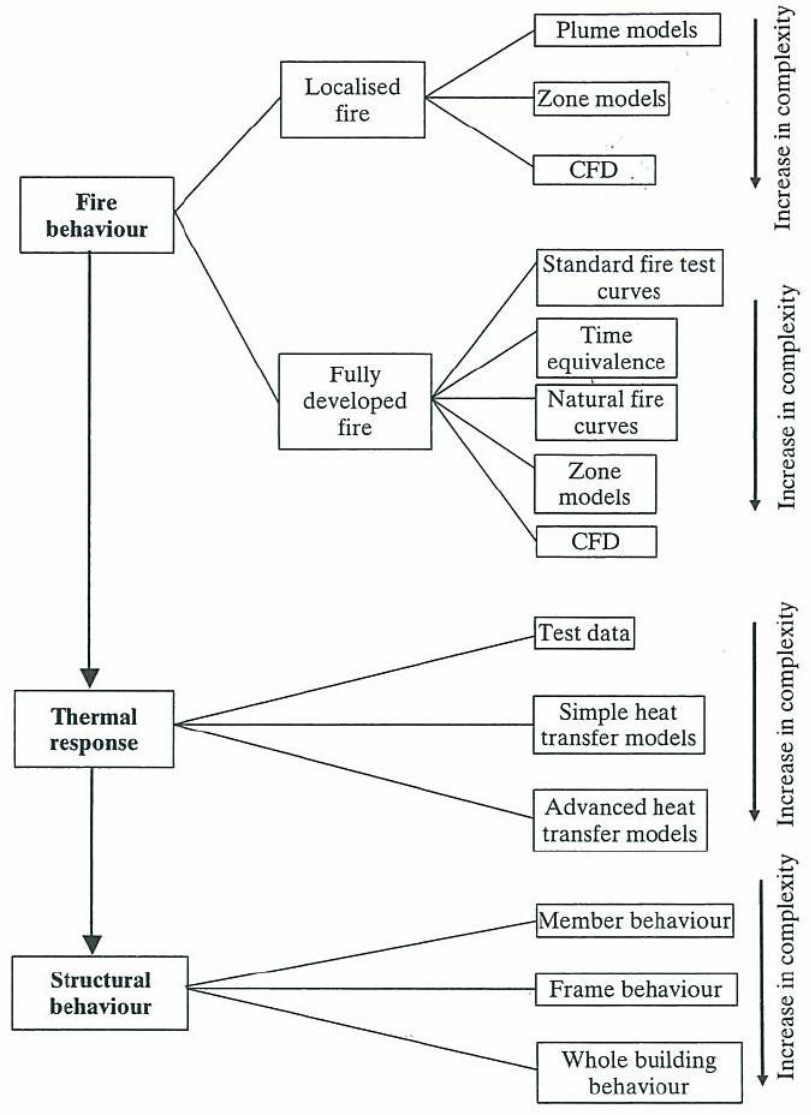

Figure 2.3: Levels of tructural fire engineering approaches (Bailey, 2009)

Dynamics (CFD) and Finite Element Method (FEM) analyses, as well as global structural behaviour. The intermediate levels include theoretical modelling and calculation techniques, which can be found in the Eurocodes, various international standards and other sources in the specific research fields, such as the study of heat transfer.

The performance based approach requires the consideration of all aspects of the structure under any type of combined action of mechanical loading and thermal loading. Wang *et al.* (2013) presents an overview of performance-based design methods that discusses the various aspects that need to be considered when designing a structural system in fire. Thermal action can be defined by a natural fire, which results in a much more realistic analysis. Any localised effects should be taken into account in a performance based design, such as localised fires that could occur at any point in time and place. The presence of active fire protection measures is also taken into account when designing a structural system, as well as any passive fire protection systems. The effect of connections between structural elements should be taken into consideration along with the effective length of the members, which allows the analysis of the global behaviour of a whole structure, rather than only single separate members.

2.3.2 Fire resistance

Fire resistance is defined as the ability of structural elements within a building, or the whole building, to resist a fire. The requirements of fire resistance are commonly based on the amount of time a structural element can satisfy specific criteria while exposed to a standard fire (Li and Wang, 2013). The temperature and load capacity of an element could also be used to measure the fire resistance of the structure (Buchanan and Abu, 2017). Preventing structural collapse and maintaining compartmentation within the building are some examples of the specific criteria to be met. It is also necessary to ensure adequate fire resistance of structural elements that support other members within the building, such as fire rated ceilings, doors and other fire protecting barriers. Failure of the latter can lead to fire spread, which could result in global structural collapse (Wald, 2016).

The Eurocodes express fire resistance by three main criteria, namely load bearing capacity (R), integrity (E) and insulation (I), which are known as the "REI"-functions. The load bearing capacity is sometimes referred to as the resistance to collapse, whereby the structure is required to maintain its mechanical resistance and ability to support main overhead members. The integrity requirement refers to the ability of the structural members and protection materials to prevent penetration of flames and hot gases through cracks and gaps caused by separating members (Wald, 2016). When the integrity of the members fail, fire spread to neighbouring compartments, thus compartmentation fails, which could lead to structural collapse. The ability of structural members to maintain thermal insulation is represented by the "I", and refers to the prevention of excessive temperature rise on the unexposed side of structural or protection members. When the insulation requirement is not satisfied, materials in the next compartment can spontaneously ignite, which could lead to compartmentation failure.

In the case of an office compartment, the walls, floors and ceilings are the critical members that need to satisfy the integrity and insulation criteria, especially at the connection interfaces. Most codes and fire design guidelines limit the average temperature rise to $140°C$ and the peak temperature rise to $180°C$. Spontaneous combustion temperatures are typically much higher. Hence, this insulation requirement is relatively conservative. These criteria could either be required separately or in combination (Vassart *et al.*, 2014). According to ECCS TC3 (2001), there are three main procedures that should be followed to determine whether the aforementioned criteria have been satisfied. The three procedures include: (a) testing of structural elements and assemblies according to harmonised standards or guidelines, (b) harmonised calculation and design methods or (c) a combination of the testing and calculation methods.

All structures require a Fire Resistance Rating (FRR) to ensure safety of occupants and the protection of property in the event of a fire. The required level of fire resistance is specified by several codes and standards and usually depends on the type of occupancy, height and size of the building and the effectiveness of active fire-fighting measures, such as an active fire brigade, sprinkler systems and adequate ventilation (ECCS TC3, 2001). In most countries fire ratings typically range from 30 minutes to 2 hours, increasing in steps of 30 minutes (ECCS TC3, 2001). Table A.1 in Appendix A indicates an example of a fire resistance design table from the appendix for fire design in the South African code governing the fire rating requirements of buildings, SANS 10400-T (SABS, 2011).

2.3.3 Standard fire curve

The standard fire curve is a nominal temperature-time relationship and dates to 1918. It is also known as the ISO 834 fire curve (ISO, 1999). The standard fire curve is widely used in standard fire tests due to the ability to repeat and reproduce the specific thermal action. This enables a standard method for determining fire resistance of structural and insulation elements (Access Steel, 2010).

Two other fire curves exist, namely the external and the hydrocarbon fire curve. The external fire curve is less intense and is used for members exposed to flames outside a building (Buchanan and Abu, 2017), such as when flames exit at the windows. When a fire burns at a higher intensity, e.g. in a building that stores petrochemical products, the hydrocarbon fire curve should be used (Buchanan and Abu, 2017). The three fire curves are depicted in Figure 2.4.

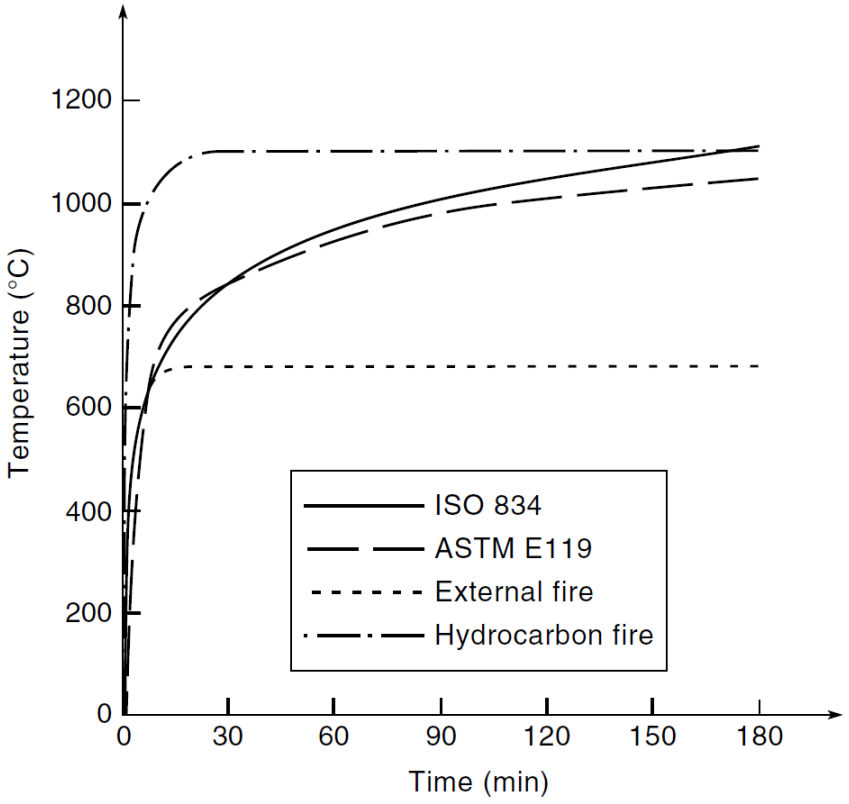

Figure 2.4: Nominal fire curves (Buchanan and Abu, 2017)

The fire curves are expressed as a uniform gas temperature (θ_g) in terms of time t, in minutes, as shown in Equations 2.3.1 to 2.3.3 (ECCS TC3, 2001).

The standard fire curve is expressed as:

$$\theta_g = 20 + 345 \log_{10}(8t + 1) \tag{2.3.1}$$

The expression for the external fire curve is:

$$\theta_g = 660(1 - 0.687 \exp^{-0.32t} - 0.313 \exp^{-3.8t}) + 20 \tag{2.3.2}$$

The hydrocarbon curve is given as:

$$\theta_g = 1080(1 - 0.325\exp^{-0.167t} - 0.675\exp^{-2.5t}) + 20 \tag{2.3.3}$$

A problem with the standard fire curve is that it was not developed based on the response of elements to a real fire. Additionally, a variety of factors that influence fire behaviour, such as fire load, ventilation characteristics and element properties are not considered. The standard fire curve consists of a steady elevation in temperature that continues to rise as time increases. It also does not consider a cooling phase, as seen in Figure 2.4. For a fire to burn for that amount of time, it requires a significant amount of fuel and the correct ventilation conditions that provide oxygen. However, in the case of a real fire, the temperature cools down as the fuel and oxygen become deficient.

2.4 Typical compartment fire behaviour

2.4.1 Fire development of a real fire

The development of a real fire depends on numerous factors, such as the size of the compartment, ventilation, fuel properties, active protective measures, etc. The time-temperature history of a real fire consists of various stages, as shown in Figure 2.5. The ignition point is where materials start to combust, which slowly heats up the compartment and enables the fire to grow (Buchanan and Abu, 2017).

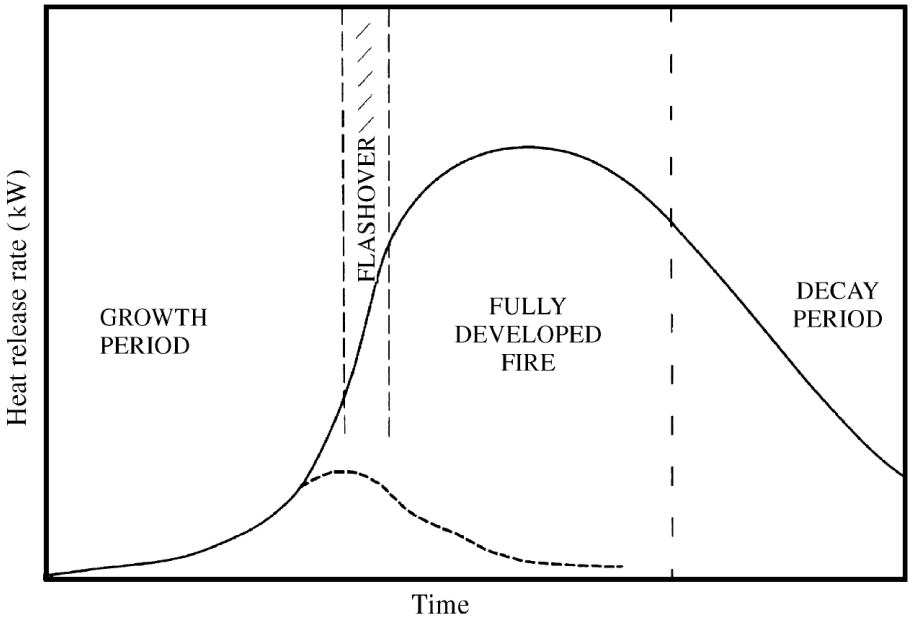

Figure 2.5: Development of a real fire (Drysdale, 2011)

Fire growth phase (pre-flashover):
The growth period burn rate is generally governed by the nature of the fuel within the room and increases as more combustible surfaces ignite. At this stage there is sufficient oxygen available for combustion to occur. Hot gases are released and cause other materials to heat up rapidly due to radiative heat transfer (Bengtsson, 2001).

Flashover:
Flashover is the rapid transition from a growing fire to a fire that is fully developed and usually occurs when the upper part of the room reaches temperatures of about $600°C$. At this point significant amounts of heat radiates from the fire and the hot gases and surfaces within the compartment, which causes all combustible material within the compartment to ignite and contribute to the burn rate and temperature in the room (Lennon, 2011).

Burning period:
After flashover, the fire enters the burning period, in which the burn rate is controlled by the ventilation available in the compartment. During the burning period, all exposed surfaces are burning due to the large amount of radiative heat flux within the compartment. It is usually in this period that structural elements within the building start to fail and where compartmentation becomes an issue, as fires are likely to spread to other compartments (Bengtsson, 2001).

Decay phase:
After burning for a certain amount of time, the fire will eventually burn out. The rate of burnout depends on the nature and amount of fuel, which is made up of all the combustible material within the compartment. As the fuel burns out, the fully developed fire can no longer be sustained, thus causing a decrease in room temperature. As the temperature in steel members cools down, some of the tensile forces that were caused by sagging are reduced. However, this can result in additional stresses in the connections, depending on the amount of axial restraint provided (Hanus, 2010).

2.4.2 Parametric fire curve

As explained above, standard fires have significantly different characteristics to real fires. The Eurocodes provide information and equations regarding parametric fires. A parametric fire is a simplified mathematical representation of a real fire time-temperature relationship. Annex A of 1991-1-2 CEN (2002) contains the calculation of the heating phase and cooling phase gas temperatures respectively, which are discussed below. An example of the application of these equations is presented in Table D.1 in Appendix D.

The heating phase gas temperature (θ_g) is calculated from:

$$\theta_g = 20 + 1325(1 - 0.324e^{-0.2t^*} - 0.204e^{-1.7t^*} - 0.472e^{-19t^*}) \quad [°C] \tag{2.4.1}$$

where:

$$t^* = t.\Gamma \quad [h] \tag{2.4.2}$$

with t as time in hours and:

$$\Gamma = \frac{(O/b)^2}{(0.04/1160)^2} \tag{2.4.3}$$

where:

$$b = \sqrt{\rho c \lambda};$$
$$\text{with limits: } 100 \leq b \leq 2200 \qquad [J/m^2 s^{1/2} K] \tag{2.4.4}$$

and the opening factor:

$$O = \frac{A_v\sqrt{h_{eq}}}{A_t};$$
$$\text{with limits: } 0.02 \leq O \leq 0.2 \qquad [m^{1/2}] \tag{2.4.5}$$

with:

ρ - density of the enclosure boundary $[kg/m^3]$;

c - specific heat of the enclosure boundary $[J/kgK]$;

λ - thermal conductivity of the enclosure boundary $[W/mK]$;

A_v - area of vertical openings $[m^2]$;

h_{eq} - weighted average of window heights $[m]$;

A_t - total area of enclosure (walls, ceiling, floor and all openings) $[m^2]$.

For a compartment consisting of a variety of materials, each with its own thermal inertia (b_i) and area (A_i) excluding openings, the combined thermal inertia (b) is given by:

$$b = \frac{\sum b_i A_i}{\sum A_i} \qquad [J/m^2 s^{1/2} K] \tag{2.4.6}$$

The time at which the maximum gas temperature (θ_{max}) is reached during the heating phase, t_{max}, depends on whether the fire is fuel or ventilation controlled. Larger openings result in more ventilation, which slows down the heating rate and reduces the temperatures. The modified time of maximum temperature (t^*_{max}) is given by:

$$t^*_{max} = t_{max}.\Gamma \qquad [h] \tag{2.4.7}$$

where:

$$t_{max} = max[0.2 \times 10^{-3}.q_{t,d}/O;\ t_{lim}] \qquad [h] \tag{2.4.8}$$

with $q_{t,d} = q_{f,d}.A_f/A_t$, as the design fire load density based on the total compartment surface area (A_t), with limits: $50 \leq q_{t,d} \leq 1000$ $[MJ/m^2]$. The limiting time (t_{lim}) is taken as 25, 20 and 15 minutes for slow, medium and fast fire growth rates, respectively. $q_{f,d}$ is the design fire load based on the floor surface area (A_f) and is given by:

$$q_{f,d} = q_{f,k}.m.\gamma_{q1}.\gamma_{q2}.\gamma_n \qquad [MJ/m^2] \tag{2.4.9}$$

where m is the combustion factor, γ_{q1} and γ_{q2} are partial factors, γ_n is the differentiation factor, and $q_{f,k}$ is the characteristic fire load density per unit floor area $[MJ/m^2]$. Values for these parameters are provided in the Eurocodes (ECCS TC3, 2001).

For a fuel controlled fire, t_{max} occurs before t_{lim}, in which case t_{max} is set equal to t_{lim}. In this case Γ is modified and t^*, as used in Equation 2.4.1, is taken as:

$$t^* = t.\Gamma_{lim} \qquad [h] \tag{2.4.10}$$

where: $\Gamma_{lim} = [O_{lim}/b]^2/(0.04/1160)^2$
with: $O_{lim} = 0.1 \times 10^{-3}.q_{t,d}/t_{lim}$

For large openings, the heating rate is further reduced by multiplying Γ_{lim} by a factor k. Hence, for $O > 0.04$, $q_{t,d} < 75$ and $b < 1160$, Γ_{lim} is multiplied by:

$$k = 1 + (\frac{O - 0.04}{0.04})(\frac{q_{t,d} - 75}{75})(\frac{1160 - b}{1160}) \tag{2.4.11}$$

After the maximum temperature has been reached, the temperatures drop in the cooling phase, as defined by:

$$\theta_g = \begin{cases} \theta_{max} - 625(t^* - t^*_{max}.x) & \text{for } t^*_{max} \leq 0.5; \\ \theta_{max} - 250(3 - t^*_{max})(t^* - t^*_{max}.x) & \text{for } 0.5 < t^*_{max} < 2; \\ \theta_{max} - 250(t^* - t^*_{max}.x) & \text{for } t^*_{max} \geq 2; \end{cases} \tag{2.4.12}$$

with:

$t^* = t.\Gamma$;

$t^*_{max} = (0.2 \times 10^{-3}.q_{t,d}/O).\Gamma$;

$x = 1.0$ if $t_{max} > t_{lim}$, or $x = t_{lim}.\Gamma/t^*_{max}$ if $t_{max} = t_{lim}$

2.5 Fire characteristics

Before analysing the effect of fire on structural elements in a building, it is important to understand fire behaviour. This section will briefly discuss the process of combustion, the basic characteristics of fire, how it behaves and the effect it has on structural elements, in this case steel members and fire insulation materials. A discussion on fire dynamics is also included in this section, along with the importance of ensuring compartmentation.

2.5.1 Combustion

Fire, or flames, is the observable effect of the process of combustion. (Balaji, 2016). According to NFPA 921 of the National Fire Protection Association (2004), a fire is defined as a rapid oxidation process (a chemical reaction) that results in the evolution of light and heat in varying intensities. The chemical combustion reaction occurs with the right mixture of oxygen in the air and a combustible fuel source with the presence of heat. The fuel feeds the fire in the form of combustible material that reaches ignition temperature due to heating, while the oxygen sustains combustion (Safety and Risk Management Office, 2017). The fire will continue to burn until the amount of oxygen, fuel or heat is insufficient. This process of combustion is known as the fire triangle, as seen in Figure 2.6.

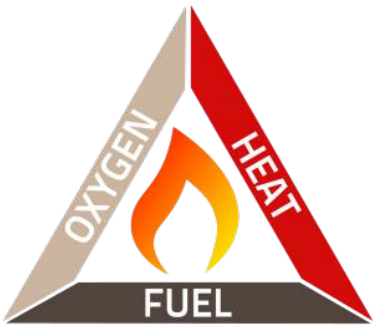

Figure 2.6: Fire triangle (Elite Fire, 2013)

Numerous causes of fire exist, many of which are caused by human activity and unforeseen accidents, such as sparks causing open flames, flammable liquids exposed to elevated temperatures, electrical wiring, heating and cooking equipment. The possibility of a fire also depends on the availability of combustible material, which includes substances such as oils, flammable liquid, gases, wood, paper, fabrics, etc. When exposed to heat, the moisture within the materials evaporate, resulting in flammable vapours that ignites when enough heat and oxygen is present. For liquid fuel, this process is called evaporation and for solid material it is referred to as pyrolysis, as shown in Figure 2.7. The point at which the material will ignite, depends on various factors, such as the quantity, geometry and moisture content of the material. The burning objects result in a reaction with the oxygen in the air, which heats up the surrounding materials. This phenomenon causes the fire to spread and could potentially lead to major disasters (Elite Fire, 2013).

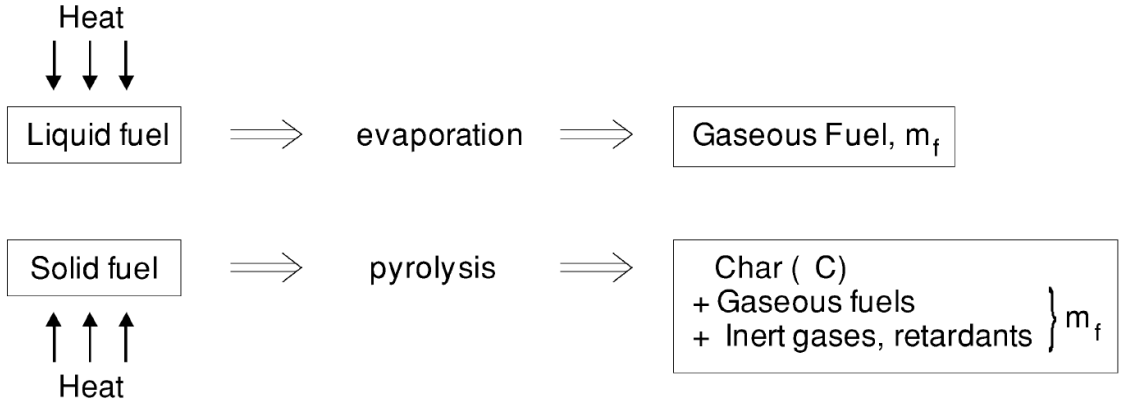

Figure 2.7: Fuel gasification in a fire (Karlsson and Quintiere, 2000)

When ensuring the safety of buildings against fires, it is important to understand how the combustion process could be managed, suppressed or even prevented. Fire safety mechanisms, such as sprinklers, reduce the amount of heat in a compartment, which allows the combustion process to decrease or stop completely. By managing the amount of oxygen available within a compartment, one could control the intensity of the fire, which is crucial when considering the lives of the fire fighters within the burning building.

2.5.2 Fire dynamics

It is obvious that larger fires have more severe consequences than smaller fires and fire protection measures are in place to prevent the growth of small fires into large ones. When

designing a structure for fire, the scale of the fire is not the only aspect to consider. It is the spread of a fire that is probably the most important aspect to consider when designing structures in fire. The prevention of fire spread to other rooms, storeys and even other buildings is known as compartmentation (Buchanan and Abu, 2017).

2.5.2.1 Compartmentation

Integrity is one of the most critical factors to consider when designing structures for the event of a fire, as discussed in Section 2.3.2. When integrity fails, compartmentation fails, which results in fire spreading from one storey to another at a pace that it becomes difficult even for large, well-equipped fire brigades to control.

Figures 2.8a, 2.8b and 2.9 show some examples of the importance of ensuring containment of a fire in tall building. The First Interstate Bank building fire burned for over three hours, destroying four floors and killing one person while 40 others were injured (Harrison, 2010). The Windsor Tower in Madrid burned for 18 to 20 hours and caused extensive structural damage. There were no automated sprinklers or other fire protection measures in place and failure of vertical compartmentation measures occurred (Bailey, 2005). In a more recent event, the Grenfell Tower fire in London is probably one of the largest fire disasters in recent times with 79 people killed and many more injured. The fire started in a faulty fridge, which soon spread across all 24 levels in less than an hour (Ruddy, 2017).

(a) First Interstate Bank building, Los Angeles (1988) (Harrison, 2010)

(b) Windsor Tower, Madrid (2005) (Fishlock, 2013)

Figure 2.8: Compartmentation failure in high rise buildings

There are four main scenarios with regard to fire spread, as discussed in significant detail in the book of Buchanan and Abu (2017). The scenarios include the spread of fire within the room of origin, fire spread to adjacent rooms, fire spread to other storeys and in a worst-case scenario, spreading of fire to other adjacent buildings.

Figure 2.9: Grenfell Tower, London (2017) (Ruddy, 2017)

There are many ways compartmentation could fail, for instance an opening could exist between two separate rooms or between certain floors. Hot gases and flames travel through ducts and cables in the ceiling, which leads to rapid fire spread. Some of the main ways fire spreads from one place to another is by flame impingement or by radiant heat transfer. The radiative and convective heat flux heats up the exposed surfaces, which in turn, through conduction, heats up members and surfaces on the unexposed sides of the floors and roofs. This causes materials on the storeys above to turn into fuel, which allows combustion to occur, thereby starting a new fire in a new compartment. As the fire develops further it travels through various compartments, which then spreads to the storeys above or below. When all or most of the combustible materials within the building has caught fire, the flames start to spread outside the building through windows and other openings. This could cause materials on, or within, the adjacent buildings to ignite, which leads to a new fire in a new building (Buchanan and Abu, 2017).

2.6 Heat transfer

To fully understand the effect a fire has on structural members, one should first understand the physics of heat transfer (Drysdale, 2011). Heat transfer is the transport of energy between different mediums due to a difference in temperature and is governed by the energy conservation principle (Patade and Chakrabarti, 2013). There are three basic processes by which heat transfer occurs, namely conduction, convection and radiation. These three modes of heat transfer could simultaneously contribute to the rise in temperature in elements within a fire compartment. One or two of the mechanisms could also occur separately, depending on the conditions in the compartment and the location under consideration (Buchanan and Abu, 2017). The three mechanisms will now be discussed in more detail.

2.6.1 Conductive heat transfer

Conduction is the transfer of heat in and through solid materials, as well as from one solid to another that are in contact with each other. Conduction can also occur between a solid and fluid where there is no relative motion adjacent to the solid (Drysdale, 2011).

Conduction occurs where a temperature gradient exists, whereby energy is transferred from the higher to the lower temperatures. With an increase in temperature there is an increase in molecular energy. Energy is then transferred from higher to lower molecular energies. This internal energy causes translational, rotational and vibrational motions within the structure of the solid material (Moran *et al.*, 2003).

This transfer of energy is measured in terms of the conductive heat flux, which represents the amount of heat that flows per unit time through a unit area with a temperature gradient of one degree per unit distance (Drysdale, 2011). The heat flux ($\dot{q}_x$"), in W/m^2, can be expressed in the one-dimensional case (x-direction) as:

$$\dot{q}_x^{"} = -k\Delta T/\Delta x \tag{2.6.1}$$

where:

k - thermal conductivity $[W/mK]$;

ΔT - difference in temperature [$^{\circ}C$ or K];

Δx - change in distance [m], usually the thickness of the material.

The thermal resistance of a material is generally influenced by the thickness and density of the material. A material with a higher density and thickness would usually result in a higher thermal resistance (Everite, 2016). The thermal conductivity (k) represents how efficiently a material can conduct heat, and therefore also influences the thermal resistance. A material with a high k-value will conduct more heat through a material as opposed to a material with a lower k-value.

2.6.2 Convective heat transfer

In his book, Drysdale (2011) defines convection as the heat transfer between solid surfaces that involves the movement of the adjacent fluids. These fluids could either be gases or liquids. Solids can be heated or cooled down by the surrounding fluids. A temperature gradient is caused by the development of a thermal boundary layer due to a temperature difference between the solid surface and the surrounding fluid. Convection has a major influence on the spread of flames in and between building compartments. The movement of hot gases and smoke from the ignition point to the ceiling and windows is also influenced by the convective heat transfer in a fire compartment (Buchanan and Abu, 2017).

Convective heat transfer could either be free or forced. Density differences within the fluid occur with an increase in temperature. As a result, buoyancy forces are induced, which then causes the movement of the fluids. This occurrence is referred to as natural or free convection. In the case of forced convection, the flow of fluids over or along the solid surface are induced by an external force. These external forces could include a fan,

a pump or even the wind (Çengel, 2008).

The heat flux generated by convective heat transfer is expressed as:

$$\dot{q}_x^{"} = h\Delta T \tag{2.6.2}$$

where:

$\dot{q}_x^{"}$ - heat flux $[W/m^2]$;

h - convective heat transfer coefficient $[W/m^2K]$;

ΔT - temperature difference of solid surface and surrounding gas or fluid [$^\circ C$ or K].

2.6.3 Radiative heat transfer

Radiative heat transfer is the transfer of energy in the form of electromagnetic waves, which requires no medium to transfer energy, unlike the case of conductive or convective heat transfer (Çengel, 2008). The temperature of an object has an influence on the amount of radiative heat that leaves the surface of the object. This intensity of radiative heat also depends on the emissivity (ϵ) of the surface (Hamerlinck, 1991), which ranges between zero (a perfect mirror-like surface) and unity (a perfect emitter). The total radiative energy emitted by a surface with a unit area is given by:

$$E = \epsilon\sigma T^4 \tag{2.6.3}$$

where σ is the Stephan Boltzmann constant ($= 5.67\text{x}10^{-8}\ W/m^2K^4$), T is the temperature of the element and ϵ, the emissivity, is defined as the ratio of the emissive power of the surface to that of a black body at the same temperature. A black body is a perfect emitter and therefore has an emissivity of 1.

The Eurocode (ECCS TC3, 2001) describes the configuration factor, also referred to as the view factor, as the ratio between the radiative heat leaving the emitting surface and the radiative heat arriving at the receiving surface. The distance and relative orientation between the two surfaces and the size of the surfaces influence the configuration factor value. The configuration, or view factor ($F_{ij} = F_{ji}$) is determined by:

$$F_{ij} = \int_i \int_j \frac{\cos\phi_i \cos\phi_j}{\pi r^2} dA_i dA_j \tag{2.6.4}$$

which can be simplified to be a two-dimensional (2D) case as:

$$\phi = \frac{|AC + BD - AD - BC|}{2|CD|} \tag{2.6.5}$$

where the distances are indicated on Figure 2.10.

Annex G of Eurocode 1991-1-2 (CEN, 2002) provides detailed information and calculations of configuration factors for various surface configurations.

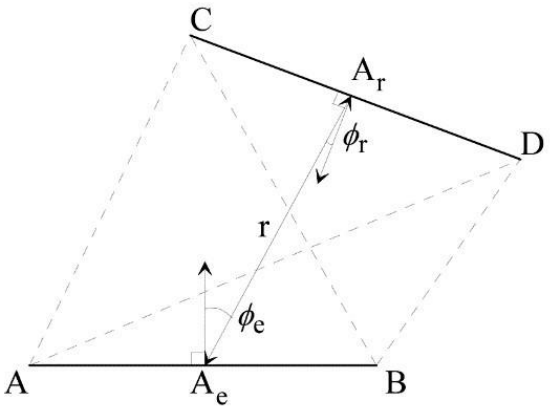

Figure 2.10: Radiative heat transfer between two infinitesimal surface areas (Franssen and Vila Real, 2012)

2.7 Steel structures in fire

2.7.1 Steel behaviour at elevated temperatures

Steel is a popular construction material and is well known for its strength in tensile applications. Steel has a good weight to strength ratio, depending on the type of section that is used. However, steel members heat up when exposed to fire, which causes sections to lose their strength and stiffness. In some cases, when steel elements reach very high temperatures, deflection limits are exceeded whilst reaction forces change due to thermal expansion (Lennon, 2011).

Due to its relatively high thermal conductivity, steel conducts heat within a steel member faster than other general construction materials, such as concrete and wood members. Furthermore, steel members are usually much thinner than other construction materials, which also contributes to the rapid heating within a section. Other factors affecting the heating rate of steel members include the type and magnitude of loads applied to the structure and the geometry of the structure (Buchanan and Abu, 2017).

The severity of the fire scenario influences how fast and by how much the steel sections heat up and, therefore, whether the structure may fail. It is important to prevent the growth of fire severity within compartments, so that the structural capacity is maintained.

2.7.2 Thermal properties of steel

As previously mentioned, the material properties of steel vary with the temperature of the steel section. Heat is transferred from the fire in the compartment to the steel member by means of convective and radiative heat transfer. In order to determine the steel section temperatures, the material thermal properties should first be calculated. The Eurocode thermal properties are used in all calculations performed in the present thesis and will be now discussed in more detail.

The density of steel stays relatively constant at 7850 kg/m^3 with a change in temperature. The thermal expansion, specific heat and thermal conductivity of steel varies quite significantly with changing temperatures, as seen in Figures 2.11, 2.12 and 2.13.

2.7.2.1 Thermal expansion

As materials heat up, they expand, some more than others. In situations where two different materials interact, such as steel and concrete in composite sections, thermal bowing can occur. Due to shielding and heat-sink effects, the bottom and top part of steel members expand at different rates (Wang *et al.*, 2013). The thermal expansion of steel varies almost linearly with respect to temperature, as seen in Figure 2.11.

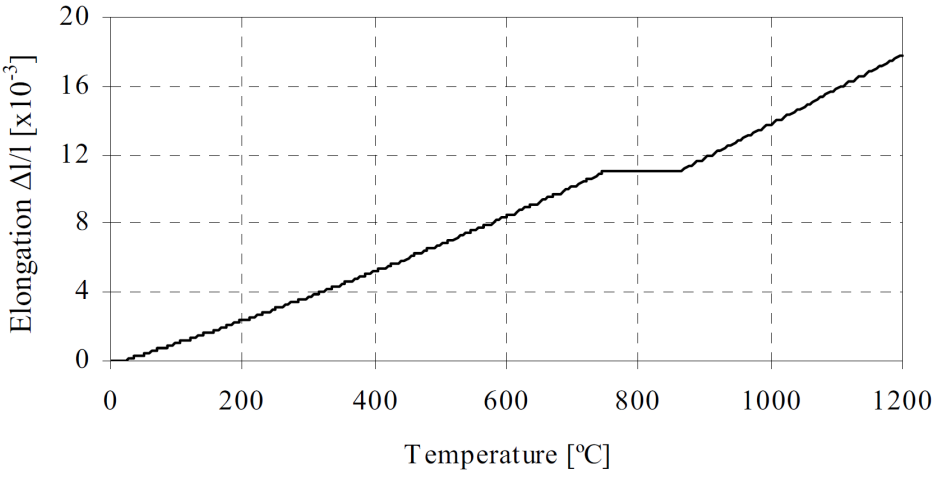

Figure 2.11: Thermal expansion of steel (Franssen and Vila Real, 2012)

The equations that describe the relationship between the thermal expansion, also known as thermal elongation, of steel and temperature are given by ECCS TC3 (2001) as:

$$\Delta l/l = \begin{cases} -2.416 \times 10^{-4} + 1.2 \times 10^{-5}\ \theta_a + 0.4 \times 10^{-8}\ \theta_a^2 & \text{for } 20°C \leq \theta_a \leq 750°C; \\ 11 \times 10^{-3} & \text{for } 750°C \leq \theta_a < 860°C; \\ -6.2 \times 10^{-3} + 2 \times 10^{-5}\ \theta_a & \text{for } 860°C < \theta_a \leq 1200°C; \end{cases} \tag{2.7.1}$$

where θ_a is the steel temperature, l is the length of the steel element at 20 $°C$ and Δl is the thermal elongation of the steel member. For simplified analyses, the Eurocode specifies a linearised thermal expansion as $\Delta l/l = 1.4 \times 10^{-5}\theta_a$ (ECCS TC3, 2001).

2.7.2.2 Specific heat

Specific heat is defined as the amount of energy (Joules) needed to be gained by a material to cause 1 kg of the material to increase by 1 $°C$ (Wang *et al.*, 2013). Specific heat of carbon steel, measured in J/kgK, varies with temperature in the manner described by Equation (2.7.2). Figure 2.12 represents this relationship.

$$c_a = \begin{cases} 425 + 0.773\ \theta_a - 1.69 \times 10^{-3}\ \theta_a^2 + 2.22 \times 10^{-6}\ \theta_a^3 & \text{for } \theta_a < 600°C; \\ 666 + \frac{13002}{738 - \theta_a} & \text{for } 600°C \leq \theta_a < 735°C; \\ 545 + \frac{17820}{\theta_a - 731} & \text{for } 735°C \leq \theta_a < 900°C; \\ 650 & \text{for } 900°C \leq \theta_a \end{cases} \tag{2.7.2}$$

where θ_a is the steel temperature.

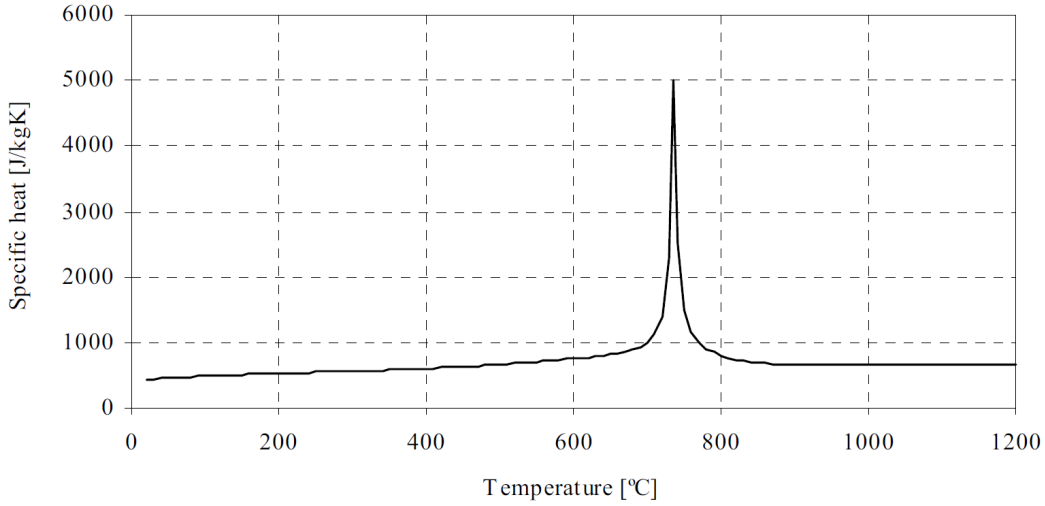

Figure 2.12: Specific heat of steel (Franssen and Vila Real, 2012)

From Figure 2.12, it can be seen that the curve reaches a peak at a temperature of $735°C$. This peak represents the crystal structure phase change of the material, which is due to an endothermic process (Wang *et al.*, 2013). For simplified calculation analyses, an average value of 600 J/kgK is used (ECCS TC3, 2001).

2.7.2.3 Thermal conductivity

Thermal conductivity represents the amount of heat transfer through a unit area with a temperature gradient of one degree per unit distance. It is a measure of how well a material can conduct heat and is given in W/mK (Wang *et al.*, 2013). For carbon steel, the thermal conductivity decreases with an increase in temperature in the manner described by Equation (2.7.3). This relationship is also shown in Figure 2.13.

$$\lambda_a = \begin{cases} 54 - 3.33 \times 10^{-2}\ \theta_a & \text{for } 20°C \leq \theta_a \leq 800°C; \\ 27.3 & \text{for } 800°C < \theta_a \leq 1200°C \end{cases} \tag{2.7.3}$$

where θ_a is the steel temperature.

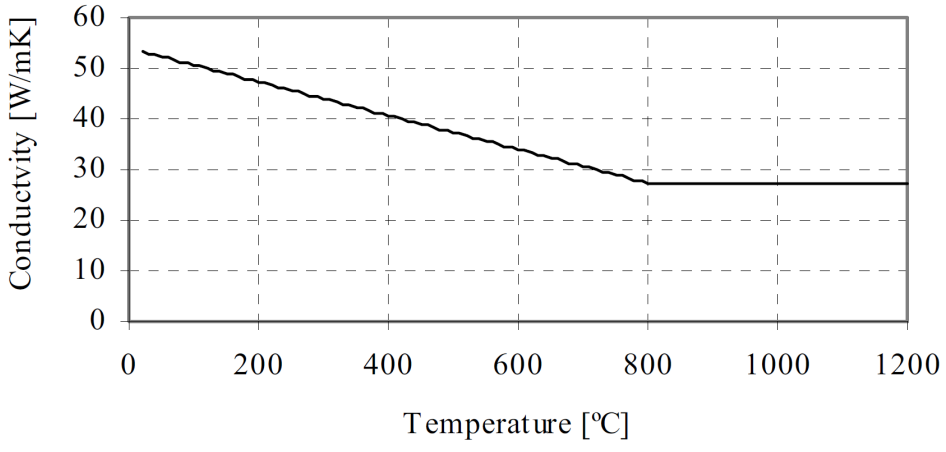

Figure 2.13: Thermal conductivity of steel (Franssen and Vila Real, 2012)

Although this is not explicitly stated in Eurocode 3, the thermal conductivity of steel is generally assumed to be reversible during cooling, which means that the thermal conductivity of steel varies according to Equation (2.7.3) during heating from $20°C$ to a temperature $\theta_{a,max}$, as well as during subsequent cooling back to $20°C$.

2.7.3 Calculating steel temperature

In order to determine the behaviour of steel structures in fire, the temperatures of the steel members should first be calculated. The steel temperatures depend on various factors, such as the gas temperature within the fire compartment, which depends on the size and geometry of the compartment. As the gas temperature rises, the heat is transferred to the structural members on and around the boundaries of the compartment through radiation and convection. Therefore, the amount of steel surfaces directly exposed to the heated gas and the nature of fire protection systems influences the rise in steel temperatures (Franssen and Vila Real, 2012).

This section will discuss important concepts of the calculation of steel temperatures and how to determine steel temperatures by using heat transfer equations for unprotected and protected sections, respectively. The effect of certain fire protection systems will also be discussed.

2.7.3.1 Steel section factor

The section factor is a parameter used in the calculation of steel temperatures that has a major influence on the rate at which temperatures rise within a steel section. Many different steel sections exist, varying from I-sections to circular hollow sections. Due to the difference in shape and thickness, the heating rate differs from section to section.

Each section has a section factor that represents the ratio of the exposed surface area to the volume of the section per unit length (A/V) resulting in a unit of m^{-1}. The section factor is sometimes referred to as the "massivity factor" and in certain cases it can be taken as the ratio of the heated perimeter to the cross-sectional area of the steel member (H_p/A). The Eurocode 3 defines the section factor for unprotected steel members as A_m/V and for protected members as A_p/V. The section factor mainly depends on the number of heated surfaces due to fire exposure for both unprotected and protected steel members. In the case of protected members, the type of insulation is also a major factor together with the number of sides insulated (Franssen and Vila Real, 2012).

It is obvious that a member with a thick section will heat up slower than a thinner section, due to the bigger cross-sectional area and therefore, a greater volume. Also, with a larger heated perimeter the section will heat up more quickly. Therefore, the higher the section factor, the faster the temperature increase in the section, and vice versa, as shown in Figure 2.14 (Franssen and Vila Real, 2012).

2.7.3.2 Unprotected sections exposed to fire

Unprotected steel sections heat up relatively quickly, especially sections with a high section factor. Simplified heat transfer equations are specified in the Eurocode 1993-1-2 (CEN, 2005) and can be used to predict steel section temperatures. These equations are based

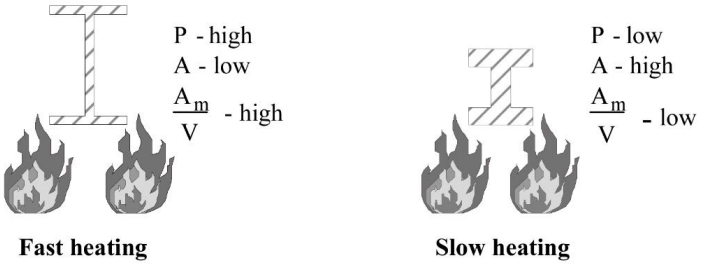

Figure 2.14: Section factor (Franssen and Vila Real, 2012)

on the assumption that the temperature is uniformly distributed within the section. The geometry of the different cross sections influences the rate of temperature increase in the section. This includes factors such as the nature of convective and radiative heat transfer, configuration factor, emissivity and other parameters, which will be discussed below. Equation 2.7.4 represents the change in temperature ($\Delta\theta_{a,t}$) over time (Δt) in an unprotected steel member.

$$\Delta\theta_{a,t} = k_{sh}\frac{A_m/V}{c_a\rho_a}\dot{h}_{net,d}\Delta t \ [^\circ C] \tag{2.7.4}$$

where:

k_{sh} - shadow effect correction factor;

A_m/V - section factor for unprotected steel members $[m^{-1}]$, with A_m, the exposed surface area of the member per unit length $[m^2]$, and V as the volume of the member per unit length $[m^3]$;

c_a - specific heat of steel, as discussed in Section 2.7.2 $[J/kg.K]$;

ρ_a - density of steel as 7850 $[kg/m^3]$;

Δt - time increment $[s]$, should be taken as $\leq 5s$;

$\dot{h}_{net,d}$ - design heat flux value per unit area, which is the sum of the convective and radiative heat flux, $h_{net,c}$ and $h_{net,r}$ respectively, as shown in Equation 2.7.5.

$$\dot{h}_{net,d} = \dot{h}_{net,c} + \dot{h}_{net,r} \ [W/m^2] \tag{2.7.5}$$

with:

$$\dot{h}_{net,c} = \alpha_c(\theta_g - \theta_m) \ [W/m^2] \tag{2.7.6}$$

where:

α_c - coefficient of heat transfer by convection, taken as 25 W/m^2K for surfaces exposed to the standard fire. On the unexposed side, where radiation is considered separately it is taken as 4 W/m^2K and when radiation is considered with convection it is taken as 9 W/m^2K;

θ_g - gas temperature within the fire compartment $[^\circ C]$;

θ_m - surface temperature of the member $[^\circ C]$.

and:

$$\dot{h}_{net,r} = \phi\epsilon_m\sigma[(\theta_r + 273)^4 - (\theta_m + 273)^4] \ [W/m^2] \tag{2.7.7}$$

where:

ϕ - configuration factor (view factor) as described in Section 2.6.3, usually taken as 1.0. When position and shape effects should be considered, Annex G of Eurocode 1 could be used to determine the configuration factor;

ϵ_m - surface emissivity of the steel member, usually taken as 0.7 for carbon steel sections and 0.8 for other materials;

σ - Stephan Boltzmann constant equal to 5.67×10^{-8} $[W/m^2K^4]$;

θ_r - effective radiation temperature of the fire environment $[°C]$;

θ_m - surface temperature of the member $[°C]$.

As previously mentioned, the heat transfer equation (Equation 2.7.4) assumes that heat is uniformly distributed throughout the steel section, which will therefore not hold for sections with a very low section factor (i.e. thick sections). A_m/V should therefore not be taken as less than 10 m^{-1} (Franssen and Vila Real, 2012). Figure A.1 in Appendix A presents the section factors for some general unprotected steel members.

When steel members are fully engulfed in a fire, the radiation temperature would be equal to the surrounding gas temperature. However, in the case where the steel member is not fully engulfed in the fire, certain parts of the member would shield other parts from the radiative heat flux transferred from the hot gas to the member. Take for instance an I-beam cross-section heated from the bottom. The bottom flange would shield some parts of the section from direct radiative heat flux, as shown in Figure 2.15 (Franssen and Vila Real, 2012).

Figure 2.15: Shielding effects due to section shape (Franssen and Vila Real, 2012)

In the case of an I-section, the correction factor k_sh could be determined as a value lower than unity as follows:

$$k_{sh} = 0.9 \ \frac{[A_m/V]_b}{[A_m/V]} \tag{2.7.8}$$

where:

$[A_m/V]_b$ - the box section factor value, which is defined as the ratio between the exposed surface area of a box perimeter around the section and the steel section volume.

For other sections k_{sh} should be calculated by:

$$k_{sh} = \frac{[A_m/V]_b}{[A_m/V]} \tag{2.7.9}$$

Some examples of box section factors are presented in Table A.2 in Appendix A.

2.7.3.3 Protected sections exposed to fire

Certain safety requirements, which vary around the world, require that most steel structures be protected against high heat fluxes for a specific amount of time. Numerous fire protection products exist that limit the rise in steel element temperatures in the event of a fire, which enable the structure to meet these safety requirements. These types of fire protection systems mainly consist of boards, sprays and intumescent paint (Franssen and Vila Real, 2015). Some of these products will be discussed in more detail through the rest of this thesis.

The simple calculation method specified by the Eurocodes (ECCS TC3, 2001) for the prediction of protected steel temperatures assumes a uniform temperature distribution throughout the cross-section. The change in temperature ($\Delta\theta_{a,t}$) over time (Δt) in a protected steel member is given by:

$$\Delta\theta_{a,t} = \frac{\lambda_p A_m/V(\theta_{g,t} - \theta_{a,t})}{d_p c_a \rho_a (1 + \phi/3)}\Delta t - (e^{\phi/10} - 1)\Delta\theta_{g,t} \geq 0 \ [^\circ C] \tag{2.7.10}$$

with:

ϕ - amount of heat stored in the protection, calculated as:

$$\phi = \frac{c_p d_p \rho_p}{c_a \rho_a}\frac{A_p}{V} \tag{2.7.11}$$

where:

A_p/V - section factor for protected steel members, where A_p is the appropriate area of fire protection material per unit length of the member and V the volume of the member per unit length;

c_a - specific heat of steel $[J/kgK]$, as discussed in Section 2.7.2;

ρ_a - density of steel $[kg/m^3]$, as discussed in Section 2.7.2;

c_p - specific heat of the insulation material $[J/kgK]$;

ρ_p - density of the insulation material $[kg/m^3]$;

λ_p - thermal conductivity of the insulation material $[W/mK]$;

d_p - thickness of the insulation material $[m]$;

$\theta_{a,t}$ - steel temperature at time t $[^\circ C$ or $K]$;

$\theta_{g,t}$ - ambient gas temperature at time t [$^{\circ}C$ or K];

$\Delta\theta_{g,t}$ - change in ambient gas temperature during time interval Δt [$^{\circ}C$ or K];

Δt - time interval [s].

Figure A.3 in Appendix A presents the section factors for some general steel members insulated by fire protection materials.

2.7.4 Gypsum boards in fire

It is important to understand the basic characteristics of insulation materials, such as gypsum, in order to determine the effect it has on the protection of steel members in a fire. Gypsum boards are the most widely used for limiting the increase in steel element temperatures, due to its favourable thermal properties that allow for good insulation and fire protecting capabilities. When the temperatures increase, gypsum dehydrates, which creates a heat barrier due to the consumption of energy that is caused by the endothermic chemical reaction of dehydration (Weber, 2012).

2.7.4.1 Material properties of gypsum

Gypsum boards are made up of a crystal lattice "needle-like" structure on a microscopic level and usually consist of calcium sulphate dihydrate ($CaSO_4 2H_2O$). Gypsum boards can also contain magnesium carbonate ($MgCO_3$), calcium carbonate ($CaCO_3$) or other materials that increase the fire resistance of the board (Kontogeorgos *et al.*, 2012). Gypsum has a relatively high porosity and contains a mixture of dry air and free moisture in the form of water vapour in the voids (Weber, 2012).

The fire performance of gypsum boards is improved by adding glass-fibre reinforcing. These boards are known as gypsum type X boards and, in some cases, may contain other additives (Buchanan and Abu, 2017). The thermal properties of gypsum type X are temperature dependent and have been determined by various authors, such as Feng *et al.* (2003), Hopkin *et al.* (2012) and Weber (2012), all of which propose different values, especially for the specific heat. This could be due to the different testing methods and equipment used as well as the specific source of the gypsum material. Weber (2012) specified the most relevant thermal properties that are generally used for gypsum boards including a heat capacity (c_p) of 1000 J/kgK, an initial density (ρ) of 820 kg/m^3 and a surface emissivity factor for the unexposed side as 0.9.

2.7.4.2 Heat transfer through gypsum boards

There are three main mechanisms of heat transfer in gypsum, namely heat conduction, vapour transportation (convection) and condensation and evaporation of water within the gypsum. The side of the gypsum board directly exposed to the fire develops a dehydration front, which consumes energy in the form of heat and releases water vapour. Convective heat transfer occurs as the water vapour travels through the gypsum board, which causes pressure to build up within the board. However, the amount of heat transferred by convection is negligible when compared to the conduction of heat through the gypsum (Weber, 2012).

In the literature it has been found that the condensation and evaporation effect have an influence on the change in temperature within the gypsum board, but only around the first 15 minutes. Temperature on the unexposed surface increases due to condensation of the water vapour. Thereafter the temperature on the unexposed surface reduces as the vapour evaporates. This results in a temperature "plateau". After all the vapour evaporates, the temperature increases again (Weber, 2012). The author mentions that heat transfer by conduction is the main mechanism and dominates the increase in temperatures through the gypsum board.

2.7.5 Steel members within voids protected by heat screens

Two general cases exist with regards to steel members that are situated in an enclosed void, where they are being protected from the radiative and convective heat from the compartment fire. One case is in the form of a composite steel beam with concrete above the section and a heat screen below, as depicted in Figure 2.16a. The heat screen could, for example, be an insulation board, such as a gypsum or fibre-cement board. The second case includes steel columns shielded on both sides by heat screens that are placed upright, as shown in Figure 2.16b (Franssen and Vila Real, 2015). This setup typically is used in drywalling systems, where cold-formed steel members are enclosed between two or more gypsum boards.

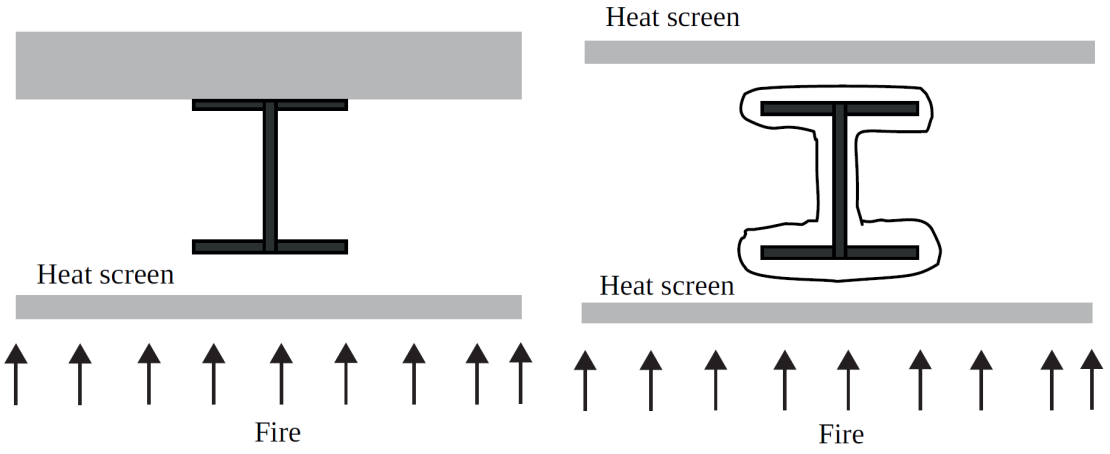

(a) Steel beam in void shielded from below (b) Steel column shielded from the sides

Figure 2.16: Horizontal (beams) and vertical (columns) heat screens protecting steel members from direct heat

ECCS TC3 (2001) provides simple rules for the case where heat screens are used to protect steelwork within voids. These rules, however, are only applicable when a gap exists between the steel member and the protective heat screen. These rules can, therefore, not be used when the steel member and heat screen are in direct contact to one another (Franssen and Vila Real, 2015). The gap prevents heat transfer by means of conduction to occur through the heat screen directly into the steel member, which typically results in lower temperatures within the steel section.

2.7.6 Advanced thermal calculation techniques

The equations for heat transfer that are provided in the Eurocodes, as described in Section 2.7.3, are based on simplified assumptions. It is assumed that the temperature through the section remains uniform, which is far from reality (Franssen and Vila Real, 2015). However, the simplified models are easier to use and in general, require less computational time and resources, as compared to an advanced model analysis.

Numerous advanced methods exist through which steel temperatures can be calculated, such as finite element analysis (FEA), computational fluid dynamics (CFD) analysis and other software programs developed by private institutions. Examples of these software include TASEF, TSLAB, MACS+, VULCAN, SAFIR, a range of fire calculation software packages provided by Arcelor-Mittal and the highly advanced commercial FE software, such as ABAQUS, ANSYS, ADINA and HEATING (Walls, 2016; Hurley *et al.*, 2016). TASEF and SAFIR were developed specifically for the fire safety analysis of structures. However, the present thesis will only focus on the finite element method using ABAQUS, which is one of the most popular FEA software programmes and is known for its powerful capabilities. ABAQUS can be used to perform various mechanical analyses, thermal heat transfer analyses, decoupled thermo-mechanical analyses as well as fully-coupled thermo-mechanical analyses (Dassault Systémes, 2015).

The accuracy of the numerical temperature calculations performed by these software packages, according to Hurley *et al.* (2016), depends on the validity of the FE model, whether the material properties are accurate and the reliability and accuracy of the algorithms within the software package itself. More information regarding the verification of numerical modelling software for determining temperatures in structures subjected to fire can be found in Wickström and Palsson (1999).

2.7.6.1 Cavity radiation in ABAQUS

The three heat transfer modes were discussed in Section 2.6, which included conduction, convection and radiation. Conduction is modelled in ABAQUS by means of "Tie" constraints between the various material surfaces, while convection and surface radiation are defined by using interactions. The convective heat transfer coefficient, along with the sink temperature are specified for the surface film condition, while the emissivity and surface temperature are specified for the surface radiation interaction. The reader is referred to the modelling process described in the ABAQUS user's guide (Dassault Systémes, 2015) for more information. The cavity radiation, however, is discussed in more detailed, due to its significance during the heat transfer analyses performed in this research.

In ABAQUS (Dassault Systémes, 2015), cavity radiation occurs between surfaces in the model that can "see" each other, where the surfaces exchange heat through radiation to one another. The surfaces that make up the cavity are referred to as facets. View factors, as discussed in Section 2.6.3, are automatically calculated by ABAQUS, which takes radiation blocking into consideration. The blocking of radiation occurs when certain parts of an object are in the way of the radiation path between two radiating surfaces (Dassault Systémes, 2015). This is also known as shadowing, as discussed in Section 2.7.3. The view factor calculations in ABAQUS are based on the work from Johnson (1987).

ABAQUS describes the radiation flux per unit area into a facet within a cavity as:

$$q_i^c = \frac{\sigma \epsilon_i}{A_i} \sum_j \epsilon_j \sum_k F_{ik} C_{kj}^{-1} ((\theta_j - \theta^z)^4 - (\theta_i - \theta^z)^4) \tag{2.7.12}$$

where:

A_i - area of facet i seeing all facets in the cavity j = 1,2,...,n;

ϵ_i, ϵ_j - emissivities of facets i and j, respectively;

σ - Stefan-Boltzmann constant ($= 5.67 \times 10^{-8}\ W/m^2K^4$);

F_{ij} - geometrical view-factor matrix;

C_{ij} - reflection matrix ($= \delta_{ij} - (1 - \epsilon_i)F_{ij}/A_i$);

θ_i, θ_j - temperatures of facets i and j, respectively;

θ^z - absolute zero temperature.

The geometrical view factor matrix is created by ABAQUS and determined from Equation 2.6.4, as provided in Section 2.6.3. For the case of a closed cavity, the ray that leaves any facet will always reach another facet within the cavity. Therefore, the lines in the view-factor matrix has to sum up to one (Schaumann and Hothan, 2002).

2.8 Cellular beams

This section provides a brief overview of cellular beams and their typical behaviour in fire. Cellular beams are essentially universal or wide flange beams with circular openings in the web, which are flexible in terms of the location and geometry of the openings, unlike castellated beam profiles (Rini, 2006).

2.8.1 Background on cellular beams

The use of cellular beams in the steel construction industry increased significantly since they were introduced 30 years ago by Westok (Ltd), a steel manufacturer part of Kloeckner metals based in the United Kingdom (UK). Cellular beams are manufactured by two processes from two respective manufacturers. One includes the cutting of universal or wide flange beams, from which the two halves of a beam are welded together, creating an expanded beam section (refer to Figure 2.17 (left)). The other method includes the automated cutting of steel plates, from which a cellular beam section is built up by automated welding of the separate plates (refer to Figure 2.17 (right). More detail on the manufacturing processes and design values of cellular beam sections are available in the literature, such as the documents on ACB Cellular Beams (ArcelorMittal, 2017*a*).

Cellular beams are suited for long spans and can allow for a wide range of floor configurations (Rini, 2006). As discussed in Chapter 1, the circular holes in the web enable services and ducts to pass through the beam, rather than underneath or above it. This allows for shallower floor depths in the overall building. The size and spacing of the web openings are not fixed values, therefore allowing for more flexible structural designs. Due to their

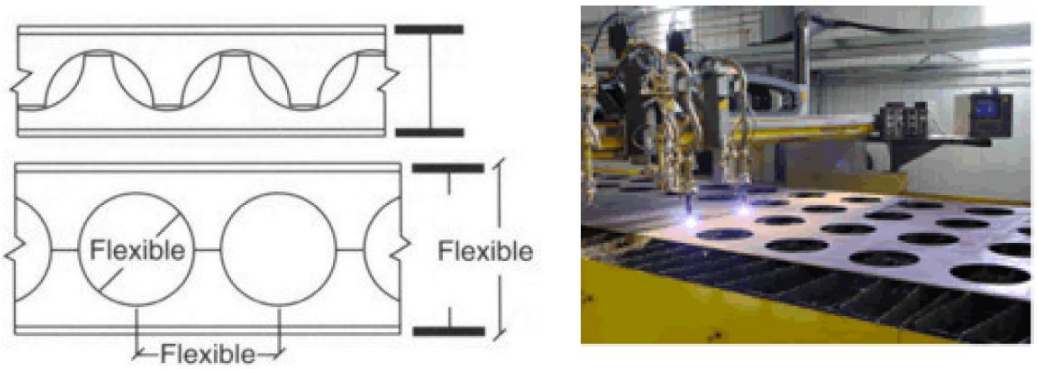

Figure 2.17: Fabrication of cellular beams with cutting and expanding process (left) and the automated plate cutting process (right) (Rini, 2006)

deeper cross-sections, cellular beams have about 2.5 times higher bending resistance than the corresponding original member, which allows for a more economical design (Mesquita *et al.*, 2015). The amount of steel used is also reduced, which results in a lower overall permanent loading on a structure. A lower permanent loading and a higher bending resistance reduce the required amount of axial support, such as columns and load bearing walls, which also reduce the total cost of the structure (Nadjai *et al.*, 2011).

However, less material in the web of cellular beams results in a reduction in shear capacity, which make them more prone to shear failure (Rini, 2006). Significant research has been conducted on the behaviour of cellular beams under ambient conditions, from which a good understanding of the various failure modes has been gained. The main failure modes include Vierendeel bending, flexural bending, failure of welds in web, web-post buckling, lateral-torsional buckling and distortional buckling (Nadjai *et al.*, 2011).

2.8.2 Behaviour of cellular beams in fire

The amount of research on cellular beams in fire has increased significantly over the past few years. Bihina *et al.* (2013) have published an article on the behaviour of composite cellular beams in fire, where they found that cellular beams with slender web posts and an asymmetrical cross-section are more likely to fail by web-post buckling. They also concluded that sections with larger or reinforced web-posts fail by flexural bending, similar to solid beam sections (Bihina *et al.*, 2013). Although the majority of experimental studies in the literature are based on single element tests, a good understanding of the fire behaviour of cellular beams has been developed (Nadjai *et al.*, 2011).

Significant research has also been done on the protection of cellular beams against fire. The work of Mesquita *et al.* (2015) includes a set of experimental fire tests on both solid and cellular steel beams that were protected with intumescent coatings, as well as being unprotected. It was found that for the unprotected sections, the web post temperature and mean flange temperature of the cellular beams were lower than the equivalent solid beam section. For the protected cellular beam sections, a small amount of shrinkage of the intumescent coating occurred around the perimeter of the openings. This allowed a small area of steel to be directly exposed to the fire, which resulted in higher temperatures compared to the solid beams. The thickness of intumescent coating required for cellular

beams depend on various factors, such as the geometry of the web openings, the thickness of the web and the width of the web post (Mesquita *et al.*, 2015).

2.9 Testing of structures in fire

Structural fire tests are widely used across the world to investigate the thermal behaviour and mechanical response of all types of structures. They are also used for validating numerous numerical and theoretical studies, such as predicting temperatures, deflections, axial forces and the overall structural behaviour of building assemblies.

2.9.1 Testing method requirements

Various international documents describe standard testing methods, such as documents from the American Society for Testing and Materials, for example standard ASTM E119 (2000), which uses a fire curve similar to the ISO standard fire to perform fire tests of building construction and materials. Another set of documents are the British Standard BS 476, which include a variety of standards on fire testing, similar to the ASTM standards. The South African Bureau of Standards (SABS) also provides a set of standards for fire testing of materials and building components and elements, which are the SANS 10177 standards, ranging from part 1 to 11. Each part of SANS 10177 describes the testing requirements for various elements in a building and different fire scenarios. The necessary apparatus and test specimen preparation are also listed in SANS 10177-2 (SABS, 2005). All of these standards provide similar requirements with regards to the fire resistance performance of the test specimens, which are based on the stability, integrity and insulation criteria, as discussed in Section 2.3.2.

2.9.2 Full-scale fire testing

The way experimental research is being conducted has changed over the past decades and research is moving towards a more full-scale performance-based approach. Bisby *et al.* (2013) mentioned that "In recent years, large-scale structural fire testing has experienced something of a renaissance." These authors present a review of full-scale non-standard structural fire engineering research that has been performed within the last couple of decades all over the world. The aim of the authors was to identify shortcomings in the research field of fire testing on a large scale, which included areas such as non-standard fire exposure, the effect of the cooling phase of a natural fire and the residual capacity after a fire, and other such factors (Bisby *et al.*, 2013).

Nadjai *et al.* (2011) conducted research on the behaviour of composite cellular steel beams in fire. Their research included a full-scale fire test on 15 m long unprotected cellular beams that behaved compositely with a concrete slab, while being exposed to a natural compartment fire. The test was used to investigate Bailey's design method, which utilizes membrane action of the composite slab. It was found that protection of the secondary beams is unnecessary, as a result of the global behaviour of the whole structure (Nadjai *et al.*, 2011). Valuable information, such as this, cannot be obtained from small-scale fire tests, which only incorporate single beam elements, due to the difference in boundary conditions. This emphasizes the need for full-scale fire tests, from which the global behaviour of structural systems can be determined.

2.9.3 Small- and medium-scale fire testing

Small- and medium-scale furnace tests are widely used to determine the thermal resistance of single elements and some small assemblies in fire. These furnace tests incorporate standard fire exposure and are usually used for research and development projects, as they are reproducible and easily controllable, which makes them useful for benchmarking and comparison purposes (Bisby *et al.*, 2013).

Due to geometry restrictions and different heat transfer parameters, small-scale models will differ somewhat when compared to full-scale fire tests. There are a variety of factors that cannot be considered in a small-scale furnace, such as the behaviour of connections, deflection behaviour and the global behaviour of the full structure. Harmathy and Lie (1970) has noted that the standard fire test does not measure the actual performance of the member being tested and it is also not a perfect comparison measurement.

In spite of the above, the heat transfer between and through test samples can be modelled relatively accurately in small-scale fire tests, whereby the thermal response can by determined (Buchanan and Abu, 2017). The focus is mainly on the insulation criteria and the integrity of the insulation boards under thermal actions and not on the structural resistance criteria. Therefore, for the purpose of this thesis, the small-scale furnace tests are sufficient, as they are primarily used for the verification of FE model simulations.

2.10 Overview of literature study

This chapter provides an in-depth background on the field of structural fire engineering, which includes various fire safety concepts and design approaches. The basics of fire characteristics, fire dynamics and structural fire resistance are discussed to gain an understanding of the processes for determining the thermal behaviour of the cellular beam structure (CBS), which was introduced in Chapter 1.

The three major criteria for determining the fire resistance of a structure include: load bearing capacity, or structural resistance (R), integrity of the structural elements (E) and the insulation of the materials (I). The requirements were briefly discussed in Section 2.3.2.

Two major design fires have been described, which are used in this work, namely the standard fire curve and the parametric fire curve. The former is also known as the ISO 834 fire and is most widely used for fire testing and serves as a benchmark for determining fire resistance, while the latter is based on Eurocode equations that closely resembles a real fire.

The main aspects of performing a thermal analysis of a steel structure are also discussed in this chapter. This includes the heat transfer mechanisms in Section 2.6, behaviour of unprotected and protected steel at elevated temperatures in Section 2.7.2 and the consideration of advanced thermal calculation models in Section 2.7.6. These sections serve as a foundation for the thermal analyses carried out in this thesis to determine the fire resistance of the CBS, in terms of the insulation and integrity requirements. Lastly, Section 2.9 provides a brief discussion on fire testing, along with the corresponding requirements.

Chapter 3

Experimental setup

3.1 Introduction

This chapter provides a detailed description of the experimental study that was performed as part of the investigation. A series of small-scale samples were tested, with each having a different configuration. The small-scale samples represent the bottom part of the sandwich floor system that was presented in Chapter 1, which is situated directly below the cellular steel beams. The rationale for the experimental study is discussed along with an overview of the small-scale fire test setup. This is followed by the preparation of the test samples and the test setup, which includes the planning and construction of the test sample assemblies, the furnace specifications, testing procedures and test data management.

3.2 Rationale for the experiments

Numerous advanced modelling software packages are available for predicting temperatures in structural systems by performing heat transfer analyses. Although these software packages are powerful, the results obtained do not necessarily replicate real world phenomena if input parameters and model formulations are not accurately defined. Furthermore, there is still a possibility of human error, such as the user incorrectly implementing analysis methods and incorporating inaccurate material properties, as discussed in Section 2.7.6. The aim of the experimental study is, therefore, to validate the numerical models discussed in Chapter 6. This is done by comparing the temperatures obtained in the small-scale fire tests with those from the FE models.

A significant number of small-scale fire tests have been conducted by various authors on cold-formed thin-walled steel panel systems in fire, which includes the work performed by Feng *et al.* (2003). These panel systems are generally used for internal partitions, cladding and lightweight floors (Feng *et al.*, 2003). However, the specific structural floor system presented in this thesis consists of a unique configuration that differs from previous experimental studies. The floor system in this thesis includes profiled steel decking, rather than cold-formed steel sections, that is "sandwiched" between layers of insulation boards. Although both configurations consist of a cavity between the insulation layers, the profiled steel decking in this thesis is continuous throughout the floor system. Therefore, the thermal behaviour of the two respective configurations will differ from one another.

Numerous composite steel-concrete structures have been tested by researchers, such as Bihina *et al.* (2013) and Nadjai *et al.* (2011). These authors performed fire tests on large-scale composite cellular beams that incorporated profiled steel decking, from which behaviour, such as composite tensile membrane action, was utilised. The structural system in the current thesis, however, does not include a concrete slab that behaves compositely with the steel beams and decking system. The small-scale furnace tests will, therefore, provide valuable information regarding the temperature distribution through the various material layers and air voids within the floor system, as well as the behaviour of the specific insulation materials used.

The validation of the numerical models allows further investigation in the form of a parametric study, as presented in Chapter 7. This will allow the determination of temperatures in various floor systems that could not be tested in the current thesis. The validated models will also assist in the planning process of the full-scale fire test, which will be conducted in the near future, by analysing potential challenges and critical temperatures.

3.3 Preparation of small-scale samples

The fire test samples were constructed in the structures laboratory workshop, situated at the Civil Engineering department of Stellenbosch University. A total of four samples, each with a different configuration, were tested to determine the temperature distribution through the specific floor sections. The samples represented only the bottom part of the larger sandwich floor system, which is situated below the cellular beams and the void. The bottom part, however, is a critical layer that protects the services situated within the void, such as cables and ducts. The insulation and integrity criteria are therefore crucial, since this bottom layer can prevent or reduce the possibility of fire spread from one floor to another.

The four samples comprised of a profiled steel sheet section with a layer of fibre-cement board (FCB) on top. Two of the samples had a single layer of ceiling board attached to the bottom, while the other two had no ceiling. The two samples without a ceiling board represent a worst-case scenario, in which the ceiling boards have detached in the event of a fire. The steel sheeting was therefore directly exposed to the severe heat from the furnace. The four sample configurations are shown in Figure 3.1, in the order of testing.

3.3.1 Materials

The following materials were used for the small-scale samples:

- 0.8 mm Voidcon VP50 steel decking;
- 9 mm Promatect-H calcium-silicate (CaSi) board, situated below the steel decking;
- 9 mm Nutec fibre-cement board (FCB), situated above the steel decking;
- 15 mm Gypsum - Firestop Rhinoboard, situated on the outer sides of the samples.

The Promatect-H CaSi-boards, which are used for the ceiling, were manufactured by Promat, who specialises in fire insulating material internationally. Their boards were provided

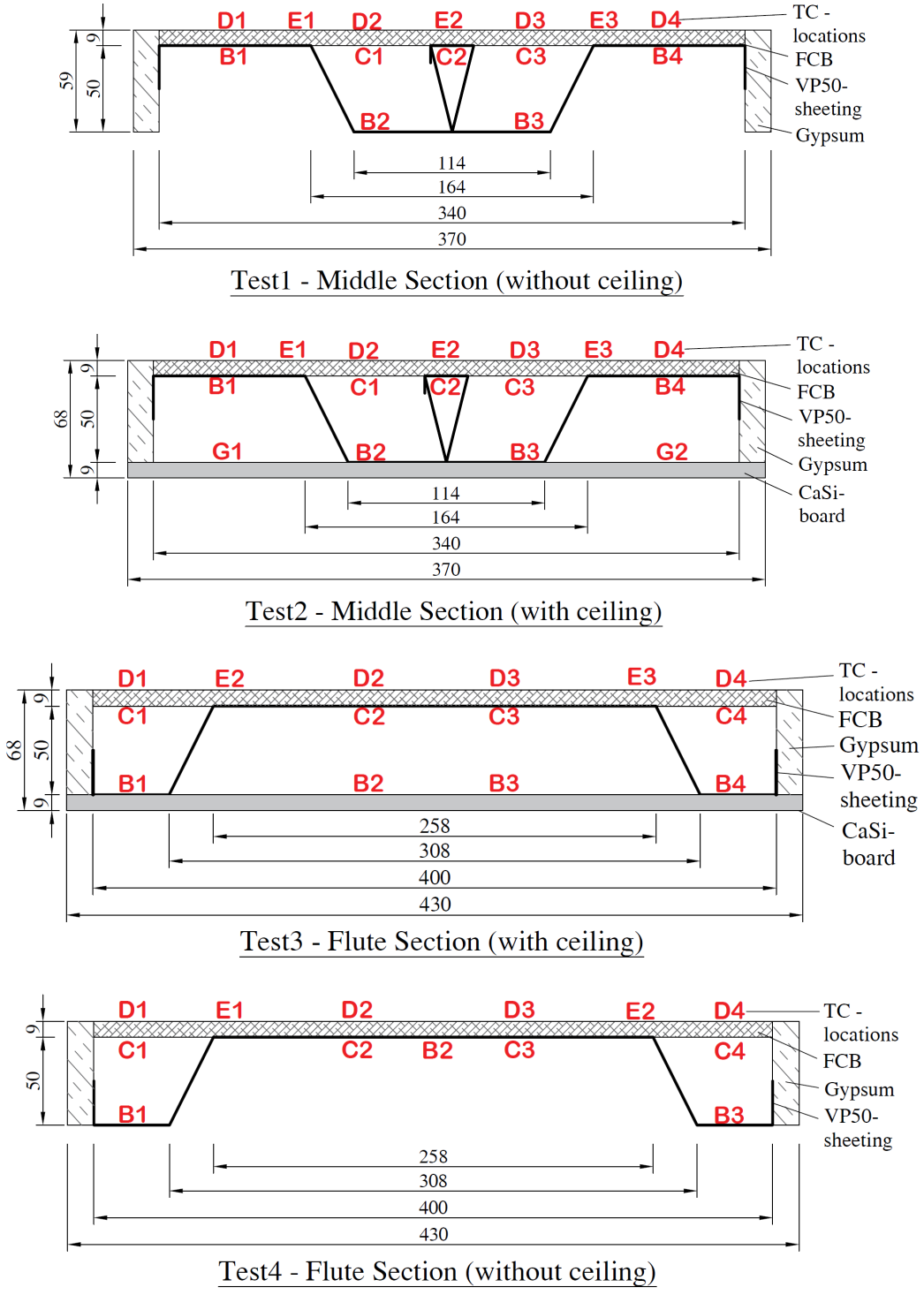

Figure 3.1: Configuration of test samples showing cross-sections with materials used and thermocouple (TC) locations

by Marley Building Systems, who is a supplier of cladding and various dry construction materials (Marley Building Systems, 2017). The ceiling system to be used in the cellular beam structure has not been finalised, or may vary from project to project. Hence, the aforementioned commonly available product with a suitable fire rating was utilised for this work. It is shown that the board specified does not provide the insulation requirement needed for the system, due to the initial thickness specified being insufficient. However, the benefit of using a thinner board in the experimental setup is that temperatures over

a much wider range are measured, thereby allowing for more calibration that would not have been possible using thicker boards.

The fibre-cement boards (FCB), used on top of the decking that form an access platform, were manufactured by Nutec (Everite, 2012*a*) and these boards come in a variety of sizes and thickness. Nutec's FCB has various benefits, such as low environmental impact, cost effectiveness, considerable tensile strength, fire- and acid-resistant and has good thermal properties (Everite, 2012*a*). The Rhinoboard Firestop, which is used to provide a fire-resistant sealant between boards, the ceiling and decking, was manufactured by Gyprock and includes glass fibre strands in the gypsum core (Gyprock, 2017). The steel decking was provided by Voidcon, who specialises in the manufacturing of composite suspended slab systems. The Voidcon decking profiles consist of an unique geometry, in which a triangular shaped overlapping of the edges of each decking panel occurs, as seen in Figure 3.1. These lightweight decking systems are cost-effective and provide high strength (Voidcon, 2014*b*).

All four samples were closed off with the gypsum on the sides, in a box-like manner, which prevented heat from within the sample from escaping out the sides. Figure 3.2 presents a three-dimensional (3D) view of the configuration for test-sample T3, as an example. Note that the front and back parts of the gypsum board box was left out to provide a clear view of the inner inner configuration. The other test samples had a similar configuration.

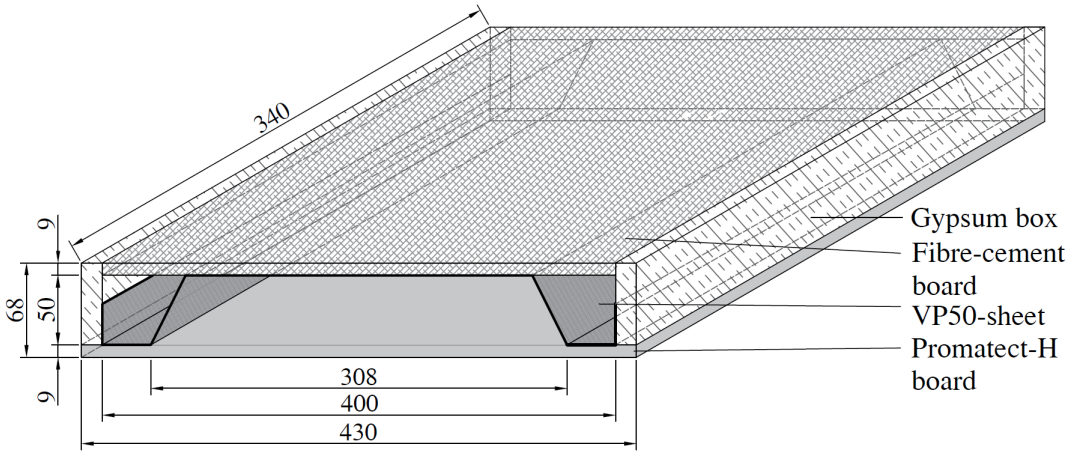

Figure 3.2: 3D configuration of test sample T3

3.3.2 Assembling test samples

The raw materials were provided in large sizes, which were 1200 x 2400 mm, 1200 x 2700 mm, 500 x 400 mm and about 400 x 3000 mm for the FCB, gypsum board, CaSi-board and the steel sheeting, respectively. Therefore, the necessary measurements were made and the materials were cut and shaped to produce the sample configurations, as depicted in Figure 3.1.

The Voidcon (VP) steel sheets that were provided comprised of flute sections with interlocking edges. These sections were cut at measured locations in the centre to produce two parts that can interlock with one another. This formed the VP middle sections for test samples T1 and T2, as shown in Figures 3.3a and 3.3b. The outer sides of these

sections were bent upwards for fixing purposes (refer to Figures 3.3c and 3.3d). The VP flute sections were bent in a similar manner and are shown in Figure 3.3e.

The insulation boards were cut according to their respective specifications, as shown in Figures 3.3f and 3.3g for the CaSi- and gypsum boards, respectively. The FCBs were also cut in this manner. Care was taken to ensure that the edges of the boards were level to create a flush finish on the sample assemblies. The gypsum boards were fitted around the steel sheets to form the box-shaped enclosure, as shown in Figure 3.3h. The FCBs were placed on top of the steel sheeting, as shown in Figure 3.4.

The type of screws used to fix the various materials to one another was a crucial part of the sample assemblies, due to the effect it has on the conduction of heat through the sample layers. Special self-drilling screws were used that cut through the steel sheeting, to which it could grip. These screws kept the insulation boards fixed to the sheeting. Flat heat screws, as seen in Figure 3.5a, were used to fix the CaSi-board ceiling to the VP steel sheeting in samples T2 and T3. This allowed a flat ceiling surface to be exposed to the high temperatures from below. Similar self-drilling screws, which had hexagonal heads, were used to fix the top FCB and side gypsum boards to the VP steel sheeting in the four test samples. Small steel brackets were specially made to keep the front and back gypsum board edges in place. Figure 3.5b presents an example of the hexagonal screws and the small steel brackets on the sample corner edges.

3.4 Furnace specifications

The fire testing was performed in a small-scale testing facility at the NES R&D Fire Test Department of NES Consult & Associates. Their testing facility incorporates a gas-fired oven (furnace), in which standard ISO 834 temperature-time tests are conducted in accordance with SABS (2005) (NES, 2017). The furnace allows for various small-scale test configurations, including both vertical (wall) and horizontal (ceiling) assemblies. The furnace consists of two gas burners, situated at the bottom of the furnace, by which heat was provided. NES (2017) uses the facility to develop rational designs for fire protection systems in terms of SABS (2011) specifications.

All of the tests that were performed in this thesis comprised of horizontal ceiling assemblies, which were exposed to the ISO 834 standard fire from below. The furnace configuration was specifically set up for the small-scale samples shown in Figure 3.1. The geometry of the small-scale samples was mainly governed by the limited size of the furnace, which allowed for maximum horizontal sample dimensions of about 500 x 400 mm (width x depth). The other crucial factor that had to be considered was the inner configuration of the furnace, which had an influence on the development of the standard fire. The configuration of the bottom part of the furnace was designed, constructed and calibrated by the research team at NES. This was done by placing fire bricks in a certain manner to guide and distribute the flow of heat, that exits the gas burners, through the bottom of the furnace and up towards the ceiling board of the test samples. Sufficient depth was provided to allow for an equal standard fire distribution that simulates a typical horizontal ceiling configuration exposed to a fire from below. This factor, along with the restricted geometry of the furnace, governed the allowable height of the test samples.

(a) VP mid section cut

(b) VP mid section bending lines

(c) Bending of section

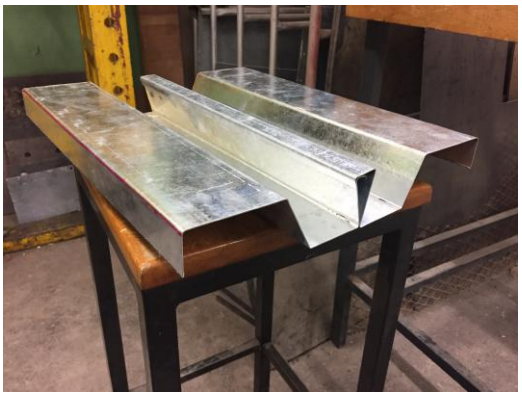

(d) VP mid section

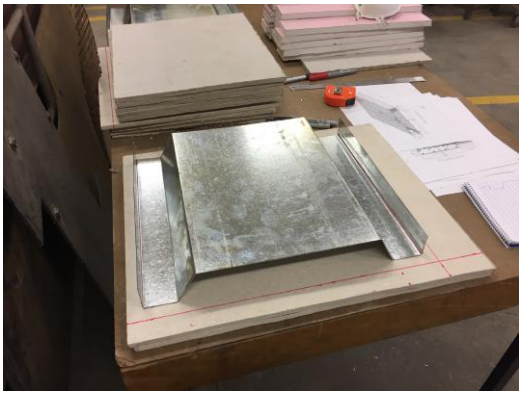

(e) VP flute section

(f) CaSi-board cutting

(g) Gypsum board cutting

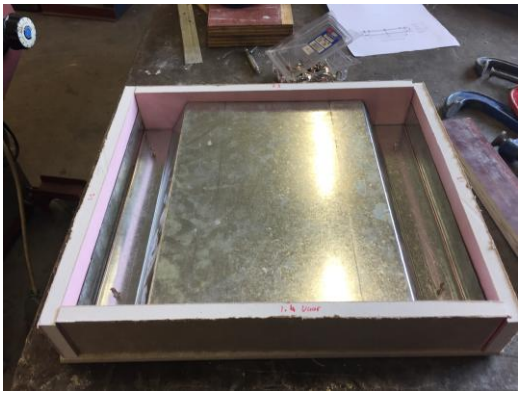

(h) Gypsum board box

Figure 3.3: Construction of test samples

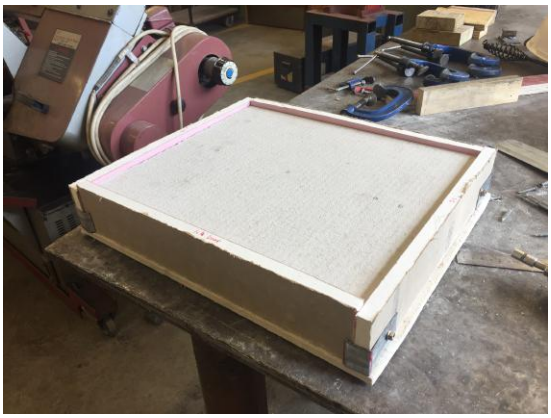

Figure 3.4: Finished assembly of test sample

(a) Screw used for fixing ceiling board

(b) Corner brackets and hexagonal screw

Figure 3.5: Fixing of insulation boards to the decking system of test samples

The test samples were situated on top of a vermiculite board, which was specifically constructed to fit inside the furnace walls. The vermiculite board had an opening of 300 x 300 mm for fire tests T1 and T2 (mid-sections) and 400 x 300 mm for tests samples T3 and T4 (flute-sections). The samples were placed so that the outer edges rested on the vermiculite board, with the opening in the middle of the sample. This allowed heat to be exposed to the bottom surface of the samples without directly exposing the bottom part of the gypsum board box. This also prevented any heat from escaping between the gypsum and vermiculite boards. Figure 3.6 presents a detailed configuration of the furnace setup.

Special fire-rated silicon was used to provide a firm bond between the sample edges and the vermiculite board. It was also used to seal any small gaps in the sample to prevent any heat from escaping. The sealants that were used are FR ASF Acrylic (Potecta, 2014), Promaseal-A (Promat, 2016) and Zwaluw Fire Sealant (Den Braven, 2017). Figure 3.7a indicates the application of the sealant to the bottom edges of the test sample. These sealants were also used to seal the screw heads on the exposed side of the test samples, as seen in Figure 3.7b.

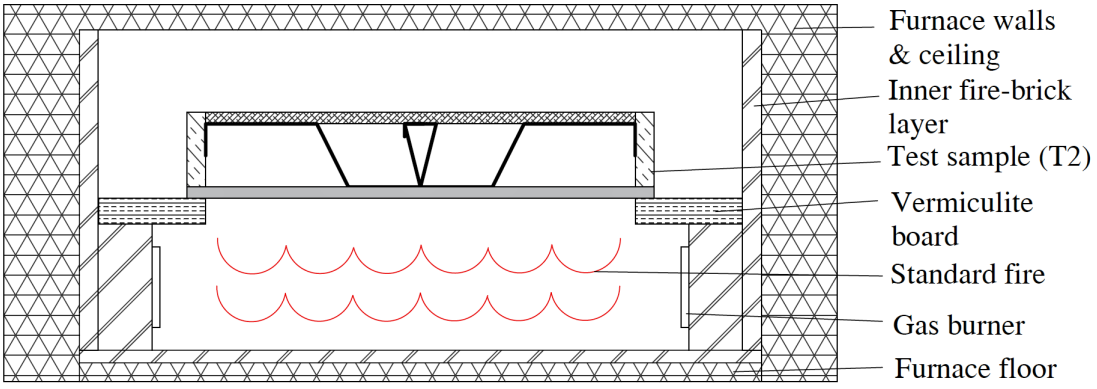

Figure 3.6: Small-scale test furnace setup with sample T2 as example

(a) Sealing of bottom edges (b) Sealing of exposed screws

Figure 3.7: Sealing bottom edges and screw heads of the test specimens

3.5 Instrumentation

Numerous types of temperature measuring devices are available in the industry, such as infrared (IR) sensors, thermometers, thermistors, resistor temperature detectors, semiconductors and the most commonly used thermocouple (TC) (Edgefx Technologies, 2017). Thermocouples were chosen for this experimental study, due to their relative cost- effectiveness and robustness (Edgefx Technologies, 2017). Thermocouples contains two dissimilar wires, by which a junction is formed at one end by fusing the two wires. A change in temperature in the sensor results in the generation of an electromotive force (EMF), which is measured in millivolts (Swift Heat, 2017).

Although all thermocouples work in a similar way, the specifications and applications of the different types could vary significantly. Due to its wide operating temperature range, Type-K thermocouples were used for measuring the temperatures in the fire tests. Type-K thermocouples can operate between temperatures of $0°C$ and $1350°C$ (Swift Heat, 2017).

The thermocouples used in the fire tests comprised of a stainless steel (316/SS) sheath

with a diameter of 4.5 mm. A 1.2 mm thick flat rectangular plate was connected to the end of the metal sheath, which allowed the thermocouples to be effectively fixed to any flat surface. A detailed layout of the plate thermocouple used in this thesis is presented in Figure B.1 in Appendix B. Various authors, such as Wickström (2010) and Sultan (2006), discussed the applicability and advantages of plate thermocouples, as opposed to the standard round tip thermocouples. Plate thermocouples have a larger area that measures both the convective and radiative heat transfer and is angled in the same direction as the surface being measured. This provides a more accurate representation of how the surface is heated, while an average temperature over the plate surface is measured.

Thermocouples were placed at the crucial surfaces within the test samples and on top of the FCB, which is referred to as the cold-face. The thermocouples were placed symmetrically on both sides across the width of the samples to account for the possibility of thermocouple failure and unequal heat distribution. The thermocouple locations for each sample are shown in Figure 3.1, as introduced in Section 3.3. The temperatures obtained at these specific locations are discussed in Chapter 4. The thermocouples were fixed at their specific locations by using screws and in some cases small bolts, as shown in Figure 3.8a. Holes were drilled through the front gypsum panel for the thermocouples that measured the inner sample temperatures. Some examples of how the thermocouple were fixed are shown in Figure 3.8.

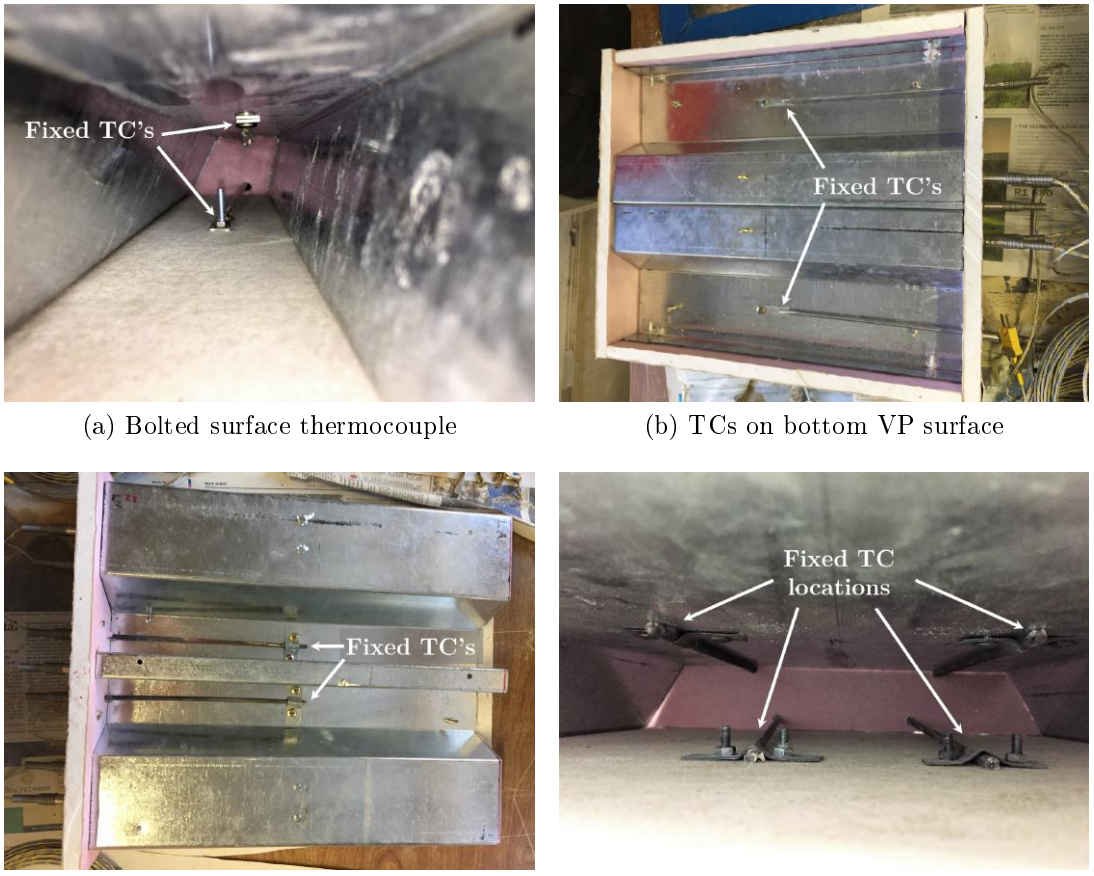

(a) Bolted surface thermocouple

(b) TCs on bottom VP surface

(c) Inner TCs fixed with brackets

(d) Top and bottom core TCs in T3

Figure 3.8: Thermocouple (TC) fixities for various locations

Four thermocouples were used to measure the gas temperature inside the furnace for monitoring the temperature and adjusting the gas supply accordingly. These were situated over the width and depth of the furnace to obtain an average furnace temperature. Three additional thermocouples were used to measure the temperatures of the surrounding environment. Two of these were located 10 mm above the top FCB surface and the other one was located at the ventilation opening, as shown in Figure 3.9.

(a) Top ambient thermocouples (b) Thermocouple at ventilation opening

Figure 3.9: Ambient thermocouple locations to measure temperature outside of the test specimens and furnace

The thermocouples were connected to a total of six Center-378 Data Logger thermometers, each having 4 input channels. These battery-operated data-loggers are compatible with a wide range of thermocouples and has a measurement range of $-200°C$ to about $1372°C$. They also have an accuracy of $0.1\%rdg + 0.7°C$ (Center, 2013). The interval, or refresh rate, of each data-logger was set to 2 seconds. Therefore, a temperature measurement was recorded every two seconds. This resulted in accurate measurements and the ability to measure any small temperature fluctuations within the test samples.

After the thermocouples were connected to their respective locations, the fire-rated sealant was applied to any gap on the edges of the test samples. Figure 3.10a shows the thermocouples fixed in place, and how the edge of the FCB were sealed to prevent any heat from escaping the samples. Each thermocouple was tagged and connected to a specific port of a data-logger to keep track of each thermocouple location and the corresponding temperature measurement. Figure 3.10b shows an example of the tagged thermocouples connected to the respective data-loggers.

3.6 Testing procedures

Before the fire tests were conducted the furnace had to be calibrated, due to the unique setup and geometry. This was done to ensure that the fire curve within the furnace resembled the ISO 834 standard fire curve as closely as possible. The temperature within the furnace was regulated by manually adjusting the amount of gas released into the furnace through the gas burners. The furnace was calibrated by using a flat steel plate with three thermocouples placed in a triangular shape in the centre. The average temperature of the plate was obtained from the thermocouples, while the plate was heated from below. The

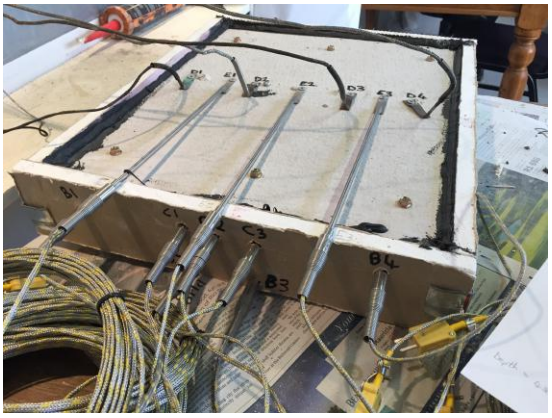

(a) Sealed sample with connected TCs

(b) TC and data-logger tags

Figure 3.10: Top thermocouples and data-logger tags for samples tested

gas regulators were adjusted in such a way that the recorded temperatures matched the standard fire curve. The specific regulator settings that resulted in an accurate representation of the standard fire curve were recorded. These were used as a guideline during the fire tests. Figure 3.11 presents the overall test setup, which includes the sample within the furnace, the thermocouples and the data-loggers, as well as the workstation where the manual readings and observations were recorded.

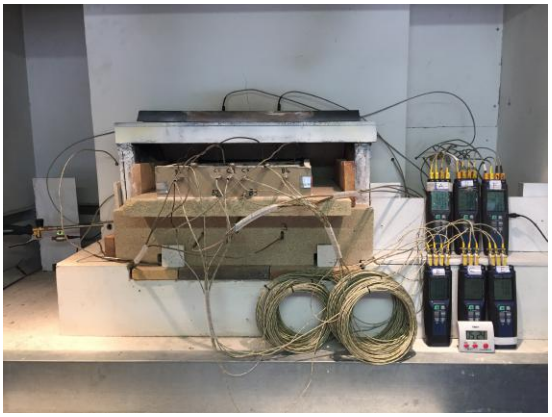

(a) Sample and instrumentation setup

(b) Testing facility layout

Figure 3.11: Testing procedures

After the fire was ignited at the start of each test, a short period of time was given for the furnace to heat up. This was done to overcome the lag in temperature rise at the start. To represent the standard fire curve, a rapid temperature rise is needed. After about 30 seconds, the data-loggers were set to start recording.

The inner furnace temperatures were manually read off from the data-loggers every minute to ensure that it followed the standard fire curve closely as possible. Upper and lower limits were applied, between which the furnace temperature had to be maintained. These were specified as 15% for the first 5 minutes, 10% for between 5 and 7 minutes and 5% for the rest of the test duration. The gas regulators were adjusted accordingly, either up

if the temperatures were too low, or down if the temperatures in the furnace were too high.

Two small ventilation openings were situated at the front of the furnace in the vermiculite board, as depicted in Figure 3.12. The openings were controlled by two square-shaped Magnesium Oxide (MgO) board blocks. The ventilation openings were used together with the adjustment of the gas regulators, to control the temperature within the furnace. All of the ventilation and gas regulator settings were recorded after each adjustment. The temperatures that were read off from the data-loggers each minute were recorded in an Excel spreadsheet as a backup in the case of an emergency, such as power failure. The temperatures on the hot face and the cold face of the test samples were also recorded every 10 minutes, along with the furnace temperature.

Figure 3.12: Ventilation openings

The test samples were carefully monitored, in between the regulation of the furnace temperature and manual data collection. These included visual observations, such as cracks, steam and external flames, as well as auditory observations. The external thermocouples and data-loggers were also monitored to ensure that the measured temperatures were accurately recorded.

At the end of each fire test, the gas burners were switched off and the furnace was left to cool down. After the samples cooled down, they were disassembled to remove the thermocouples, which were used in the next fire test. The furnace was cleaned and set up for the next test sample. The data-loggers were also disconnected from the sample and connected to the computer, from which the temperature data was downloaded and saved for further analyses.

3.7 Conclusion

This chapter discussed the experimental setup of the fire tests that were used for validation purposes. A total of four fire tests were conducted, in which each sample was exposed to a 60-minute standard fire. The aim was to test the bottom layers of the sandwich floor system to determine how heat is transferred through the floor layers and the air cavities.

The preparation of the test samples was discussed and the various material layers was defined, along with the corresponding thermal properties. The materials included the 9

mm Promatect-H CaSi ceiling board, the 0.8 mm Voidcon VP50 steel sheeting, a 9 mm FCB on top and 15 mm gypsum board strips that enclosed the test sample. The sample configurations are presented in Figure 3.1. A detailed discussion on the sample assemblies was also included.

The four horizontal (ceiling) fire tests were conducted at the NES R&D fire testing facility in a gas-fired furnace. The furnace is approximately 500 mm wide and 400 mm deep. The temperature within the furnace was regulated with four thermocouples to ensure that the ISO 834 fire curve was followed accurately.

Type K plate thermocouples were used to measure the temperatures at various locations within the test samples. The thermocouples were fixed with screws and bolts, in order to secure a tight connection and to allow good contact between the thermocouples and the measured surfaces. Between six and seven thermocouples measured the unexposed side of the test samples, while the rest were located in the upper and lower stud sections, as well as in the core sections.

The temperature data was recorded with a total of six data loggers, from which the data was obtained for further analysis. During the fire tests, readings were also recorded manually every minute, in case of power failure, etc. The temperature within the furnace was regulated continuously by adjusting the gas regulators and the ventilation openings, which was situated in front of the furnace. Observations were made during the tests to document any relevant occurrences.

Chapter 4

Discussion of experimental results

4.1 Introduction to experimental results

The results obtained from the experimental investigation carried out in Chapter 3 are presented and discussed in this chapter. The temperatures that were measured at the specific thermocouple locations are presented for the four test samples. This section also provides an overview of the thermal behaviour of the test samples, which are described in terms of the fire resistance failure criteria. Observations that were made during testing are also included in this section.

4.2 Temperature results from fire tests

After each test the temperature data was retrieved from the data-loggers. The temperature history from each thermocouple was exported and saved in respective MS Excel spreadsheets. The data was analysed to determine the temperature development through the respective samples. Various temperature points on each sample were grouped together into separate sections, in order to present the overall thermal behaviour of each sample.

The average furnace temperature calculated is based on the temperatures from the four thermocouples that were situated in the furnace, which were denoted as A1, A2, A3 and A4, respectively. The average furnace temperatures of each test were compared to the standard fire curve to determine whether the samples were exposed to an accurate representation of a standard fire. The combined sections of thermocouple locations are shown in Table 4.1 for samples T1 and T2 and in Table 4.2 for sample T3 and T4. Samples T1 and T4 had no thermocouples on the core bottom, due to the absence of a ceiling board.

Although the test samples were used to validate the Finite Element (FE) models, the fire resistance criteria were also determined. The insulation criteria for each sample was defined by limiting the average unexposed surface temperature, referred to as the cold face (CF) temperature, to $160°C$. This included the assumed ambient temperature of $20°C$. The integrity of the insulation materials was visually inspected, whereby cracks were identified in various parts of the samples.

It should be noted that the specific setup and conditions of the fire tests were different to the configuration of the full-scale structure. Therefore, the thermal performance is only applicable to the specific configuration of the small-scale samples. Different dimensions

Table 4.1: Thermocouple location grouping for Test 1 & 2

TC location description for VP50 middle section		
Location	Sample T1	Sample T2
Bottom core	N/A	G1, G2
Top core	B1, B4	B1, B4
Bottom stud	B2, B3	B2, B3
Top stud	C1-C3	C1-C3
CF on stud	E1-E3, D2, D3	E1-E3, D2, D3
CF off stud	D1, D4	D1, D4

Table 4.2: Thermocouple location grouping for Test 3 & 4

TC location description for VP50 flute section		
Location	Sample T3	Sample T4
Bottom core	B2, B3	N/A
Bottom stud	B1, B4	B1, B3
Top inside	C1-C4	C1-C4, B2
CF on stud	E2,E3, D2, D3	E1,E2, D2, D3
CF off stud	D1, D4	D1, D4

and layouts would result in different thermal behaviour. However, the general thermal behaviour provides an understanding of similar configurations that also include voids between a steel decking system, such that it can be used for validating numerical models in the following chapter. These models are then applied to the entire structural system.

4.2.1 Test 1 - Middle VP section without ceiling

The middle VP50 steel section, which contains the stud with the interlocking triangle in the middle, was tested in sample T1. Figure 4.1 presents the sample configuration and the thermocouple locations where temperatures were measured.

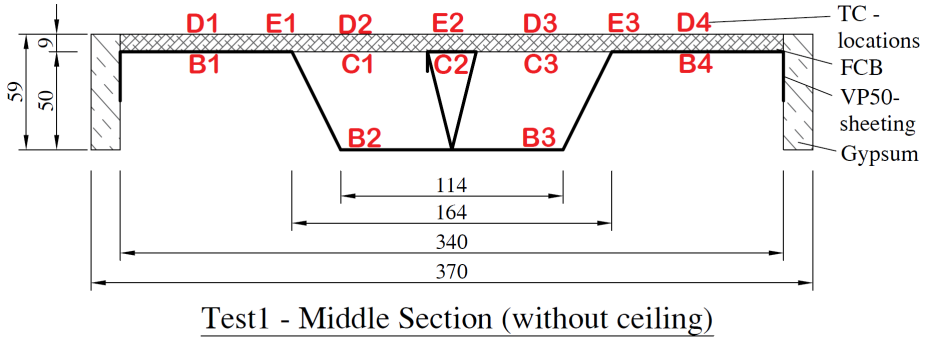

Figure 4.1: Thermocouple locations for test sample T1

The measured temperatures for test sample T1 are presented in Figure 4.2. It can be seen that the standard fire curve was followed relatively closely. Although the furnace temperature was a bit lower between 2 and 5 minutes, it was still higher than the lower

limit. The exposed temperature remained between the upper and lower limits throughout the full duration of the test.

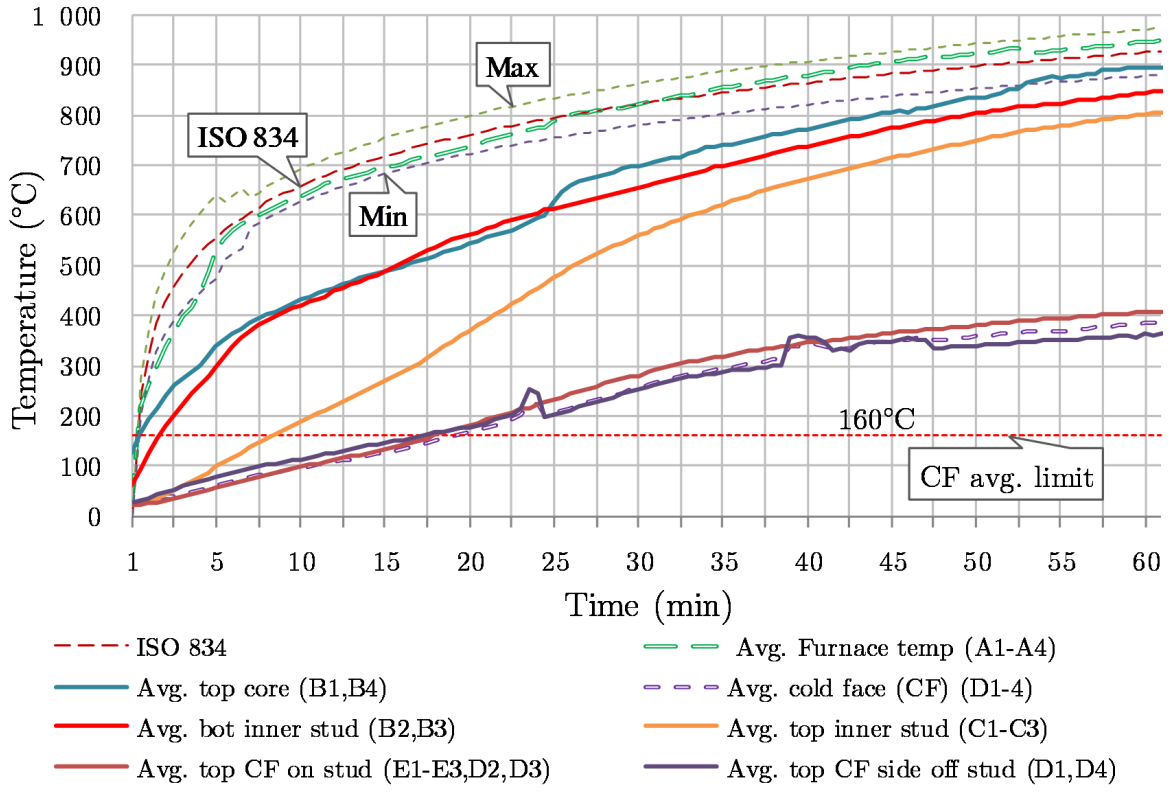

Figure 4.2: Temperatures from Test 1

The thermocouples located at B1 and B4 were directly exposed to the hot furnace gas and therefore resulted in the highest temperature. However, thermocouples B2 and B3 resulted in similar temperatures, even though they were shielded by the VP steel sheeting. This is due to the very thin steel section that has a high conductivity. However, the VP sheeting did shield most of the radiative and convective heat transfer from the furnace fire to the inner stud locations. This is evident in the relatively lower temperatures of the top inner stud section of the sample, denoted by C1-C3, when compared to the steel temperatures. However, as the steel temperature increased, the radiation from the decking to the other components within the sample cavities became more important. This resulted in high temperatures within the stud section at the end of 60 minutes, as shown in Figure 4.2.

After a duration of about 10 minutes, steam started to become visible from the top of the FCB, as seen in Figure 4.3a. This was the moisture from the gypsum boards that evaporated, through which heat was released into the surrounding environment. When water evaporates it reduces the rate of heat rise in a specimen as energy is consumed in the phase change process. Smoke became visible after 25 minutes of exposure. At this stage the temperatures in the gypsum boards were high enough for the paper on its sides to char and produce smoke. As this happened the gypsum board paper turned brown from the bottom upwards, as seen in Figure 4.3b.

The thermocouple located at the left-hand side on the cold face (D1) failed after about 23 minutes. The effect of this can be seen by the spikes on the graph for the average outer

(a) Steam from gypsum boards (b) Charring of outer gypsum paper

Figure 4.3: Observations during Test 1

cold face temperature, which was determined from thermocouples D1, D2, D3 and D4. From the graph it can be seen that the average allowable temperature on the unexposed surface (CF), as specified in SANS 10400-T (SABS, 2011), was surpassed at about 20 minutes. The sample therefore failed the insulation criteria.

The steel temperature was taken as the average between the thermocouples that were situated directly on the steel sheeting. These were thermocouples B1 to B4, which were located in the top core and bottom stud sections of sample T1, as shown in Table 4.1. The steel temperature increased rapidly to approximately $420°C$ within the first ten minutes of the test. This is also the melting temperature of the galvanizing on the steel sheeting (Hamerlinck, 1991). Hence, it can be assumed that the galvanizing started to melt after 10 minutes into the fire test.

It was noted during the test that the VP steel sheeting started to expand and caused an upward bowing-effect, which can be seen in Figure 4.4a. For a temperature of 850 degC and a length of 430 mm the expansion of steelwork would be 5 mm, based on the simplified thermal expansion coefficient of 1.4×10^{-5}, as discussed in Section 2.7.2. This could not be accommodated in the frame and resulted in the top FCB cracking in the middle across the whole width of the sample, as shown in Figure 4.4b. The cracking sounds could be heard during the fire test. Note that the gypsum boards on the sides were also cracked at a similar position, as shown for that of the FCB, due to the thermal bowing of the steel.

It is clear from the images that the crack occurred in the line of the thermocouple fixing screws. The screws weakened the FCB, due to the concentration of holes over the relatively small surface area. Therefore, the FCB cracked more readily when the steel started to expand. However, in the case of a real structure, there would be no extra fixities that could further weaken the FCB, although this does highlight that fixing details may need to be carefully considered. Figure 4.5 presents the result from fire test T1, which indicates the exposed steel surface.

Unfortunately, most of the plate thermocouples were damaged in the fire test of sample T1. The plates that were used for fixing purposes melted off during the fire test, which may have had an effect on the temperature results. However, it seems that there was no sudden jump (increase) or drop (decrease) in the measured temperatures from these

(a) Thermal bowing (b) Cracked FCB

Figure 4.4: Integrity failure of sample T1

(a) Exposed VP50 sheeting (b) Damaged insulation boards

Figure 4.5: Aftermath of test T1 indicating discoloured sheet and charred sides

thermocouples. The only irregularities ("spikes") were those caused by the faulty thermocouple (D1) on the unexposed surface. The wrong weld material was used during the manufacturing of the thermocouples, which was acknowledged by the manufacturer after the test. For the tests that followed, special brackets were made from steel sheeting strips to fix the thermocouples to their specific locations. The thermal properties of the steel strips were similar to those of the thermocouple material (stainless steel), hence it had a negligible influence on the temperature readings. The thermocouples were fixed in such a way that the tip of the thermocouple, where the measurement is taken, made good contact with the specific surface. This ensured accurate temperature readings.

4.2.2 Test 2 - Middle VP section with ceiling

Test sample T2 had a similar configuration to sample T1, with the only difference being the Promatect-H (CaSi) ceiling board. Two additional thermocouples (G1 and G2) were installed in the sample to measure the average temperature on the unexposed side of the ceiling board, as depicted in Figure 4.6.

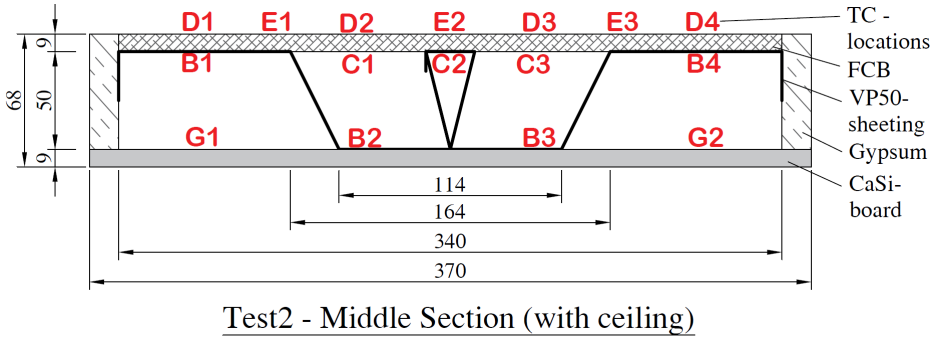

Figure 4.6: Thermocouple locations for test sample T2

Similar testing procedures were performed for the four tests, as described in Section 3.6. This included the adjustment of the gas regulator and ventilation openings. The sealant was applied to the edges of the ceiling surface to prevent heat from escaping, as can be seen in Figure 4.7. The thermocouple arrangement can also be seen in this figure. Note that there was no thermocouple placed at location D1, due to the failure in the previous test. Therefore, only the temperature at D4 was used in further analyses for that location.

Figure 4.7: Test sample T2 placement and TC arrangement

The temperature development through sample T2, as measured at the specified thermocouple locations, is presented in Figure 4.8. It can be seen that an accurate representation of the standard fire curve was maintained over the full duration of the fire test T2. By comparing the results for test samples 1 and 2, it is clear that the 9 mm CaSi-board made a considerable difference in the temperature development through the sample layers. The temperatures in sample T1 were roughly twice as high as those in sample T2.

The steel temperatures were obtained from the upper core and bottom stud sections of test sample T2. Figure 4.8 shows that the steel temperatures at the bottom stud were higher than that of the top core. This was due to the direct contact between the steel at the bottom of the stud section and the ceiling board, through which heat was conducted. It was noted that the temperature directly on top of the CaSi- ceiling board was higher than those of the bottom stud. Although both of these locations are on the same level within the sample, the thermocouples on the bottom stud were protected by the thin steel sheeting.

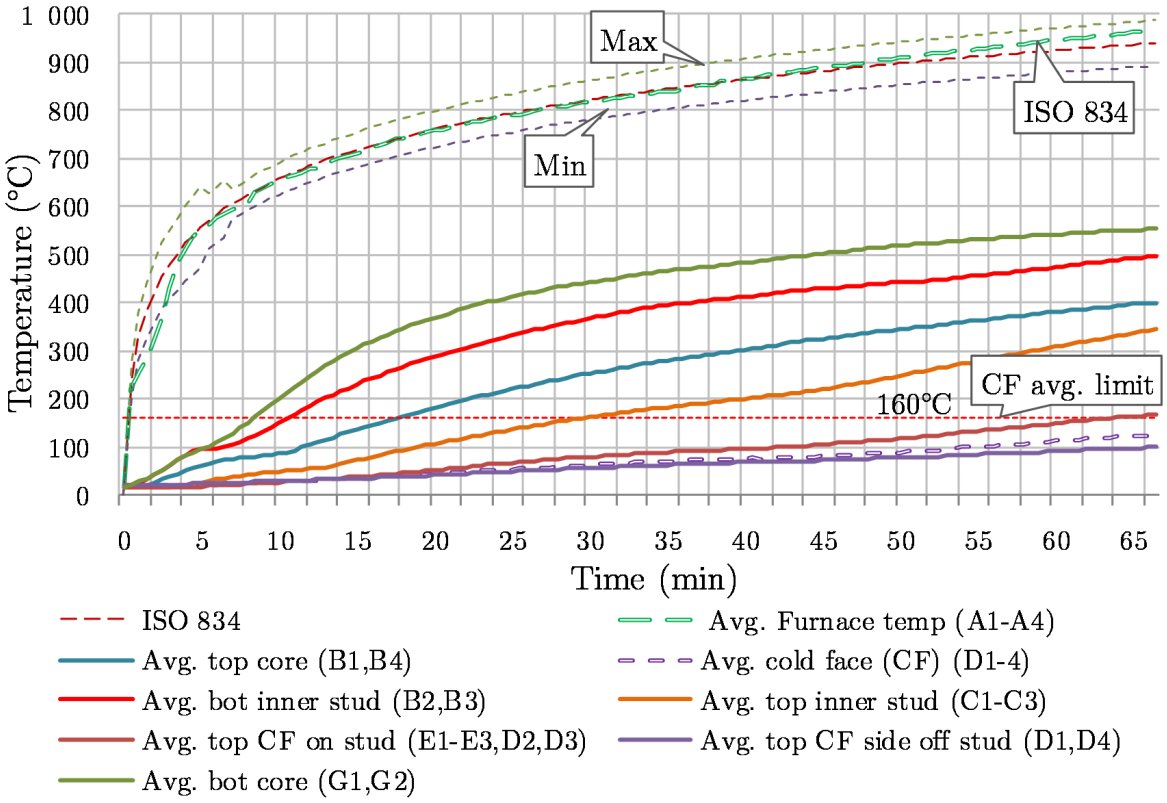

Figure 4.8: Fire test 2 results

The unexposed surface, which is the top of the FCB, performed significantly better than sample T1. The average temperatures on the cold face (CF) did not reach the insulation criteria limit of 160°C until 64 minutes. The ceiling board effectively protected the upper sections of the test sample against the hot radiative and convective heat fluxes from the furnace.

Figure 4.9a presents the overall setup of test sample T2 with the connected thermocouples and data-loggers. During the test of sample T2, similar behaviour of the gypsum boards was observed as discussed previously for test sample T1. These observations included steam, due to the evaporation of the moisture within the gypsum boards, as well as some flames at the back of the test sample, as seen in Figure 4.9b. The flames were a result of the outer gypsum paper igniting, due to the high temperature at the back of the furnace. The test sample for Test 2 performed relatively well, as no major damaged was caused to the insulation boards. From Figure 4.10a it can be seen that no large cracks were present in the CaSi- ceiling board, which were directly exposed to the severe furnace fire. However, few small cracks, which cannot be easily seen with the naked eye, appeared across the width of the ceiling board, as depicted in Figure 4.10b on the unexposed side of the ceiling board. The stain marks from the heated VP steel sheeting, which was caused due to the melting of the galvanizing, can also be noted in this figure.

The galvanizing on the steel sheeting melted, due to the increase in temperature in the steel, as shown in Figure 4.11a. From this image, it can be seen that the back of the test sample was exposed to higher temperatures. This could possibly be due to the sample being a bit too long for the available furnace depth, or due to an uneven fire temperature distribution within the furnace. This will be discussed further in Section 5.3.4. The steel

(a) Sample T2 setup (b) Ignition of back gypsum paper

Figure 4.9: Observations during Test 2

(a) Exposed side of CaSi-boad (b) Unexposed side of CaSi-board

Figure 4.10: Test sample T2 ceiling board

temperature at the bottom stud (B2 and B3) and the top core (B1 and B4) were measured as 380°C and 475°C, respectively, at the end of the test, which are just below and just above the melting temperature of galvanizing. The FCB on the unexposed side of the sample remained intact with no major cracks, as shown in Figure 4.11b. Therefore, it can be assumed that the VP steel sheeting did not expand significantly during the fire test.

(a) Melted galvanised sheeting (b) Unexposed insulation boards

Figure 4.11: VP steel sheet and FCB conditions after testing sample T2

4.2.3 Test 3 - Flute VP section with ceiling

The sample that was tested in Test 3 consisted of the flute section of the Voidcon VP50 steel profile. No stud was present in these sections. However, a larger (wider) cavity was present in the middle part of the sample. It was expected that the thermal behaviour for this specific configuration will differ from that of test samples T1 and T2, due to the lack of radiative heat transfer shielding effects. Various factors could influence this, such as the different steel geometry that could lead to different conductive heat transfer behaviour. Also, cavity radiation is crucial in test sample T3, due to the reduced influence of the troughs providing a shielding mechanism, such as the stud section in test samples T1 and T2. The configuration and thermocouple locations are shown in Figure 4.12.

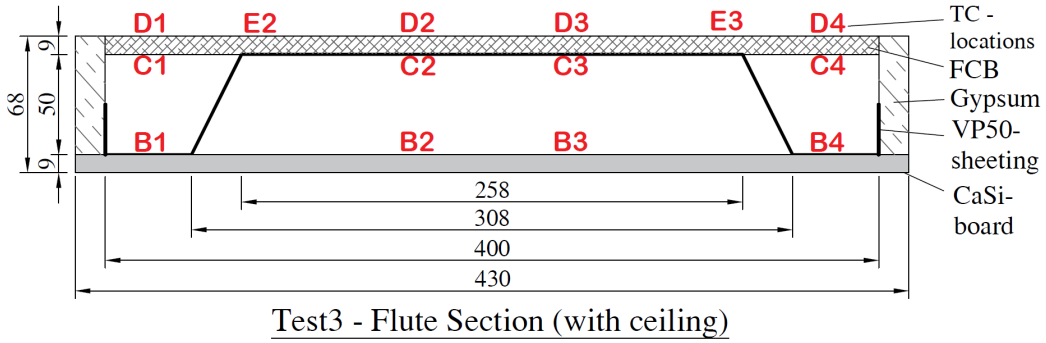

Figure 4.12: Thermocouple locations for test sample T3

The temperature results obtained from test sample T3 are shown in Figure 4.13. The average furnace temperature followed the standard fire curve with minimal deviation up to about 16 minutes, after which a drop occurred, although results were still within the required tolerance range, which were specified as 5% below the standard fire curve. It should be noted that the actual furnace temperatures are used for FE modelling in the following chapter so such a drop does not significantly affect overall predicted results. After adjusting the gas regulator and ventilation of the furnace, the furnace temperature increased to follow the standard fire curve for the rest of the test duration.

The thermal performance of the Promatect-H (CaSi) ceiling board in sample T3 was relatively similar to that of sample T2. The difference between the bottom core temperature of these two test samples were only about $45°C$ at the end of 60 minutes, which were measured at locations G1 and G2 for sample T2 and B2 and B3 for sample T3. The ceiling board temperature in test sample T3 increased more rapidly than in sample T2, by approximately 20 to 30% within the first 20 minutes, as seen in Figure 4.13. This was due to the positioning of the thermocouples, which were located in the middle of test sample T3 where the intensity of the heat was higher, as compared to the outer sides of the test sample. The 20 to 30% lower temperature in the ceiling board for test sample T2 could also be due to the to the specific geometry of the VP sheeting. In test sample T2 the middle stud section shielded some of the radiation within the cavities. In the case of test sample T3, less steel was present in the cavity that could shield the surrounding layers from the cavity radiation.

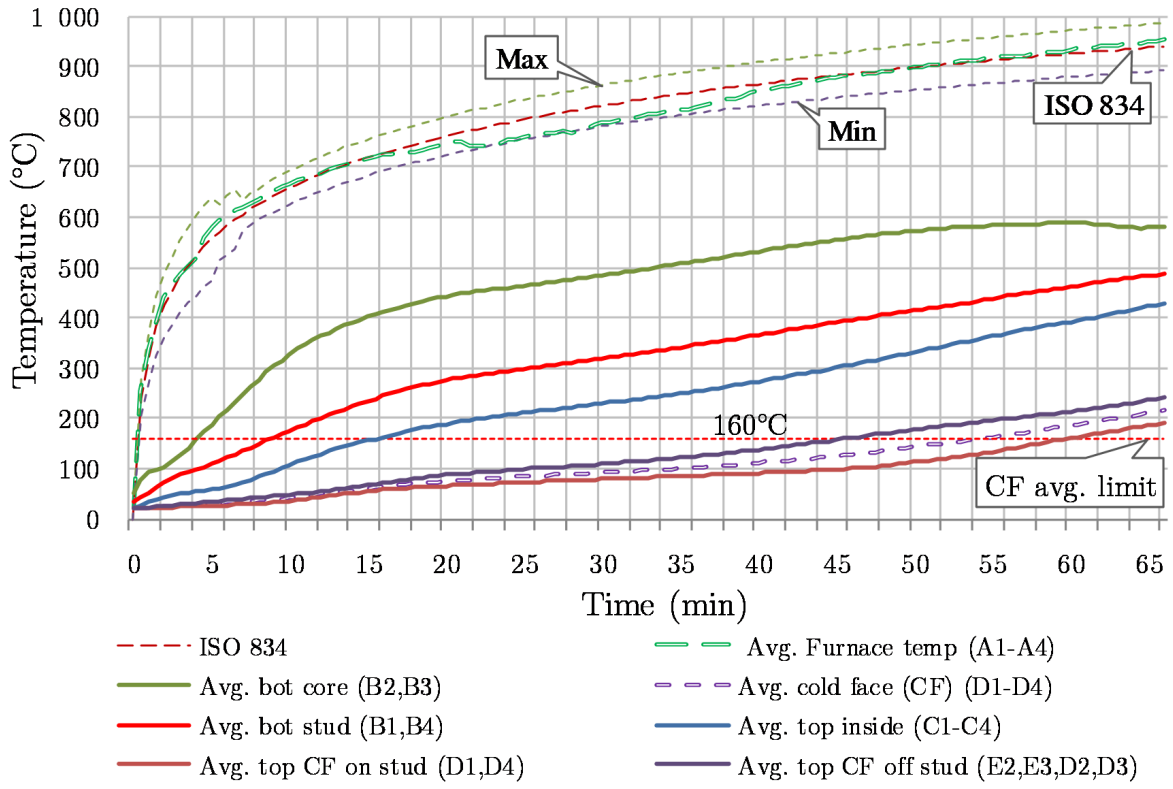

Figure 4.13: Temperatures obtained from Test 3

Although test sample T2 consisted of a higher concentration of steel in the middle of the sample, it was found that the temperatures obtained for the unexposed surface on top of the FCB (D1 to D4) was approximately 40% lower than for sample T3. From Figure 4.13 it can be seen that the insulation temperature limit was surpassed by the temperatures obtained on the cold face (CF) of sample T3 at about 52 minutes. The CF temperatures for sample T2 were less than the 160°C limit throughout the full duration of the 60-minute test. It is therefore evident that the radiation within the cavity is the governing heat transfer mechanism and that the conduction of heat through the steel in the stud section has a lower influence in comparison to the cavity radiation.

The increase in the average steel temperatures obtained in sample T3 was approximately 14% lower than for sample T2 for the first 30 minutes of the test duration. This was due to a similar reason as explained above in terms of the distribution of the furnace intensity. The bottom stud steel section was positioned on the outer sides of sample T3 (locations B1 and B4), which is where the furnace intensity is lower, as compared to the middle of the sample (locations B2 and B3 in sample T2). However, the average steel temperature of the two test samples, T2 and T3, were similar towards the end of the 60 minutes, with a difference of only 3%. For the first 30 minutes of the test, the average steel temperature in the core of sample T3 was approximately 10% lower than for sample T2. This is a result of the CaSi- ceiling board and the small air void that acts as a protecting insulation layer beneath the steel on the top of the core section. However, as the temperature increased in the sample, the cavity radiation became more dominant, which resulted in a 10°C higher temperature for test sample T3, relative to sample T2. This again shows the effect of cavity radiation and the shielding effect of the stud section in sample T2.

Observations that were made during the testing of sample T3 included the discolouring of the outer gypsum paper and the sealant on the bottom edges of the sample, as shown in Figure 4.14a. These outer sections turned brown as the temperatures increased through the sample. A small amount of charring was also visible at the back of the test sample, which can be seen in Figure 4.14b.

(a) Discolouring of sample edges (b) Charring of gypsum paper

Figure 4.14: Test 3 observations

It was observed that the steel section in test sample T3 did not expand by a significant amount, which is consistent with the 2 mm expansion expected for a steel length of 340 mm at 60 minutes, based on the steel temperature of $461°C$, as determined from the simplified expansion coefficient discussed in Section 2.7.2. Cracking sounds were heard only after about 52 minutes. From Figure 4.15a it can be seen that small cracks appeared on the exposed side of the ceiling board, where the major crack spanned across the full width of the sample. No cracks were visible on the unexposed surface of the FCB during testing. However, a small crack was noted on the underside of the FCB after the sample was taken out of the furnace, as shown in Figure 4.15b. From the images in Figure 4.15 it can also be noted that the gypsum boards were damaged. The gypsum boards became more brittle as the moisture evaporated due to the heat increase through the sample.

(a) Exposed ceiling board cracks (b) Damaged insulation boards

Figure 4.15: Test 3 aftermath

4.2.4 Test 4 - Flute VP section without ceiling

Test sample T4 had a similar configuration compared to sample T3, but in this case the ceiling board was neglected. The steel sheeting was therefore directly exposed to the fire. The configuration and thermocouple locations are shown in Figure 4.16. The middle part of the flute section only consisted of the thin layer of steel with the 9 mm FCB on top that provided resistance to the hot gases from below. Therefore, the temperature increase on the unexposed side of the sample was primarily due to conduction.

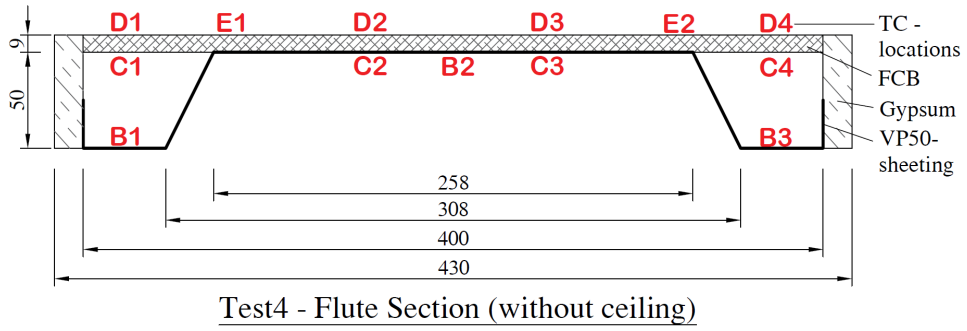

Figure 4.16: Thermocouple locations for test sample T4

The temperatures for sample T4 are shown in Figure 4.17. The effect of the ceiling board can clearly be seen when comparing the results from samples T3 and T4. In general, the absence of the ceiling board (sample T4) yielded between 40 and 65% higher temperatures than for the sample with a ceiling board (sample T3). The temperatures variation between samples T3 and T4 are similar to that of samples T1 and T2, illustrating relatively consistent furnace behaviour, although this is discussed further below.

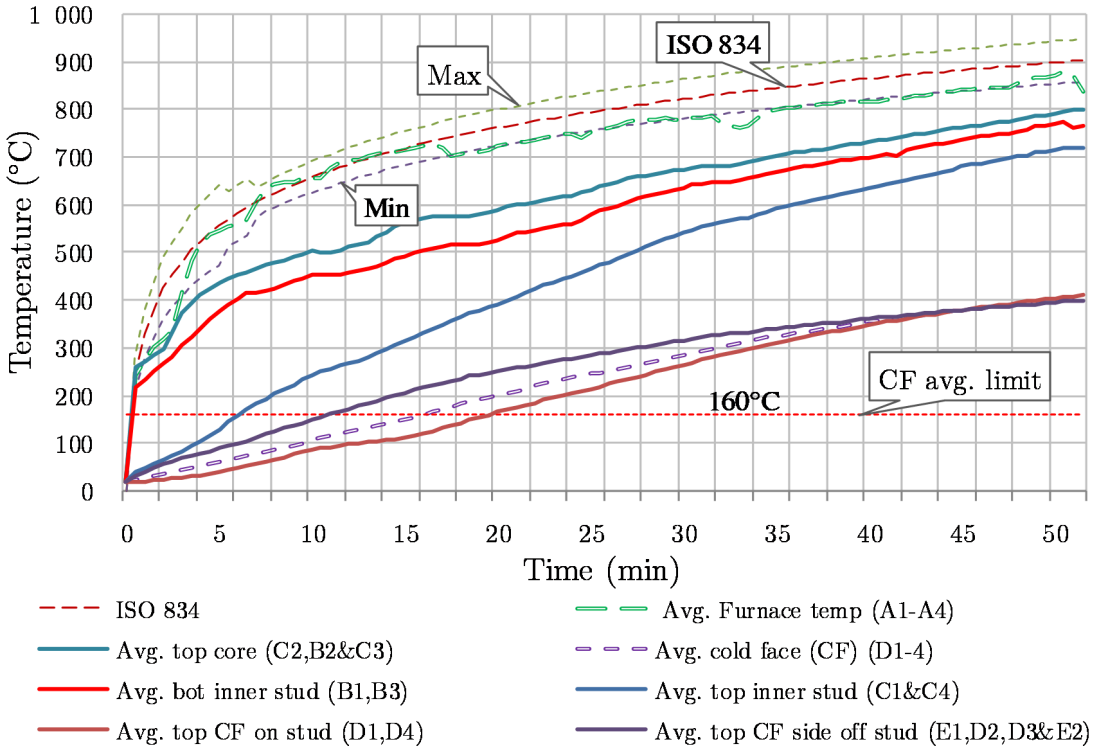

Figure 4.17: Temperatures from Test 4

The average furnace temperature during the testing of sample T4 did experience fluctuations and dropped below the required minimum tolerance between the first 2 to 4 minutes and then again at about 33 minutes, as shown in Figure 4.17. It can be seen that the furnace temperature bordered the minimum curve between 18 and 46 minutes. This may have resulted due to problems related to the control of the gas regulators. Another possible explanation could be that the gas containers providing fuel to the burners were nearly empty, which caused a reduction in the pressure at which the gas is released. However, as discussed above, the actual fire temperatures have been used to calibrate numerical models in the next chapter, so this variation will be accounted for.

The temperature on the exposed steel sheeting increased rapidly, both at the top core section (C2, B2 & C3) and the bottom inner stud sections (B1, B3). A steel temperature of approximately $400°C$ was reached within the first 7 minutes of testing, as seen on Figure 4.17. The small difference between the two sections is due to the thin steel layer of the VP sheeting, which shielded most of the radiative and convective heat transfer from the furnace. The test was stopped just after 50 minutes, due to the risk of damaging the thermocouples that were directly exposed to the furnace fire, as temperatures in excess of $800°C$ were recorded at the top core section.

The insulation board on the unexposed side of the sample failed within the first 15 minutes in terms of the insulation criteria, as shown on Figure 4.17. The rapid increase in the steel temperature heated the top FCB through conduction in the middle part of the sample. The steel stud sections on the outer sides of the sample radiated heat across the small cavities, which heated the top FCB.

Steam from the outer gypsum boards was observed very early in the test, as shown in Figure 4.18a. Smoke and charring of the gypsum boards also occurred relatively early, as compared to the other test samples. This is due to the shape of the steel sheeting, which provided negligible shielding to the unexposed surfaces. Relatively large cracks appeared due to the significant expansion and thermal bowing of the heated steel sheeting, as shown in Figure 4.18b. Therefore, the structural integrity of the top FCB failed.

(a) Steam from gypsum boards (b) Cracking of FCB

Figure 4.18: Test 4 observations

Figure 4.19 shows the steel sheeting and unexposed FCB after testing. The galvanizing on the steel sheeting melted, similar to the result from test sample T1, as shown in Figure

4.19a. The steel sheeting underwent significant bowing during the heating from below, while the expansion of the 340 mm steel section was calculated to be in the order of 4 mm at 50 minutes. The original shape and profile was regained after the test as the steel cooled down. From Figure 4.19b it can be seen that a significant number of cracks developed across the top FCB. A large crack formed along the fixing positions where the screws reduced the integrity of the insulation board.

(a) Exposed steel sheeting (b) Cracked unexposed FCB

Figure 4.19: Test 4 aftermath

4.3 Main findings and observations

A total of four small-scale fire tests were conducted, in which the samples were exposed to a standard furnace fire curve from below. The various locations of the thermocouples were discussed for each test sample, along with the temperatures that were measured at the respective locations. Some comparisons were made between the two different VP sheeting configurations, as well as between the samples with a ceiling board and those without a ceiling board. Observations that were made during and after each fire test were discussed and some examples were presented.

From the temperature results obtained for each of the test samples, it was found that the presence of the 9 mm Promatect-H ceiling board makes a significant difference in terms of the temperatures within the sample. Temperatures for the test samples without a ceiling board were approximately 40 to 64% more (representing a difference of 250°C to 370°C at 60 minutes) as compared to the corresponding ceiling board sample temperatures. It was also found that the intensity of the heat from the furnace was significantly higher in the middle part of the test samples as compared to the outer sides. As a result, the

ceiling board temperatures were slightly higher for test sample T3.

The stud section of the VP steel sheeting provided shielding to the surrounding materials within the cavities of test sample T2. Test sample T3, on the other hand, had no stud section in the middle that could shield some of the radiative heat transfer in the cavity. It was, therefore, found that the temperatures on the unexposed side of the FCB were slightly higher in test sample T3 than for sample T2. Test samples T1, T3 and T4 failed the insulation criteria, in which the limiting average unexposed temperature was defined as $160°C$. The unexposed surface temperature in test sample T2 did not exceed this limiting temperature, as shown in Figure 4.8. This was due to the shielding effect of the inner stud geometry.

General observations that were made during the four tests included steam being emitted from the gypsum boards and cracks that appeared in the FCB on top of the samples. Another observation that was made during each of the four tests, was the discolouring of the surrounding gypsum boards. The increased heat experienced by this section caused the outer gypsum paper and the sealants that were applied on the bottom edges of each sample to turn brown. Charring of the gypsum paper also occurred in all four tests and flames could be seen at the back of test sample T2, due to the gypsum paper that ignited during testing.

From the various images provided in this section, it can be seen that the integrity of the insulation boards is significantly less than the required 60-minute fire rating. Hence, when designing and specifying the ceiling system for the SAISC cellular beam structure it is pivotal that the integrity of ceiling systems is maintained, and they can accommodate the movements experienced by the structure. If the ceiling system fails, it is likely that compartmentation will be lost and fires can spread throughout the building. Only minor cracks appeared in the CaSi- ceiling board for both of the ceiling board test samples. The expansion of the steel sheeting caused the insulation boards to crack. Therefore, by limiting the increase in steel temperature within the samples, the expansion could be reduced and in turn, the cracks could be reduced. Fixing details in the SAISC structure would need to be designed to accommodate the expected expansion of the ceiling and decking system to ensure that ceilings do not crack and fail during fires.

Chapter 5

Validation of Finite Element models

5.1 Introduction

This section will discuss the validation studies that were performed to verify the procedures that were performed in ABAQUS. Firstly, the preliminary validation studies are discussed, from which basic modelling methods and parameters are investigated. Thereafter, the verification of Finite ELement (FE) models representing the experimental tests will be performed by using the experimental results presented in Chapter 4.

5.2 Preliminary validation studies

Before the execution of the experimental FE verification models, three FE studies from various researchers have been performed. This is used to validate the specific modelling methods that have been conducted in this work for the simulation of heat transfer. The validation case studies that have been performed included an insulated steel cross-section, cold-formed thin-walled steel panel systems in fire and a new slim-floor beam system under standard fire loading.

All of these studies address the simulation of conductive, convective and radiative heat transfer, as well as cavity radiation that occurs in the voids of the structural systems. By comparing temperatures predicted in this work with those in the literature it is observed that behaviour obtained from both theoretical and experimental investigations compare well with the methodologies developed in this work.

5.2.1 Insulated HE200B steel section

The first case study considers 2D heat transfer modelling of a fire protected steel section that is encased by an insulation board and uniformly exposed to the standard fire (ISO, 1999) on all four sides, as originally presented by Wickström and Palsson (1999). An HE200B steel section and a 10mm Promatect Calcium-Silicate (CaSi) board were used in the analysis. The steel section was positioned such that two small air cavities existed above and below the section, as presented in Figure 5.1. The results from the literature consist of the steel temperature as calculated by two 2D finite element analyses in software packages called TASEF and HEATING (Wickström and Palsson, 1999).

The cross-section has also been analysed by Jeffers *et al.* (2013) using an ABAQUS model, from which a good correlation was found between the temperature results when compared to those obtained from the TASEF and HEATING models developed by Wickström and Palsson (1999). Therefore, only the TASEF results from Wickström and Palsson (1999) were used for comparison purposes in this validation study, which is discussed below.

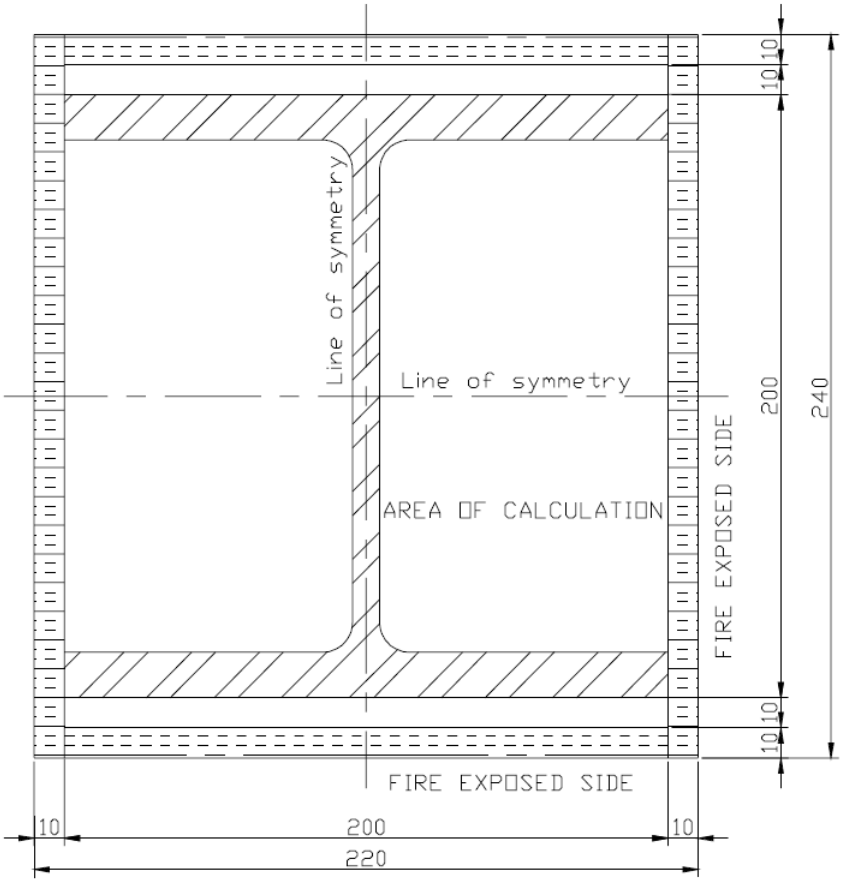

Figure 5.1: Insulated HE200B steel section (Wickström and Palsson, 1999)

An ABAQUS model, similar to that of Jeffers et al, was set up in this work to validate the modelling procedure performed by the current author. The setup was modelled as a 2D shell with solid homogeneous sections, which were assigned to both the steel and the insulation board. The material properties used for the steel and insulation board are presented in Table 5.1. The thermal conductivity of the two materials was dependent on temperature and varied bi-linearly as shown in Table 5.1. The emissivity was taken as 0.8 for all surfaces.

Table 5.1: Thermal properties for steel and insulation

Material	Density	Specific heat	Emissivity	Conductivity (W/mK)		
Name	$\rho\ (kg/m^3)$	$c_p\ (J/kgK)$	ϵ	$0°C$	$800°C$	$1200°C$
Steel	7850	600	0.8	54	27.3	27.3
CaSi	870	1130	0.8	0.174	0.188	0.188

A standard 2-hour fire was applied to the outer surfaces of the insulation board by means of convective and radiative heat transfer interactions. Similar heat transfer parameters that were used in the original literature were used by the author of this thesis. The convective heat transfer coefficient was taken as 25 W/m^2K and the emissivity as 0.8, as specified in ECCS TC3 (2001). The cavity radiative heat transfer in the enclosure was applied on all surfaces that encloses the corresponding cavity.

In this work and in the original literature an initial analysis was performed with only radiative heat transfer within the cavities between the insulation board and the steel section, through which the average surface temperature history of the inner surface of the insulation board was determined and saved. A second heat transfer analysis was then performed whereby a temperature amplitude was created that included the temperature history determined in the first analysis. The convective heat transfer could then be applied to the steel section surfaces as a surface film condition interaction, which consisted of the temperature history from the previous analysis. The convective heat transfer coefficient was taken as 1.5 W/m^2K and 2 W/m^2K in the smaller voids and larger voids respectively (refer to Figure 5.1).

Numerous analyses were performed using the ABAQUS model developed in this work, in which the number of elements in the mesh were varied to determine the influence it had on the accuracy of the steel temperatures. The increment size in the heat transfer time step was also varied. It was found that by increasing the number of elements within the steel section and insulation board more accurate results are obtained. Also, by decreasing the size of the increment in the heat transfer step, more accurate temperatures were obtained. Similar analysis procedures could therefore be followed for determining the steel and other material temperatures for other ABAQUS models. An approximate mesh size of 2.5 mm and a fixed time step increment of 10 seconds was used in the ABAQUS model, developed by the current author, in this validation study.

The temperature at the midpoint of the bottom flange was used as a reference point, at which the results could be compared. A difference of 0% was obtained in the results from the ABAQUS model developed in this work, compared to the models from the original authors, Wickström and Palsson (1999), using TASEF. Tables 5.2 and 5.3 present the correlation between the ABAQUS and TASEF results for the cavity radiation only analysis and the cavity convection analysis respectively. Hence, the ABAQUS model developed in the research described here correlates well with all of the results obtained by Wickström and Palsson (1999) and Jeffers *et al.* (2013).

Table 5.2: Comparison of temperatures obtained here using ABAQUS and Wickström and Palsson (1999) (TASEF), considering only cavity radiation

Time	ABAQUS	TASEF 357	Difference
min	Temperature ($°C$)	Temperature ($°C$)	%
0	20	20	0.00
30	229	226	0.01
60	519	518	0.00
90	736	736	0.00
120	879	879	0.00

Table 5.3: Comparison of temperatures obtained here using ABAQUS and Wickström and Palsson (1999) (TASEF), for cavity radiation and inner convection (I-C)

Time	ABAQUS (I-C)	TASEF 357 (I-C)	Difference
min	Temperature ($°C$)	Temperature ($°C$)	%
0	20	20	0.00
30	241	246	0.02
60	537	536	0.00
90	747	746	0.00
120	884	885	0.00

The results obtained from this validation study were also compared to the results from the theoretical Eurocode equations, which were discussed in Section 2.7.3. It was found that both calculation methods yielded similar results. It can therefore be concluded that the procedure used in the ABAQUS analysis yields accurate element temperatures in comparison to the results in the literature.

5.2.2 Cold-formed thin-walled steel panel systems in fire

Numerous studies have been performed by various authors on the thermal and mechanical behaviour of cold-formed thin-walled steel panel systems in fire. These systems are widely used in buildings as wall panels in the form of partitions for dividing compartments and usually consist of cold-formed steel channel sections that are sandwiched between two layers of gypsum board. They are also referred to as Light-gauge Steel Frame (LSF) systems. Ariyanayagam *et al.* (2017) investigated the thermal behaviour of these systems under natural fire conditions while being subjected to a mechanical load. Numerical studies of non-load-bearing LSF walls in fire have been performed by Rusthi *et al.* (2015), while Keerthan and Mahendran (2012) compared gypsum plasterboard and Magnesium Oxide (MgO) board lined LSF walls in fire through performing numerical analyses. Most of these authors conducted experimental fire tests that were used to validate FE models.

This validation study will discuss the research performed by Feng *et al.* (2003), who investigated the thermal performance of these systems in fire. These authors conducted a series of small-scale fire tests on eight samples with different configurations. These tests were compared to FE analyses that were performed in ABAQUS. The various test samples included LSF systems with a single layer of gypsum boards, double layer gypsum boards, lipped and unlipped channel sections, mineral wool insulated wall sections and sections with and without a hole in the web. The tests were used to compare different configurations with each other and to validate the numerical models developed by the authors. Figure 5.2 presents two of the samples that were tested by Feng *et al.* (2003).

The structural configurations investigated by Feng *et al.* (2003) have a certain degree of similarity to the sandwich system investigated in this work. In both cases an air cavity is formed between the insulation members, in which cavity radiation plays a crucial role. Although the aforementioned authors performed a significant number of tests, only one of them was used in this validation study. The aim of this study was to determine whether the modelling procedure for cavity radiation in an enclosed void was accurate. Further information on the tests and FE analyses performed can be obtained in their research paper (Feng *et al.*, 2003).

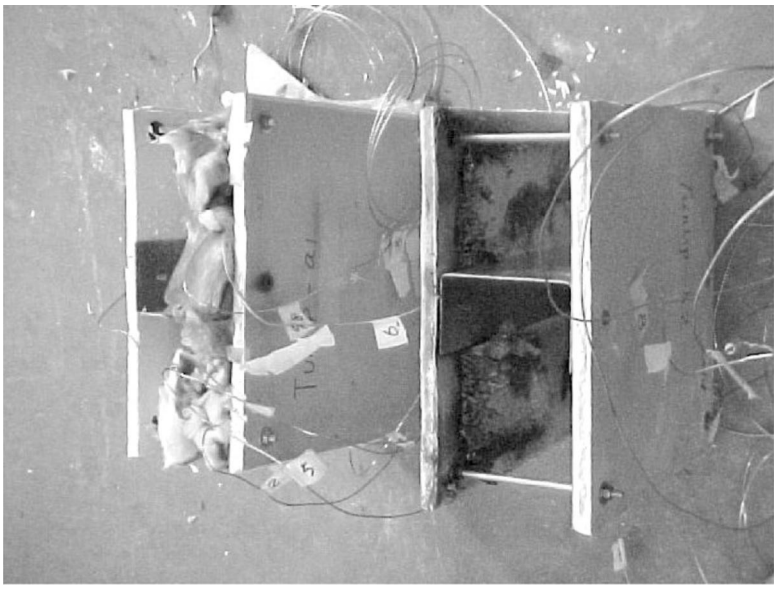

Figure 5.2: Insulated Unlipped channel with gypsum boards (Feng *et al.*, 2003)

5.2.2.1 Model configuration and parameters

The LSF sample that was used in this validation study consists of a single lipped channel section, with dimensions 100 x 54 x 15 x 1.2 mm, with a single layer of gypsum board on each side without any mineral wool insulation within the void and without the service hole in the web. It was found that this configuration was sufficient for investigating the behaviour of cavity radiation within the wall system. The layout of the specific configuration is shown in Figure 5.3.

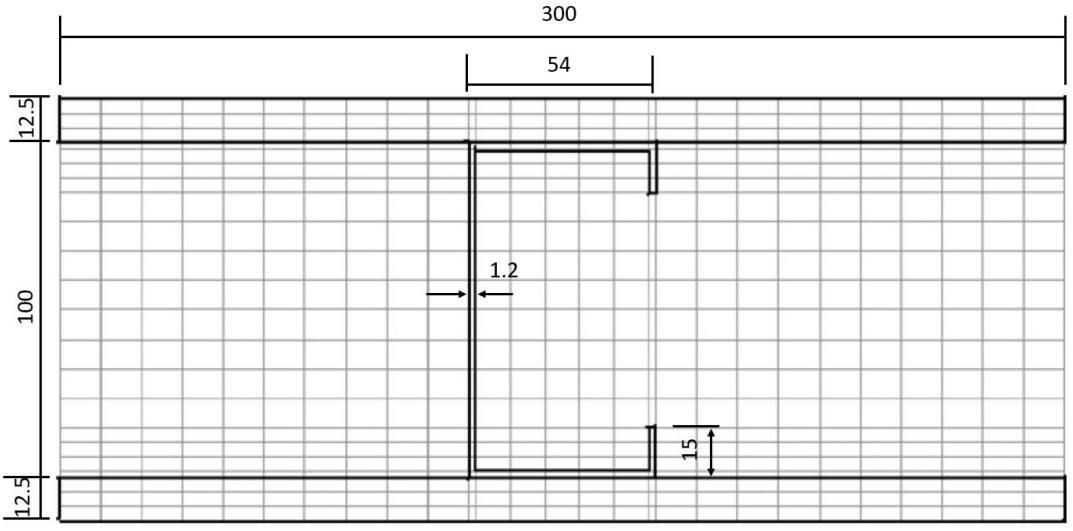

Figure 5.3: Layout of lipped channel section (Adapted from Feng *et al.* (2003))

The modelling parameters are discussed in Feng *et al.* (2003), which includes the thermal boundary conditions on the exposed and unexposed surfaces. These authors defined the convective heat transfer coefficient (h), modelling using the film coefficient in ABAQUS, as 25 W/m^2K and 10 W/m^2K on the exposed and unexposed sides respectively. In terms

of radiative heat transfer, a value of 0.3 was used for the resultant emissivity on the exposed side, according to Shahbazian and Wang (2013). The emissivity for the unexposed side was taken as 0.8 (Feng *et al.*, 2003). The same authors discussed the problem of cavity radiation, which had to be considered for the void in the wall panels. Section 2.7.6.1 presented the concept of cavity radiation and how it is utilised in ABAQUS, along with the equation used in the analyses.

The ABAQUS FE model developed here included the above mentioned thermal properties and heat transfer coefficients for the exposed and unexposed surfaces. The cavity conditions, however, were not clearly specified in the paper of Feng *et al.* (2003). Therefore, the emissivity for the cavity radiation was derived based on the combination of the emissivities of the material surfaces within the cavity. These were taken as 0.9 and 0.4 for the gypsum and the cold-formed steel section, respectively. The resultant emissivity within the cavity was determined as 0.38 from Equation 5.3.2, and is discussed in more detail below.

Convection was also simulated in the FE analysis performed by the current author. Average temperatures were determined in an initial FE analyses on the inner surface of the upper gypsum board and on the top surface of the cold-formed steel section (stud), similar to the procedure of the first validation study in this chapter. The convective heat transfer coefficients within the cavity were estimated as 4 and 2 W/m^2K for the outer and inner steel stud sections, respectively. The estimated values were based on the relatively small values that were assumed by Wickström and Palsson (1999) in the previous validation study. Convection was then applied to all of the unexposed surfaces within the cavity as surface film conditions in the interaction functionality of ABAQUS, which incorporated the average temperatures and convection coefficients.

5.2.2.2 Material properties

The material properties that were used for the steel section are provided in the Eurocode 1993-1-2 (CEN, 2005), as discussed in Section 2.7.2. British Gypsum Fireline board was used by Feng *et al.* (2003), and the material properties were defined and validated in their study. This was done by testing and modelling a 12.5 mm fireline gypsum board section and comparing the respective results. A summary of the material properties that were used are presented in Table 5.4.

5.2.2.3 Comparison of results

The assembled parts were connected with ties in ABAQUS to allow conductivity to occur from the gypsum board through to the steel channel section and into the gypsum board on the unexposed side. A predefined temperature of $20°C$, which is the assumed ambient temperature, was applied to the whole model. The temperature distribution through the panel system at the end of a 120 minute fire exposure are presented in Figure 5.4. Temperatures were determined at the points corresponding to those used in Feng *et al.* (2003) and is shown on FE model in the figure. The temperature nodes are denoted as "FE node 1", for example. The temperatures that were predicted by Feng *et al.* (2003) while using ABAQUS are denoted by the letter "P" and the temperatures that were measured during the fire tests in Feng *et al.* (2003) are given by the letter "T". Node

Table 5.4: Thermal properties of FE beam model materials

Material name	Density ρ (kg/m^3)	Conductivity k (W/mK)	Specific heat c_p (J/kgK)
Steel	7850	$54 - 3.33 \times 10^{-2}\ \theta$ at $(20°C \leq \theta \leq 800°C)$ 27.3 at $(800°C \leq \theta \leq 1200°C)$	$425 + 0.773\ \theta - 1.69 \times 10^{-3}\ \theta^2 + 2.22 \times 10^{-6}\ \theta^3$ at $(20°C \leq \theta < 600°C)$ $666 + \frac{13002}{738-\theta}$ at $(600°C \leq \theta < 735°C)$ $545 + \frac{17820}{\theta-731}$ at $(735°C \leq \theta < 900°C)$ 650 at $(900°C \leq \theta \leq 1200°C)$
Gypsum - Type X	727.1	0.2 at $10°C$ 0.218 at $150°C$ 0.103 at $155°C$ 0.3195 at $1200°C$	925.04 at $10°C$ 941.5 at $95°C$ 24572.32 at $125°C$ 953.14 at $155°C$ 1097.5 at $900C°C$

With θ as the surface temperature in $°C$.

number 1 is located on the unexposed surface, node 2 is on the steel channel section and node 3 is situated on the exposed surface, as depicted in the figure.

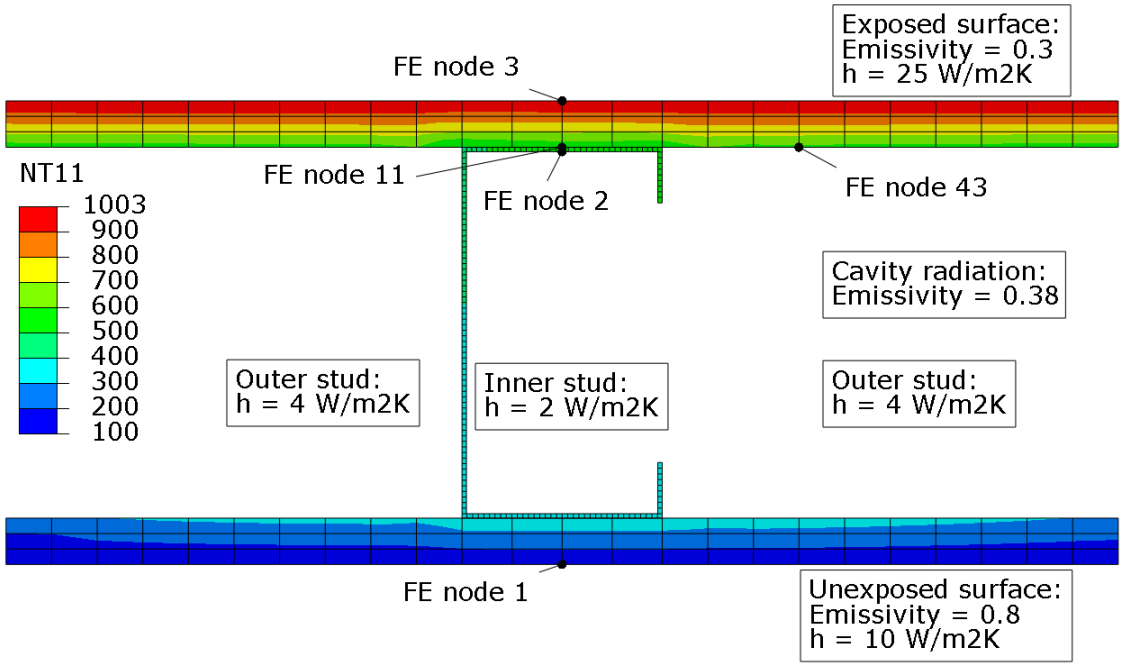

Figure 5.4: Validation study 2 - Predicted temperatures in ABAQUS model at 120 minutes

During the initial analysis, the average inner cavity temperatures were determined from nodes 11 and 43 for the inner and outer stud cavities, as indicated on the FE model in Figure 5.4. These temperatures were then applied in the second FE analysis as a surface film condition interaction. The interaction with temperatures from node 11 were applied to the inner stud surfaces, while the temperatures from node 43 were applied to the top surface of the lower gypsum board and the outer stud surfaces. The assumed heat transfer parameters that were used are also shown in the figure.

The temperature curves obtained by Feng *et al.* (2003) were compared with the numerical results that were obtained here using ABAQUS. From Figure 5.5 it can be seen that the FE temperatures agreed well with the predicted (ABAQUS) results from Feng *et al.* (2003), with typical variations in results being less than 7%.

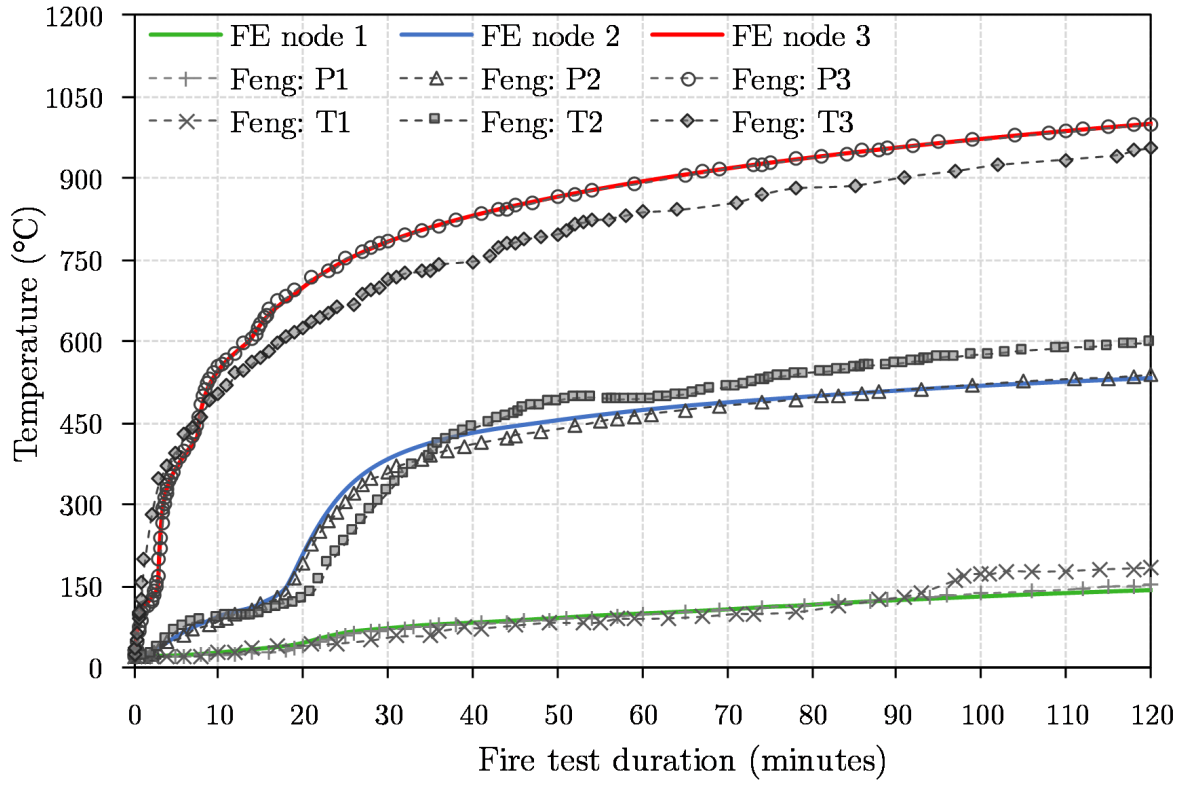

Figure 5.5: Comparison between ABAQUS model (coloured lines) and results from Feng *et al.* (2003), including predicted (P) and test (T) results (grey lines and data points)

From 5.5 it can be observed that the heat transfer through the steel panel assemblies were therefore accurately simulated by utilising ABAQUS. More specifically, the modelling parameters for the cavity radiation and inner convection into the cavity were appropriate. Although the cavity in the panel system was open to the ambient temperature of $20°C$ during testing, similar modelling techniques could be applied for closed cavities. This will be discussed in the following part of this section.

5.2.3 Cavity radiation modelling in a slim-floor beam system

Schaumann and Hothan (2002) discussed the modelling of a new slim floor beam system that was designed by Kuhlmann, Fires & Leukart (2000). The system consists of a UPE 240 section and a European U-profile with parallel flanges (ArcelorMittal, 2017*b*), with dimensions of 240 x 90 x 7 x 12.5 mm for the height, width, web thickness and flange thickness, respectively. The U-profile is welded to a steel plate and forms a "hat-shape" profile, which is connected to a concrete slab with the use of shear studs, as shown in Figure 5.6. The original authors investigated the thermal behaviour and the mechanical load bearing capacity of the slim-floor system (Schaumann and Hothan, 2002). However, only the thermal behaviour comparison of the cavity will be analysed in this work.

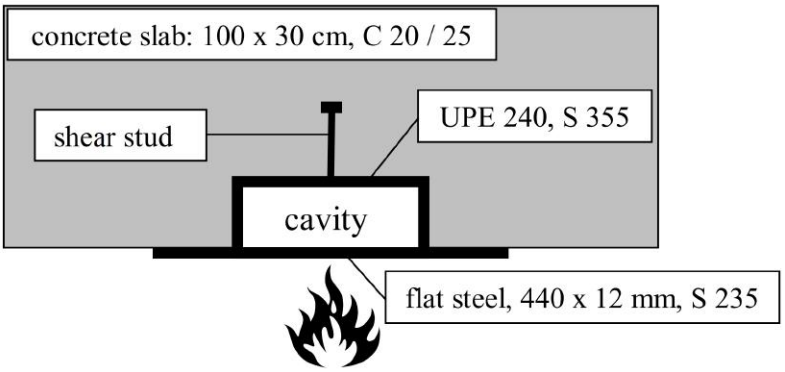

Figure 5.6: Slim-floor composite beam configuration (Schaumann and Hothan, 2002)

A two-dimensional (2D) heat transfer analysis of the slim-floor system was performed here to develop a further understanding of cavity radiation modelling in ABAQUS. The temperature results are compared below to those obtained by Schaumann and Hothan (2002). Two models have been analysed, one considering cavity radiation, while the other model neglected the radiative heat transfer within the cavity. The FE models were exposed to a 2-hour standard fire, which was applied to the bottom surface as interactions in ABAQUS (Dassault Systémes, 2015), as discussed in the previous validation study. The convective and radiative heat transfer was modelled as a surface film condition and surface radiation, respectively. The analyses comprised of a heat transfer time step with a time period of 7200 seconds, which were automatically divided into increments with a maximum size of 10 seconds. A maximum allowable temperature change of $10°C$ per increment was specified in the heat transfer step.

The thermal properties of the steel and concrete were based on the Eurocodes as specified in ECCS TC3 (2001). The heat transfer through the steel plate, into the cavity and through the surrounding UPE and concrete layers was simulated by using four-node linear solid elements, denoted by DC2D4 in ABAQUS (Dassault Systémes, 2015). The contact surfaces between the steel and concrete sections were constrained by using "Ties", to allow conduction through the various material layers.

A similar mesh, as defined by Schaumann and Hothan (2002), was assigned to the FE models by seeding the model edges using a specific number of elements. The FE model of the slim-floor beam system, along with the mesh configuration and the two points at which the temperatures were determined and compared, are shown in Figure 5.7.

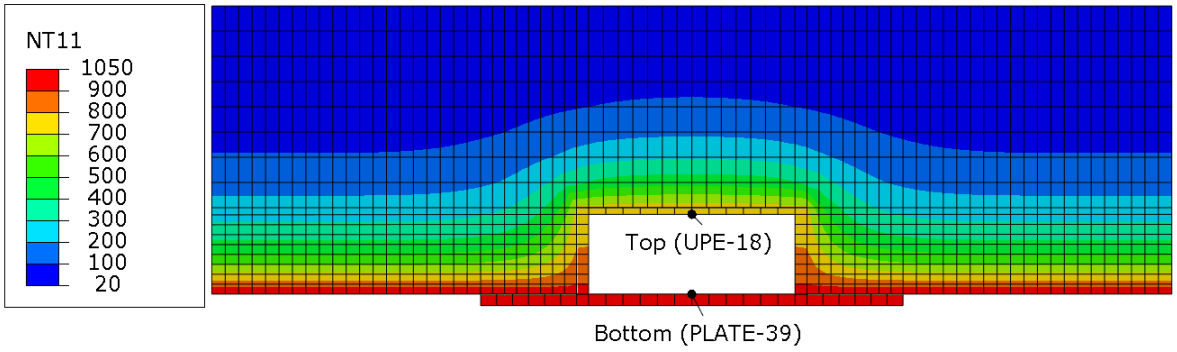

Figure 5.7: FE model of the Slim-floor beam system

The temperature distribution through the model that included cavity radiation is also depicted in Figure 5.7. The shear stud was neglected during the FE analyses, due to the focus being on the cavity behaviour as was done by the authors Schaumann and Hothan (2002), and shear studs only being present at intervals.

The boundary conditions in the FE model included the emissivities and heat transfer coefficients for the respective material surfaces, based upon values provided by the original authors. The emissivity for the steel and concrete surfaces on the exposed side were taken as 0.56. The convective heat transfer coefficient was defined as 25 W/m^2K and 9 W/m^2K for the exposed and unexposed sides, respectively. An emissivity value of 0.56 was also assumed for the inner surfaces of the closed cavity. Conductive and convective heat transfer within the cavity were neglected (Schaumann and Hothan, 2002), due to radiation being the governing mode of heat transfer at high temperatures. According to Schaumann and Hothan (2002), negligible heat loss occurred at the unexposed side of the concrete slab. Therefore, the radiative heat transfer from the unexposed surface was not considered. An initial ambient temperature of 20°C was assumed.

5.2.3.1 Results comparison

The temperature results obtained by Schaumann and Hothan (2002), along with the results obtained from the FE analyses, are depicted in Figure 5.8. The black and grey dotted lines with the markers represent the results from Schaumann and Hothan (2002), while the red and blue lines are the temperatures obtained from the FE analyses performed here. CR and noCR, denotes the models with and without the consideration of cavity radiation, respectively. The temperatures were determined at the top ("t") and the bottom ("b") of the cavity, as shown in Figure 5.7.

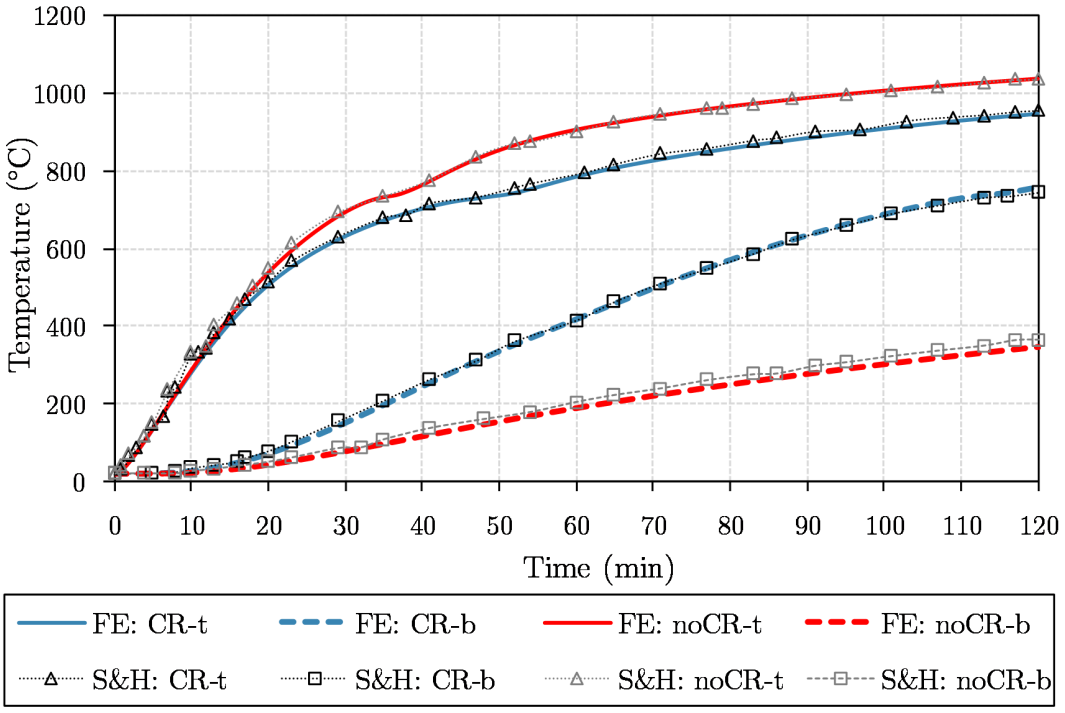

Figure 5.8: Comparison of predicted temperatures from the ABAQUS model and Schaumann and Hothan (2002), both including cavity radiation (CR) and neglecting it (noCR)

From Figure 5.8 it is clear that a good correlation has been obtained between the respective results from Schaumann and Hothan (2002) and the model used in this research. The difference in predicted temperatures is typically less than 10% between the models. The radiative heat transfer in the cavity was therefore accurately modelled, relative to the original authors. The influence of cavity radiation on the thermal behaviour of the slim-floor system is evident in Figure 5.8. It can be seen that the cavity radiation (CR) resulted in higher temperatures at the top surface of the cavity, compared to the model without cavity radiation (noCR). Heat is therefore emitted from the top surface of the steel plate into the cavity towards the inner cavity surfaces, comprising of the UPE-section. The amount of heat that radiates from the plate increases with a rise in temperature, as seen in Figure 5.8. As the temperature of the top surface within the cavity increases, heat is radiated back into the cavity, which results in lower temperatures at the top of the cavity. This can also be noted in the figure.

It is evident that cavity radiation is a crucial component to consider during heat transfer analyses, in order to accurately simulate the thermal performance of a structural system, such as the slim-floor beam system.

5.3 Verification of fire-test FE models

From the previous section it has been shown that the modelling procedures implemented in this work can predict the thermal response of structural elements with a level of accuracy comparable to that of models in the literature.

This section will now describe the FE models that have been developed in ABAQUS to simulate the thermal behaviour of the experimental fire test samples, which were discussed in Chapter 3. The aim is to verify the FE models by comparing the predicted temperatures obtained from the ABAQUS analyses to the temperatures that were physically measured during the fire tests. The verification process allows for the development and calibration of a model to understand and predict the behaviour of the flooring system presented in this work. Ultimately, the verification of the FE models provides the basis for further development of larger scale FE models for the prediction of the thermal behaviour within the sandwich floor system, as presented in Chapter 1. The larger scale FE models include the prediction of the cellular beam and inner floor temperatures.

The appropriate modelling parameters were determined during the verification process. These parameters include the heat transfer variables, such as emissivity and convective heat transfer coefficients, as well as the thermal properties of the materials.

5.3.1 FE modelling of test samples

The FE models developed are based on the geometry and dimensions of each respective test sample shown in Figure 3.1, as described in Section 3.3. Two-dimensional (2D) shell elements were used to analyse the test samples in ABAQUS. Therefore, only the cross-section of each sample was modelled, while neglecting the depth of the section. The use of 2D elements is sufficient for the heat transfer analyses, due to an assumed uniform distribution of temperature across the depth of the samples. A major advantage

of 2D-modelling is that the computational time is significantly less than for 3D-modelling.

Each homogeneous material layer in the FE models was created as a separate part, to which a solid section was assigned. Each assembled model contained three parts, which included the Promatect-H (CaSi) ceiling board, the Voidcon VP50 steel sheeting, the inner fibre-cement board (FCB) and the gypsum board on the sample sides. The different parts, each with its corresponding material properties, was assembled to form the cross-sectional FE models shown in Figure 5.9. This figure also includes the locations at which the temperatures were determined in ABAQUS, the mesh configuration and the temperature distribution at 60 minutes for the test samples. The locations are annotated in terms of the material and specific node on that material section. In FE sample T1, for example, FCB-113 indicates that the point is located at node 113 on the fibre-cement board (FCB).

A transient heat transfer analysis was performed to determine the temperature distribution for each of the test samples. The analyses were performed in a heat transfer step with a time period of 3600 seconds (60 minutes), except for test sample T4. Test T4 was terminated after about 50 minutes, as discussed in Chapter 4, which was therefore analysed with a time period of 3000 seconds. ABAQUS automatically divides the time period into smaller time steps (increments). The initial, minimum and maximum increment sizes were specified as 0.1, 0.0036 and 20 seconds, respectively. The allowable temperature and emissivity change per increment were limited to a maximum of $20°C$ and 0.1, respectively. Two physical constants were defined in the ABAQUS model attributes, namely the absolute zero temperature ($-273.15°C$) and the Stefan-Boltzmann constant ($\sigma = 5.67e^{-8}$). The FE models were analysed with a medium-sized mesh, as seen in Figure 5.9. A global seed size of 0.005 m was defined for the insulation materials and 0.001 m for the Voidcon sheeting. It was found that a finer mesh resulted in a negligible difference in temperatures for the respective test models. Two-dimensional (2D) 4-node linear heat transfer elements (DC2D4) were assigned to the models in the FE analyses.

5.3.2 Material properties of FE models

The respective material manufacturers, namely Promat (2016), Voidcon (2014*a*), Everite (2012*a*) and Gyprock (2017), provide technical material specifications in their brochures, with values listed in Table 5.5. The required thermal properties of the materials for performing heat transfer analyses in ABAQUS included the density (ρ), thermal conductivity (k) and the specific heat (c_p). In most cases, these properties are dependent on temperature, such as defined in the study performed by Feng *et al.* (2003) for the gypsum boards. However, most of the technical specifications provided by the respective manufacturers include constant thermal properties, such as the conductivity or specific heat at a specific temperature. The material properties for the gypsum board and the FCB were therefore modelled as constant values in the respective ABAQUS models. However, with the gypsum boards and FCB being at the side and top, respectively, they are exposed to lower temperatures and the models are less sensitive to their specified properties. Temperature dependent properties of the materials should be experimentally determined in further investigations, from which more accurate FE models could be developed.

The thermal properties of the Voidcon steel sheeting were assumed to be similar to those of normal carbon steel. A detailed discussion of the thermal properties of steel is presented in Section 2.7.2, as well as in the study performed by Feng *et al.* (2003). The density,

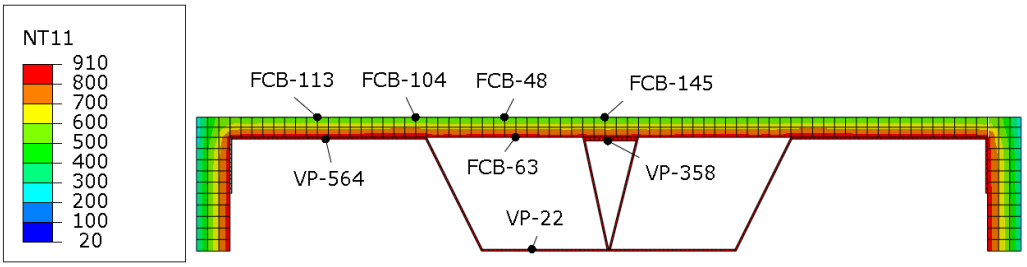

(a) Test 1

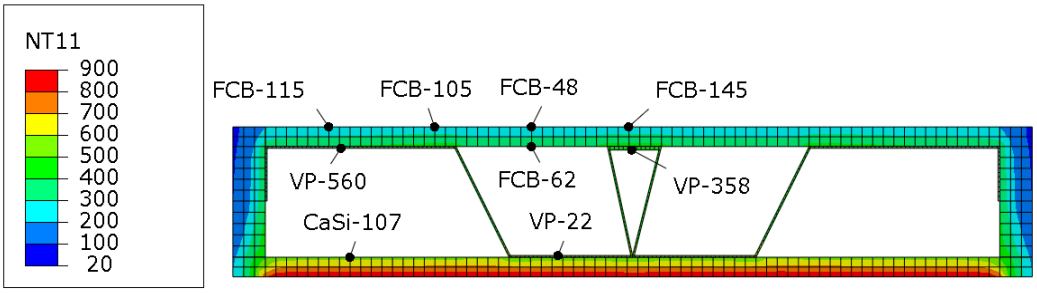

(b) Test 2

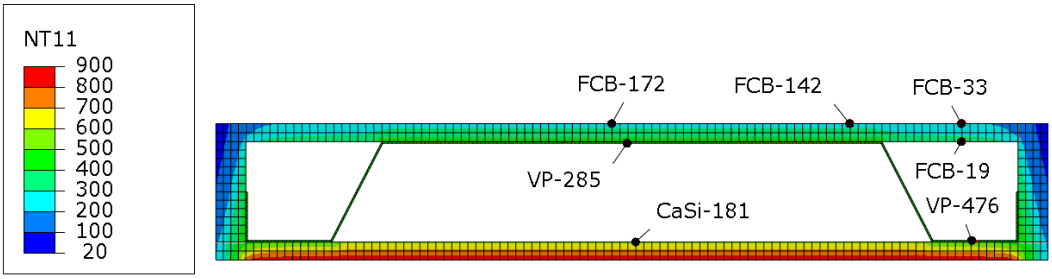

(c) Test 3

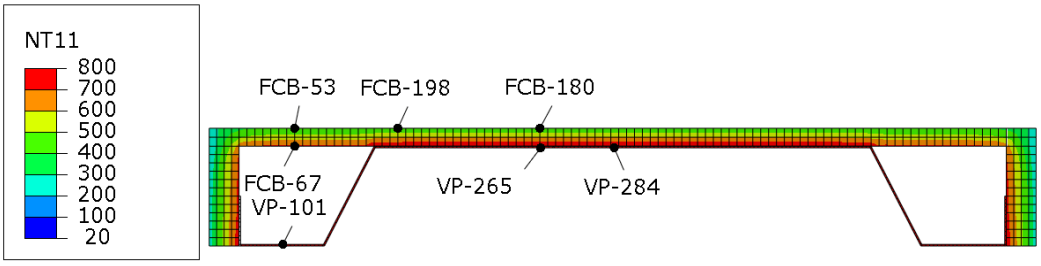

(d) Test 4

Figure 5.9: ABAQUS models with temperature points after a 60 minute standard fire

specific heat and a bilinear relationship between temperature and the conductivity of the Promatect-H (CaSi) boards were used in the FE analyses, which is based on the values specified by Wickström and Palsson (1999), as described in Table 5.1. The density and thermal conductivity of the FCB were obtained from the product specifications (Everite, 2012*b*), while the specific heat was based on the value for light fibreboard, as described by The Engineering ToolBox (2017). The thermal properties of the insulation materials are summarised in Table 5.5.

The emissivity value of materials varies between different sources in the literature. Although the emissivity of a material depends on the temperature of the material surface,

Table 5.5: Thermal properties for insulation materials in FE models

Material name	Density ρ (kg/m^3)	Conductivity k (W/mK)	Specific heat c_p (J/kgK)
Gypsum board	1440	0.48	840
Fibre-cement board (FCB)	1400	0.19	2500
Promatect-H board (CaSi)	870	0.174 at $0°C$ 0.188 at $250°C$	1130

constant values were used, due to the uncertainty of the specific material properties. The Eurocode specifies a default surface emissivity (ϵ) value of 0.8 (ECCS TC3, 2001), which is generally used for steel sections. However, it was found that the emissivity of gypsum and fibre-cement boards is typically about 0.9, according to Hurley *et al.* (2016).

Galvanized steel profiles experience a change in surface conditions with a rise in temperature, as discussed in Section 4.2. Elich and Hamerlinck (1990) conducted an extensive investigation on the radiative heat transfer properties of galvanized steel, such as the emissivity value. Initially, galvanized sheeting has a relatively low emissivity in the range of 0.25, depending on the level of oxidation and how clean the surface is. At a temperature of $420°C$ the zinc coating melts, after which the emissivity of the steel sheeting increases to a value in the range of 0.8 (Elich and Hamerlinck, 1990). A bi-linear emissivity- temperature relationship was therefore defined for the galvanized steel sheeting in the test-sample FE models. An initial emissivity of 0.42 was assumed, as obtained from Hurley *et al.* (2016) for a galvanized steel roofing material. The emissivity of carbon steel, taken as 0.8, was used for temperatures exceeding $420°C$. A summary of the assumed emissivity values for each material are presented in Table 5.6.

Table 5.6: Surface emissivity of sample materials

Material	Emissivity
CaSi - board	0.8
Fibre-cement board	0.9
Gypsum board	0.9
Galvanized steel	0.42 at $20°C$ 0.8 at $420°C$

5.3.3 Heat transfer modelling considerations

The modelling procedure used for the LSF validation study, as presented in Section 5.2.2, was performed in a similar manner for the FE models representing the test samples. The components of the flooring system were linked together by applying constraints in the form of ties. These constraints simulated the contact between the different materials by connecting the degrees of freedom, thereby conducting heat through the model.

The FE models were exposed to the actual temperature-time relationships (fire curves) that were measured in the small-scale furnace for the respective fire test samples, as presented in Chapter 4. An average furnace temperature was determined for each test, which was applied to the exposed surface of the respective FE models. The convective and radiative heat transfer coefficients were incorporated in the ABAQUS heat transfer analyses on the exposed, unexposed and cavity surfaces. These heat transfer parameters were defined as interactions, which included the surface film condition, surface radiation and cavity radiation. The surface film condition incorporated the convective heat transfer coefficient, while the surface emissivities were defined in the surface and cavity radiation interactions.

Initially, a series of FE analyses of the test samples were performed based on the heat transfer coefficients and emissivity values specified by the Eurocodes as 0.8 and 25 W/m^2K, respectively. It was found that the FE models representing the test samples were sensitive to the surface and cavity emissivity values. This presents a challenge to accurately model results as these values are not precisely known. Hence, in this work a sensitivity analysis on input parameters was conducted. Initially, the temperatures obtained from the FE analyses were much higher than the measured temperatures from the tests for an exposed surface emissivity of 0.8. This could have been due to the relatively small size and configuration of the small-scale furnace, which were discussed in Section 3.4. According to Feldman (2006), the ratio between the test sample surface area and the radiative surface area of the furnace has an influence on the surface emissivities. Other factors, such as the furnace material, ventilation conditions and gas and flow properties could also influence the heat transfer parameters. Also, the complexity of the flow makes it difficult to measure the velocity within a furnace (Beyler *et al.*, 2007). Most of these parameters were unknown during the execution of the fire tests. The exact values for the convective coefficient and surface emissivity could therefore not be determined.

A variety of emissivity values, ranging from 0.6 to 1.0, and heat transfer coefficients between 5 and 25 W/m^2K were investigated for gypsum plasterboard assemblies in a thesis conducted by Jones (2001). The heat transfer parameters were varied in a similar manner during the FE modelling of the test samples in this research to determine the appropriate values for the exposed and unexposed surfaces. It was found that the change in the convective heat transfer parameter on the exposed side of the samples had a negligible influence on the temperature distribution through the models. A convective coefficient of 25 W/m^2K was therefore used for all FE models, as typically specified in the literature. However, the emissivity of the exposed surface had a considerable effect on the temperature in the FE models. A high radiative coefficient results in heat being lost from the surface of the exposed element, leading to lower predicted temperatures. Numerous authors in the literature used a variety of emissivity values, such as Shahbazian and Wang (2013) and Feng *et al.* (2003), where emissivities between 0.3 and 0.8 were specified for the exposed and unexposed surface, respectively. A number of these authors investigated the behaviour of gypsum plasterboard assemblies in a standard fire, which comprised of small-scale tests, similar to that proposed in this work. Wang *et al.* (1995) used an effective emissivity of 0.5 for the exposed side within the furnace. Higher emissivities in the range of 0.7 to 0.8 were used by Hopkin *et al.* (2012) and Thomas *et al.* (1997).

During the FE modelling of the test samples, an emissivity of 0.3 on the exposed side was assumed, which resulted in a good agreement with the test results. This value was also used by Feng *et al.* (2003), who investigated similar sample sizes of cold-formed panel sys-

tems in a small-scale furnace, as discussed in Section 5.2.2. The radiative and convective heat transfer from the unexposed surfaces were considered separately. The emissivity of the unexposed gypsum and FCB surfaces were applied to the outer boundaries of the FE models, which were taken as 0.9, as shown in Table 5.6.

The Eurocode specifies a heat transfer coefficient of 4 W/m^2K for the unexposed side when radiation is considered separately. However, this relatively low coefficient value resulted in higher temperatures on the FCB than those obtained from the fire tests. The heat transfer coefficient was increased to a value of 10 W/m^2K. This value is commonly used by various authors in the literature, such as those discussed in the validation studies at the beginning of this chapter. Authors, such as Jones (2001) and Thomas *et al.* (1997), specified convective coefficients on the unexposed side as 12 and 9 W/m^2K, respectively (Keerthan and Mahendran, 2012). The use of the higher coefficient value could also be justified by the significant amount of steam that was produced by the gypsum boards during the fire tests. This observation was discussed in Section 4.3. The steam from the gypsum convected heat to the surrounding environment, which acted as a heat sink.

A summary of the surface emissivity, convective heat transfer coefficient and the corresponding sink temperature for the specific sample surfaces are shown in Table 5.7. The sink temperatures FT_TC-A correspond to the average furnace temperature, that were measured with the thermocouples (TC) in the fire tests (FT). Data-logger A was used to record the furnace temperatures.

Table 5.7: Heat transfer coefficients for the FE test models

Location	ϵ	α_C (W/m^2K)	Sink Temperature $(°C)$
Exposed Surface (Bot)	0.3	25	FT_TC-A
Unexposed Surface (Top)	0.9	10	20
Sides (Gypsum)	0.9	10	20

5.3.3.1 Configuration factors

The absence of a ceiling board in test samples T1 and T4, resulted in a non-uniform surface geometry to be exposed to the furnace fire. Therefore, configuration factors had to be determined for these two test samples. Although the depth of the samples is relatively small, the varying distance between the sample surfaces and the flames had an influence on the configuration factors. The configuration factors were taken as unity for samples T2 and T3, due to the presence of a ceiling board on the exposed side. It was also assumed that the configuration factor of the voids within the samples is equal to one.

The 2D simplified equation, given by Equation 2.6.5 in Section 2.6.3, was used to determine the configuration factors for the respective VP steel surfaces within test samples T1 and T4. The exposed steel surfaces and the dimensions for the calculation of the configuration factors are presented in Figure 5.10 and 5.11 for sample T1 and T4, respectively.

A specific geometry was defined for each surface in terms of the points A, B, C and D, as defined in Figure 2.10. The distances between these points were determined and used in

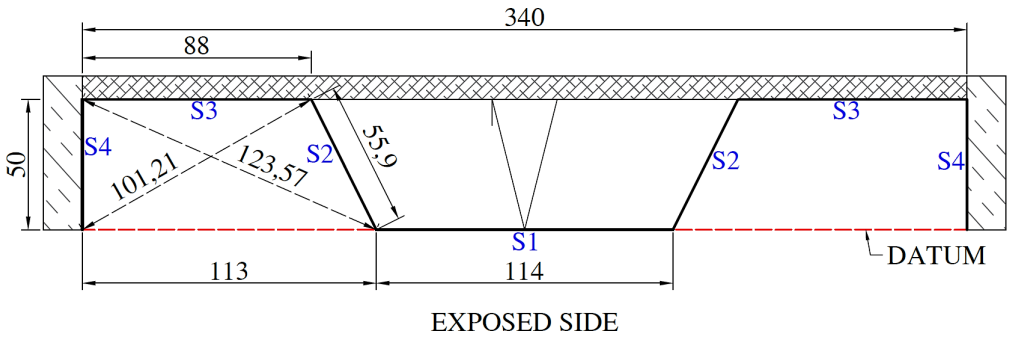

Figure 5.10: Configuration factor calculation parameters for sample T1

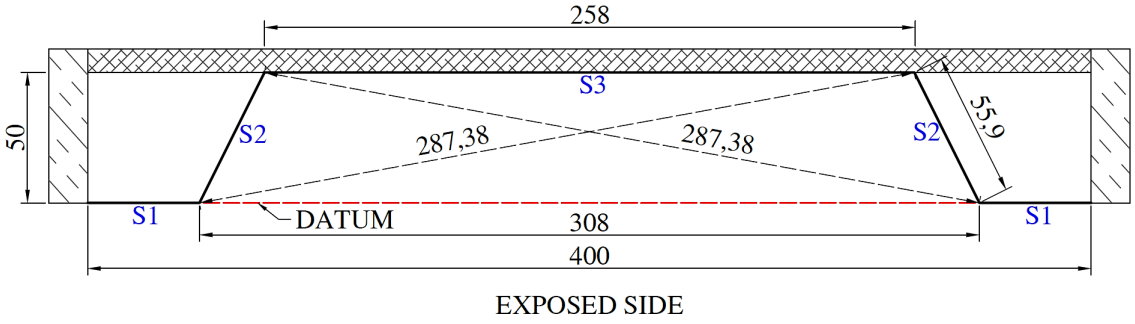

Figure 5.11: Configuration factor calculation parameters for sample T4

Equation 2.6.5 to calculate the configuration factor for the respective surfaces in the two samples without a ceiling board. The surfaces are denoted by S1, S2, S3 and S4, as shown in Figures 5.10 and 5.11. It can be seen that both samples T1 and T4 are symmetrical about the vertical centre-line. The configuration factors for the left and right side of the sample were therefore equal.

The furnace test samples were situated on top of a vermiculite board, as discussed in Section 3.3. The openings in the vermiculite board, also described in Section 3.3, allowed the heat from the furnace to be concentrated on the bottom area of the test samples. As previously discussed, the opening for test samples T1 and T2 were 300 x 300 mm, while for samples T3 and T4 the opening was 400 x 300 mm. The heat flow within the furnace and through the openings was turbulent and unpredictable. A simplification was made by assuming that the heat from the furnace was directly emitted onto the bottom surface of the test samples. This means that the bottom exposed surface of the samples, which are located on the red "DATUM line in Figures 5.10 and 5.11, had a configuration factor of 1.0. These surfaces, denoted by S1, were thus fully exposed to the furnace temperature without any shielding effects. The calculated distances and configuration factors are presented in Tables 5.8 and 5.9 for test sample T1 and T4, respectively.

The configuration factors were multiplied by the emissivities of the respective surface materials, as depicted in the tables above. In both samples, the exposed surfaces consisted of the VP steel sheeting, for which two emissivity values were defined in Table 5.6. The radiative heat transfer on the exposed surfaces were applied as separate interactions for each surface and its corresponding factored emissivity, which takes the shielding and non-uniform surface geometry effects into consideration.

Table 5.8: Calculation of the configuration factor (ϕ) for test sample T1

Distance	Surface			
(mm)	S1 (botStud)	S2 (sideStud)	S3 (topCore)	S4 (sideCore)
AB	300.0	113.0	113.0	113.0
CD	114.0	55.9	88.0	50.0
AC	113.0	101.2	50.0	0.0
BD	113.0	0.0	55.9	123.6
AD	227.0	113.0	101.2	50.0
BC	227.0	55.9	123.6	113.0
ϕ	1.00	0.61	0.68	0.39
$\epsilon.\phi$ $(< 420°C)$	0.42	0.25	0.28	0.17
$\epsilon.\phi$ $(\geq 420°C)$	0.8	0.48	0.54	0.32

Table 5.9: Calculation of the configuration factor (ϕ) for test sample T4

Distance	Surface		
(mm)	S1 (botStud)	S2 (sideCore)	S3 (topCore)
AB	400.0	308.0	308.0
CD	46.0	55.9	258.0
AC	0.0	0.0	55.9
BD	354.0	287.4	55.9
AD	46.0	55.9	287.4
BC	400.0	308.0	287.4
ϕ	1.00	0.68	0.90
$\epsilon.\phi$ $(< 420°C)$	0.42	0.29	0.38
$\epsilon.\phi$ $(\geq 420°C)$	0.8	0.55	0.72

5.3.3.2 Cavity radiation within samples

Radiation within the cavities is transferred between two or more different materials. The cavities include a combination of the steel sheeting, gypsum, FCB and the Promatect-H (CaSi) board, each with its corresponding surface emissivity. However, when defining cavity radiation in ABAQUS only a single emissivity value is required. Therefore, an effective emissivity value had to be determined, by which the emissivities of the various materials were combined. Numerous authors, such as Hopkin *et al.* (2012), Kay *et al.* (1996) and Buchanan and Abu (2017), describes a resultant emissivity (ϵ_{res}) relationship that incorporates two different surface emissivities as:

$$\epsilon_{res} = \frac{1}{1/\epsilon_e + 1/\epsilon_r - 1} \tag{5.3.1}$$

which could also be expressed as:

$$\epsilon_{res} = \frac{\epsilon_e.\epsilon_r}{\epsilon_r + \epsilon_e - \epsilon_e.\epsilon_r} \tag{5.3.2}$$

where ϵ_e and ϵ_r are the emissivity of the emitting and receiving surfaces, respectively.

Throughout the literature, these expressions are mostly used to determine the resultant emissivity between a fire, or gas, and an exposed material surface. However, the expression in Equation 5.3.2 was used to determine the effective emissivity within each of the cavities in the FE models while incorporating the respective surface emissivities, as defined in Table 5.6. The cavity within the larger stud section of the test models comprised of the VP steel and FCB, which resulted in an effective cavity emissivity of 0.38 at $20°C$ and 0.67 at $420°C$, where the galvanizing on the steel sheeting start to melt. The cavity formed by the core, or flute section, of the samples consisted of the VP steel sheeting and the CaSi-board. Hence, the effective emissivity was determined as 0.4 at $20°C$ and 0.73 at $420°C$. The smaller stud cavity only consisted of the VP steel surface. Therefore, only the steel emissivity was used, as tabulated in Table 5.6.

5.3.4 Comparison of experimental and numerical results

Temperatures were determined from the FE models at the same locations at which the thermocouples were placed within each test sample. Due to the significant amount of data points obtained during the experiments, some of these locations with the same thermal behaviour were grouped together by taking the average temperatures of the specific location measurements. The groups included the average top surface (avgTop) and the average top stud (avgStudT) temperatures. Figures 5.12, 5.13, 5.14 and 5.15 shows the comparison of the results from the respective fire tests and the corresponding ABAQUS FE models. Each of the locations are represented by a specific colour, as seen in the figures. The dotted lines depict the numerical temperatures from ABAQUS, while the marked solid lines represent the fire test results, as discussed in Chapter 4.

In general, there is a good correlation between the numerical and experimental model temperatures for each of the four samples. The increase in temperature obtained in the FE models followed a similar trend to those measured from the fire tests. Also, the maximum temperatures reached at the end of the 60-minute fire exposure were similar for the experimental and numerical models.

The locations on the exposed side of the FE models accurately predicted those obtained in the test, with differences typically ranging between 5 and 12%, for all samples. The difference in temperatures obtained on the unexposed side of the samples ranges between 5 and 21%, in which the FE models slightly under predicted the temperatures for samples T1, T3 and T4.

The interior locations also yielded fairly accurate results, with temperature differences of approximately 10 to 20%, as seen for samples T1 and T2, which consist of the middle stud section. The temperatures obtained at location C1/C4 for samples T3 and T4 correlated reasonably well, in the order of 6%, as depicted in Figures 5.14 and 5.15. The simulation of the cavity radiation in these parts of the test samples was therefore fairly accurate and the assumed emissivities were appropriate. This is also evident in Figure 5.13 for locations B1/B4, for an average temperature difference of approximately 10%.

The temperature distribution for the respective FE models at the end of the test duration can be seen in Figure 5.9. From these distributions it can be noted that the temperature

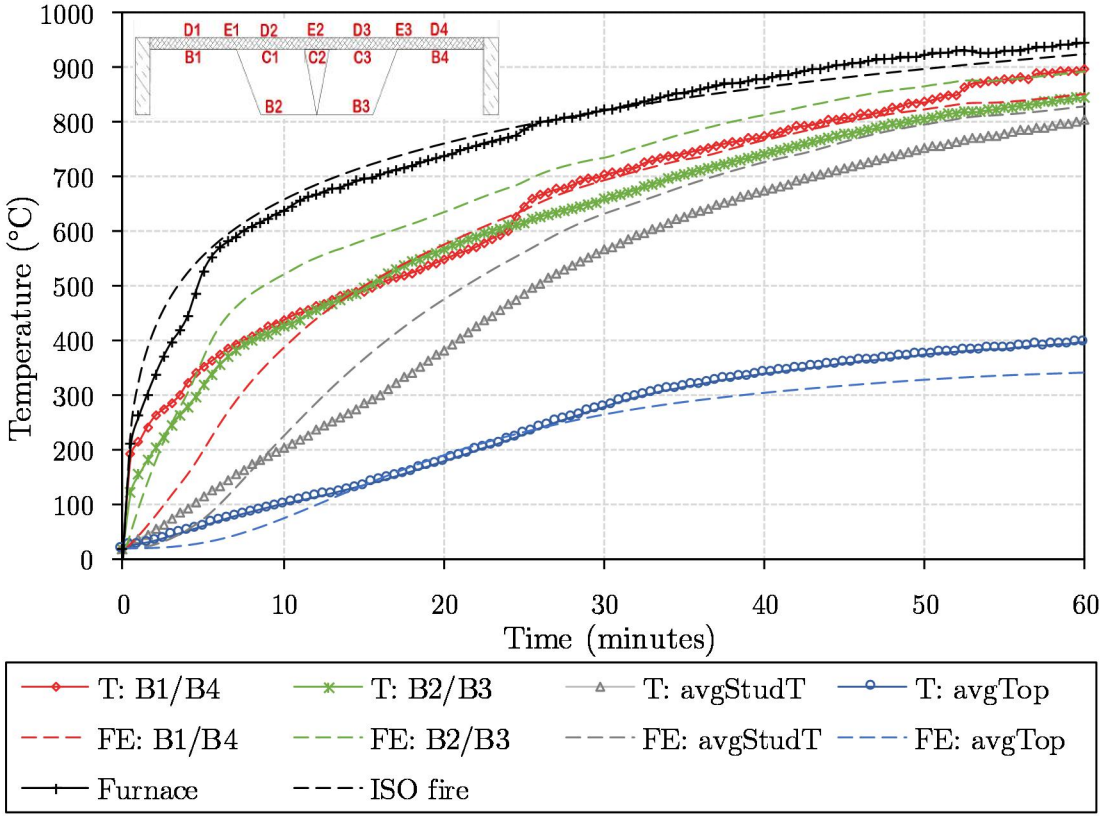

Figure 5.12: Comparison between test & ABAQUS results for sample T1

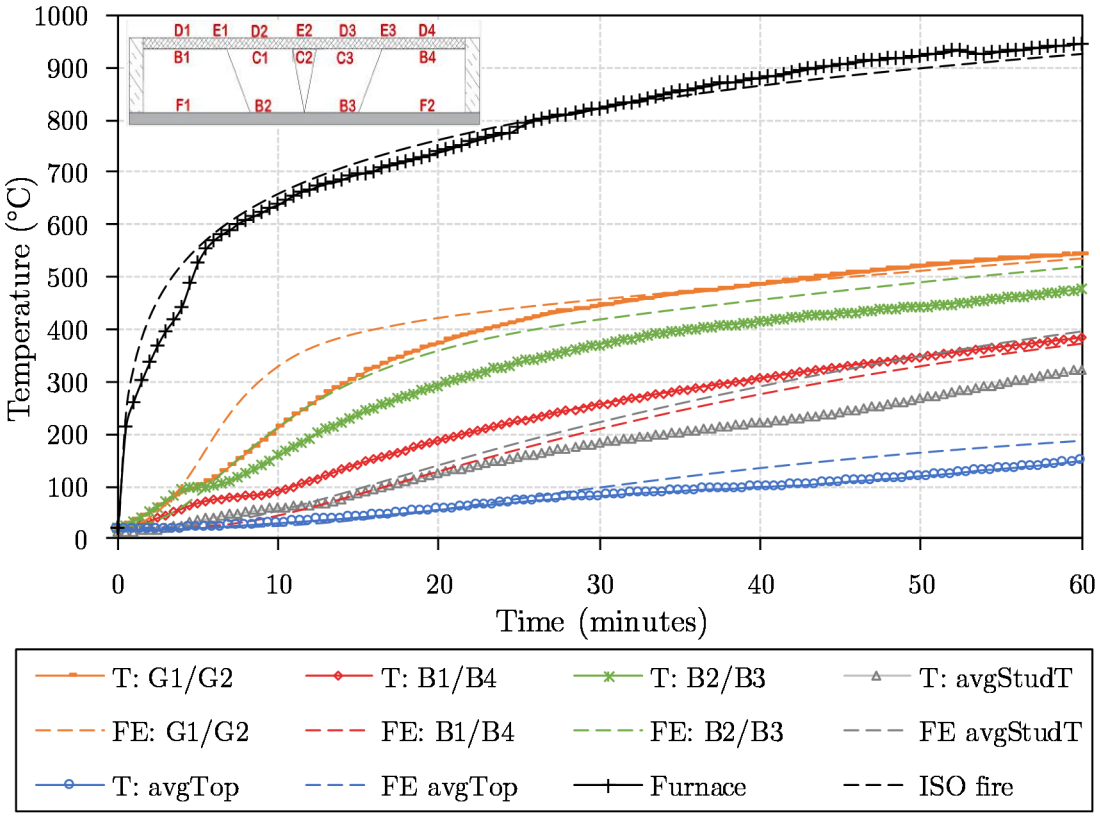

Figure 5.13: Comparison between test & ABAQUS results for sample T2

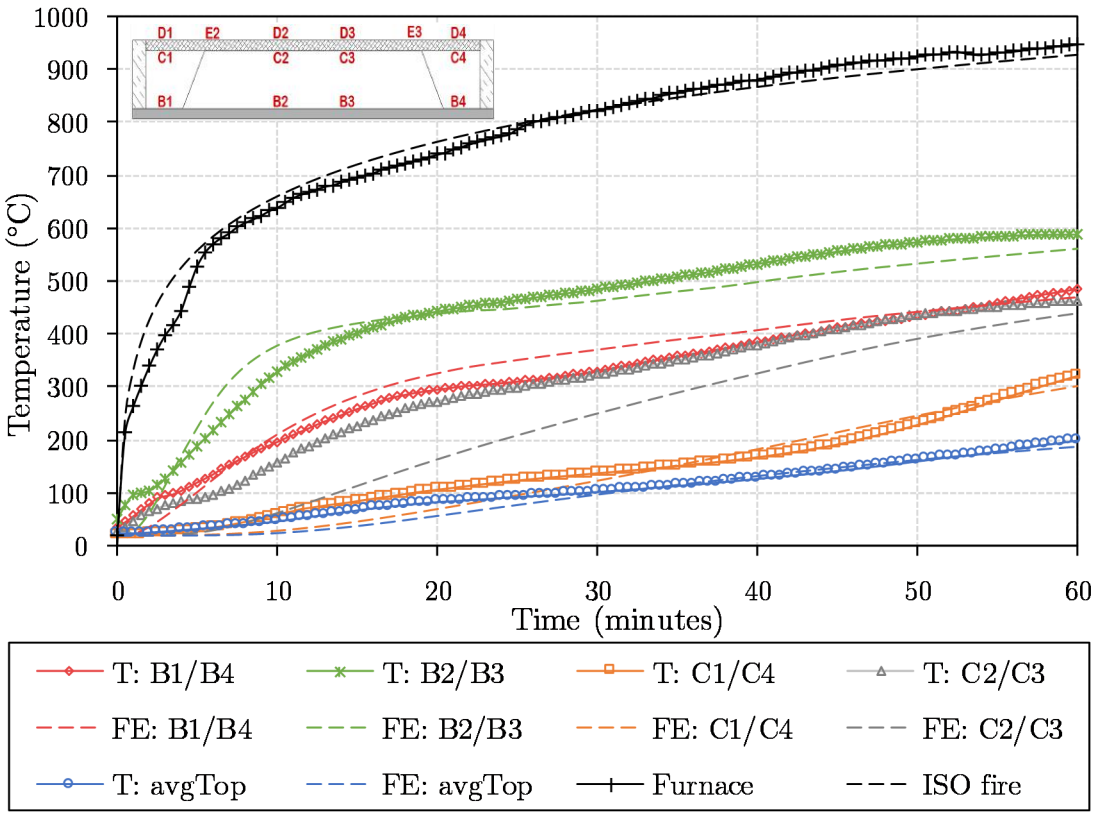

Figure 5.14: Comparison between test & ABAQUS results for sample T3

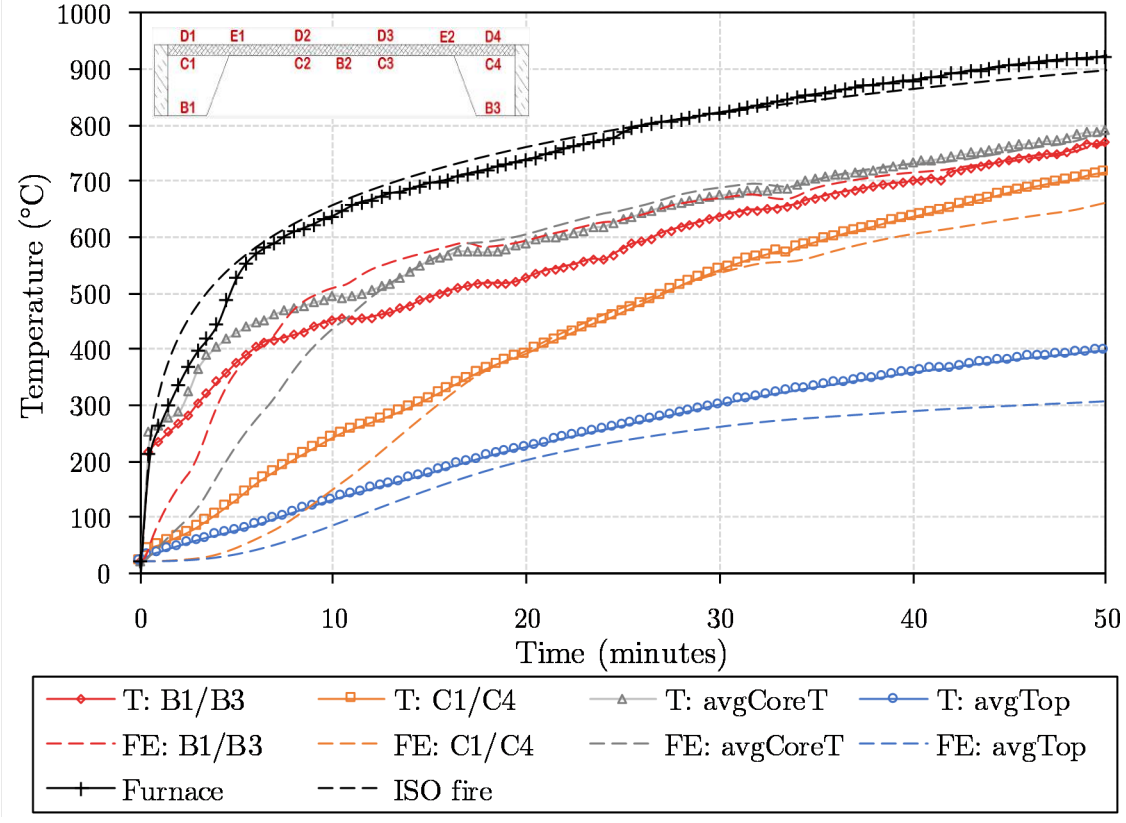

Figure 5.15: Comparison between test & ABAQUS results for sample T4

in the lower section of the gypsum boards for test samples T2 and T3 was higher than in the upper section. This agrees with the observations made during the fire tests, in which charring and ignition of the gypsum paper occurred on the bottom outer corners. This was due to the conductive heat transfer from the fire exposed CaSi-board into the lower part of the gypsum boards. Also, no change in colour occurred at the top section of the gypsum boards during the tests, which agrees with the relatively low temperatures, as seen at these locations for samples T2 and T3 in Figure 5.9. Appropriate thermal properties were therefore assumed, and the temperature distributions were accurately simulated.

However, localized variations occurred at some locations in the result comparison between the test sample and FE model. For sample T4 it was found that the FE models predicted lower temperatures within the first 10 to 15 minutes, as seen in Figure 5.15. Thereafter the FE model temperatures increased and correlated with the test results for the rest of the duration. The cold face (CF) temperatures obtained from sample T4 in the test were approximately 25% higher than for the corresponding FE model. This could be due to the uncertainties that existed in the assumed thermal properties for the insulation material, which included the CaSi, gypsum and fibre-cement boards. Also, numerous variables within the specific furnace configuration were unknown during the fire tests, which may have led to the slightly lower CF temperatures in the FE model.

Differences, in the order of 25 to 40%, were obtained for the average top stud (C1, C2, C3) and top core (C2, C3) temperatures, for sample T2 and T3, respectively. From Figure 5.14 it can be seen that the FE model predicted lower temperatures for the first 30 minutes when compared to the fire test measurement, with a temperature difference in the range of $110°C$. Thereafter the temperature difference gradually decreased to roughly 5% at 60 minutes. These temperature variations could be due to incorrect thermal properties of the ceiling and fibre-cement boards or due to the unique configuration of the steel profile. The increase in temperature of the bottom part of the steel sheeting could have caused the steel profile to experience thermal bowing, which was observed during the fire tests, as discussed in Section 4.2. It is possible that a small opening occurred between the two steel sheets that were joined together to form the middle stud section, thereby allowing more heat to be transferred to the upper layers through convection and radiation. Another reason for the slight variations could be that the heat from the furnace was not evenly distributed over the bottom surface of the test samples, particularly for sample T2, which was noted after the test was conducted. The area at which the furnace fire was concentrated was shown in Figure 4.11a. This may have resulted in a lower overall temperature distribution across and through sample T2. Hence, the FE model predicted slightly higher temperatures at the inner top layer of the stud section, as discussed above.

The FE analyses of the test models simulated ideal conditions, specifically with regards to the contact between the various materials. The "Tie" constraints that were used in the FE models represented perfect contact and conduction between the material surfaces. However, small air gaps may have occurred between the materials that were in contact with each other, due to irregular surface shapes or insufficient fixing. Although the conduction across the small gap would be negligible, the gap radiation would have a considerable influence on the surface temperatures (Feng *et al.*, 2003). Therefore, these small imperfections may have caused some variability in the surface temperature results in the four test samples.

5.4 Concluding remarks on the validation of FE models

Various validation studies were performed in this chapter to determine the suitability of ABAQUS (Dassault Systémes, 2015) for the simulation of heat transfer through various structural systems. During the three initial validation studies, a thorough understanding of heat transfer modelling was gained, which included convective, conductive and radiative heat transfer parameters. Thereafter, FE models representing the four test samples were developed for comparison with the results obtained from the fire tests, as discussed in Chapter 4.

The validation studies included investigations that were performed by Jeffers *et al.* (2013), Feng *et al.* (2003) and Schaumann and Hothan (2002), all of which incorporated the modelling of cavity radiation that occurs within voids. Good correlations were obtained between the results from the FE analyses performed by the author of this thesis and those from the respective original authors. The temperature results were presented in Sections 5.2.1, 5.2.2 and 5.2.3 for the insulated steel section, cold-formed steel wall panel system and the slim-floor beam system, respectively. It should be noted that in the tests where experimental data was used there was a variation in predicted results vs. test measurements, as also observed in this work.

The fire test FE models were discussed in Section 5.3 and are depicted in Figure 5.9. The crucial heat transfer modelling issues were discussed, which included the thermal boundary conditions and the material thermal properties. The emissivity of 0.8 specified by the Eurocodes caused a significant over-prediction of temperatures throughout the test samples. It was found that an emissivity of 0.3 for the exposed surface was appropriate, as it resulted in reasonably good correlations for the FE models. This relatively low emissivity value was also used by authors Feng *et al.* (2003) in their experimental validation study. The emissivity of the unexposed surfaces were based on the specific material emissivity values, as specified in Section 5.3. General convection coefficients of 25 and 10 W/m^2K were applied to the exposed and unexposed surfaces, respectively. The ambient temperatures and the cavity radiation parameters were also discussed, along with the configuration factors for test sample T1 and T4.

From the results presented in Figures 5.12, 5.13, 5.14 and 5.15, it was seen that generally a good correlation between the numerical FE model and experimental sample temperature results is observed. The temperatures on the exposed side of the test samples typically differed by only 5 to 12%, while on the unexposed side a variation between the different results of 5 to 21% was obtained. The interior locations, such as the top stud layers for sample T3 and T4 also correlated well, with a difference of approximately 6%. Observations that were made during the fire tests were also justified by noting the temperature distribution through the test samples at 60 minutes, as depicted in Figure 5.9. Here it could be seen that the lower part of the gypsum board reached temperatures of approximately 200 to 300°C for the ceiling board models and roughly 400°C for the models without a ceiling board. This agreed with the charring, discolouring and burning of the gypsum board paper that were observed during the fire tests.

Some variations in temperatures were found between the FE models and the test results.

However, this only occurred at certain locations within the samples. Reasons for the variation in results include the uncertainty of material thermal properties, which has a significant influence on the thermal performance of a structural system. Also, thermal bowing occurred during the tests, which could have resulted in some layers losing contact with one another. The conduction and radiation transfer modes may, therefore, have been influenced.

Nonetheless, relatively good correlation existed between the experimental and numerical results, whereby the trends of temperature increase were accurately predicted from the ABAQUS models. Hence, the modelling parameters and the simulation of the conduction and cavity radiation through the system accurately represent the thermal behaviour of the fire test samples, while taking the shielding effects of the unique geometries into account.

Through the various validation case studies and the verification of the FE test models, it was found that ABAQUS can be used to perform heat transfer analyses on various structural assemblies. However, care should be taken when defining the input parameters, due to the significant influence they can have on the results of an FE analysis, such as the thermal material properties and heat transfer parameters. The knowledge that was gained in this chapter will now be used to develop larger FE models for the sandwich floor system in the structure that was introduced in Chapter 1.

Chapter 6

Thermal Finite Element analysis of sandwich floor system

6.1 Introduction

Large-scale fire testing provides significant insights into the thermal and structural behaviour of real structures, but tests can be expensive and usually require a significant amount of resources. The Finite Element Method (FEM) provides a way to analyse full-scale structures and to predict temperatures, deflections and stresses under a variety of circumstances, for a significantly reduced cost. ABAQUS (Dassault Systémes, 2015) was therefore used in this thesis to simulate the thermal performance of the sandwich floor system in the full-scale structure, which was described in Section 1.1.2. The aim is to predict the temperatures through the floor system, but most specifically the steel beam and inner floor temperatures. The predicted temperatures can then be used to evaluate the structural system in terms of the integrity and insulation failure criteria, as discussed in Section 2.3.2. The valuable information obtained from the FE analyses will aid in the planning and design of the full-scale fire test that will be performed on the cellular beam structure (CBS) in the future. The temperatures predicted in this thesis were used in the structural FE modelling of the CBS, as discussed in the thesis of Kloos (2017).

This chapter contains a detailed discussion on the development of the FE models representing the sandwich floor system and the cellular steel beams within the voids, along with the temperature results obtained. The FE beam models are used to simulate the heat transfer through the various material layers, while incorporating the relevant parameters, such as thermal properties, boundary conditions and interactions of the various surfaces and cavities. The temperatures of the cellular steel beams were determined, along with the average inner floor temperature for insulation purposes.

6.2 Development of FE models

The FE beam analyses in this thesis were performed by using 4-node linear heat transfer quadrilateral elements (DC2D4). These elements are the default element type for the simulation of 2D diffusive heat transfer models in ABAQUS (Dassault Systémes, 2015).

An illustration and a brief overview of the cellular beam structure (CBS) was shown in Figure 1.1 and discussed in Section 1.1.2. Also included, was the general configuration of

the various layers within the sandwich floor system. The sandwich floor consists of two different cellular beam configurations for the primary and secondary beams. The ceiling layers within each bay are carried by two hot-rolled C160x65 beams, which are referred to as the channels. These channels are connected to the secondary beams with knee-braces, which are C100x50 channel cross-sections. The secondary beams are built-up cellular beams that are supported by the primary cellular beams, which in turn, are supported by the columns. The secondary cellular beams consist of a cross-section in the form of the letter J, to which an additional angle is welded during the assembly process. Although the additional angle that is welded to the J-beam results in a I-shaped beam, the secondary beam will be referred to as the J-beam. The angle has no significant influence on the structural behaviour. However, the angle can shield some of the radiation in the floor cavities, which can influence the steel temperature results significantly. Therefore, the angle will be analysed with the J-beam. The primary beam and the channels are referred to as the P-beam and C-beam, respectively. Detailed drawings on the various CBS elements are provided in Appendix C.

The secondary cellular beams (J-beams) are level with the bottom of the Bond-Dek sheeting, while the primary cellular beams (P-beams) are situated on top of the Bond-Dek. Two different FE models were therefore developed to determine the temperatures in the two beams. An additional FE model was developed for the channels (C-beams), which was also situated on top of the Bond-Dek profile. Figure 6.1 depicts the lower configuration at the cellular beams within the sandwich floor.

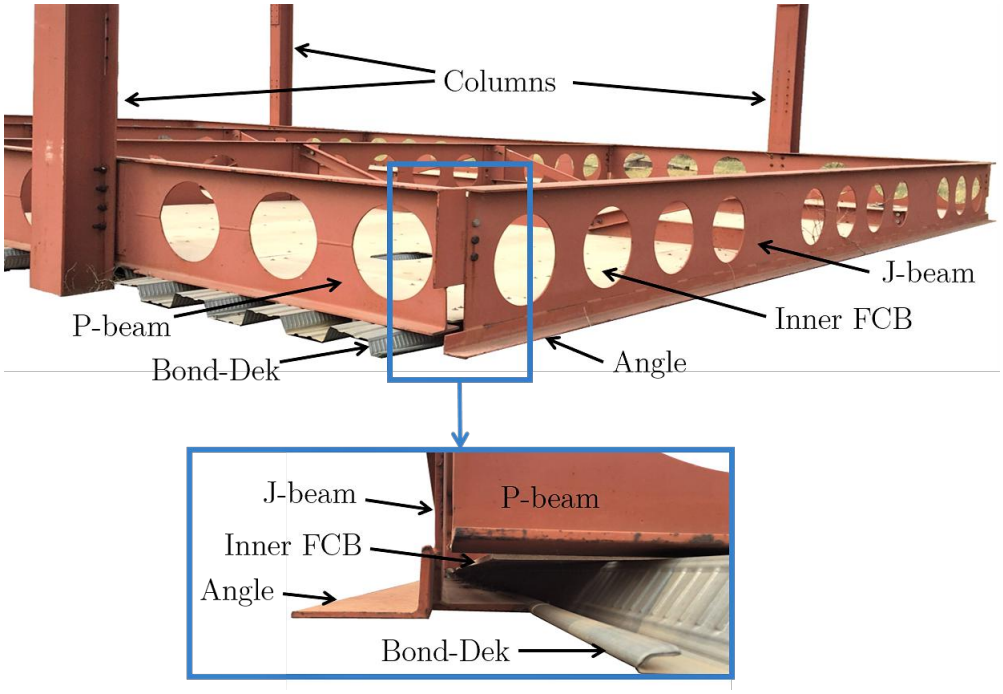

Figure 6.1: Sandwich floor beam configuration

The FE beam models were developed in a similar manner to that of the fire test samples, as discussed in Section 5.3. However, some of the input parameters, such as the heat transfer coefficients and thermal material properties, have been adjusted due to the difference in geometry of the steel decking system and the material that was used for the actual ceiling, namely gypsum type X. These parameters were based on the initial

"prototype" specifications of the CBS, which includes the 0.8 mm Bond-Dek sheeting, a 15 mm gypsum type X ceiling board and a 9 mm FCB on the inner floor layer, as well as on the top of the floor system. However, this chapter identifies shortcomings in the specifications, such as the required ceiling board thickness to satisfy the insulation and integrity criteria. These shortcomings are then addressed in Chapter 7, where the parametric investigation highlights what should be done.

The FE models in Section 5.3 simulated the heat transfer through the fire test samples in the furnace, which consisted of different surrounding environment conditions than those present in a real fire scenario. Some of the input variables for the work developed in this chapter are, therefore, different in the larger FE beam models of the sandwich floor system. The input parameters for the FE beam models are discussed below in Section 6.3.

Figures 6.2, 6.3 and 6.4 depicts the FE model configurations for the secondary beam (J-shaped), primary beam (P-beam) and C-beam (channel), respectively. Full sandwich floor cross-sections were used during the two-dimensional (2D) FE analyses to obtain a continuous distribution through the height of the cross-section of the cellular beams. For the J-beam model, the profiled cross-section of the Bond-Dek was included. However, for the P-beam and channel models the orientation of the decking is perpendicular to the cross-section of the beams. Therefore, the profiled shape of the Bond-Dek was not directly considered, but rather two separate 2D analyses have been performed, for each of the P-beam and channel models. This account for when the decking trough is against the ceiling board, and when the decking flute is against the bottom beam flange.

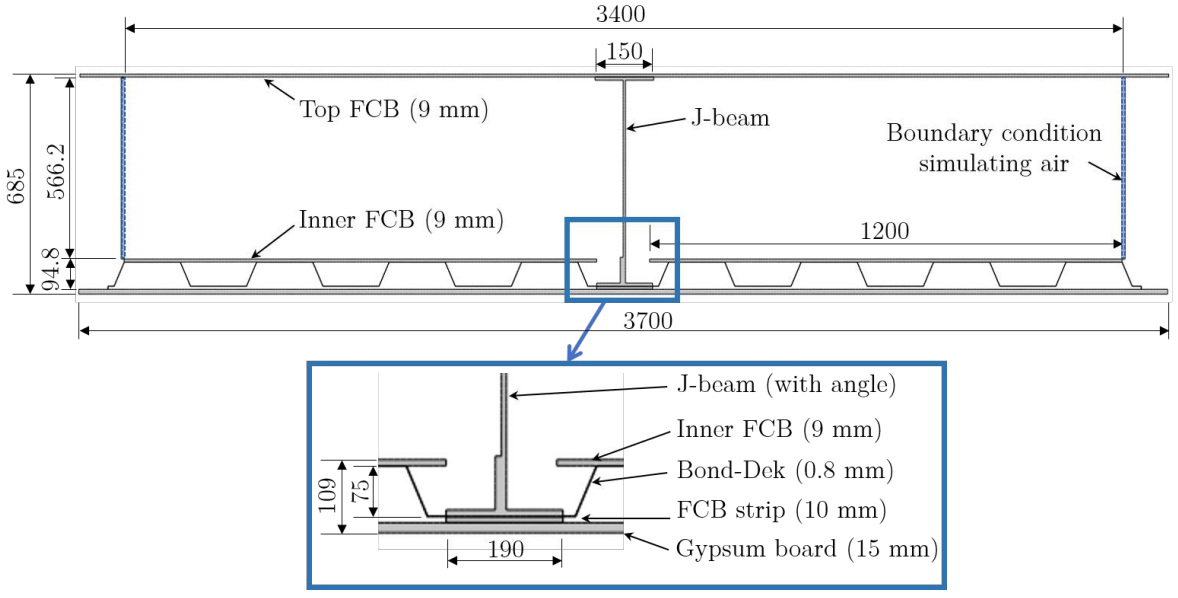

Figure 6.2: FE model configuration for J-beam

In reality the floor voids are closed off by the surrounding beams and insulation boards. Radiative heat transfer then heats up the various surfaces within the cavity. In order to utilize the cavity radiation functionality in ABAQUS, additional boundary conditions were added to the open ends of the beam models. Therefore, a non-uniform temperature distribution can be simulated within the voids, as opposed to a constant cavity temperature. These boundary conditions were modelled as edge layers, which were created as

separate 2D shell parts, to form a closed cavity. The thermal properties of air were assigned to these material layers to minimize the effect it has on conduction and convection at the edges, thereby simulating the cavity radiation as accurately as possible.

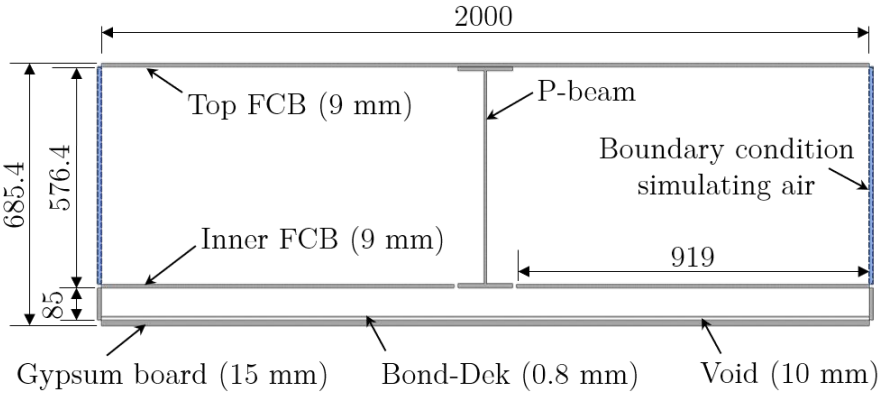

(a) P-beam (Bottom Bond-Dek section)

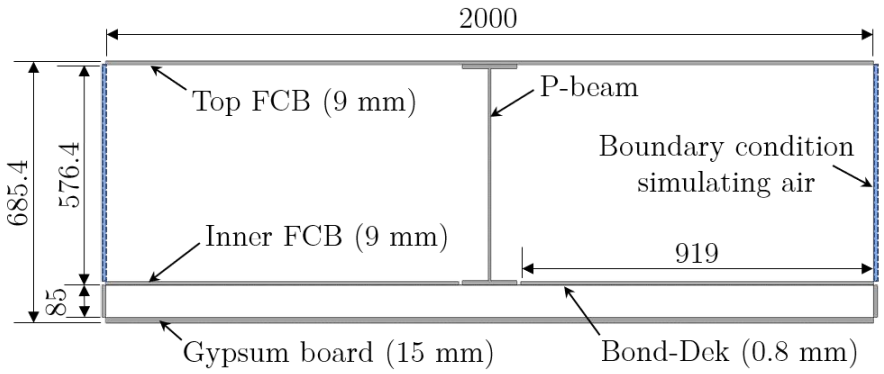

(b) P-beam (Top Bond-Dek section)

Figure 6.3: FE model configuration for P-beam analyses

The cellular beam structure (CBS) contains a steel strip that holds the steel sheeting in place directly underneath the C160x65 channels, which can have an influence on the heat transfer through the floor system. This 100 x 10 mm steel strip was therefore also included in the FE analyses for the C-beam models, as shown in Figure 6.4.

Preliminary FE analyses on the J-beam model highlighted that there was insufficient thermal protection to the bottom flange of the J-beams. Therefore, the bottom part of the floor system was adjusted by including an additional 10 mm thick fibre-cement board strip along the length of the bottom flange of the J-beam. The strip was situated in between the bottom flange and the ceiling board, as shown in Figure 6.2. The additional insulation strip reduced the amount of conductive heat transfer into the bottom flange. Also, the strip created a small gap of air between the ceiling board and the Bond-Dek sheeting, which significantly reduced the heat conducted into the sheeting from the ceiling board. This, in turn, results in lower inner floor temperatures.

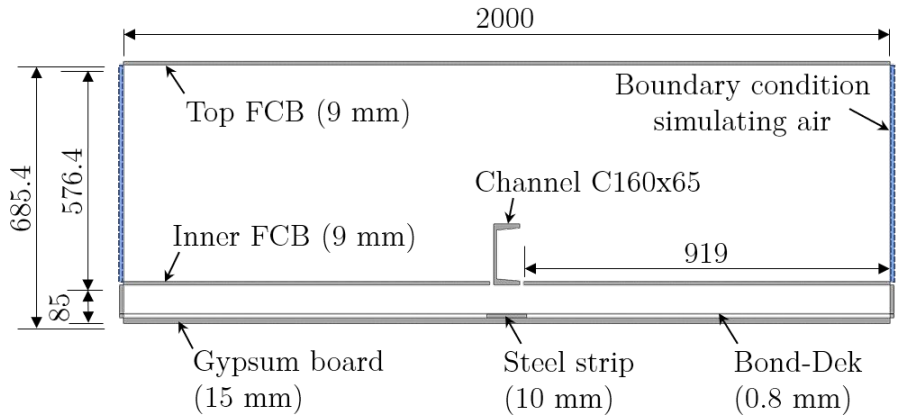

(a) P-beam (Bottom Bond-Dek section)

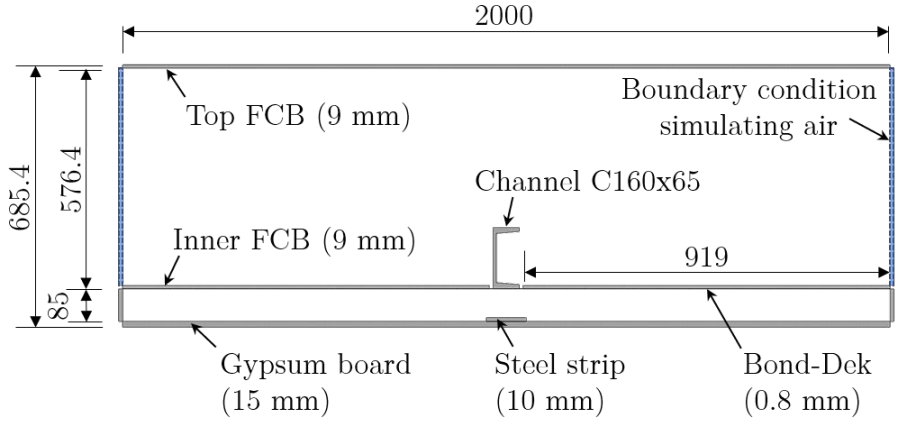

(b) P-beam (Top Bond-Dek section)

Figure 6.4: FE model configuration for P-beam analyses

6.3 Input parameters for FE beam models

The accuracy of FE models depend on various factors, such as those discussed in Section 2.7.6, which includes the input parameters defined by the user. The general input parameters used in this thesis for all three FE beam models are presented in this section, which includes the element type, material thermal properties, thermal boundary conditions and interactions and the mesh configuration. Although most of these parameters remain constant between the various beam models, the thermal interactions for each individual model was different due to the geometric differences.

6.3.1 Model & element description

The sandwich floor system has been modelled in a two-dimensional (2D) space, for each of the three FE beam models. As discussed in Section 5.3.1, 2D modelling allows for shorter computational durations, while yielding accurate results.

All of the FE beam analyses were performed by using shell elements, which only consisted of the cross-sectional geometry for the 2D case. These elements were sufficient for simulating the heat transfer through the floor system, while assuming a constant heat

distribution across the depth of the section. The thermal properties that were assigned to the respective material layers within each of the beam models are discussed below.

6.3.2 Material properties

In practice the material properties of the various elements could range depending on what products are utilised. For the purposes of this research, the properties were assumed to be similar to those found in the literature, which were discussed in Chapter 5. It would be necessary to ensure that products specified for the construction of the CBS system provide a similar thermal performance to those specified in this work, or the model would need to be adjusted based on the modified parameters. The thermal properties for the cellular steel beams and the Bond-Dek steel sheeting were based on the values specified for steel in the Eurocodes, as discussed in Section 2.7.2. These properties were also used for the FE validation studies in Chapter 5. Both the inner and top fibre-cement boards were assigned similar material properties to those used for the validation of the small-scale fire test FE models, which were presented in Table 5.5.

The gypsum type X ceiling-board has a higher fire resistance than conventional gypsum boards, as discussed in Section 2.7.4, due to the significant difference in their thermal properties. The specific ceiling-board has not yet been finalised for the cellular beam structure. Therefore, the thermal properties for the gypsum board in the FE beam models were assumed to be similar to those used by Feng *et al.* (2003), which were presented in Table 5.4 in Section 5.2.2. The thermal properties of the material that represented the air layer at the edges of the beam models were based on the values provided in Table A.23 of the SFPE Handbook of Fire Protection Engineering (Hurley *et al.*, 2016). The thermal properties of all the materials used in the thermal analyses for the FE beam models are summarised in Table 6.1.

Table 6.1: Thermal properties of FE beam model materials

Material name	Density ρ (kg/m^3)	Conductivity k (W/mK)	Specific heat c_p (J/kgK)
Steel	7850	$54 - 3.33 \times 10^{-2}\ \theta$ at $(20°C \leq \theta \leq 800°C)$ 27.3 at $(800°C \leq \theta \leq 1200°C)$	$425 + 0.773\ \theta - 1.69 \times 10^{-3}\ \theta^2 + 2.22 \times 10^{-6}\ \theta^3$ at $(20°C \leq \theta < 600°C)$ $666 + \frac{13002}{738-\theta}$ at $(600°C \leq \theta < 735°C)$ $545 + \frac{17820}{\theta-731}$ at $(735°C \leq \theta < 900°C)$ 650 at $(900°C \leq \theta \leq 1200°C)$
Fibre-cement board (FCB)	1400	0.19	2500
Gypsum - Type X	727.1	0.2 at $10°C$ 0.218 at $150°C$ 0.103 at $155°C$ 0.3195 at $1200°C$	925.04 at $10°C$ 941.5 at $95°C$ 24572.32 at $125°C$ 953.14 at $155°C$ 1097.5 at $900°C$

With θ as the surface temperature in $°C$.

The radiative heat transfer between materials depends on the emissivity of a surface. The surface emissivities of the materials used in the FE beam models were discussed and summarized in Table 5.6 in Section 5.3.2.

6.3.3 Boundary conditions and thermal interactions

The boundary conditions of the FE beam models were defined on the outer and inner surfaces of the floor system. The main boundary condition is that of the ceiling boards, which are directly exposed to a fire in any given compartment. The ceiling boards play a crucial role in protecting the upper floor layers, such as the steel beams and services.

A worst-case scenario was also considered, in which the ceiling board was neglected during the FE beam analyses. The aim was to simulate what would happen if the ceiling board detached during a fire, which can be a result of structural integrity failure of the gypsum board. Although this case is unlikely to occur, these analyses gave an indication of the elevated steel temperatures that can be expected, along with the structural behaviour of the steel members within the CBS. The FE models with and without the ceiling board are denoted by "C" (ceiling) and "noC" (no ceiling), respectively.

An ambient temperature of $20°C$ was assumed for each of the FE models. The ambient temperature was applied to all surfaces within each model as a predefined field variable. This was defined in the initial step of the FE analyses. The heat transfer through the sandwich floor system was simulated, whereby a one-hour standard fire was applied to the exposed side of the ceiling surface. The duration of the fire was based on the required fire resistance rating for three to ten storey office buildings, according to SANS 10400-T (SABS, 2011), as discussed in Section 2.3.2 and shown in Table A.1 in Appendix A.

The 60-minute standard fire was applied in a similar manner as was done for the test verification models, as discussed in Section 5.3. The standard temperature-time history was added as an amplitude in the FE model (refer to Equation 2.3.1 and Figure 2.4). This amplitude was used as an input temperature for the convective and radiative heat transfer interactions, respectively, on the exposed side of the gypsum ceiling-board. Convection was applied as a surface film condition with a heat transfer coefficient of 25 W/m^2K, as prescribed by EN 1991-1-2 (CEN, 2002). An emissivity value of 0.7 was assumed for the radiative heat transfer from the standard fire exposure.

The various material surfaces that were in contact with each other were connected by using the "Tie" constraint, similar to the FE analyses in the validation studies, which were discussed in Chapter 5. The purpose of the air material on the sides of the FE beam models were only to form a closed cavity for the view factor calculation during the FE analyses. Therefore, no ties were assigned to the contact surfaces between these air materials and the rest of the sandwich floor layers to prevent additional heat being conducted.

The convective and radiative heat transfer modes were modelled by defining them with their respective parameters in the interaction module for the heat transfer time step. These parameters, which includes the convective heat transfer coefficient and the emissivity, varied significantly through the beam model cross-sections. Only radiative heat transfer was taken into account on the inside of the sandwich floor system, by means of cavity radiation, due to the negligible influence of the convective heat transfer within the voids. The various heat transfer boundary condition interactions for the J-beam, P-beam and C-beam models are discussed below.

6.3.3.1 J-beam model interactions

In the floor system three different cavity sections have been specified to model the air voids in the system, as shown in Figure 6.5. Different emissivities were then applied to the respective cavity surfaces. The three cavities are the bottom-cavity, inner-cavity and the beam-cavity. The bottom cavity consists of the void between the gypsum ceiling-board and the bottom surface of the Bond-Dek sheeting, while the voids between the Bond-Dek sheeting and the inner fibre-cement board (FCB) are referred to as the inner cavity. The large void that contains the steel beam with the top FCB layer and the top surface of the inner FCB are denoted as the beam-cavity. The surrounding surfaces for the bottom, inner and beam cavities are depicted in Figure 6.5 in blue, green and red, respectively.

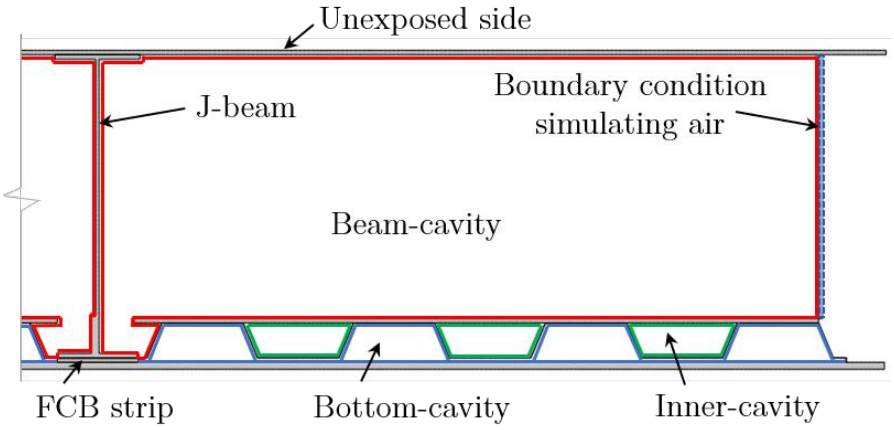

Figure 6.5: Voids for cavity radiation in J-beam FE model

The cavity radiation in the FE beam models was incorporated in a similar manner to that of the test verification models in Chapter 5. Equation 5.3.2 was used to determine a resultant emissivity value within each cavity by taking the emissivities of the various material surfaces into consideration. An emissivity of 0.8 was assumed for the gypsum board and the steel beams (ECCS TC3, 2001), while a value of 0.9 was used for the fibre-cement boards, as discussed in Section 5.3. The bottom and inner cavities contained Bond-Dek sheeting, for which the emissivity changes from about 0.42 to 0.8 after the galvanized coating melts off at about $420°C$, as discussed in previous chapters. The resultant emissivities for the J-beam model cavities are summarised in Table 6.2.

Table 6.2: Cavity emissivities for FE beam models

Cavity	ϵ	T ($°C$)
Bottom	0.38	20
	0.67	420
Inner	0.4	20
	0.73	420
Beam	0.73	20

The interactions on the unexposed side of the top FCB included a heat transfer coefficient of 4 W/m^2K with an emissivity of 0.9, which were applied as a surface film condition and a surface radiation in the heat transfer time step, respectively. These values are recommended by the Eurocodes (ECCS TC3, 2001). The air material at the ends of the sandwich floor model allowed heat to be transferred through convection with a heat transfer coefficient of 9 W/m^2K.

6.3.3.2 P-beam and C-beam model interactions

Two FE models were developed for both the P-beam and C-beam, as discussed above and shown in Figures 6.3 and 6.4. Average temperatures were obtained by combining the results from the two respective FE analyses for each of the two beam sections.

The cavity radiation was modelled in a similar manner to that of the J-beam model, with the different void characteristics. The P-beam model with the bottom Bond-Dek section included the bottom cavity, which comprised of the top surface of the gypsum board and the bottom surface of the Bond-Dek sheeting. The inner cavity above the sheeting included the bottom flange of the steel beam and the inner FCB surfaces, which also formed part of the larger beam cavity. The top Bond-Dek section P-beam model only comprised of the bottom cavity between the sheeting and ceiling board and the larger beam cavity. The emissivities that were applied to the various cavity surfaces were specified in Table 6.2.

6.3.3.3 No-ceiling model interactions

The standard fire curve was directly applied to the bottom surface of the Bond-Dek sheeting for the "no ceiling" models. The temperature-time relationship was applied by incorporating three different view factors, due to the non-uniform exposed surface of the Bond-Dek. The product of the configuration factor and emissivity for each surface was determined in an equivalent manner to the method discussed in Section 5.3.3.1, in which Equation 2.6.5 was used to determine the configuration factor.

The bottom surface of the sheeting was assigned a configuration factor of unity, due to the direct exposure to the fire. The radiative heat transfer to the side and top surfaces in the flutes of the sheeting are slightly blocked by the lower section of the sheeting. The configuration factors determined were 0.64 and 0.81 for the side and top surfaces, respectively. These configuration factors were multiplied by the surface emissivity of the sheeting, which is 0.42 at $20°C$ and jumps to 0.8 at $420°C$, due to the melting of the galvanizing. However, an average value was determined, as only a constant emissivity value can be used when defining surface radiation in ABAQUS. However, as discussed in Section 5.3 this does not have a significant influence on calculated temperatures. The product of the configuration factor and emissivity for the bottom surface, side surface and the top surface of the sheeting were determined as 0.6, 0.4 and 0.5, respectively.

The convective heat transfer coefficient on the exposed surface was taken as 25 W/m^2K, as discussed for the previous FE models. The cavity radiation is modelled similarly to the "ceiling" models, as discussed above for the beam-, inner- and bottom-cavity. The heat transfer parameters used in the boundary interactions for the unexposed surfaces were also similar to the models with the ceiling board.

6.4 Sensitivity analysis of the beam-cavity radiation

From previous investigations, such as the numerical validation studies and the test verification modelling in Section 5.3, it is evident that cavity radiation has a significant influence on the thermal performance of structural floor systems. Due to the significant number of variables that exist within the sandwich floor system of the CBS, the exact emissivity of the beam cavity is unknown. A sensitivity analysis was therefore performed on the emissivity value of the beam cavity, as presented in Figure 6.5.

A series of FE analyses were performed, in which the emissivity of the cavity surfaces was varied. Figures 6.6 and 6.7 depicts the J-beam and inner FCB temperatures obtained for a surface emissivity of 0.5, 0.6, 0.8 and 0.9, respectively, for the bottom flange (BF), lower web (LW), upper web (UW) and the top flange (TF). A significant variation in predicted temperatures is observed for the upper flanges when surface emissivity values are varied. Cavity radiation, therefore, did not have a significant influence on the bottom flange of the beam section. This is due to conduction having a much greater influence on results. Also, the Bond-Dek sheeting has a shielding effect on the lower part of the beam. The upper web and top flange have limited shielding within the beam-cavity and are therefore more susceptible to cavity radiation. The difference in temperatures due to the varying emissivities ranged between 18 and 20% for the upper beam section, while less than 6% differences were obtained in the lower beam temperatures.

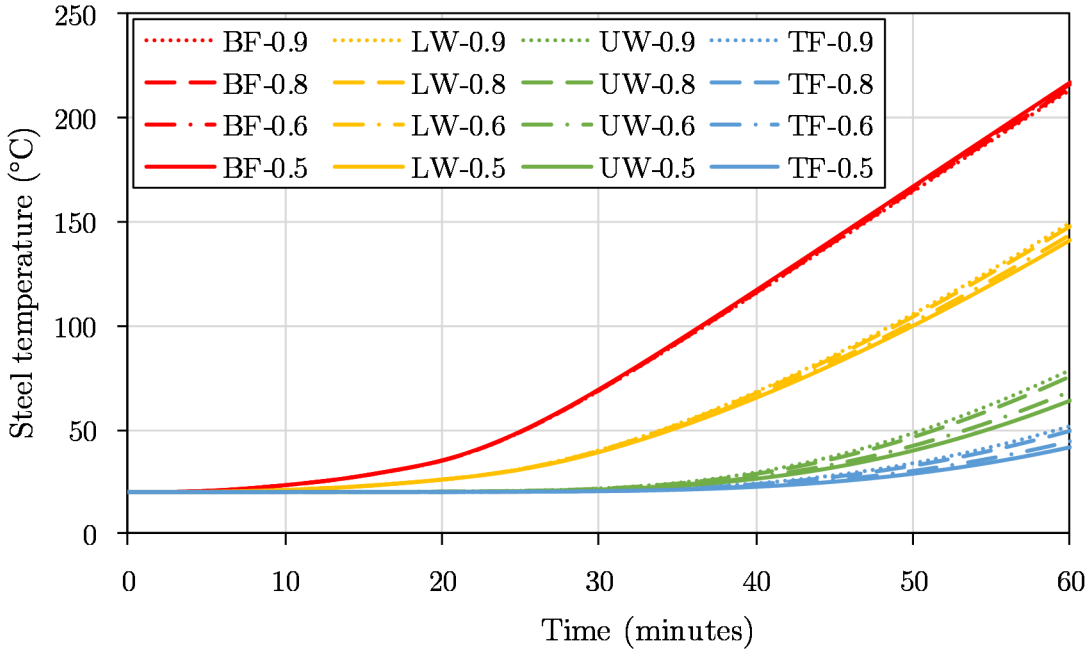

Figure 6.6: Steel temperatures of J-beam model with various beam-cavity emissivities

A similar effect is noticed in Figure 6.7 for the average inner FCB surface temperature. A higher FCB surface emissivity results in more heat being emitted from the FCB into the cavity and surrounding surfaces. The inner FCB surface temperature is approximately $20°C$ higher for an emissivity of 0.5, compared to 0.9. Consequently, for the beam temperatures, a surface emissivity of 0.5 resulted in slightly lower temperatures when compared to an emissivity of 0.9. A temperature difference of $10.2°C$ and $14.7°C$ were noted from

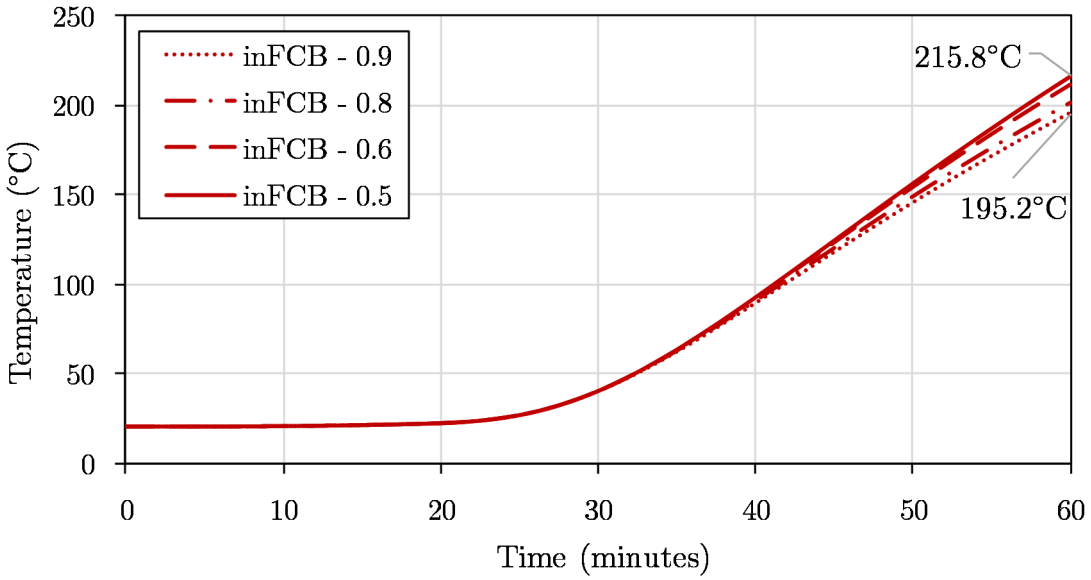

Figure 6.7: Inner FCB temperature for J-beam with various beam-cavity emissivities

Figure 6.6 for the top flange and upper web, respectively. Therefore, the higher the emissivity, the lower the temperature will be of the emitting surface and the higher the temperature will be for the receiving surfaces. From Figure 6.7 it can be seen that the temperatures for the various emissivities start to vary only from about 40 minutes of standard fire exposure, which is approximately at $80°C$. Thereafter the correlation between the temperatures decreases until the end of the analysis. This shows that the effect of cavity radiation is more dominant at higher temperatures.

In this work a surface emissivity of 0.73 has been specified for the beam cavity, based on the parameters specified in Section 6.3.3. From the results above, it can be observed that even if the emissivity in real structures does vary within the range of 0.5-0.9 (although more probable to be near the calculated value), results will not be significantly different from those predicted.

6.4.1 Mesh configuration

A structured mesh was used for the quadrilateral elements within the insulation boards and steel beams, which ensures a neat square mesh configuration. For the Bond-Dek, the structured technique resulted in some elements being distorted. Therefore, a free mesh technique with a medial axis algorithm was used to overcome this issue, after which the distortion was reduced by minimizing the mesh transition (Dassault Systémes, 2015).

Mesh configuration has a significant influence on the accuracy of results of FE analyses. A smaller seed size yields more accurate results, due to the larger number of elements and hence, a larger number of element nodes. However, a finer mesh requires a longer analysis duration, which limits the amount of analyses that can be performed. A sensitivity analysis was therefore performed to determine a seed size that can be analysed in a relatively short amount of time, while yielding accurate results.

The P-beam model was used to analyse the effect of different mesh sizes. Three analyses

were performed, in which the element seed size of the ceiling board was varied between fine (5 mm), medium (10 mm) and coarse (20 mm). The average temperatures in the bottom flange (BF), lower web (LW), upper web (UW) and the top flange (TF) are depicted in Figure 6.8.

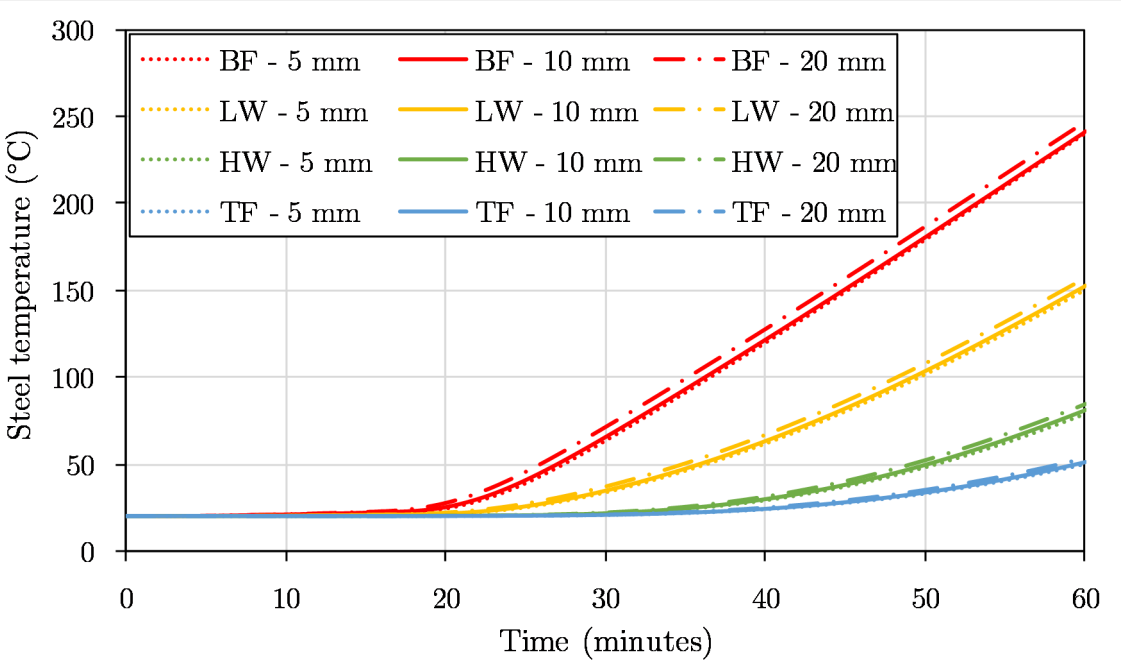

Figure 6.8: P-beam temperatures for different mesh sizes

It can be noted that the difference between the temperatures for the fine and the medium mesh are negligible at all four locations within the beam. The coarse mesh yielded slightly higher temperatures of about $8°C$ more in the bottom flange. The medium mesh, with seed size of 10 mm, has thus been chosen for the ceiling board in the FE analyses performed in this thesis, due to the good accuracy and relatively short analysis duration. The seed size for the rest of the material layers were kept constant throughout all of the FE beam analyses. The mesh sizes are summarized in Table 6.3. It should be noted that each element in the mesh consists of integration points. For these FE models, one element contains four temperature points.

Table 6.3: FE beam models mesh configuration

Material	Seed size
Gypsum (ceiling)	10 mm
J - beam	4 mm
P - beam	5 mm
C - beam	5 mm
Bond-Dek sheeting	4 mm
Inner FCB	4.5 mm
Top FCB	10 mm
Air material (sides)	1000 mm

The element seed size for the steel beams was chosen as shown above to ensure a mesh with two elements across the flange and web thickness, in order to obtain accurate results through the beam cross-sections. For a similar reason, the 9 mm inner fibre-cement board (FCB) were meshed with a seed size of 4.5 mm. The Bond-Dek sheeting with a thickness of 0.8 mm was meshed with a relatively small seed size of 4 mm. The number of elements in the top FCB and the air material on the sides was not as crucial during the simulation of heat transfer by conduction, which allowed for a larger seed size to be used. The general mesh configuration for the J-beam model is presented in Figure 6.9, which is similar for the P-beam and C-beam models.

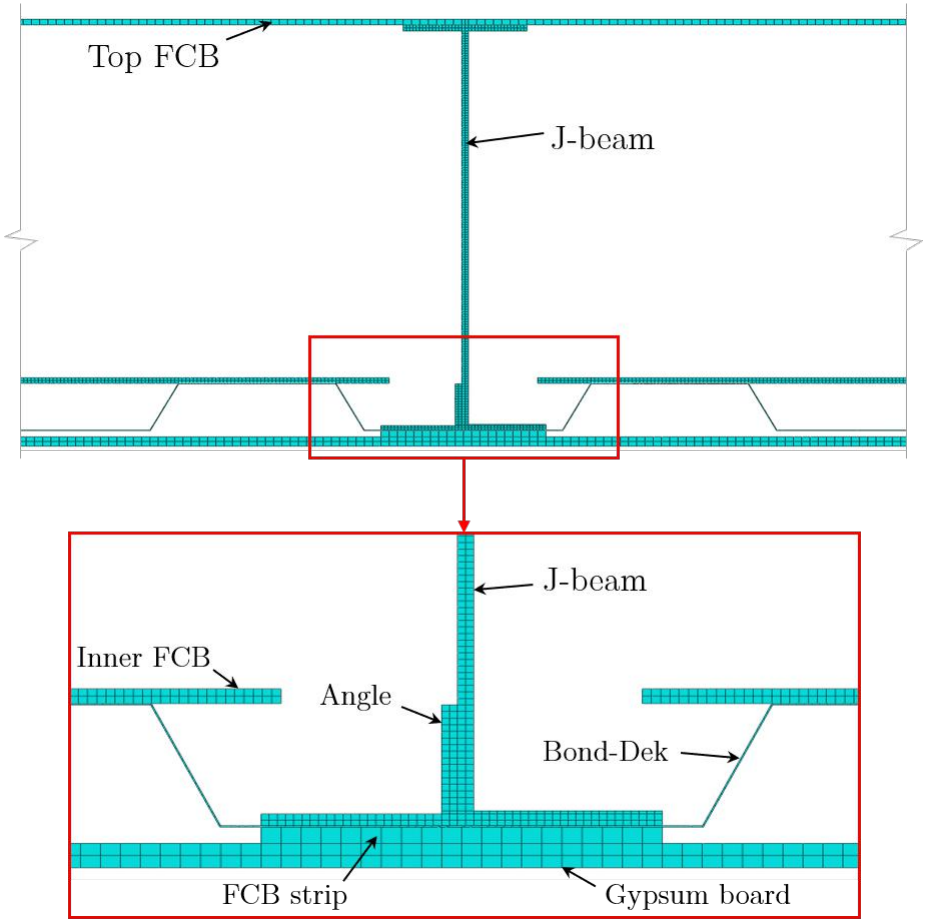

Figure 6.9: Mesh configuration for the J-beam model

6.5 FE analysis procedure

The FE beam analyses were performed in a similar manner to the validation studies and the fire test verification analyses, as described in Section 5.3. The FE analyses included an initial step, in which the ambient temperature of $20°C$ was assigned to the whole model, and a transient heat transfer step, in which the heat transfer through the sandwich floor system was simulated.

A time period of 3600 seconds was defined during the transient heat transfer step, which corresponded with the input duration of the standard fire. The total analysis time pe-

riod was divided into smaller increments automatically in the heat transfer step module of ABAQUS (Dassault Systémes, 2015). A maximum number of increments were set to 100000 to ensure convergence, while defining the minimum and maximum time increment size limitations as 0.036 and 10 seconds, respectively. The maximum allowable temperature and emissivity change per increment were set to $10°C$ and 0.1, respectively.

6.6 Results of FE analyses

The temperatures obtained from the FE analyses provide the input for future modelling of the CBS, and have been used by Kloos (2017) to determine the structural behaviour of the CBS, as discussed at the beginning of this chapter. These temperatures have been determined for various points on the beam cross-sections within the FE models to allow an accurate representation of the average temperature distribution through the height of the beams. As discussed previously, both the case of the ceiling remaining intact (C) and the ceiling failing (NoC), have been considered. Figures 6.10, 6.11 and 6.12 show the temperature distribution across the height of the J-beam, P-beam and channel (C-beam) ceiling models, respectively, after a 60 minute standard fire exposure.

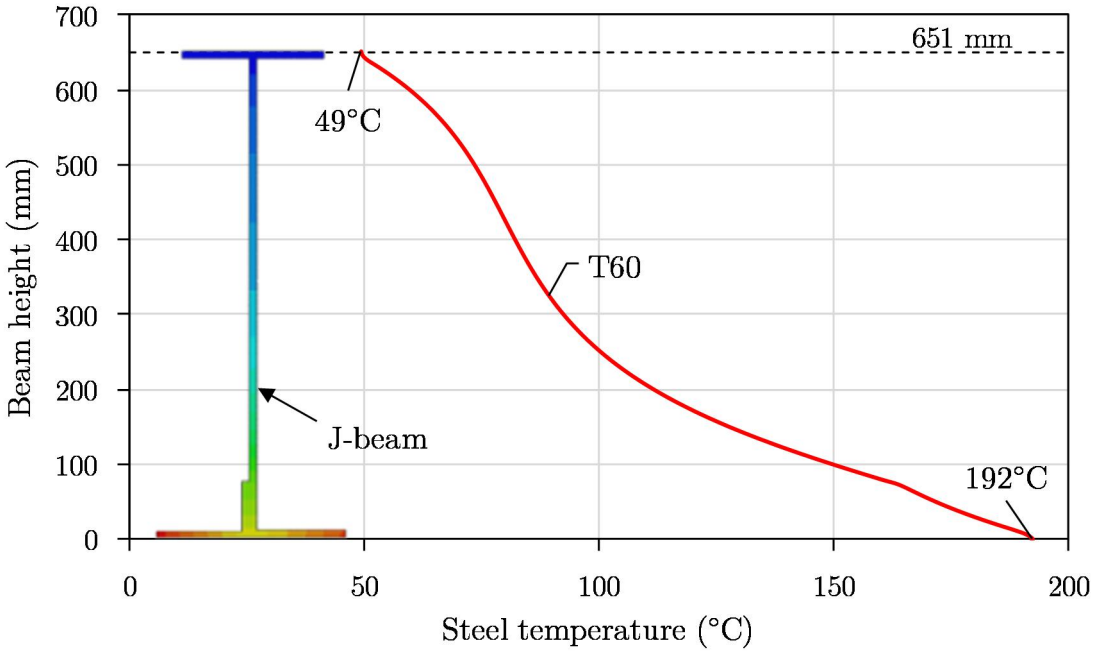

Figure 6.10: J-beam temperature distribution after a 60 minute standard fire

The temperatures are measured on the centre-line of each beam section, which runs through the middle of the bottom flange, the web and the middle of the top flange. It is clear from the predicted temperature distributions that the temperature varies significantly through each of the beam cross-sections. The temperatures are higher in the lower part of the beams, which is to be expected, due to the system being heated from below. The temperature difference between the bottom and top flange for the J-beam and P-beam models were $143°C$ and $184°C$, respectively. The lower channel section height had a difference of $83°C$, which is significantly lower than for the two cellular beams.

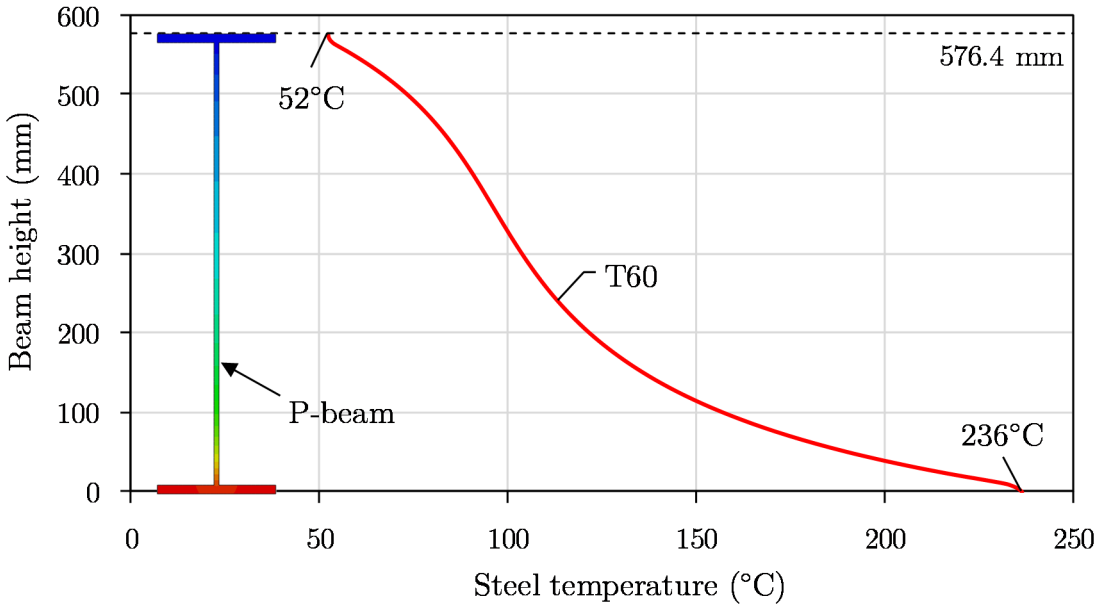

Figure 6.11: P-beam temperature distribution after a 60 minute standard fire

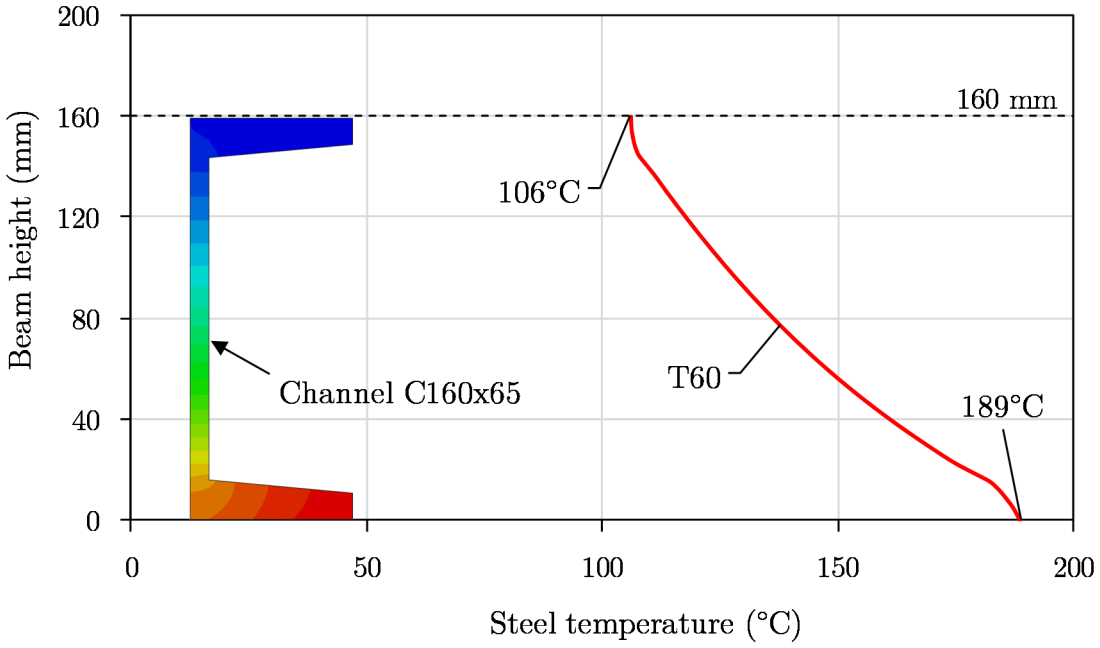

Figure 6.12: Channel temperature distribution after a 60 minute standard fire

When modelling structures in fire a constant temperature is typically specified for the web of a section. Due to the large depth of beams it was deemed necessary to have more than one temperature zone for the web. Therefore, the beams were divided into sections that consisted of an average temperature of the specific section. The J-beam model was divided into four sections, which consisted of the bottom flange (BF), top flange (TF), lower web (LW) and the upper web (UW). A total of eleven temperature points was used, which included four in the bottom flange containing the angle, two in the lower web, two in the upper web and three in the top flange. The temperature points within each of the four sections were combined to obtain an average temperature for each respective section.

The P-beam model was also divided into four sections, similar to the J-beam model, for which the average temperature in each section was determined from a total of ten points across the height of the steel beam section. Due to the relatively low height of the web, the channel section (C-beam) was only divided into three sections. These were the bottom flange (BF), web (W) and the top flange (TF).

6.6.1 J-beam temperatures

Figure 6.13 presents an example of the resulting temperature distribution after a 60-minute standard fire heat transfer analysis of the J-beam model when the ceiling is assumed to remain in place.

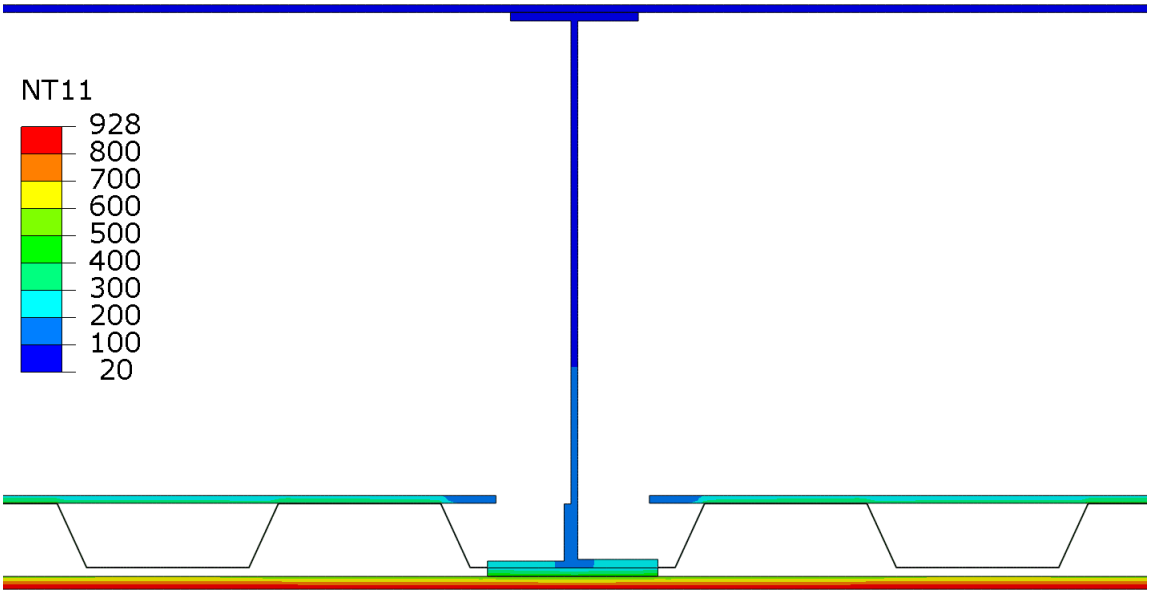

Figure 6.13: FE J-beam model temperature distribution, while assuming the ceiling board remains intact

Figure 6.14 presents the J-beam temperatures that were determined from the FE analysis for a 60-minute standard fire for both the ceiling (C) and no ceiling (noC) models, which are depicted by the solid and dashed lines, respectively. The colour of the lines indicates the specific section within the beam, namely the BF in red, LW in yellow, UW in green and the TF in blue. The temperatures for the P-beam and channel analyses are presented in a similar manner in Figures 6.15 and 6.16, respectively.

As one would expect, the no ceiling model yielded significantly higher temperatures than for the ceiling model, with a difference in temperature ranging between $300°C$ and $450°C$ in the four sections. These higher temperatures reduce the stiffness and increase the expansion of the steel, which results in larger deflections and higher axial forces in the steel beam. This emphasizes the importance of the ceiling board for providing sufficient insulation to the steel beam and upper floor layers. It is therefore crucial to ensure that the integrity of the ceiling board is satisfied.

From the FE results it was noted that the temperatures obtained within the steel beam are fairly low, with a maximum temperature of $215°C$ in the bottom flange. This is due

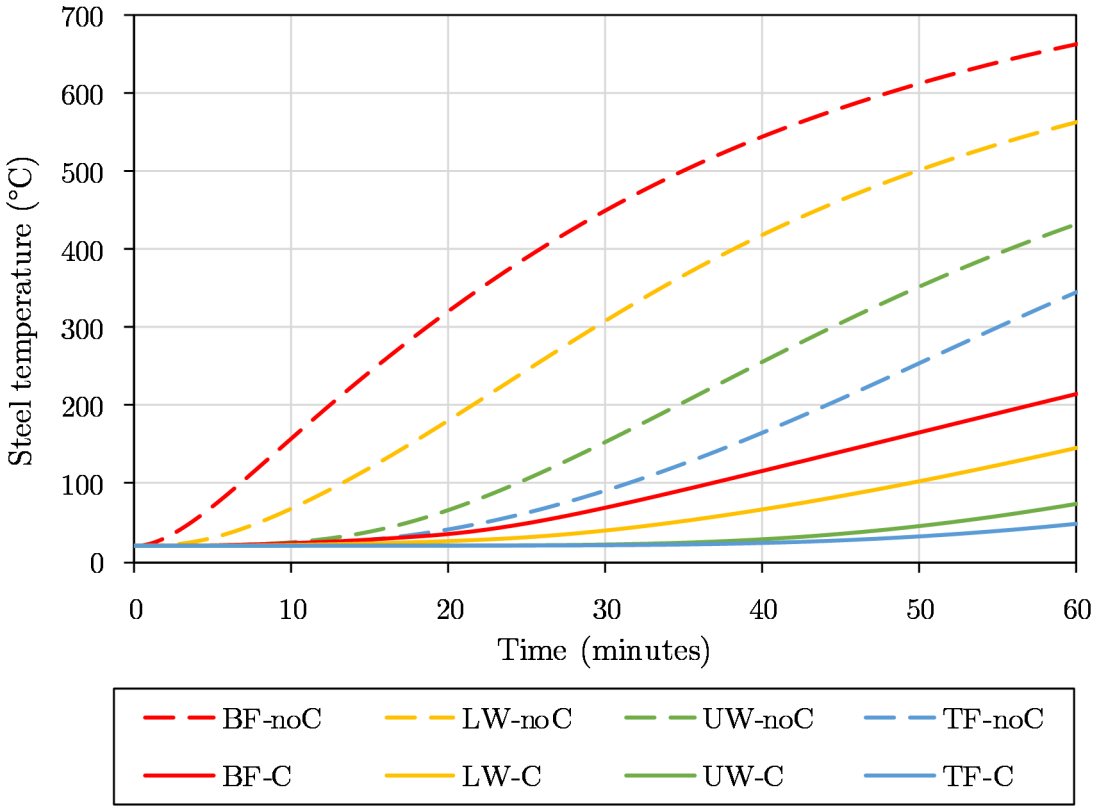

Figure 6.14: Steel temperatures for J-beam with and without ceiling (C and noC)

to the performance of the ceiling system, which is similar to the validation studies, as discussed in Chapter 5. The FE analysis yielded a temperature difference of 70°C between the bottom flange and the lower web, as well as between the lower web and upper web sections. The relatively high conductivity of steel resulted in the upper sections of the J-beam heating up. Heat was also radiated from the top surface of the inner fibre-cement boards towards the web and top flange sections. However, with the rise in temperature within the steel beam, heat was radiated back into the air cavity, which in turn resulted in lower steel temperatures in the top section of the J-beam. The ambient conditions on the unexposed side of the top FCB acted as a heat sink, which also contributed to the relatively cooler temperatures in the top sections of the J-beam.

For a J-beam length of 7.925 m and at a temperature of 215°C, which was obtained in the bottom flange, the longitudinal expansion would be approximately 24 mm, based on the simplified constant expansion coefficient of 1.4×10^{-5}, as provided in the Eurocode 1993-1-2 (CEN, 2005). It would be essential to design the ceiling system to accommodate such strains to ensure that it does not fail.

6.6.2 P-beam temperatures

The primary beam (P-beam) has a similar temperature distribution to that of the secondary beam (J-beam), for the ceiling and no ceiling models, as shown in Figure 6.15. Both the J-beam and P-beam analyses yielded temperatures that range between approximately 360°C and 713°C for the no ceiling models and between 45°C and 222°C for the ceiling models, as seen in Figure 6.15. Therefore, by ensuring that the ceiling board stays

intact, the steel beam temperatures can be kept relatively low.

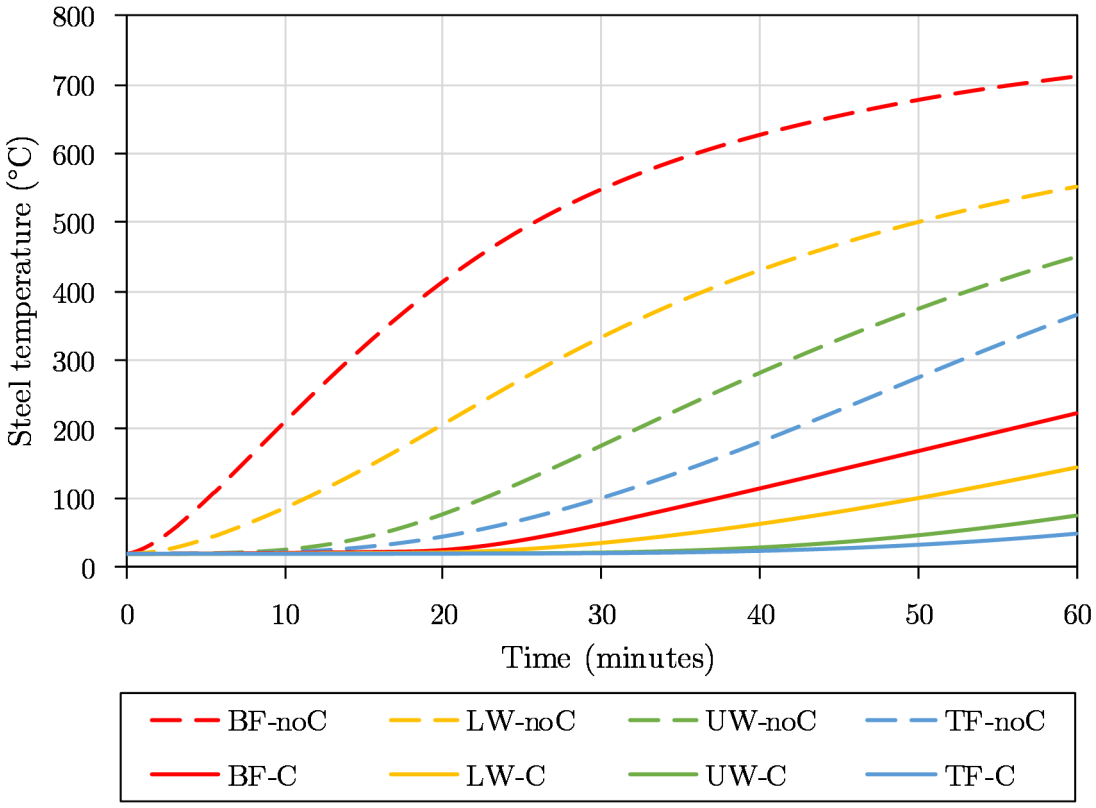

Figure 6.15: Steel temperatures for P-beam with and without ceiling (C and noC)

The temperature difference between the ceiling and no ceiling models were approximately 490°C for the bottom flange, 409°C and 375°C for the lower and upper web, and 319°C for the top flange. It is clear that the temperature difference of the various parts of the beam is not constant. The difference in temperature between the ceiling and no ceiling models reduces when moving up in the beam section. Therefore, some of the heat from below is distributed through the air cavities and the outer material layers.

With a maximum temperature of 222°C in the bottom flange for the ceiling model and a beam length of 4.24 m, the estimated longitudinal expansion is approximately 13.2 mm. The expansion of the steel beam in the no ceiling model is 42.3 mm, based on the bottom flange temperature of 712°C and a beam length of 4.24 m. Large expansions can result in major cracks occurring across the ceiling board, thus resulting in the failure of structural integrity. Care should therefore be taken when fixing the ceiling boards. By allowing some amount of expansion, the strain within the ceiling board can be reduced. This, in turn, can prevent major cracks to form during a fire.

6.6.3 Channel temperatures

The channel (C-beam) FE analysis yielded similar results to that obtained for the J-beam and the P-beam. However, due to the significantly lower section height, the top flange of the channel experienced higher temperatures than the top flange of the other two beams. The maximum average temperature at 60 minutes was 176°C in the bottom flange, 129°C

in the web and 96°C in the top flange, as shown in Figure 6.16. Once again, it is evident that the ceiling board plays a crucial role in limiting the steel temperatures in the upper part of the floor system. The difference in beam temperatures between the ceiling and no ceiling models were found to be in the range of 410°C to 531°C.

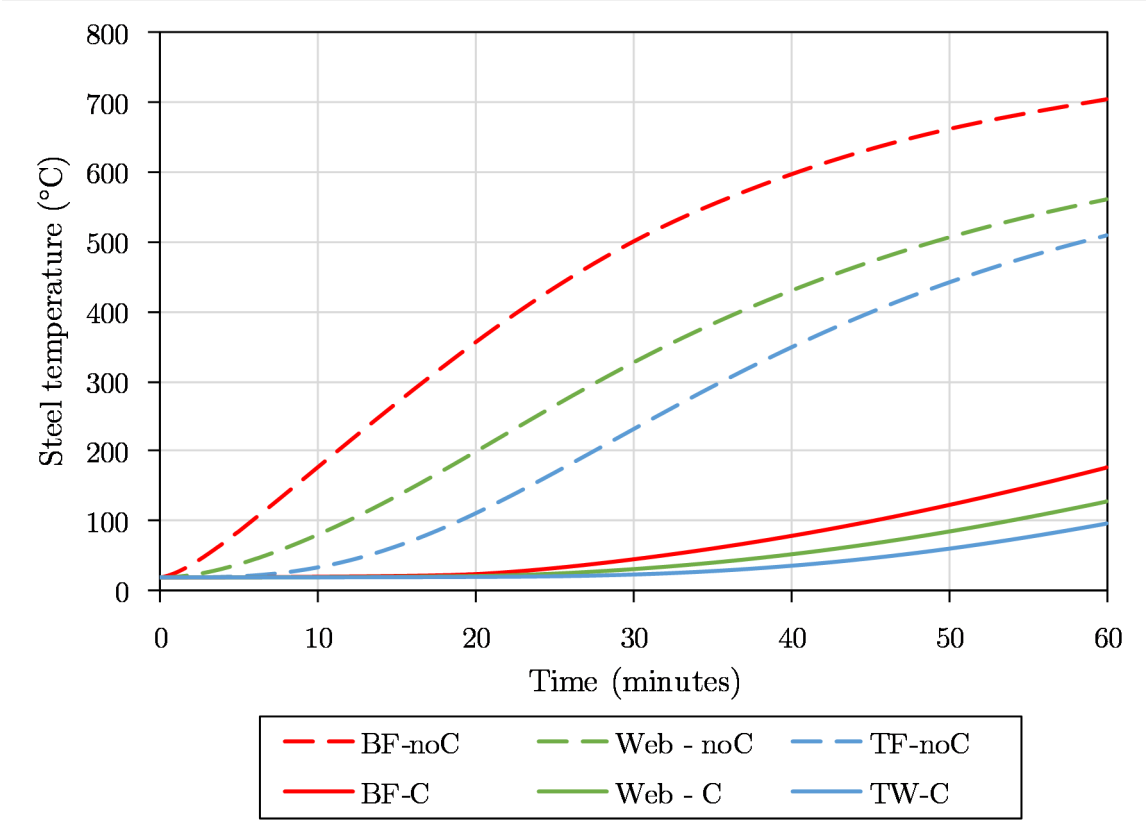

Figure 6.16: Steel temperatures for channel C160x65 with (C) and without ceiling (noC)

6.6.4 Inner floor temperatures

According to the insulation criteria in SANS 10400-T (SABS, 2011), the allowable average unexposed temperature is limited to 140°C, while the maximum (peak) temperature allowed on the unexposed surface is 180°C. This is to prevent any combustible substance igniting due to the increase in temperature, as discussed in Chapter 2. It was generally found that for all of the beam models, the unexposed surface on the top FCB layer satisfied the criteria, i.e. the top of the suspended computer floor is well within temperatures allowed to prevent fire spread. This was due to the significant depth of the floor and the big void, which reduced the heating rate of the top FCB. However, the inner FCB serves as the floor layer on which all services and access flooring pedestals will be located, i.e. it must be ensured that cables, ducting and services in the floor do not get exposed to high temperatures and potentially catch fire. Therefore, it is crucial that this layer also satisfies the insulation criteria described above.

Figure 6.17 shows the average temperature on top of the inner FCB layer (inFCB), i.e. the one supporting carrying services, within the sandwich floor system after a 60 minute standard fire exposure. The secondary beam (J-beam), primary beam (P-beam) and

channel (C-beam) models are denoted as Jb, Pb and Cb, respectively. The no ceiling (noC) models are indicated by the dashed lines, while the ceiling (C) models are presented by the solid lines.

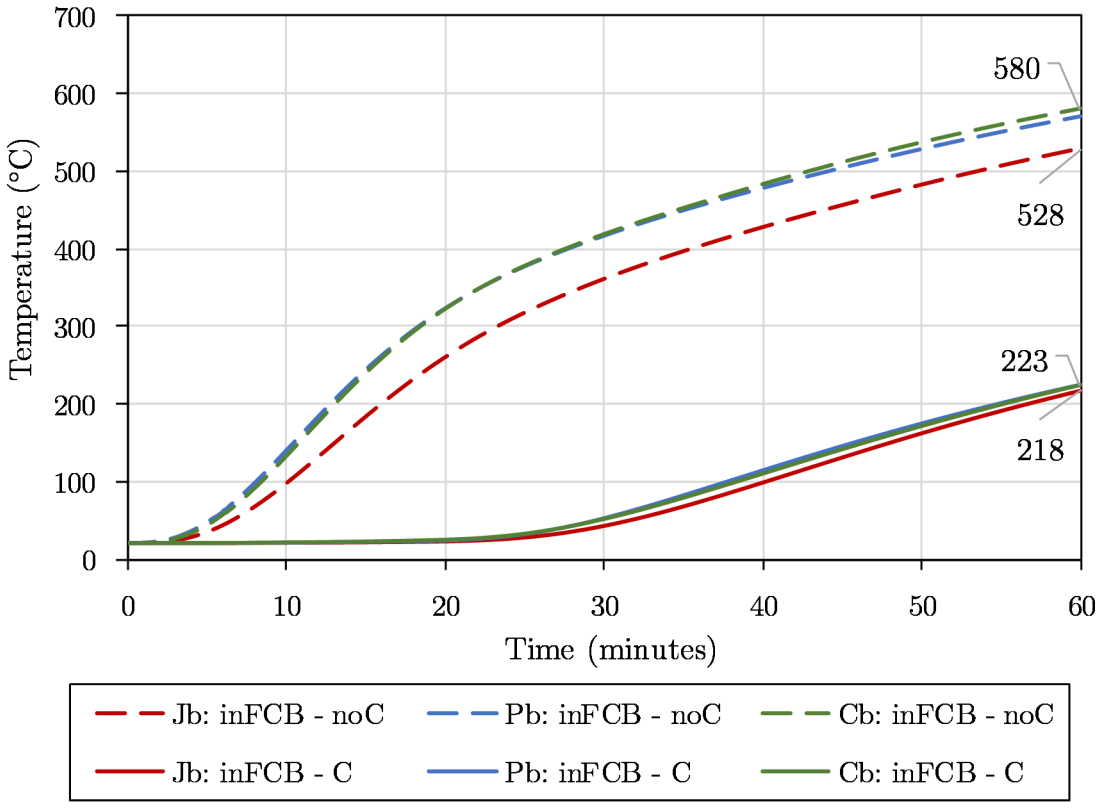

Figure 6.17: Average inner FCB surface temperatures for J-beam (Jb), P-beam (Pb) and channel (Cb) with and without a ceiling board (C and noC) for a 60 minute standard fire

It can be seen that the average temperatures obtained for the P-beam and C-beam models correlate with one another, while the J-beam model resulted in relatively lower temperatures with a difference of approximately $5°C$ for the models containing a ceiling board and $40°C$ for the models without a ceiling board. The slight difference is due to the variability between the FE beam model geometries. The J-beam model included the varying profile of the Bond-Dek sheeting, while the P-beam and C-beam models did not. From Figure 6.17 it is clear that the no ceiling models yielded significantly higher temperatures on the inner FCB when compared to the ceiling models, similarly to the beam temperatures discussed previously. The temperature difference ranges between $322°C$ and $357°C$.

It can be noted that the average floor temperatures obtained from the FE beam analyses do not satisfy the insulation criteria. With an initial temperature of $20°C$, the average temperature increase exceeds the insulation limit by $60°C$. Also, a maximum peak temperature increase of $248°C$ was determined, which exceeds the insulation peak criteria by $68°C$. This means that some of the services within the floor system could potentially ignite, which can lead to the spread of fire to adjacent compartment. The failure of compartmentation could eventually lead to major loss of property or even overall structural collapse. The temperature rise within the inner FCB layer could be reduced by increasing either the ceiling or inner FCB thickness or even a combination of the two. However, a

more detailed parametric investigation is performed in Chapter 7.

After a 60-minute standard fire analysis on the ceiling models, the temperature within the Bond-Dek steel sheeting varied between approximately $500°C$ and $440°C$, for the bottom and top steel sections, respectively. The expansion of the sheeting was taken as 1.4×10^{-5}, which is equivalent to that of carbon steel. Therefore, by assuming a constant temperature of $500°C$ throughout the whole sheeting layer of 7.925 m in length, an expansion of 55.5 mm is expected in the longitudinal direction. This relatively high expansion of the Bond-Dek sheeting can have detrimental effects on the inner FCB and the ceiling board. It is highly possible that thermal bowing could occur, as seen during the small-scale fire tests that were discussed in Chapter 3. The linear expansion and thermal bowing of the steel sheeting can cause cracks in the boards, which leads to an integrity failure. Heat and flames will then be able to spread instantly into the floor system and into the adjacent compartments. This would also heat up the steel beams more rapidly, thus reducing their strength and stiffness.

By increasing the ceiling thickness, the temperature increase in the Bond-Dek sheeting would be reduced, thus resulting in less expansion and thermal bowing, which improves the integrity of the floor system. Also, by allowing some amount of flexibility between the fixities in the boards, the strain caused by the expanding steel can be reduced, thereby preventing major cracks. Special screws that allow for small movements of the insulation boards should be used to ensure that minimal cracks occur.

6.7 Conclusion

This chapter presents a detailed discussion on the development and analysis procedures of the finite element (FE) beam models performed in ABAQUS (Dassault Systémes, 2015). These models comprised of the primary beam (P-beam), secondary beam (J-beam) and channel (C-beam), along with the insulation boards and Bond-Dek steel sheeting. The predicted temperatures in this chapter formed part of a decoupled analysis, to provide input for those wishing to carry out a structural fire analysis on the CBS, as done by Kloos (2017). At first, the beam model geometries, thermal properties and heat transfer parameters were discussed, after which the steel beam temperatures from the respective beam models were discussed, along with the inner floor and sheeting temperatures.

Temperatures were determined from various locations within each of the beam sections to ensure a reasonable accuracy. It was found that the J-beam and P-beam had a highly non-uniform temperature distribution, while the temperature through the channel varied almost linearly, as seen in Figures 6.10, 6.11 and 6.12, respectively.

In general, the ceiling models yield temperatures that are higher in the lower part of the beam section. The steel temperatures ranged between $48°C$ and $220°C$ for the J-beam and P-beam models, and between $95°C$ and $176°C$ for the channel. The temperature rise in the steel beams is relatively low, with a maximum temperature of only about $220°C$, which means that the steel beams would still have sufficient strength. Conversely, the temperatures obtained for the no ceiling (noC) models yielded significantly higher temperatures than the ceiling models, which is to be expected. Generally, the temperature difference between these two models is in the range of $300°C$ to $500°C$ for the FE beam

models. These analyses indicated what could happen in the case of full integrity failure of the ceiling board, thus emphasizing the need to ensure proper fixing of insulation boards.

The unexposed surface of the top fibre-cement board (FCB) did not exceed $50°C$, which is $90°C$ below the average insulation limit of $140°C$. However, the inner FCB reached temperatures in excess of $200°C$, exceeding the average limit by $60°C$. The maximum peak temperature of $180°C$ was exceeded by $68°C$. Therefore, the sandwich floor system does not satisfy the insulation requirement. This means that some of the services within the floor void could ignite, which leads to fire spread.

The expansion of the Bond-Dek sheeting was determined as 55.5 mm for a length of 7.925 m and an average temperature of $500°C$. This is for one bay in the case of a typical CBS layout, with a 60-minute standard fire exposed to the bottom ceiling board surface. A linear expansion of this magnitude, along with the thermal bowing of the steel sheeting, could cause major cracks to occur in the insulation boards. A similar occurrence was noted during the small-scale fire tests, as discussed in Chapter 3, in which major cracks were caused by the expansion of the steel sheeting. As soon as cracks appear in the ceiling board, the fire could spread more rapidly, whereby integrity is lost. The relatively low steel beam temperatures also cause small expansions in the longitudinal directions of the beam, which were in the range of 13 to 23 mm for the ceiling models and between 41 and 71 mm for the no ceiling models. The expansion of the beams, however, depends on the fixing at the supports. These were investigated during the structural analyses, which were performed by Kloos (2017).

The large strains caused by the expansion of the steel can be reduced by allowing some amount of movement between the insulation boards, as well as at the fixities, such as using special self-drilling screws that allow small movements around the screw. However, this should be done without reducing the effectiveness of the insulation. Integrity should be ensured by allowing some flexibility in the insulation boards, in order to account for the thermal bowing of the steel. The thermal expansion of the steel, as well as the temperatures on the inner FCB layer can be reduced by increasing the ceiling thickness. Another way to lower the temperatures in the inner FCB is to increase its own thickness. A detailed parametric investigation will now be performed in Chapter 7 to investigate such aspects.

Chapter 7

Parametric investigation

7.1 Introduction to parametric studies

In the previous chapters, a thorough understanding of the thermal behaviour of the sandwich floor system and the various fire test samples have been gained by using ABAQUS to perform Finite Element (FE) Analyses. The number of physical fire experiments that can be performed is limited, due to the significant amount of resources and monetary aspects involved with them. In the experiments conducted specific design criteria and layouts were considered. However, it is important to understand how the predicted results in previous chapters may change as design criteria vary. Hence, in this chapter a parametric investigation is conducted through which it is identified how parameters influence the thermal behaviour of the sandwich floor system. Several authors in the literature have used FEM tools for performing parametric studies on all sorts of structural systems. One example is the work of Feng *et al.* (2003) as discussed in Chapter 1, in which different configurations of various cold-formed thin-walled steel panel systems were analysed.

In the FE analyses of Chapter 6, it was found that the sandwich floor system does not satisfy the insulation criteria. The temperatures on the inner fibre-cement board (FCB) exceeded the required average temperature increase limitation of $140°C$ above ambient temperature. Therefore, the specified insulation boards, which include the 15 mm gypsum type X ceiling board and the inner 9 mm FCB, are not sufficient. By increasing the boards' thicknesses, the amount of heat conducted through the ceiling into the upper floor system is reduced, which is necessary for satisfying insulation requirements.

This chapter, therefore, presents various FE analyses, in which some of the floor system parameters were varied and compared to one another with regards to fire resistance. These parameters include the type and depth of the profiled galvanized steel decking, the type of materials used for the ceiling and inner insulation board and the thickness of the insulation materials. Figure 7.1 depicts the FE model configuration of the J-beam, which was used for the parametric investigation. The parameters which are varied are shown in red with the different dimensions and profiles. All dimensions are in millimetres (mm).

All of these analyses had a similar modelling procedure to the models discussed in Chapter 6 and were performed with similar heat transfer parameters, time step increments and mesh configurations. The boundary conditions, which include the 1-hour standard fire exposure to the ceiling, were used. As an example, a worst-case parametric fire curve

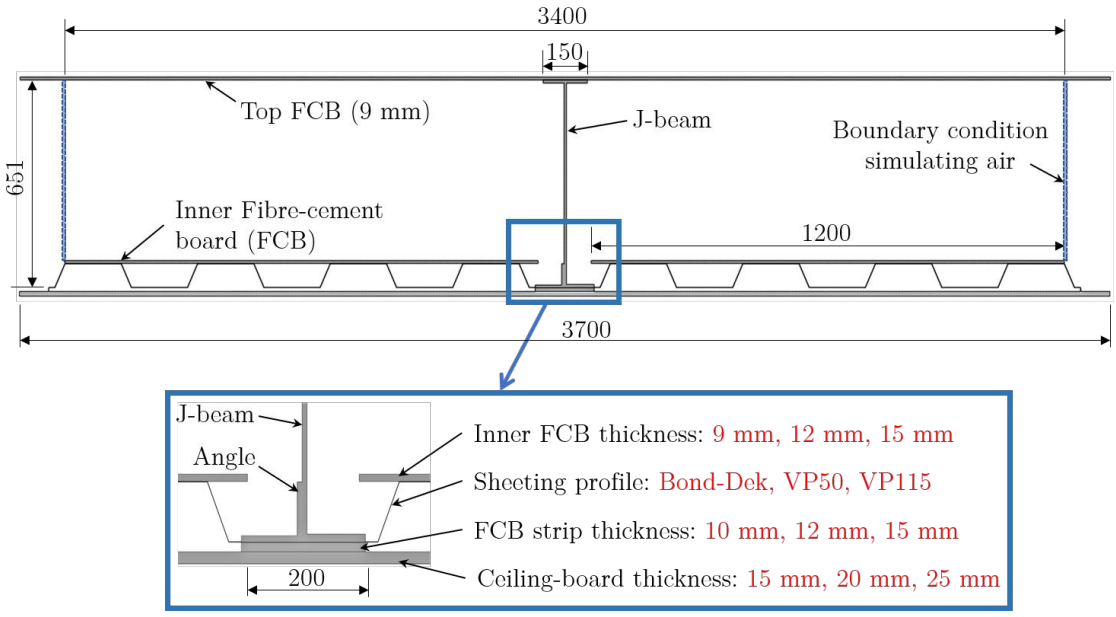

Figure 7.1: FE model configuration for J-beam, indicating various parameters that were changed during the parametric investigation (indicated in red)

for the specific compartment was also determined, which was used by Kloos (2017) to simulate the heating and cooling effects of a real fire on the structural behaviour of the CBS. The thermal behaviour of the two fire models is compared with one another below.

7.2 Ceiling board type and thickness

The ceiling board acts as a fire barrier to reduce the amount of heat that is transferred through the floor system, thus limiting the temperature rise on the unexposed side of the inner insulation boards. It is crucial to satisfy the insulation criteria to prevent the possibility of fire spread, as discussed in Section 2.3.2. During the FE beam analyses, as discussed in Chapter 6, it was clear that the single 15 mm layer of gypsum type X ceiling board was not sufficient in terms of the insulation criteria. The average temperature rise in the inner FCB was predicted as $200°C$, as opposed to the $140°C$ limit.

This section therefore investigates the influence of the type and thickness of the ceiling board. The different materials investigated for the ceiling were Gypsum Type X and Promatect-H Calcium Silicate, which was used in the small-scale fire tests. The thickness of the ceiling board was varied between 12 mm and 25 mm. The aim of this was to determine a suitable thickness that will satisfy the insulation criteria by ensuring that the average temperature rise in the inner floor layer remains below $140°C$.

The temperature increase in the inner FCB that was obtained for the various ceiling board models are presented in Figure 7.2. The dashed and solid lines depict the analyses with the Promatect-H Calcium Silicate (CaSi) board and the gypsum type X (Gyp) board, respectively. The different colours represent each of the various board thicknesses, in millimeters, and are indicated by the numbers 12, 15, 20 and 25.

It can be seen that for the first ten minutes of standard fire exposure, the temperature

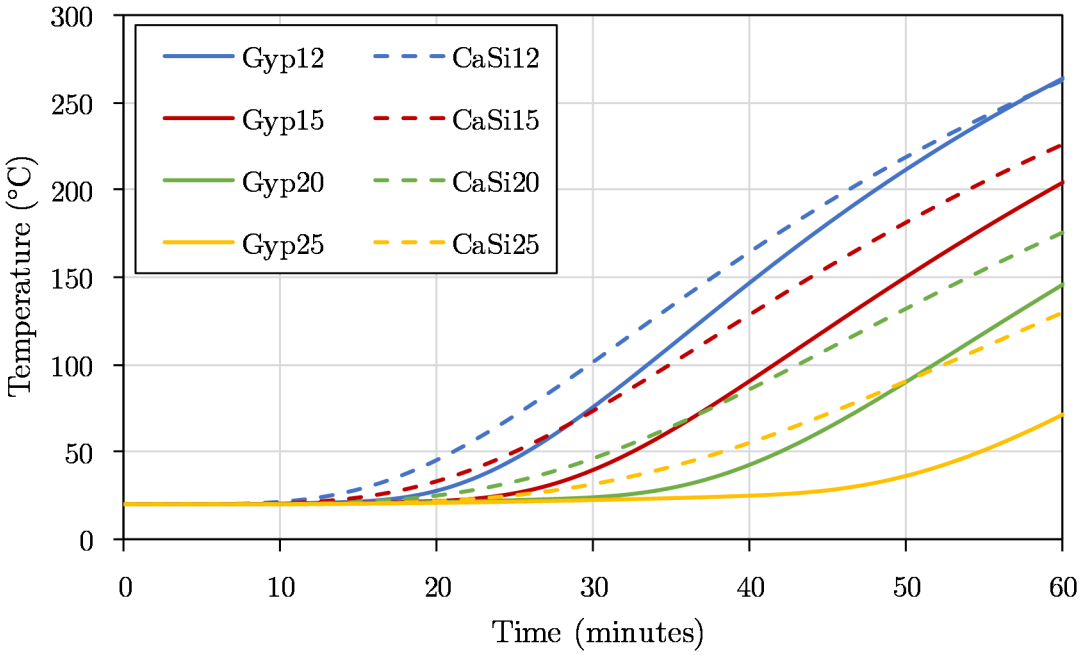

Figure 7.2: Comparison of the inner FCB temperatures for Promatect-H and gypsum type X ceiling boards with various thickness

within the inner FCB remained similar for all the configurations at the assumed room temperature of 20°C. Thereafter, the temperature increase for the various board models differed significantly. It was noted that the CaSi-board models yielded higher temperatures than the gypsum type X models. Also, the difference in temperature results between these two board models increased with a higher board thickness. From Figure 7.2 it can be seen that the temperature in the inner FCB after 60 minutes was approximately 57°C higher for the 25 mm CaSi-board model, when compared to the gypsum model with the same board thickness. The 15 and 20 mm models resulted in temperature differences between 20 and 30°C for the gypsum and CaSi-board models.

It is therefore evident that the gypsum type X board generally performed better than the CaSi-board, with regards to insulation. Reasons for this are discussed below. Figure 7.2 indicates that both the 25 mm CaSi- and gypsum boards satisfied the insulation criteria limit of 140°C, with a temperature increase of 110°C and 52°C, respectively. The 20 mm gypsum board also satisfied this limit, with an average temperature increase of 126°C. The rest of the board models yielded temperatures that exceed the limit between 16°C, for the 20 mm CaSi-board, and 103°C, for the 12 mm gypsum and CaSi-boards. It should, however, be noted that the thermal properties that were used for the respective board materials were based on values obtained from the literature, as discussed in Section 6.3.2. These properties differ significantly between various products and manufacturers. The temperatures obtained from these FE analyses, therefore, are only applicable to the specific thermal properties implemented into the FE material models.

The temperature results obtained for the various ceiling board models only indicate whether the floor systems satisfy the insulation criteria. These temperatures are also based on the assumption that no cracks occur in the ceiling board and that it remains intact, thus assuming that the structural integrity is ensured. However, the structural

integrity of the ceiling boards are difficult to model numerically, as it is impossible to accurately predict when and where cracks would occur.

Although the gypsum type X board performed more favourably in terms of the insulation criteria, it is not necessarily the case when considering the structural integrity of the ceiling boards. It is likely that the CaSi-board may perform better in comparison to the gypsum board, depending on the amount of moisture present within the board. Gypsum boards typically have a moisture content of approximately 17.5% (Feng *et al.*, 2003), while Promatect-H boards consist of a 6% moisture content (Promat, 2016). A higher moisture content leads to more shrinkage at elevated temperatures, due to the evaporation of the water particles, as discussed in Section 2.7.4. Shrinkage cracks occur as the board contracts, which result in more heat seeping into the floor cavity. It is thus possible that fewer cracks would occur in the CaSi-board, which could result in lower temperatures compared to a cracked gypsum type X board.

7.3 Fibre-cement board (FCB) strip thickness

The fibre-cement strip that was applied below the bottom flange of the J-beam formed part of the ceiling board. The thickness of the strip was varied between 9, 12 and 15 mm, while using the 15 mm gypsum ceiling board. It was found that the thickness of the FCB strip had a negligible impact on the inner floor temperatures. A change in beam temperatures was observed for the different strip thickness, as depicted in Figure 7.3.

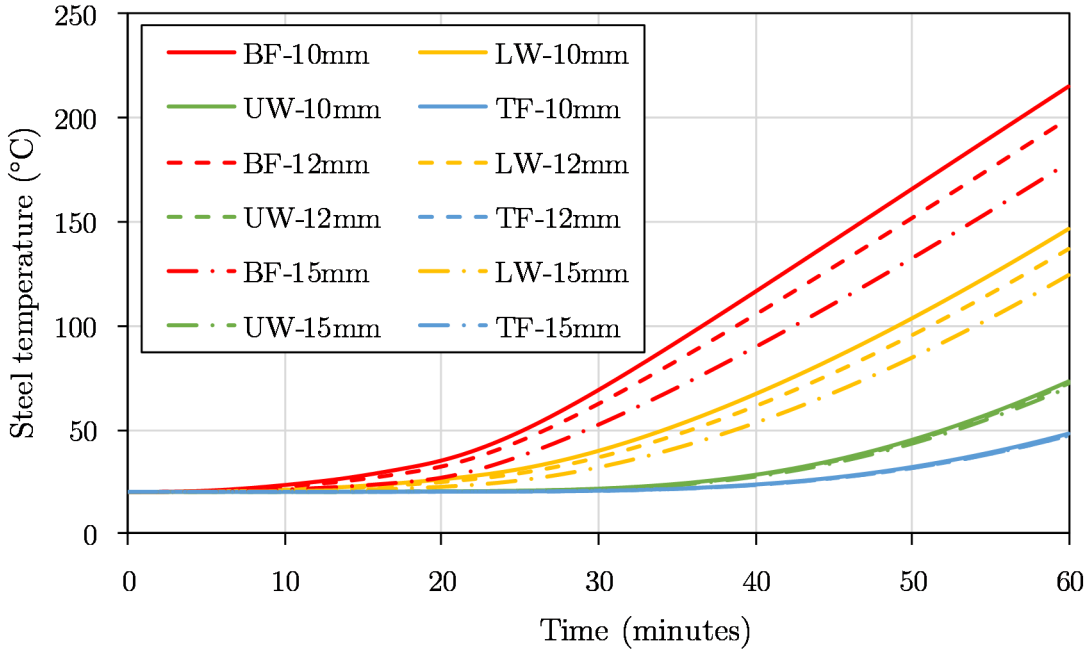

Figure 7.3: Comparison of the beam temperatures for varying FCB strip thickness

It was noted that the upper web and top flange sections are not significantly influenced by the thickness of the strip. These sections had approximately a zero percent difference in the steel temperature after the 60 minute standard fire duration, as seen in Figure 7.3. Conversely, the lower parts of the beam seem to be significantly influenced by this

parameter. By increasing the thickness of the FCB strip from 10 to 12 mm, the temperature increase in the bottom flange is reduced by 16°C. A further increase in thickness from 12 to 15 mm, resulted in a 36°C reduction in the bottom flange steel temperature. The lower web resulted in similar steel temperature variations. The difference in temperature between the 9 and 15 mm thickness was determined as 22°C. Although the steel temperatures are reduced, the insulation criteria is still not satisfied.

7.4 Internal insulation board thickness

In addition to the ceiling board, the thickness of the inner fibre-cement board (FCB) was also varied, relative to its current thickness of 9 mm, to determine the effect it has on the temperature the top of it experienced during a 60-minute standard fire. As mentioned previously, the inner FCB forms the base of the access floor on which the services will be located. The structural integrity and insulation of the inner FCB is thus crucial, which can be improved by increasing its thickness.

Figure 7.4 presents the average inner floor temperature for different inner FCB floor thickness, including a 9, 12 and 15 mm board thickness. It can be seen that the 9 mm board resulted in significantly higher temperatures, due to the shorter distance through which heat has to be conducted. The 12 mm board yielded a 37°C reduction in temperature compared to the 9 mm board. Similarly, the difference between the 15 mm and 12 mm board is 38°C. This indicates that the temperature increase in the inner FCB is inversely proportional to the thickness of the board, which is to be expected when considering the conductivity through the material, as discussed in 2.6.1.

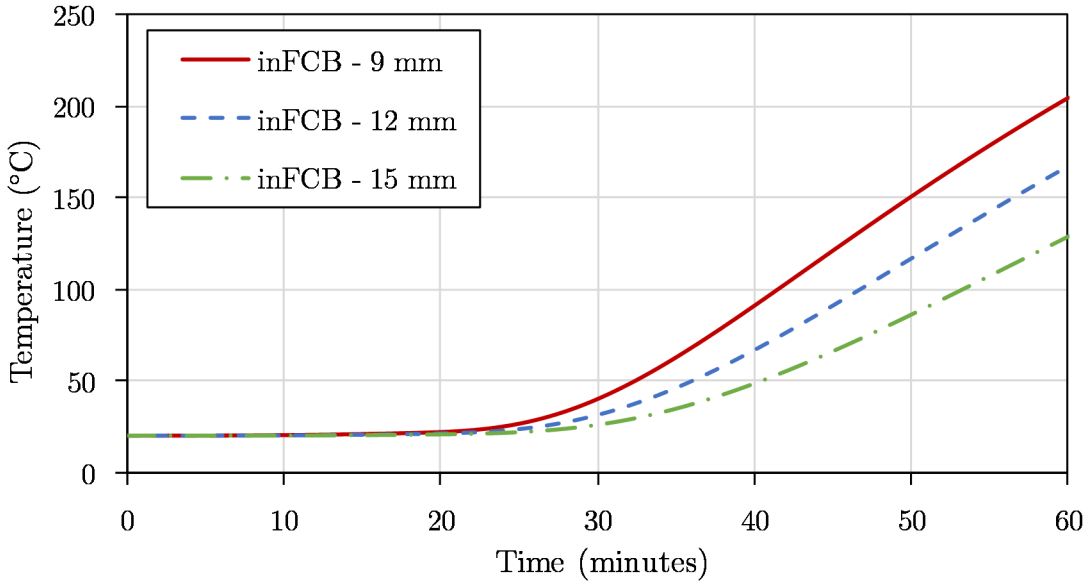

Figure 7.4: Comparison of temperatures for varying inner FCB thickness

It was found that the 15 mm FCB satisfied the insulation criteria, with an average temperature increase of 109°C. The 9 mm and 12 mm board both exceed the average limit of 140°C, by 44°C and 8°C, respectively. Therefore, a reasonably and economically efficient solution would be to increase the thickness of the inner FCB. However, the thicker board

results in more weight, which increases the overall weight of the structure. The density of the FCB is almost double that of the gypsum board, as was shown in Table 6.1. Hence, it will be more efficient to increase the gypsum ceiling board thickness, although cost considerations are likely to govern the final specifications.

7.5 Bond-Dek vs Voidcon decking profiles

The initial configuration of the modular sandwich floor system contains Bond-Dek, which has a depth of 75 mm and an average flute width of 225 mm. Another type of steel decking was investigated, namely Voidcon (Voidcon, 2014*b*), which was used in the small-scale fire tests, refer Section 3. The geometry of the Voidcon sheeting differs significantly from the Bond-Dek, as can be seen in the product's design tables (Voidcon, 2014*a*).

The discussion regarding the fire tests in Section 4.2 included comments on the specific geometry of the Voidcon sheeting, in which the influence of the small overlapping triangle on the heat transfer within the voids was highlighted. Hence, here the influence of the various decking profiles and depths is investigated. The Bond-Dek sheeting, as specified for the CBS, was compared to two Voidcon profiles, namely the VP50 and the VP115, which has a depth of 50 mm and 115 mm, respectively. The configuration for the three different sheeting profiles are depicted in Figure 7.5.

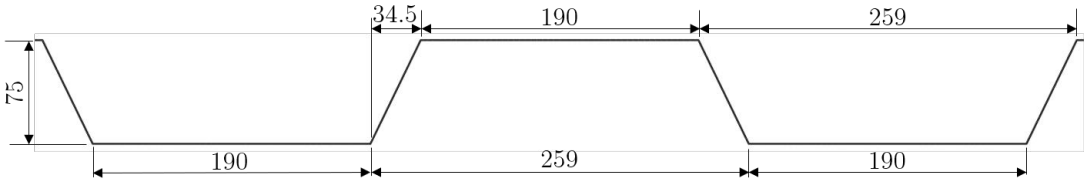

(a) Bond-Dek (BD) profile

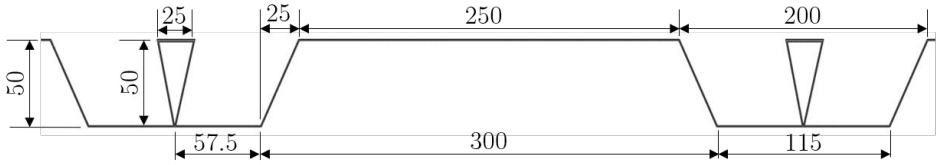

(b) Voidcon VP50 profile

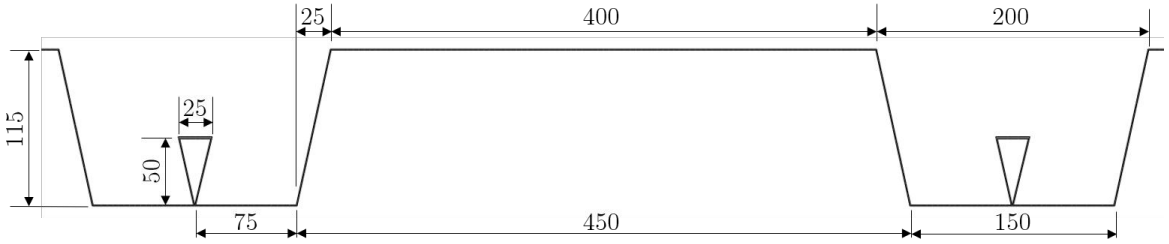

(c) Voidcon VP115 profile

Figure 7.5: Sheeting configuration for the various profiles used in the parametric study

Figure 7.6 presents the average inner floor temperatures for the J-beam model, incorporating the Bond-Dek (BD), VP50 and VP115 steel sheeting profiles. A good correlation was found between the aforementioned profile models. The difference between the floor

temperatures for the Bond-Dek and VP50 models is negligible. It can be seen that the three models yielded similar temperatures up to a duration of 30 minutes, after which a difference between the VP115 and the other two profiles is noted. The temperatures were approximately $10°C$ lower for the relatively deeper VP115 profile. The deeper profile consists of more air, which allows the cavity temperatures to cool down.

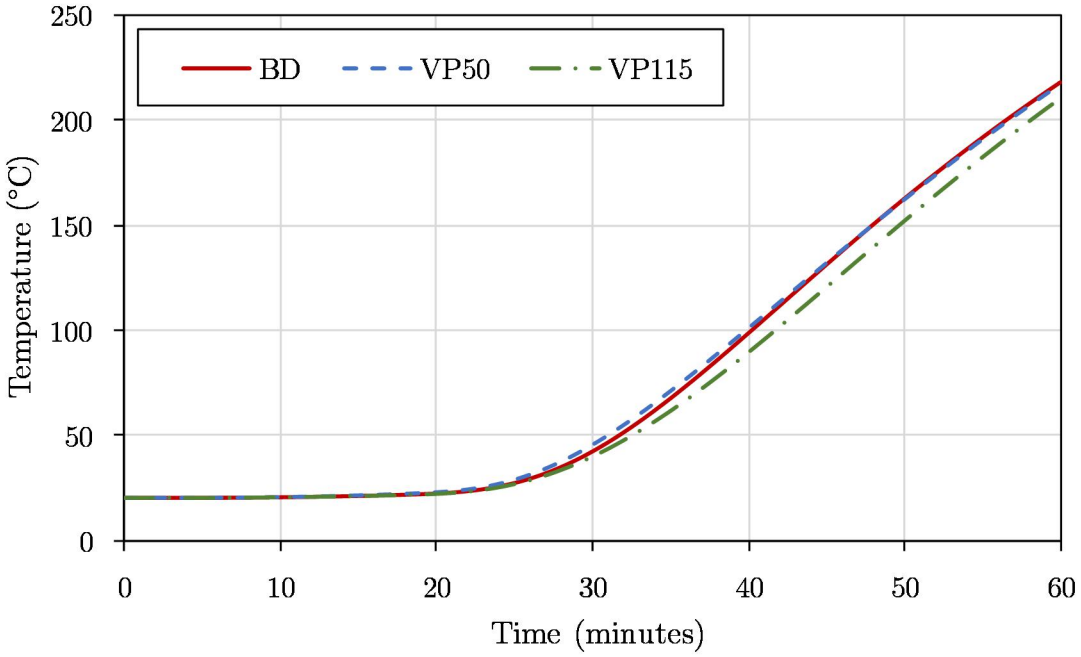

Figure 7.6: Comparison of the inner FCB temperatures between the Bond-Dek (BD) and two Voidcon (VP50 and VP115) decking profiles

The steel temperatures were also predicted for the three models, however, the FE analyses yielded similar results for the three respective models. The steel temperature differences were less than $10°C$. It is therefore clear that the profile and depth of the steel sheeting does not have a significant influence on the temperatures obtained within the floor system. This is beneficial in that different decking systems could be specified without the flooring system needing to be thermally evaluated each time.

7.6 Parametric fire exposure

The FE beam analyses that were discussed in Chapter 6 have, up to this point, incorporated a 60-minute standard fire, which was exposed to the bottom ceiling surface. In this section, a parametric fire is determined for the specific compartment characteristics of the CBS, which provides a more realistic fire as opposed to the standard fire. The parametric fire was calculated from the equations provided in the Eurocode 1991-1-2 (CEN, 2002), which were discussed in Section 2.4.2, and with further details contained in Appendix D.

The aim of this section was to investigate the behaviour of the CBS when exposed to a more realistic, but very intense temperature-time relationship, which includes a heating and a cooling phase. The standard fire lacks a cooling phase; hence some behavioural aspects are neglected during analyses that incorporate this type of thermal loading. The

temperatures that were obtained below from the parametric fire analyses have been used by Kloos (2017) to determine the effect of the cooling phase on the axial forces experienced in the cellular beams.

This section discusses the assumptions made for the input variables used for the calculation of the parametric fire curve. The results from the FE analyses are then presented, along with a discussion of the results.

7.6.1 Determination of the parametric fire curve

The parametric fire curve was determined for a compartment that was based on the CBS configuration, as presented in Figure C in Appendix C. The calculations include various characteristics that are not taken into account for a standard fire curve, such as the ventilation, design fire load, building size and the boundary conditions and materials.

A worst case parametric fire was determined as an example to investigate how the CBS performs when subjected to a very high peak temperature during the heating phase and a significant cooling effect. The temperature-time relationship obtained from the calculations was added as an amplitude in ABAQUS and applied to the bottom exposed ceiling surface. The modelling procedure of the parametric fire was similar to that of the 60-minute standard fire analyses, as discussed in Section 6.3.3.

The size of the compartment was taken as 12.75 x 8.5 x 2.56 m, while assuming a significant amount of ventilation in the form of 1 door and 4 windows. The sizes were taken as 1 x 2 m for the door and 3.85 x 1.54 m for the windows, which resulted in an opening factor (O) of 0.1, as determined from Equation 2.4.5. The calculation procedure provided in Annex A of EN 1991-1-2 (CEN, 2002) was used to determine the heating and cooling phase of the parametric fire curve. The main assumptions that were made during the calculation are summarized in Table D.1.

From Figure 7.7 it can be seen that the standard fire (black dashed line) and the parametric fire (red solid line) differ significantly, in this case. The standard fire increases rapidly within the first 5 minutes, after which it heats up gradually. The temperature continues to increase during the 2-hour duration, after which a temperature of $1049°C$ is reached. The parametric fire consists of a shorter, but more intense heating phase, as well as a rapid cooling phase. It can therefore be expected that the parametric fire would result in significantly different temperatures within the steel members.

Based on the assumptions discussed above, a parametric fire with a peak temperature of $1188°C$ was obtained, as shown in Figure 7.7. In general, such a high peak is unlikely (even though mathematically predicted by EN 1991-1-2 (CEN, 2002)), but included to consider a very intense fire. Initially, the temperature in the compartment increased rapidly until the peak temperature was reached at 20 minutes. Thereafter, the temperature dropped linearly over a duration of 20 minutes. At 40 minutes, the fire cooled down to the assumed room temperature of $20°C$, after which the temperature in the compartment remained constant on the room temperature for the full duration.

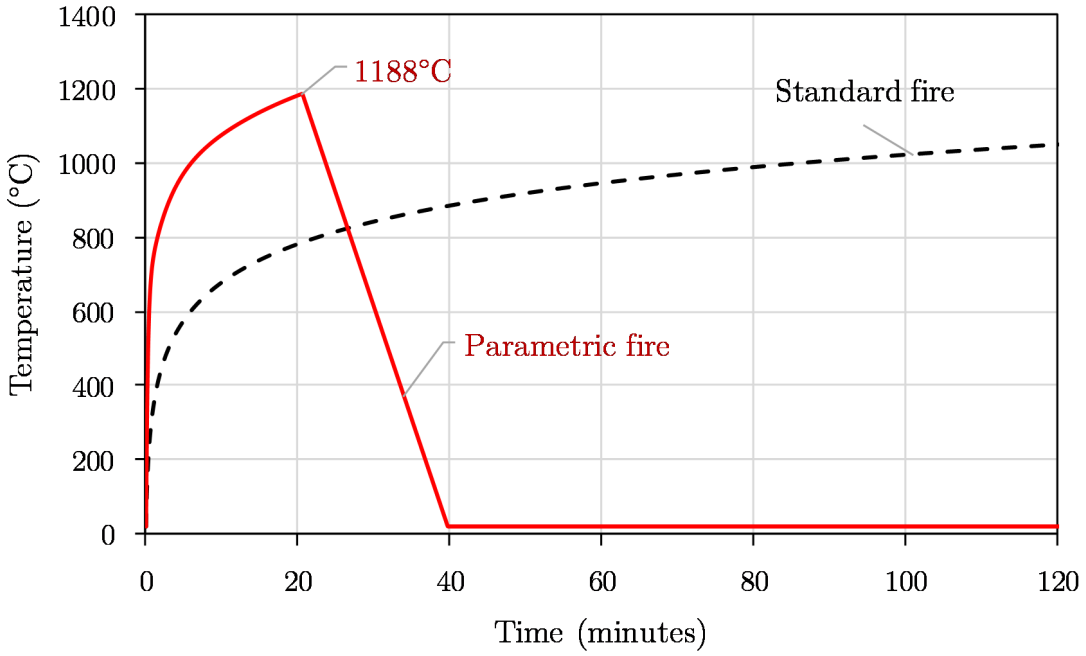

Figure 7.7: A 2-hour parametric fire curve for the CBS and the standard fire curve

7.6.2 Results and discussion

The FE parametric fire models were analysed for a duration of 120 minutes to allow the steel to cool down. Figures 7.8, 7.9 and 7.10 depicts the temperatures of the J-beam (secondary), P-beam (primary) and C-beam (channel) for the parametric fire analysis ("parF"). The results from the 1-hour standard fire analyses ("stdF") are also presented on each of the respective figures. The average temperature in the various sections are indicated by different line colours, similar to the FE beam model results in Section 6.6.

All of the analyses performed for the three FE beam models exposed to a parametric fire, yielded significantly higher temperatures within the first 40 minutes, when compared to the standard fire results. This means that the total energy released by the parametric fire was higher for the first 40 minutes, based on the specific compartment ventilation and fuel assumptions, as discussed above. The bottom flange of the J-beam in the parametric fire analysis reached approximately $58°C$ higher temperatures than the corresponding standard fire analysis in the first 40 minutes. This is due to the significantly higher temperature to which the ceiling was exposed. As a result, heat was conducted more rapidly through the ceiling board and into the bottom flange of the beams. Heat was then further conducted through the steel beam sections, due to the high conductivity of steel.

After 40 minutes, the temperature in the beam sections decreased, due to the cooling phase of the exposed temperature on the ceiling board. Hence, the total energy released by the parametric fire decreased relative to the energy released by the standard fire, as seen in Figure 7.8 between approximately 50 and 60 minutes. The bottom flange temperatures of the beam sections decreased more rapidly than the upper parts of the beams. This is due to the heat still being conducted inside the beam section, from the hotter bottom part to the top cooler part. Also, due to the heat capacity of the various insulation materials, heat continues to be radiated into the beam cavities. Temperature gradients

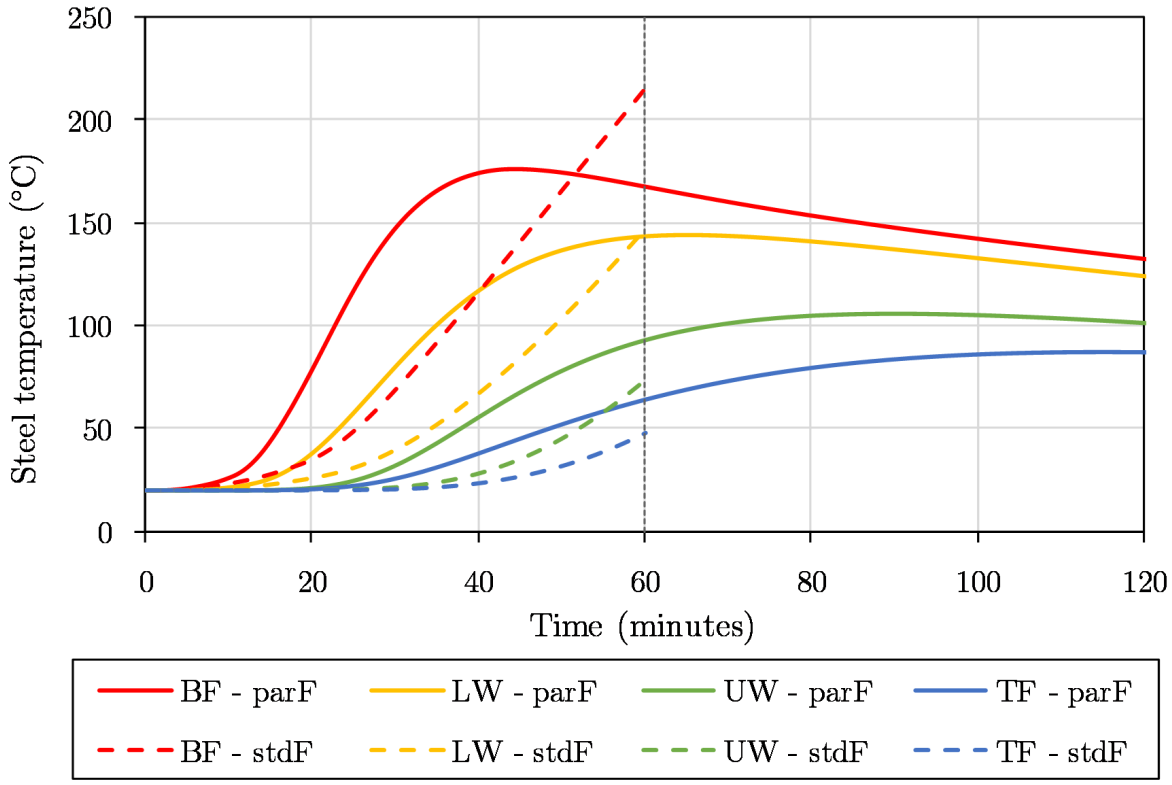

Figure 7.8: Temperatures for J-beam during a 2-hour parametric fire (parF) and a 1-hour standard fire (stdF)

still exist within the floor system, which causes a slow cooling effect.

Nonetheless, the temperatures at the end of the 60-minute duration, from the two thermal analyses differ significantly for the bottom flange and the upper part of the J-beam. At the 60 minutes, the parametric fire analysis resulted in a $49°C$ lower temperature in the bottom flange of the J-beam than the standard fire analysis. For both the upper web section and the top flange of the J-beam, more energy was released, in terms of heat, by the parametric fire analysis over the 60-minute duration, with a difference of approximately 28%. This is due to the high temperatures experienced in the bottom flange that were transferred to the upper parts of the beam through conduction, as mentioned above. It is thus evident that the average void temperature remained relatively high during the cooling phase of the parametric fire analysis.

The results obtained for the J-beam and P-beam are fairly similar to one another. However, the P-beam model yielded approximately $15°C$ higher temperatures. This is due to the extra FCB layer of insulation below the bottom flange of the J-beam, which reduces the heat conducted through the beam and floor system. The steel temperatures start increasing at approximately 10 minutes for the parametric fire models, as opposed to a duration of 15 to 20 minutes for the standard fire models. This is a result of the higher temperature at the initial stage of the parametric fire, due to the higher energy being released when compared to the relatively low energy released by standard fire. However, it should be noted that significantly higher temperatures would occur in a standard fire analysis at the end of 120 minutes. This is due to the continuous increase in energy being released, as opposed to the cooling phase of a parametric fire.

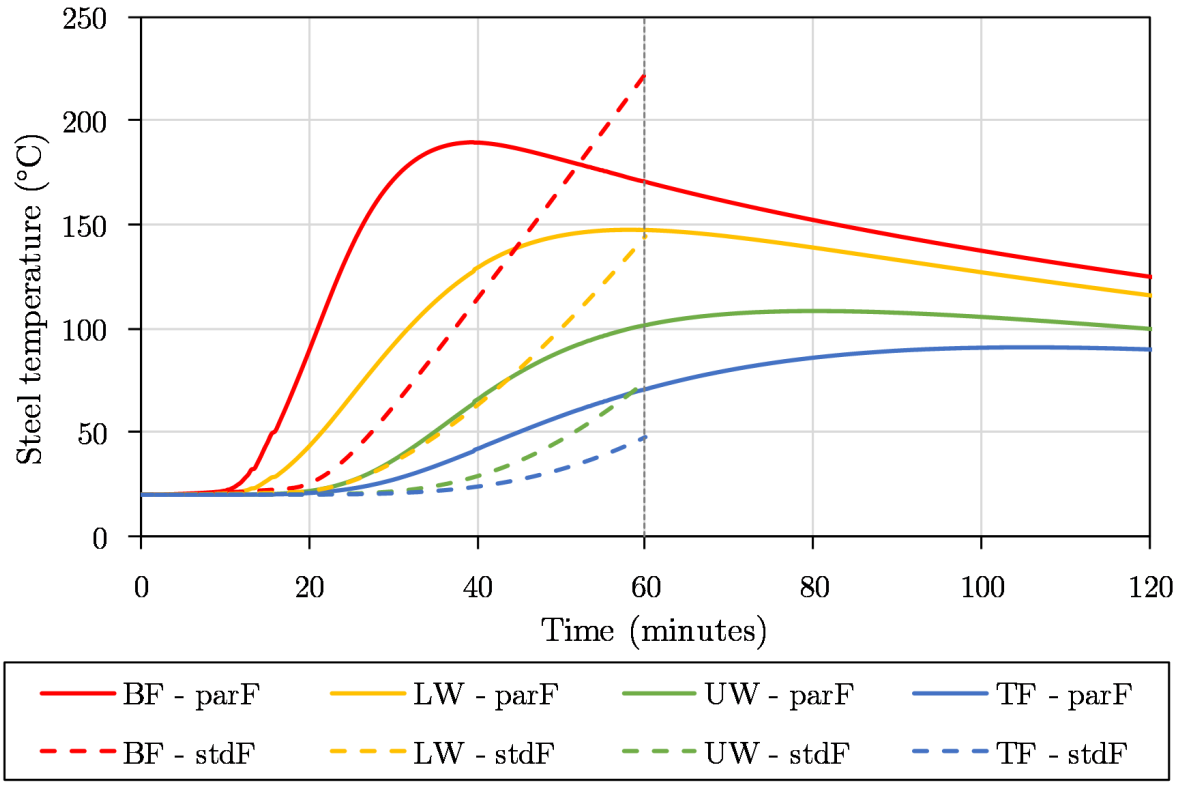

Figure 7.9: Temperatures for P-beam during a 2-hour parametric fire (parF) and a 1-hour standard fire (stdF)

The energy released by the parametric fire was, again, higher during the first 40 to 50 minutes, where a temperature of 189°C was obtained in the bottom flange. After 50 minutes, the temperature of the standard fire yielded higher temperatures for the bottom flange. The peak temperature reached in the parametric fire analysis is approximately 52°C lower than for the standard fire analysis. However, the upper part of the FE beam models for the parametric fire analyses was approximately 24°C to 31°C hotter at 60 minutes than for the standard fire analyses. This was due to the same reasons as explained above for the J-beam.

Similar behaviour can be noted for the channel section as compared to the J-beam and P-beam models. However, the whole channel section seemed to cool down at a slower rate, with only a 29°C reduction in temperature over the last 60 minutes of the 2-hour parametric fire exposure. This can be due to the reduced section height, which is subjected to the higher temperatures emitted from the lower part of the floor void. Heat is also conducted through the steel; hence heat is lost at a slower rate. When compared to the standard fire analysis, it can be seen that a significantly higher heating rate occurred in the parametric fire analysis, in which 46 to 58% higher temperatures were obtained in the bottom flange and upper channel sections, respectively. However, at the end of 60 minutes, a 20°C higher temperature was obtained in the bottom flange for the standard fire analysis. The continuous heating phase of the standard fire resulted in the beam models heating up to temperatures higher than those obtained in the parametric analyses.

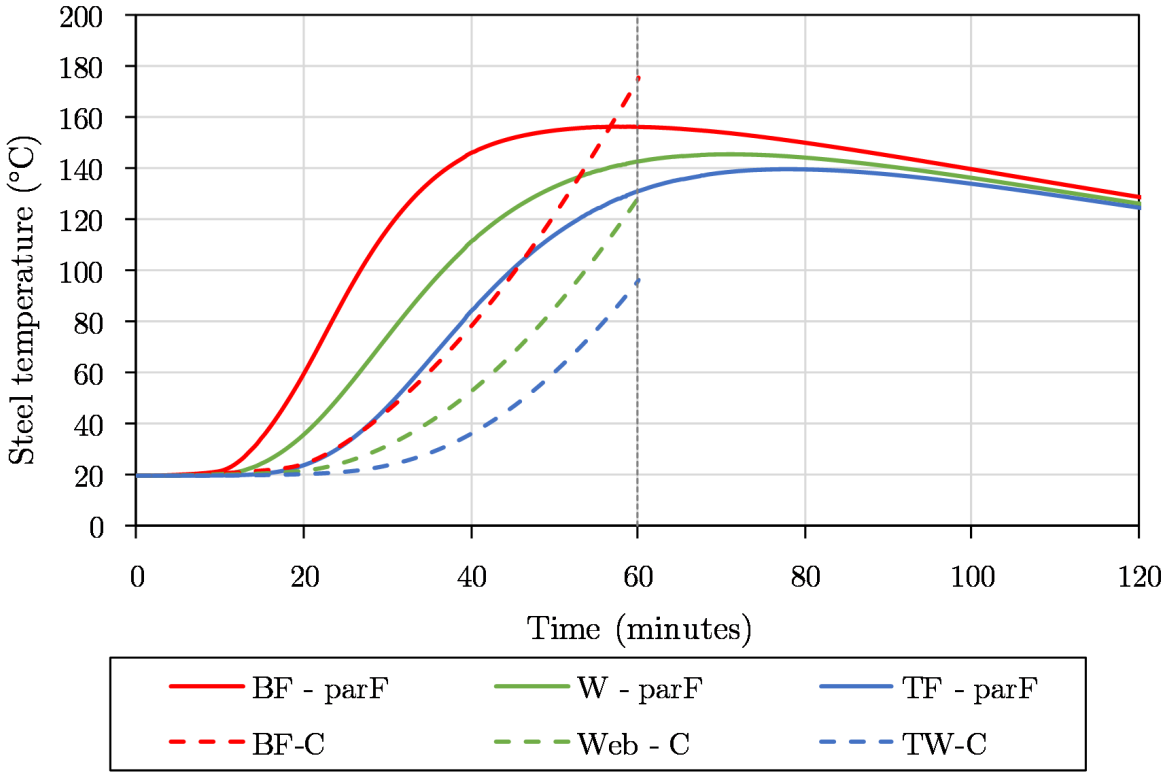

Figure 7.10: Temperatures for channel during a 2-hour parametric fire (parF) and a 1-hour standard fire (stdF)

7.7 Conclusion of parametric investigation

During the FE beam analyses that were performed in Chapter 6 it was found that the floor system does not satisfy the insulation criteria for a 60-minute standard fire, which is based on the average temperature increase and maximum peak temperature increase limitations, as discussed in Section 2.3.2. Various parameters within the floor system could be adjusted to ensure that the CBS meets the required fire resistance. This section therefore investigated the influence of various parameters on the average temperature increase on the inner FCB, which forms the base of the access flooring and services. These parameters included the type and thickness of the ceiling board, the thickness of the FCB strip below the bottom J-beam flange, the thickness of the inner FCB, and the profile and depth of the steel sheeting, which is located between the ceiling board and the inner FCB.

It was found that the use of Promatect-H CaSi-boards resulted in higher inner floor temperatures than the gypsum type X ceiling boards. This, however, could be due to the specific thermal properties that were chosen from the literature for the two respective materials. These properties differ from one product to another, hence it should be noted that the temperatures obtained from the FE analyses are only applicable to the specific properties used in this thesis, although these are based upon validated data in the literature from Feng *et al.* (2003). The lower temperatures obtained by using the gypsum boards could also be due to the relatively higher moisture content, as compared to the CaSi-board, which has a cooling effect on the floor system as the water evaporates. However, the higher moisture content in gypsum board makes it more prone to shrinkage cracks, which leads to an increased risk of integrity failure of the ceiling board.

The thickness of the ceiling boards was varied between 12, 15, 20 and 25 mm. For the CaSi-boards, only the 25 mm board satisfied the insulation criteria, while the 12, 15 and 20 mm boards exceeded the 140° limitation by a temperature increase ranging between $16°C$ and $100°C$. The 20 and 25 mm gypsum boards also satisfied the insulation criteria for a 60-minute standard fire, while assuming that cracks would not occur.

The thickness of the fibre-cement strip below the bottom J-beam flange was varied between 10, 12 and 15 mm to determine the effect it has on the steel temperatures. It was found that by increasing the thickness of the strip, it had a negligible effect on the average temperature increase of the inner FCB. However, the difference in temperatures obtained in the J-beam ranged between $177°C$ and $216°C$ in the bottom flange and between $124°C$ and $147°C$ in the lower web sections for the respective strip thicknesses. These significant differences are due to the additional insulation that the strip provides, which reduces the amount of heat being conducted through to the bottom flange. The upper parts of the J-beam were not influenced by this parameter, due to the significant amount of radiative heat transfer from the insulation boards to the upper part of the beam within the cavity.

The influence of the internal FCB was also investigated by varying its thickness between 9, 12 and 15 mm. From Figure 7.4 it was clearly seen that by increasing the thickness of the board, the average temperature increase on the inner FCB was significantly reduced. A temperature difference of up to $38°C$ was obtained for a 3 mm increase in board thickness. Only the 15 mm FCB satisfied the insulation criteria, with a 15 mm gypsum type X ceiling board and Bond-Dek sheeting.

The steel sheeting profile and depth was varied between the originally specified Bond-Dek sheeting with a depth of 75 mm and the two Voidcon profiles, which included the VP50, as used in the small-scale fire tests, and the VP115, with depths of 50 mm and 115 mm, respectively. It was found that the profile of the steel sheeting did not have a significant influence on the average temperature increase on the inner FCB, as seen on Figure 7.6 for the Bond-Dek and VP50. The VP115, which is 65 mm deeper than the VP50 and 40 mm deeper than the Bond-Dek, resulted in a slightly lower temperature increase with a difference of $9°C$. The temperature increase for all three decking systems exceeded the insulation criteria limitations, while assuming a 15 mm gypsum ceiling board and a 9 mm inner FCB. However, due to their negligible influence on the increase in steel and inner floor temperatures, any decking system can be used, as long as it satisfies the structural stability requirements.

To conclude with regards to the insulation criteria, it can therefore be decided to either increase the thickness of the ceiling board to at least 20 mm or increase the inner FCB thickness to 15 mm. Both of the former adjustments satisfy the insulation criteria, based on the assumed thermal properties and assuming a FCB strip of 10 mm and Bond-Dek sheeting. However, these parameters could be adjusted together, whereby both the ceiling and inner FCB thickness could be increased. Also, it is probable that the gypsum type X ceiling could undergo integrity failure due to shrinkage cracks and flexural cracks, especially when the steel sheeting experiences thermal bowing, as discussed in Section 6.6.4. Another crucial aspect to consider is the fixing of the ceiling boards. As discussed for the fire tests in Chapter 4, it was shown that the fixing screws weaken the ceiling board, which increases the chance of cracks occurring, thereby causing fire to spread to adjacent

compartments. Proper fixing procedures should therefore be executed. The boards should also be fixed in such a way to allow for some amount of movement, which would reduce the stress in the boards.

This chapter also discussed the application of a very intense parametric fire for the specific compartment, which is based on the general CBS layout in Figure C and the basic assumptions summarized in Table D.1 in Appendix D. A worst case parametric fire was derived from the Eurocode equations, which were discussed in Section 2.4.2. The temperatures that were obtained from the FE analyses were significantly different to those obtained for the FE beam models under a 60-minute standard fire, as discussed in Chapter 6. Generally, it was found that the steel temperatures initially increased more rapidly for the parametric fire models, due to the higher initial temperature and the higher peak temperature value of $1188°C$. The steel temperatures gradually decreased from approximately 40 minutes, due to the cooling phase of the parametric fire curve. The main difference between the parametric and standard fire models is the decrease in steel temperature with time, which does not occur in a standard fire analysis. The steel temperatures obtained from the parametric analyses above have been used to determine the axial stresses within the steel beams and the whole CBS, as a result of the cooling effect. More information regarding the structural behaviour on the CBS is available in Kloos (2017).

Chapter 8

Conclusions and recommendations

8.1 General overview

The goal of this thesis was to investigate the thermal behaviour of a novel cellular beam structural system in fire, which has been developed by the Southern African Institute of Steel Construction (SAISC). The cellular beam structure (CBS) was introduced in Chapter 1, along with the description of the sandwich floor system. Thermal analyses were performed, based on heat transfer principles, to determine the temperatures of the steel beams and unexposed surfaces within the floor system. The investigation formed part of a decoupled thermo-mechanical analysis, in which the temperatures obtained from the thermal analyses were used as input for the structural analyses performed by Kloos (2017). The overall goal was to determine the structural fire resistance of the modular structural system. The objectives of this thesis identified in Chapter 1 have been addressed as discussed below.

An extensive literature study was conducted in Chapter 2, to gain a thorough understanding of structural fire engineering and the resistance requirements necessary to be met for ensuring the safety of a structural system in fire. A background to fire behaviour, steel behaviour in fire and structural fire testing was presented in the literature review. Heat transfer principles were also discussed, which assist in understanding the mechanisms by which heat is transferred through structural systems.

An experimental study was performed, in which a series of small-scale sandwich samples were tested in a furnace, as discussed Chapter 3. Four samples, each consisting of a different configuration, were exposed to a 60-minute standard fire from below. The aim of the fire tests was to validate the use of finite element (FE) models that simulate the heat transfer through the sandwich floor system of the CBS. Temperatures were measured, with thermocouples (type K), at various locations within the test samples. The experimental results were analysed and discussed in Chapter 4, which included the observations made during testing and the comparison of the different sample configurations.

In addition to the experimental validation of FE models, three studies from the literature were used to validate the basic heat transfer modelling process conducted in ABAQUS. These initial validation studies highlighted various modelling considerations, which included the material thermal properties, thermal interactions and boundary conditions, as discussed in Chapter 5. The FE modelling of the small-scale fire test samples were also

discussed in Chapter 5, which included the comparison of the experimental and numerical results.

Larger two-dimensional (2D) FE models were developed based on the thermal modelling parameters derived from the validation studies in Chapter 5. These models represented the sandwich floor system of the CBS, which included the cellular beams, steel sheeting and the various insulation boards. A detailed discussion on the development of these beam models was provided in Chapter 6, along with the FE heat transfer modelling parameters and analysis procedure. Three respective models were developed for the primary beam, secondary beam and the channel, all of which were exposed to a 60-minute standard fire from below. The results obtained from the FE beam analyses were also discussed in Chapter 6, which are summarised below.

A parametric investigation was conducted in Chapter 7, in which certain parameters of the FE beam models were varied to determine the effect they have on the thermal behaviour of the floor system. The parameters that were changed included the type and thickness of the insulation boards and the geometry of the steel sheeting. Also included as part of the parametric investigation was the development of a parametric fire, which was based on an assumed office compartment configuration that yielded a very intense fire curve. The aim of the parametric fire analyses was to determine the thermal behaviour of the steel beams and floor layers when exposed to a real fire scenario that includes a cooling phase, as opposed to the continuous temperature increase of a standard fire curve.

8.2 Project findings

The results obtained throughout this thesis are summarised in this section. This includes the experimental and numerical results of the fire tests, and the comparison thereof, which were discussed in Chapters 4 and 5. Following this is a summary of the results from the various FE beam analyses in Chapter 6 and parametric investigation in Chapter 7. For a more detailed discussion of the models and their results, refer to the respective chapters mentioned above.

8.2.1 Experimental results

The four small-scale fire test samples were exposed to the ISO 834 standard fire, which was manipulated by regulating two gas burners. These were adjusted according to the temperature readings from four thermocouples that were located inside the furnace. Two ventilation openings, situated in the front of the furnace, allowed manual control of the amount of air that enters the furnace, thus controlling the heat.

From the measured temperature results discussed in Chapter 4, it was found that the standard fire curve was traced with significant accuracy, with the furnace temperature staying within 10% of the ISO 834 curve for the full duration of each test.

Two samples were tested without a ceiling board, in order to replicate a possible worst-case scenario, in which the ceiling boards detach during a fire. The temperatures obtained from these "no ceiling" tests were generally 40 to 60% higher than the corresponding "ceiling" test samples. Thus, the ceiling board has a significant influence on the thermal behaviour

of the test sample, as seen in the aftermath images provided in Chapter 4. Large cracks occurred in the FCB on the unexposed side, which was due to the significant expansion of the steel sheeting during the elevated temperatures.

Two different cross-sections of the VP50 sheeting were tested, one with the flute section and another with a stud section in the middle of the sample, which was formed at the connection between two sheets. From the unexposed surface (cold face) temperatures of the test samples, it was found that the middle stud section in sample T2 yielded approximately 40% lower temperatures, compared to sample T3. This indicates that the radiation in the void was blocked by the stud section, which resulted in lower temperatures on the cold face of the sample.

8.2.2 Validation results

The preliminary validation studies performed in Chapter 5 included the heat transfer modelling of an enclosed steel I-section from Jeffers *et al.* (2013), cold-formed steel wall panel system from Feng *et al.* (2003) and a slim-floor beam system investigated by Schaumann and Hothan (2002). ABAQUS models were developed for each of the above-mentioned systems to validate the modelling process used here, especially for modelling cavity radiation in assemblies containing voids between materials. The results obtained in this research showed significant correlation with the results from the respective original authors of each study.

In general, a good correlation was found between the temperatures measured during the fire tests and the numerical test model results obtained from ABAQUS. The variation in temperatures for the exposed side of the samples were less than 12% and less than 21% for the unexposed sides. The internal temperatures differed by approximately 6%, which indicates that the models accurately simulated the heat transfer through the test samples. Despite of some localized temperature variations, the general trend of the temperature distributions of the FE models was accurate. Hence, ABAQUS was found suitable for modelling the heat transfer through the sandwich floor system.

8.2.3 FE beam analysis results

The FE beam models consisted of the primary beam (P-beam), secondary beam (J-beam) with the additional angle welded to the bottom flange, and the channel (C-beam). Two models were developed for each of these beams, one with the ceiling board intact (C) and another without the ceiling board (noC). This simulated a worst-case scenario where the integrity of the ceiling board fails completely, similar to what was done in the fire tests. The predicted steel beam temperatures were used by Kloos (2017) as input to perform numerical analyses to predict the structural behaviour of the CBS.

It was found that the temperature distributions through the steel beams were highly non-uniform. Temperatures decreased significantly towards the upper part of the beam sections, due to the heating that was applied from below. Therefore, the maximum temperature was obtained in the bottom flange of the beam sections, which was approximately $220°C$ for the P-beam and J-beam, and $176°C$ for the channel.

The average temperature increase on the unexposed surface of the top fibre-cement board (FCB) never exceeded $50°C$, which is well below the insulation requirement limitation of $140°C$. The maximum peak temperature increase limitation of $180°C$ was also satisfied at this layer. However, the inner FCB also had to satisfy the insulation criteria, due to the services that are situated on top of this inner floor layer. It was found that the average and peak temperature increase in the inner FCB exceeded the insulation criteria limitations by $60°C$ and $68°C$, respectively. This could cause the cables or other services in the floor to ignite, which leads to fire spread and thus compartmentation failure.

The Bond-Dek steel sheeting, which is situated between the ceiling board and the inner FCB, also experienced a significant temperature increase and reached an average temperature of $500°C$. It was seen during the small-scale fire tests that the steel sheeting undergoes significant expansion and warping when exposed to elevated temperatures. It was determined that a linear expansion of 55.5 mm can occur in the sheeting for a length of 7.925 m and a temperature of $500°C$. This could potentially result in undesirable stresses within the insulation boards that causes cracks to occur. This was evident in the fire tests, where large cracks appeared in the FCB due to the thermal bowing of the steel sheeting.

However, all of these predicted temperatures are based on the assumption that the ceiling board does not fail in terms of integrity, which means that no cracks occur within the gypsum type X ceiling board. In real life, it is impossible to ensure, with 100% certainty, that the ceiling board will not fail. Hence, the worst-case scenario served as an example of what might happen in terms of thermal behaviour. The "noC" analyses yielded significantly higher temperatures in the beams and insulation boards, with a temperature variation of approximately $300°C$ to $500°C$ for the various FE models.

Although the steel beam temperatures remained relatively low, while assuming no integrity failure of the ceiling board, the CBS failed with regards to the insulation criteria.

8.2.4 Parametric investigation results

From the parametric investigation, it was found that the type and depth of steel sheeting has a negligible influence on the temperature increase within the floor system. The temperature variation between the 75 mm deep Bond-Dek and the 115 mm Voidcon sheeting was less than $10°C$ over the 60-minute standard fire duration. It was also found that the thickness of the FCB strip, situated between the ceiling board and the bottom flange of the J-beam, has a negligible influence on the average temperature increase in the inner FCB. However, the temperature in the lower part of the J-beam decreases by approximately $16°C$ when there is an increase from 10 mm to 12 mm thickness, and $21°C$ from a 12 mm to a 15 mm thickness. Nonetheless, based on the results obtained from the FE beam analyses in Chapter 6, the CBS fails in terms of the insulation criteria. Hence, the inner FCB temperature needs to be reduced.

While considering the insulation materials, it was found that the thickness of the ceiling board and the inner FCB have the most significant influence on the temperature increase within the floor system. By increasing the inner FCB by 3 mm, from 9 to 12 mm and from 12 to 15 mm, the temperature increase can be reduced by approximately $37°C$. A floor system configuration that consist of a 15 mm gypsum type X ceiling-board, Bond-

Dek sheeting and a 15 mm inner FCB, was found to satisfy the insulation criteria, while assuming no integrity failure in the ceiling board.

With regards to the ceiling board, it was clear from the comparison that the gypsum type X resulted in a lower temperature increase in the inner FCB than the Promatect-H CaSi-board with a similar thickness. The variation in temperatures between the two materials increased significantly with an increase in board thickness, as shown in Figure 7.2. It was found that a 20 mm gypsum type X board would satisfy the insulation requirement with a Bond-Dek sheeting and a 9 mm FCB on top, while only a 25 mm CaSi-board satisfied this requirement.

However, gypsum has a significantly higher moisture content compared to CaSi-boards, which in this case are 17.5% and 6% respectively. Most of the moisture evaporates when exposed to elevated temperatures, which means that gypsum can experience more shrinkage cracks, despite the cooling effect it may have. These cracks cause localized hot spots on the unexposed inner floor layer, which could be detrimental and lead to fire spread from within the floor system. Cracks are difficult to model numerically, due to the uncertainty of exactly where and when they might occur, as well as what the size of the cracks would be. However, it is possible that the CaSi-board can ensure a higher reliability in terms of structural integrity.

It should also be noted that the results obtained are highly dependent on the thermal properties of the materials used in the FE analyses. The properties of the gypsum type X board were based on values obtained from Feng *et al.* (2003), as discussed in Section 6.3.2. Alternative thermal properties may result in significantly different results.

It is evident throughout this research that the integrity of the ceiling board is a crucial aspect for satisfying the fire resistance criteria, especially when considering the extent of thermal bowing the steel sheeting experiences during elevated temperatures. Hence, it is necessary to provide sufficient insulation on the exposed side of the floor layer to ensure low temperatures within the steel sheeting.

Although the parametric fire is unrealistic for a standard office compartment fire scenario, it provided valuable information regarding the thermal and structural behaviour of the CBS. The effect of the cooling phase on the axial forces within the steel beams could be investigated, which are discussed by Kloos (2017). As for the thermal analyses, it was found that the parametric fire generally resulted in a more rapid temperature increase in the first 40 minutes. After 60 minutes, the standard fire resulted in approximately $20°C$ higher temperatures. It should be noted that in the case of a 120-minute standard fire, the temperature variation would be significantly higher when compared to the parametric fire. Hence more energy would be released by a standard fire curve.

To conclude, the CBS would satisfy the insulation and integrity requirements for a 60-minute standard fire, by incorporating a gypsum type X ceiling-board with a thickness of at least 20 mm, or by increasing the thickness of the inner FCB to 15 mm, or a combination of the two. Although using a 25 mm ceiling-board instead will be conservative, this will ensure the integrity of the ceiling board with a higher reliability. The increase in sheeting temperature will be reduced, which reduces the bowing experienced within the insulation boards, provided that the ceiling boards are securely fixed and allow for some expansion

to occur at the fixities.

8.3 Recommendations & future research

Extensive research has been conducted in this project on the thermal behaviour of the CBS through performing numerous FE analyses in ABAQUS. Also, a good understanding has been developed on the fire resistance requirements of the CBS. However, this section concludes with some recommendations for future investigations with regards to the fire resistance of the CBS.

This thesis performed 2D heat transfer analyses, which provided accurate temperatures to a reasonable extent. However, the effect of the cellular holes in the beams should be included for future work. Hence, 3D analyses should be performed on the cellular beam models to investigate the heat transfer in multiple directions within the floor system. This should include the heat transfer through the holes of the cellular beams within the ceiling void.

Once the insulation materials are finalised for the CBS, the specific thermal properties should be determined experimentally, in order to improve the accuracy of the FE heat transfer models.

Additional parametric investigations should be conducted to investigate various ceiling configurations that would provide better protection against fire, such as modelling suspended ceiling systems with cold-formed channel sections.

The work performed in this thesis provides a foundation for the planning and execution of a full-scale fire test. It is recommended that medium-scale fire testing should be conducted to test a section of the sandwich floor system that includes a cellular beam. Through these fire tests, the numerical beam models in this thesis can be validated, which include the assumed heat transfer parameters and material properties.

Appendices

Appendix A

Fire design tables

This appendix includes the general fire resistance requirements table from SABS (2011), which indicates the fire rating required for a standard office building between 3 and 10 storeys. Also included in this appendix are tables describing the section factor for unprotected and protected steel elements that are used during heat transfer calculations, as discussed in Chapter 2.

Table A.1: Stability of structural elements or components from SANS 10400-T (SABS, 2011)

Type of occupancy	Class of occupancy	Stability (min)				
		Single-storey building	Double-storey building	3 to 10 storey building	11 storeys and more	Basement in any building
Entertainment and public assembly	A1	30	60	120	120	120
Theatrical and indoor sport	A2	30	60	120	120	120
Place of instruction	A3	30	30	90	120	120
Worship	A4	30	60	90	120	120
Outdoor sport	A5	30	30	60	90	120
High risk commercial services	B1	60	60	120	180	120
Moderate risk commercial services	B2	30	60	120	120	120
Low risk commercial services	B3	30	30	90	120	120
Exhibition hall	C1	90	90	120	120	120
Museum	C2	60	60	90	120	120
High risk industrial	D1	60	90	120	180	240
Moderate risk industrial	D2	30	60	90	120	180
Low risk industrial	D3	30	30	60	120	120
Plant room	D4	30	30	60	90	120
Place of detention	E1	60	60	90	120	120
Hospital	E2	60	90	120	180	120
Other institutional (residential)	E3	60	60	120	180	120
Medical facilities	E4	30	30	Not applicable	Not applicable	120
Large shop	F1	60	90	120	180	120
Small shop	F2	30	60	120	180	120
Wholesalers' store	F3	60	90	120	120	120
Office	G1	30	30	60	120	120
Hotel	H1	30	60	90	120	120
Dormitory	H2	30	30	60	120	120
Domestic residence	H3	30	30	60	120	120
Detached dwelling house	H4	30	30	60	Not applicable	120
Hospitality	H5	30	30	Not applicable	Not applicable	120
High risk storage	J1	60	90	120	180	240
Moderate risk storage	J2	30	60	90	120	180
Low risk storage	J3	30	30	90	90	120
Parking garage	J4	30	30	30	90	120

NOTE 1 Unprotected steel may be used in the structural system of all single-storey and certain double-storey buildings in spite of the fact that in many cases such structural members would not comply with the requirements of this table. The practice is regarded as safe for all practical cases that are likely to occur in single-storey construction, but the possible consequences of early distortion or collapse should be considered in the design of double-storey buildings in order to be certain that escape routes will be able to serve their purpose for the required period. Particular care should be exercised where thin sections are used or in "space-frame" type structures.

NOTE 2 A further problem arises in the application of the requirement of 4.2. Distortion or collapse of any structural member should not cause loss of integrity or stability in any external wall facing a site boundary or another building as this might lead to non-compliance with the safety distance requirement. Where such a situation occurs, it would be necessary either to protect the steel to the extent required to attain the stability given in this table or to regard such wall as being of type N for the purposes of 4.2.

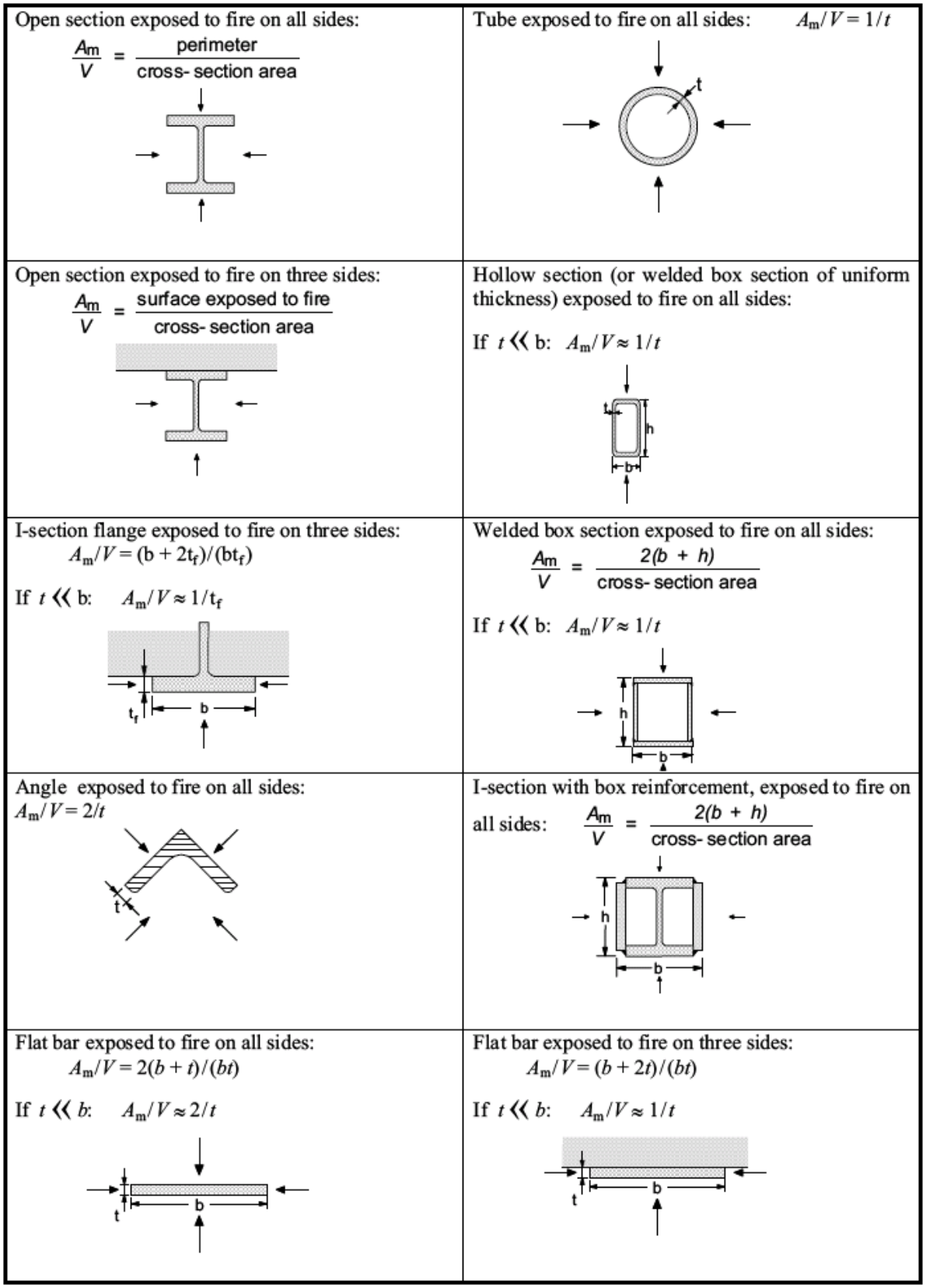

Figure A.1: Section factor of unprotected steel sections from EN1993-1-2 (CEN, 2005)

Sketch	Section factor $[A_m / V]_b$
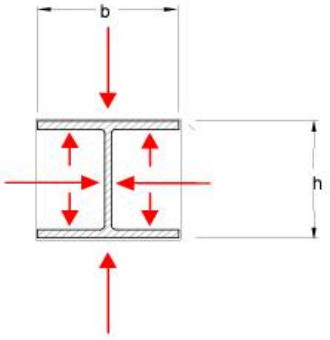	$\frac{2(b + h)}{\text{Steel cross-Section area}}$
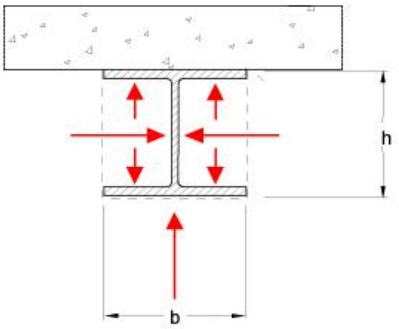	$\frac{2h + b}{\text{Steel cross-Section area}}$
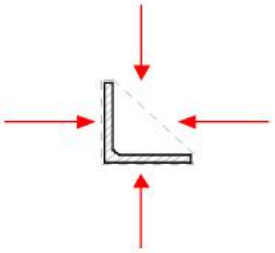	$\frac{\text{box perimeter*}}{\text{Steel cross-Section area}}$

* The dotted line defines the box perimeter that corresponds to the smallest box surrounding the section (Franssen J-M, *et al.*, 2009)

Figure A.2: Box section factor value (Franssen and Vila Real, 2015)

Sketch	Description	Section factor (A_p/V)
	Contour encasement of uniform thickness	$\frac{\text{steel perimeter}}{\text{steel cross-section area}}$
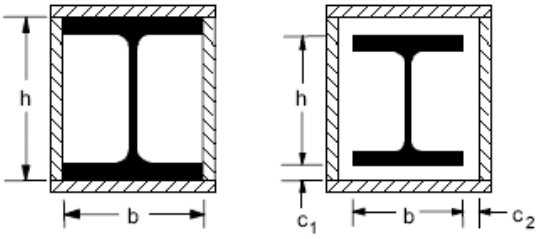	Hollow encasement of uniform thickness)[1]	$\frac{2(b+h)}{\text{steel cross-section area}}$
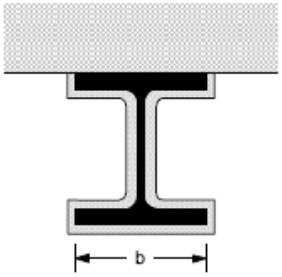	Contour encasement of uniform thickness, exposed to fire on three sides	$\frac{\text{steel perimeter - } b}{\text{steel cross-section area}}$
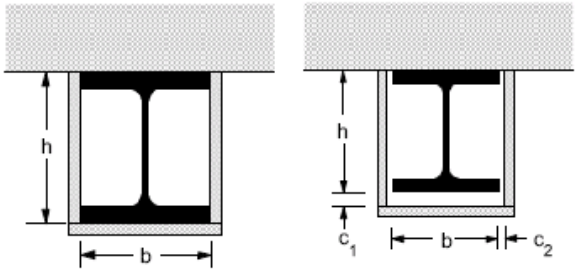	Hollow encasement of uniform thickness, exposed to fire on three sides)[1]	$\frac{2h+b}{\text{steel cross-section area}}$
)[1] The clearance dimensions c_1 and c_2 should not normally exceed $h/4$		

Figure A.3: Section factor of protected steel sections from EN 1993-1-2 (CEN, 2005)

Appendix B

Plate thermocouple layout

This appendix provides a detailed drawing of the plate thermocouple that was used for measuring the temperatures during the fire test, as discussed in Chapter 4.

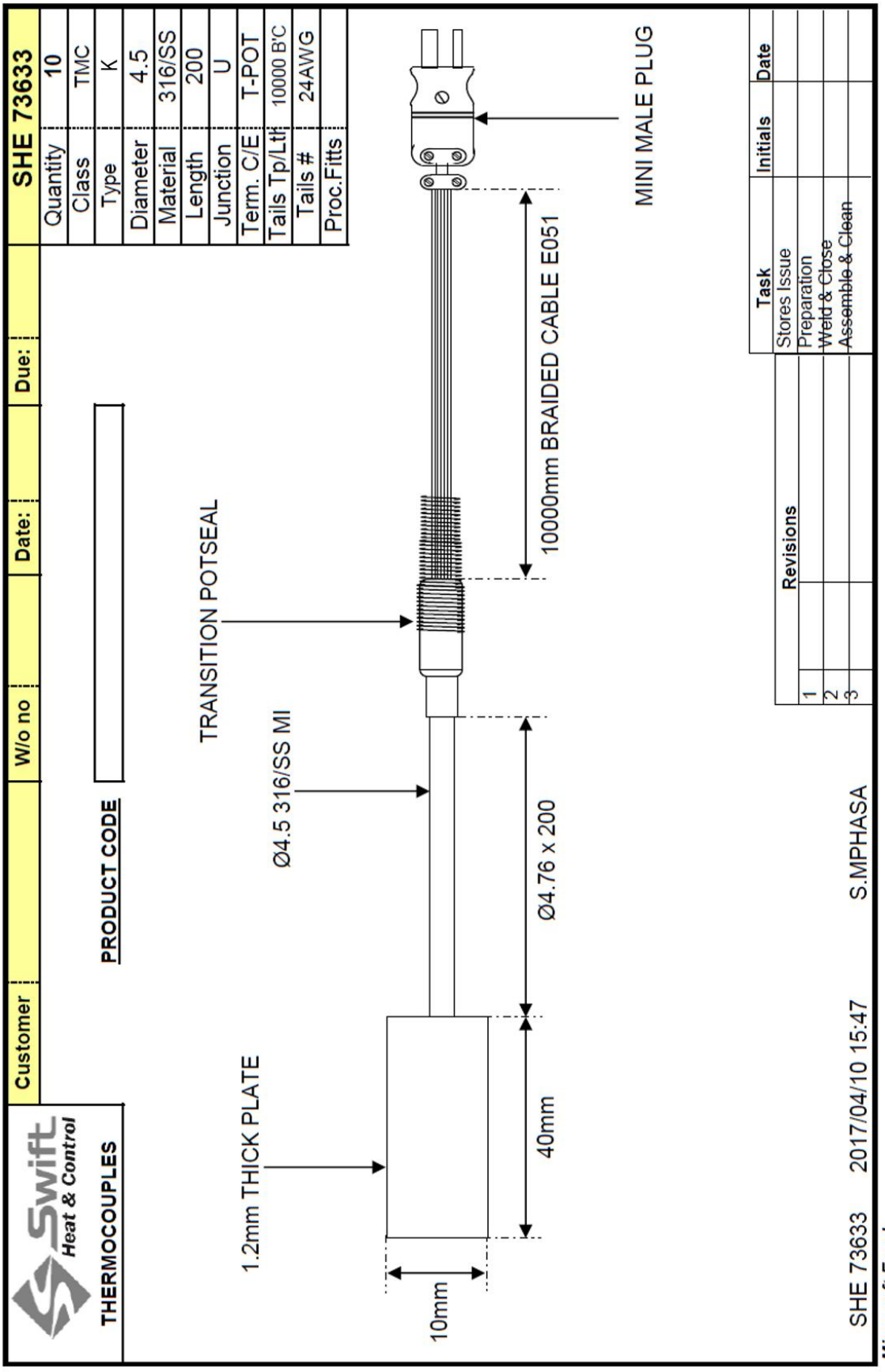

Figure B.1: Plate thermocouple layout

Appendix C

Detailed drawings

The relevant detailed shop drawings, as provided by Amanuel Gebremeskel from the SAISC, are presented in this appendix. These drawings were used to determine the geometry of the beam sections in the FE analyses performed in Chapter 6, and include:

- G2: General Arrangement Drawing
- A-CB47: Primary beam (P-beam)
- A-PA70: Secondary beam (J-beam)
- W-M109: Additional angle for J-beam
- W-M116: Channel (C-beam)
- W-P124: Steel plate (situated below the Bond-Dek sheeting)

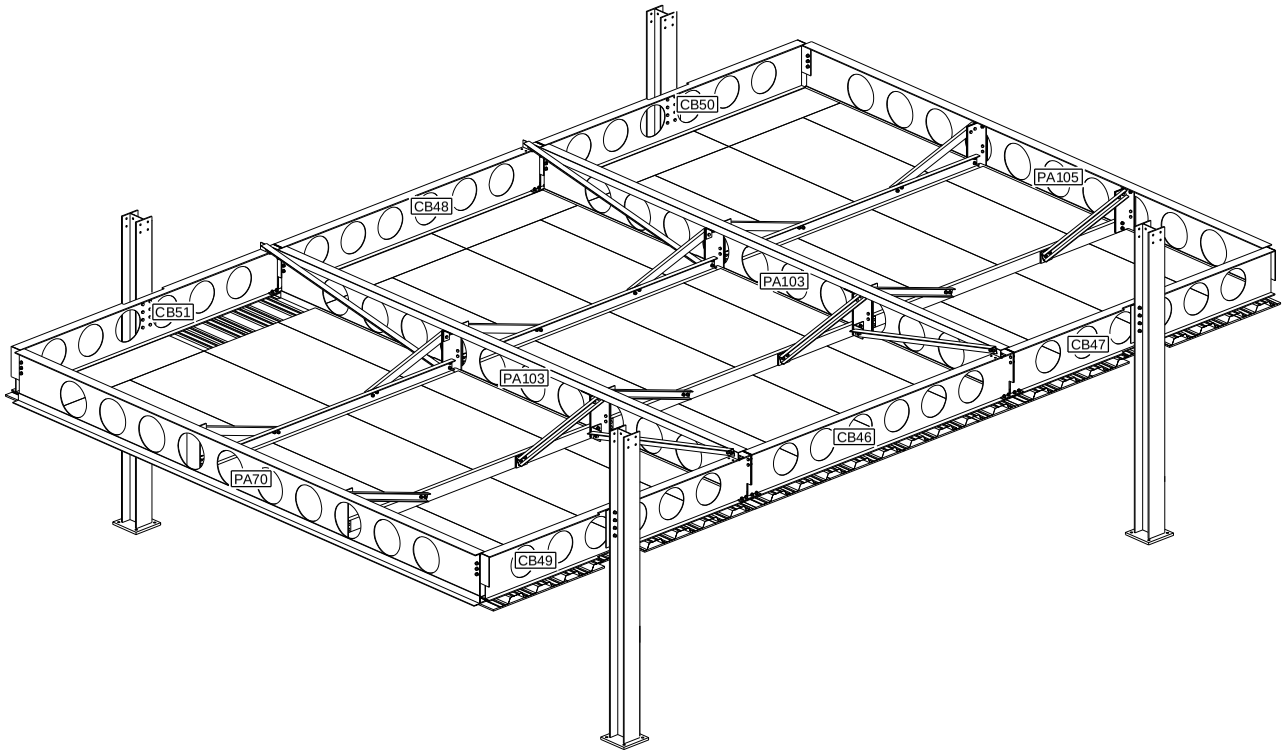

Model :- New model 4

Rev	Mark	Revision Description	Date

SAISC
Dry Floor Panel and Modular Access Floor
Research
Power Street Germiston

Drawing title
A3 General Arrangement Drawing

Draw C Schoeman &
Scale 1:50
Issued
Revised
Project Number 1
Drawing G [2]
Rev 0

POWERED BY TEKLA A TRIMBLE COMPANY

Supplied by
Cadex SA (Tekla's SA Reseller)
Tel +27 11 463 1857/3641 Fax +27 11 463 9445
P O Box 411340
Craighall 2024, South Africa
info@CadexSA.com

Tekla Structures

Prepared using Tekla Structures® (www.tekla.com)

Phase number & name	Qty
1 Phase 1	1

Prepared using Tekla Structures® (www.tekla.com)

Model : - New model 4

General Notes: All steelwork to comply with SANS 2001:CS1 & SANS 1921-3
All welds 6mm continuous fillet welds unless noted otherwise
All butt welds full penetration welds unless noted otherwise
Mark assembly at position shown for correct site orientation
All holes to be 22DIA for M20 bolts unless noted otherwise

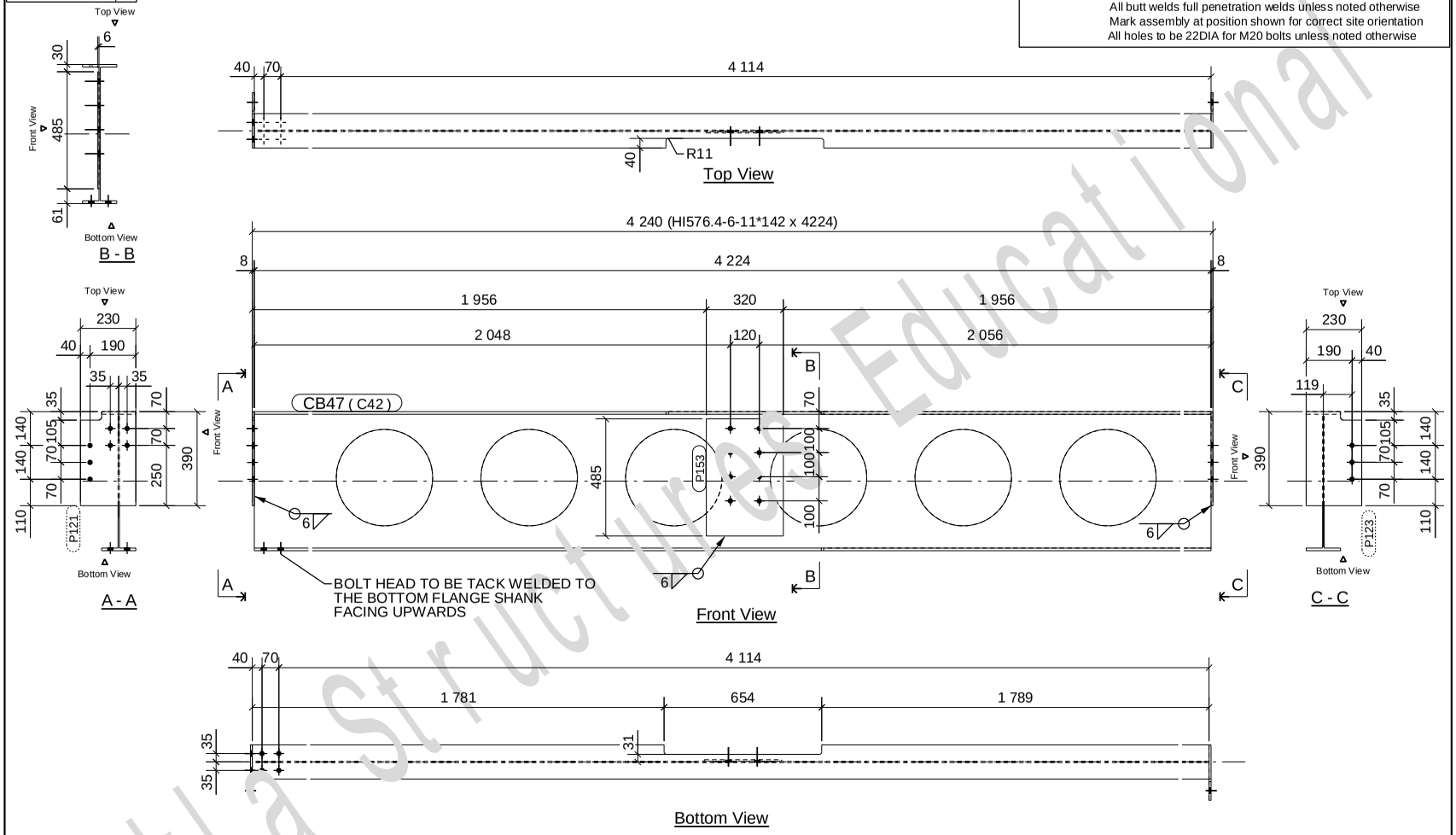

Material list for 1 BEAM assembly marked CB47 - only 1 is required

Mark	No	Profile	Length	Grade	Paint area	Mass
C42	1	HI576.4-6-11*142	4224	S355JR	5.7	213.9
P121	1	PLT8*230	390	S355JR	0.2	5.6
P123	1	PLT8*230	390	S355JR	0.2	5.6
P153	1	PLT6*320	485	S355JR	0.3	7.3
Total for 1 assembly					6.4	232.5

Tekla Structures

1 'BEAM' required marked CB47

Rev	Mark	Revision Description	Date

SAISC
Dry Floor Panel and Modular Access Floor
Research
Power Street Germiston

Supplied by
Cadex SA (Tekla's SA Reseller)
Tel +27 11 463 1857/3641 Fax +27 11 463 9445
P O Box 411340
Craighall 2024, South Africa
info@CadexSA.com

POWERED BY TEKLA A TRIMBLE COMPANY

Draw C Schoeman &
Scale 1:15
Issued
Revised
Project Number 1
Assembly Drawing A [CB.47]
Rev 0

Phase number & name	Qty
1 Phase 1	1

Prepared using Tekla Structures® (www.tekla.com)

Model :- New model 4

General Notes: All steelwork to comply with SANS 2001:CS1 & SANS 1921-3
All welds 6mm continuous fillet welds unless noted otherwise
All butt welds full penetration welds unless noted otherwise
Mark assembly at position shown for correct site orientation
All holes to be 22DIA for M20 bolts unless noted otherwise

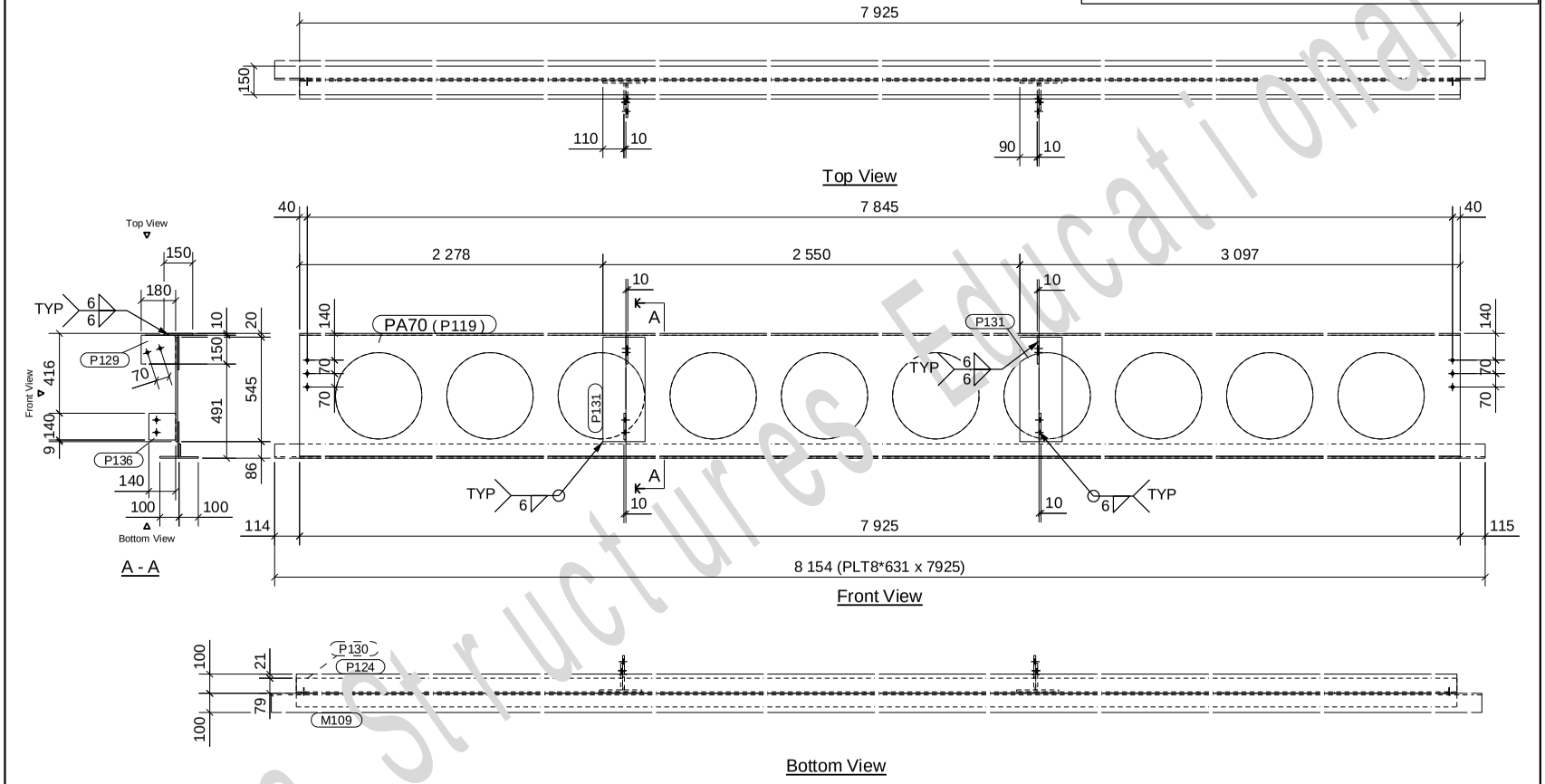

Material list for 1 Plate assembly marked PA70 - only 1 is required

Mark	No	Profile	Length	Grade	Paint area	Mass
M109	1	L100*75*8	8154	S355JR	2.9	86.4
P119	1	PLT8*631	7925	S355JR	7.1	314.0
P124	1	FL10*100	7925	S355JR	1.7	62.2
P129	2	FL10*150	180	S355JR	0.1	4.2
P130	1	FL10*150	7925	S355JR	2.5	93.3
P131	2	PLT10*220	545	S355JR	0.5	18.8
P136	2	PLT10*140	140	S355JR	0.1	3.1
Total for 1 assembly					14.9	582.1

1 'Plate' required marked PA70

Rev	Mark	Revision Description	Date

SAISC
Dry Floor Panel and Modular Access Floor Research
Power Street Germiston

Supplied by
Cadex SA (Tekla's SA Reseller)
Tel +27 11 463 1857/3641 Fax +27 11 463 9445
P O Box 411340
Craighall 2024, South Africa
info@CadexSA.com

POWERED BY TEKLA A TRIMBLE COMPANY

Draw C Schoeman & Scale 1:20
Issued
Revised
Project Number 1
Assembly Drawing A [PA.70] Rev 0

Tekla Structures

Phase	Qty
Phase 1	4

Prepared using Tekla Structures® (www.tekla.com)

Model :- New model 4

General Notes: All steelwork to comply with SANS 2001:CS1 & SANS 1921-3
All profile notches to have 11mm radius unless noted otherwise

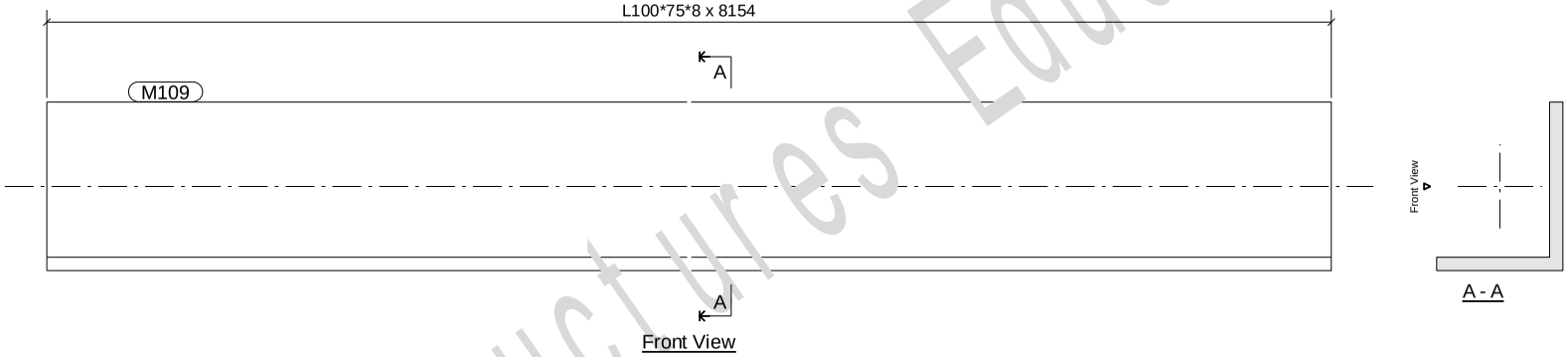

The part shown is required for the following assemblies:-

3	required for 3 'Beam' assemblies marked A115
1	required for 1 'Plate' assembly marked PA70

Material list for 4 parts named 'Beam'

Mark	Profile	Grade	Length	Paint Area	Mass
M109	L100*75*8	S355JR	8154	2.9	86.4
		Total for 4 parts	32616	11.4	345.7

Tekla Structures

Rev	Mark	Revision Description	Date

SAISC
Dry Floor Panel and Modular Access Floor Research
Power Street Germiston

Supplied by
Cadex SA (Tekla's SA Reseller)
Tel +27 11 463 1857/3641 Fax +27 11 463 9445
P O Box 411340
Craighall 2024, South Africa
info@CadexSA.com

POWERED BY TEKLA A TRIMBLE COMPANY

Draw C Schoeman &
Scale 1:2.5
Issued
Revised
Project Number 1
Workshop Drawing W [M.109]
Rev 0

Phase	Qty
Phase 1	3

Prepared using Tekla Structures® (www.tekla.com)

Model :- New model 4

General Notes: All steelwork to comply with SANS 2001:CS1 & SANS 1921-3
All profile notches to have 11mm radius unless noted otherwise

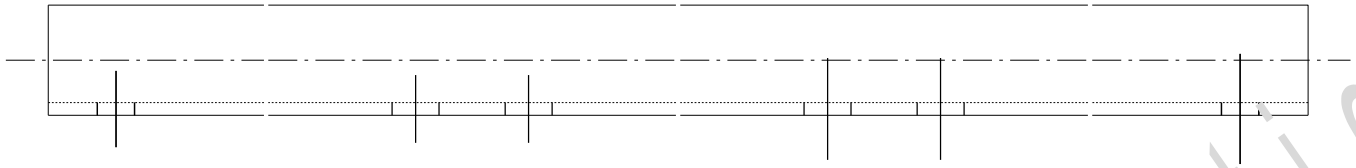

Bottom View

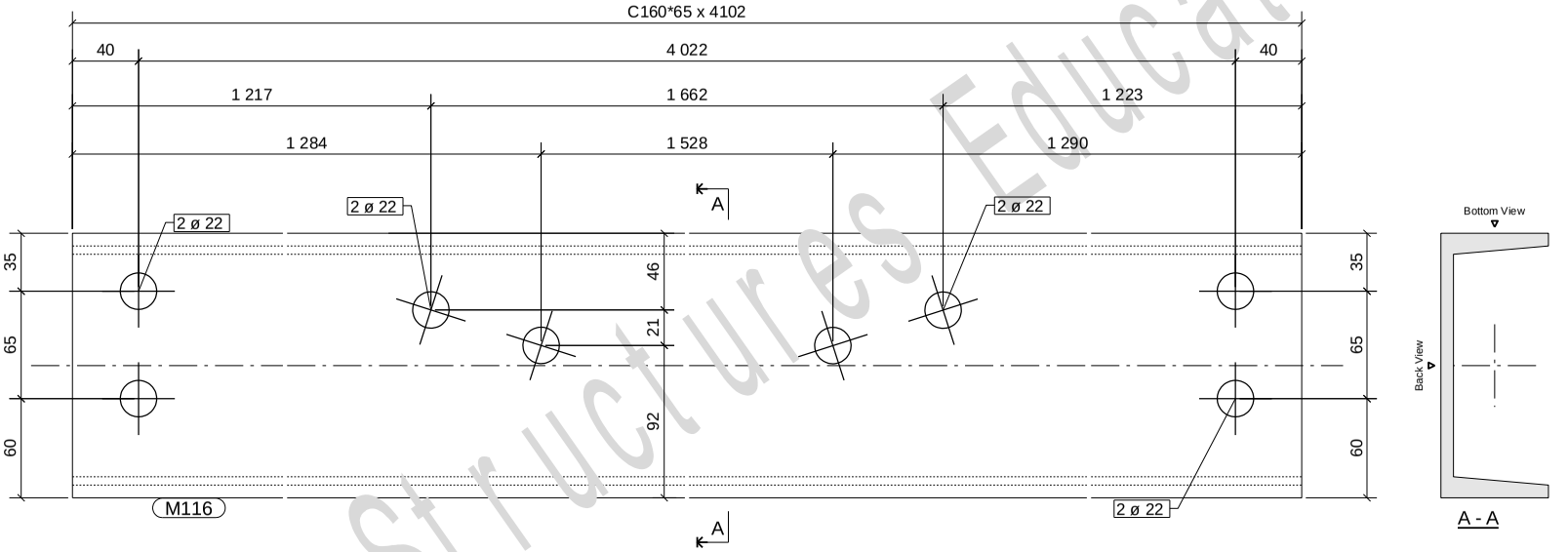

A - A

Back View

The part shown is required for the following assemblies:-
3 required for 3 'Purlin' assemblies marked A122

Material list for 3 parts named 'Purlin'

Mark	Profile	Grade	Length	Paint Area	Mass
M116	C160*65	S355JR	4102	1.1	78.3
		Total for 3 parts	12306	3.2	235.0

Tekla Structures

Rev	Mark	Revision Description	Date

SAISC
Dry Floor Panel and Modular Access Floor
Research
Power Street Germiston

Supplied by
Cadex SA (Tekla's SA Reseller)
Tel +27 11 463 1857/3641 Fax +27 11 463 9445
P O Box 411340
Craighall 2024, South Africa
info@CadexSA.com

POWERED BY TEKLA A TRIMBLE COMPANY

Draw C Schoeman &
Scale 1:2.5
Issued
Revised
Project Number 1
Workshop Drawing W [M.116] Rev 0

Phase	Qty
Phase 1	4

Prepared using Tekla Structures® (www.tekla.com)

Model :- New model 4

General Notes: All steelwork to comply with SANS 2001:CS1 & SANS 1921-3
All profile notches to have 11mm radius unless noted otherwise

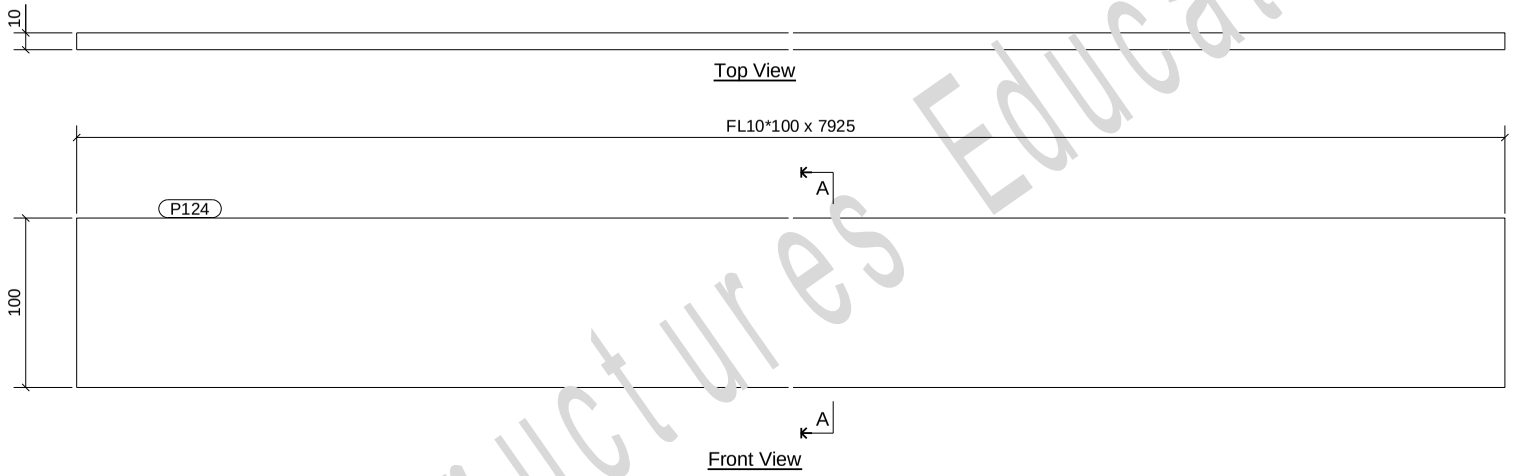

The part shown is required for the following assemblies:-

1	required for 1 'Plate' assembly marked PA70
2	required for 2 'Plate' assemblies marked PA103
1	required for 1 'Plate' assembly marked PA105

Material list for 4 parts named 'Plate'

Mark	Profile	Grade	Length	Paint Area	Mass
P124	FL10*100	S355JR	7925	1.7	62.2
		Total for 4 parts	31700	7.0	248.8

Tekla Structures

Rev	Mark	Revision Description	Date

SAISC
Dry Floor Panel and Modular Access Floor Research
Power Street Germiston

Supplied by
Cadex SA (Tekla's SA Reseller)
Tel +27 11 463 1857/3641 Fax +27 11 463 9445
P O Box 411340
Craighall 2024, South Africa
info@CadexSA.com

POWERED BY TEKLA A TRIMBLE COMPANY

Draw C Schoeman &
Scale 1:2.5
Issued
Revised
Project Number 1
Workshop Drawing W [P.124]
Rev 0

Appendix D

Parametric fire calculation assumptions

Assumptions made for the parametric fire calculation are presented in this appendix. The calculation was based on the Eurocode equations in 1991-1-2 (CEN, 2002), as discussed in Section 2.4.2. Refer to Section 7.6 for the steel beam temperatures obtained for the parametric fire exposure.

Table D.1: General assumptions for the parametric fire curve calculation

Dimensions of compartment			
Floor length	L =	12.75	m
Floor width	B =	8.5	m
Floor height	H =	2.56	m

Ventilation opnenings			
Opening type	Window	Door	Other
Quantity	4	1	0
Width (m)	3.85	1	0
Height (m)	1.54	2	0

Basic assumptions			
Occupancy Type:		Office	
Fire load density: qf,k =	511	MJ/m2	(80% Fractile)
Factor (γ_n) =	1.0	(Active safety measures)	
Activity factor (γ_{q2}) =	1.0	(Office)	
Combustion factor:	m = 0.8	(Cellulosic material)	

Compartment boundaries			
Boundary/Material	ρ (kg/m^3)	k (W/mK)	c_p (J/kgK)
Floor - FCB	1260	0.17	2500
Ceiling - Gypsum	1440	0.48	840
Walls - Gypsum	1440	0.48	840

List of References

Access Steel (2010). Data: Nominal temperature-time curves, structural fire engineering to eurocodes.
Available at: https://sites.google.com/site/structuralfire/fire-curves (Cited on page 13.)

ArcelorMittal (2017*a*). ACB Cellular Beams. ArcelorMittal Europe - Long Products: Sections and Merchant Bars.
Available at: http://sections.arcelormittal.com/fileadmin/redaction/4-Library/1-Sales_programme_Brochures/ACB/ACB_EN.pdf (Cited on page 33.)

ArcelorMittal (2017*b*). Upe - channels with parallel flanges.
Available at: http://www.constructalia.com/prg/selfware.pl?id_sitemap=67#&.WaR4TCgjG1s (Cited on page 72.)

Ariyanayagam, A.D., Poologanathan, K. and Mahendran, M. (2017). Thermal modelling of load bearing cold-formed steel frame walls under realistic design fire conditions. *Advanced Steel Construction*, vol. 13, no. 2, pp. 160–189. (Cited on page 68.)

ASFP (2014). *The Yellow Book - Fire protection for structural steel in buildings.* 5th edn. Hampshire, UK: Association of Specialist Fire Protection. (Cited on page 10.)

ASTM E119 (2000). Standard test methods for fire tests of building construction and materials. Standard, American Society for Testing and Materials (ASTM International), Conshohocken, Pa. (Cited on page 35.)

Bailey, C. (2005). The windsor tower fire, madrid.
Available at: http://www.mace.manchester.ac.uk/project/research/structures/strucfire/CaseStudy/HistoricFires/BuildingFires/default.htm (Cited on page 19.)

Bailey, C. (2009). Science and technology developments in structural fire engineering. *Structural Engineering International*, vol. 19, no. 2, pp. 155–164. (Cited on pages ix, 10, and 11.)

Balaji, K.P. (2016). Fire resisting buildings. SlideShare. Slide 2.
Available at: https://www.slideshare.net/balakp/fire-resisting-buildings (Cited on page 17.)

Bengtsson, L.G. (2001). *Enclosure Fires.* Swedish Rescue Services Agency, Karlstad, Sweden. (Cited on pages 14 and 15.)

Beyler, C., Beitel, J., Iwankiw, N. and Lattimer, B. (2007). Fire resistance testing for perfomance based fire design of buildings: final report. *Quincy, MA: The Fire Protection Research Foundation, Batterymarch Park.* (Cited on page 79.)

Bihina, G., Zhao, B. and Bouchaïr, A. (2013). Behaviour of composite steel–concrete cellular beams in fire. *Engineering Structures*, vol. 56, pp. 2217–2228. (Cited on pages 34 and 38.)

Bisby, L., Gales, J. and Maluk, C. (2013). A contemporary review of large-scale non-standard structural fire testing. *Fire science reviews*, vol. 2, no. 1. (Cited on pages 1, 5, 35, and 36.)

Buchanan, A.H. and Abu, A.K. (2017). *Structural Design for Fire Safety*. 2nd edn. John Wiley & Sons. ISBN 0470972890,9780470972892. (Cited on pages ix, 9, 12, 13, 14, 19, 20, 21, 23, 30, 36, and 82.)

Çengel, Y.A. (2008). *Introduction to thermodynamics and heat transfer*. 2nd edn. McGraw-Hill New York. ISBN 0390861227. (Cited on page 22.)

CEN (2002). *Eurocode 1: Actions on Structures. Part 1-2 : General Actions - Actions on structures exposed to fire*. Brussels: European Committee for Standardization. EN 1991-1-2. (Cited on pages 15, 22, 95, 117, 118, and 146.)

CEN (2005). *Eurocode 3: Design of steel structures - Part 1-2: General rules - Structural fire design*. Brussels: European Committee for Standardization. EN 1993-1-2. (Cited on pages xii, 26, 70, 105, 134, and 136.)

Center (2013). Center 378 data logger thermometer. Tech. Rep., Center Technology Corp. Available at: `http://bim-instruments.com.sg/uploads/Center%20378.pdf` (Cited on page 46.)

Dassault Systémes (2015). *Abaqus 2016 Documentation*. Dassault Systémes Simulia Corporation, Providence, RI, USA. Software: Abaqus/CAE v2016. Available at: `http://50.16.225.63/v2016/` (Cited on pages 5, 32, 73, 87, 89, 99, 102, and 109.)

Den Braven (2017). Zwaluw fire sealant 1200°*c*. Tech. Rep., Den Braven. Available at: `https://www.denbraven.com/en/products/technologies/t8/fire-sealant-1200c_7311/datasheet.pdf/` (Cited on page 43.)

Drysdale, D. (2011). *An Introduction to Fire Dynamics*. 3rd edn. Chichester: John Wiley & Sons. ISBN 0470319038,9780470319031. (Cited on pages ix, 14, 20, and 21.)

ECCS (1999). Explanatory document for eccs no 89 "euro-nomogram" fire resistance of steel structures. *Brussels*. (Cited on page 10.)

ECCS TC3 (2001). *Model Code on Fire Engineering*. ECCS publication No. 111. Brussels: European Convention for Constructional Steelwork. ISBN 92914700065. (Cited on pages 12, 13, 16, 22, 24, 25, 29, 31, 67, 73, 78, 96, and 97.)

Edgefx Technologies (2017). Know about various types of temperature sensors. Available at: `https://www.edgefx.in/6-different-types-of-temperature-sensors-with\discretionary{-}{}{}their-specifications/` (Cited on page 44.)

Elich, J.P. and Hamerlinck, A. (1990). Thermal radiation properties of galvanized steel and its importance in enclosure fire scenarios. *Fire safety journal*, vol. 16, no. 6, pp. 469–482. (Cited on page 78.)

Elite Fire (2013). Back to basics with the fire triangle. Available at: `http://www.elitefire.co.uk/basics-fire-triangle/` (Cited on pages ix and 18.)

Everite (2012*a*). *The benefits of Nutec Fibre Cement*. Everite Building Products. Available at: `http://www.everite.co.za/EN/Content/Pages/ABOUT` (Cited on pages 40 and 76.)

Everite (2012*b*). *Nutec Flat Sheets*. Everite Building Products.
Available at: `http://www.everite.co.za/Uploads/Files/Flat%20sheets_Tongue%20and%20Groove%20Apr%2019%202012.pdf` (Cited on page 77.)

Everite (2016). *The Facts about Nutec's Thermal Properties*. Everite Building Products. (Cited on page 21.)

Feldman, M.R. (2006). Thermal testing of type b packages in furnaces per astm standard practice e 2230. *Packaging, Transport, Storage & Security of Radioactive Material*, vol. 17, no. 3, pp. 137–141. (Cited on page 79.)

Feng, M., Wangand, Y.-C. and Davies, J.M. (2003). Thermal performance of cold-formed thin-walled steel panel systems in fire. *Fire Safety Journal*, vol. 38, no. 4, pp. 365–394. (Cited on pages xi, 30, 37, 68, 69, 70, 72, 76, 79, 86, 87, 94, 111, 114, 122, 127, and 129.)

Fishlock, M. (2013). Materials found in the construction of high-rise buildings.
Available at: `http://www.highrisefirefighting.co.uk/material.html` (Cited on pages ix and 19.)

Franssen, J.-M. (2005). Structures in fire, yesterday, today and tomorrow. *Fire Safety Science*, vol. 8, pp. 21–35. (Cited on page 8.)

Franssen, J.-M. and Vila Real, P. (2012). *Fire design of steel structures Eurocode 1: Actions on structures ; Part 1-2: General actions – Actions on structures exposed to fire ; Eurocode 3: Design of steel structures ; Part 1-2: General rules – Structural fire design*. ECCS Eurocode design manuals. ECCS : Ernst & Sohn, Berlin. ISBN 9783433601600. (Cited on pages ix, 23, 24, 25, 26, 27, and 28.)

Franssen, J.-M. and Vila Real, P. (2015). *Fire design of steel structures: Eurocode 1: actions on structures, part 1-2: General actions - Actions on structures exposed to fire: Eurocode 3: design of steel structures, part 1-2: General rules - Structural fire design*. ECCS Eurocode design manuals, 2nd edn. Ernst & Sohn. (Cited on pages xii, 29, 31, 32, and 135.)

Gales, J., Maluk, C. and Bisby, L. (2012). Large-scale structural fire testing-how did we get here, where are we, and where are we going? (Cited on page 1.)

Gyprock (2017). Rhinoboard firestop.
Available at: `http://www.gyproc.co.za/products/walls/rhinoboard-firestop-0` (Cited on pages 40 and 76.)

Hamerlinck, A.F. (1991). *The behaviour of fire-exposed composite steel/concrete slabs*. Technische Universiteit Eindhoven, Eindhoven. (Cited on pages 22 and 53.)

Hanus, F. (2010). *Analysis of simple connections in steel structures subjected to natural fires*. Ph.D. thesis, University of Liege, Liege, Belgium. (Cited on page 15.)

Harmathy, T. and Lie, T. (1970). Fire test standard in the light of fire research. In: *Fire Test Performance*. ASTM International. (Cited on page 36.)

Harrison, S. (2010). First interstate bank fire.
Available at: `http://framework.latimes.com/2010/10/06/first-interstate-bank-fire/` (Cited on pages ix and 19.)

Hopkin, D., Lennon, T., El-Rimawi, J. and Silberschmidt, V. (2012). A numerical study of gypsum plasterboard behaviour under standard and natural fire conditions. *Fire and Materials*, vol. 36, no. 2, pp. 107–126. (Cited on pages 30, 79, and 82.)

Hurley, M.J., Gottuk, D., Jr., J.R.H., Harada, K., Kuligowski, E., Puchovsky, M., Torero, J.L., Jr., J.M.W. and Wieczorek, C.J. (2016). *SFPE Handbook of Fire Protection Engineering*. 5th edn. Springer - Verlag New York. (Cited on pages 32, 78, and 94.)

ISO (1999). Iso 834 fire-resistance tests - elements of building construction. parts 1-12. (Cited on pages 13 and 65.)

Jeffers, A., Wickström, U. and McGrattan, K. (2013). Documentation of the Solutions to the SFPE Heat Transfer Verification Cases. Case 15 – 2D Heat Transfer in a Composite Section with Cavity Radiation. (Cited on pages 66, 67, 87, and 127.)

Jones, B. (2001). Performance of gypsum plasterboard assemblies exposed to real building fires. (Cited on pages 79 and 80.)

Karlsson, B. and Quintiere, J. (2000). *Enclosure fire dynamics*. Environmental and energy engineering series, 1st edn. CRC Press. (Cited on pages ix and 18.)

Kay, T., Kirby, B. and Preston, R. (1996). Calculation of the heating rate of an unprotected steel member in a standard fire resistance test. *Fire Safety Journal*, vol. 26, no. 4, pp. 327–350. (Cited on page 82.)

Keerthan, P. and Mahendran, M. (2012). Numerical modelling of non-load-bearing light gauge cold-formed steel frame walls under fire conditions. *Journal of fire sciences*, vol. 30, no. 5, pp. 375–403. (Cited on pages 68 and 80.)

Kloos, M. (2017). *An investigation into the structural behaviour of a novel cellular beam structure in fire*. Master's thesis, Stellenbosch University, Stellenbosch. (Cited on pages 5, 89, 102, 109, 110, 112, 118, 124, 125, 127, and 129.)

Kontogeorgos, D., Wakili, K.G., Hugi, E. and Founti, M. (2012). Heat and moisture transfer through a steel stud gypsum board assembly exposed to fire. *Construction and Building Materials*, vol. 26, no. 1, pp. 746–754. (Cited on page 30.)

Lennon, T. (2011). *Structural Fire Engineering*. ICE Publishing. (Cited on pages 9, 15, and 23.)

Li, G. and Wang, P. (2013). *Advanced Analysis and Design for Fire Safety of Steel Structures*. Advanced Topics in Science and Technology in China, 1st edn. Springer Science & Business Media. ISBN 978-3-642-34392-6,978-3-642-34393-3. (Cited on page 12.)

Marley Building Systems (2017). Product range.
Available at: `http://www.marleybuildingsystems.co.za/product-range/` (Cited on page 39.)

Mesquita, L., Gonçalves, J., Gonçalves, G., Piloto, P. and Kada, A. (2015). Intumescente fire protection of cellular beams. In: *X Congresso de Construção Metálica e Mista*, pp. 623–630. CMM-Associação Portuguesa de Construção Metálica e Mista. (Cited on pages 34 and 35.)

Moran, M.J., Shapiro, H.N., Munson, B.R. and DeWitt, D.P. (2003). *Introduction to thermal systems engineering : Thermodynamics, Fluid mechanics, and Heat Transfer*. Wiley. ISBN 9780471204909. (Cited on page 21.)

Nadjai, A., Bailey, C., Han, S.-H., Vassart, O., Zhao, B., Hawes, M., Franssen, J.-M. and Simms, I. (2011). Full-scale fire test on a composite floor slab incorporating long span cellular steel beams. *The Structural Engineer*, vol. 89, no. 21, pp. 18–25. (Cited on pages 1, 34, 35, and 38.)

National Fire Protection Association (2004). *NFPA 921: Guide for fire and explosion investigations*. National Fire Protection Association. (Cited on page 17.)

NES (2017). NES consult & associates.
Available at: `http://www.nesconsult.co.za/` (Cited on page 41.)

Olivier, V. (2012). Basic design methods of en1991-1-2. Brussels: Workshop 'Structural Fire Design of Buildings according to the Eurocodes'. (Not cited.)

Patade, H.K. and Chakrabarti, M. (2013). Thermal stress analysis of beam subjected to fire. *International Journal of Engineering Research and Application*, vol. 3, no. 5, pp. 420–424. (Cited on page 20.)

Potecta (2014). Protecta fr asf acrylic. Tech. Rep., Potecta.
Available at: `http://docs.wixstatic.com/ugd/4243cc_9be49ad6fd594fcd9698794a70bf1589.pdf` (Cited on page 43.)

Promat (2016). Promaseal-a. Tech. Rep., Promat International.
Available at: `http://www.promat-see.com/en/products/promaseal-a` (Cited on page 43.)

Promat (2016). Promatect-h.
Available at: `http://www.promat-see.com/en/products/promatect-h` (Cited on pages 76 and 114.)

Rein, G. (2012). Introduction to fire dynamics for structural engineers. Lecture notes - Training School for Young Researchers, COST TU0904, Malta. School of Engineering, University of Edinburgh. (Cited on pages ix and 9.)

Rini, D. (2006). *Critical behavior of long span cellular beams in fire*. Ph.D. thesis, Faculty of the Graduate School of the University of Maryland, College Park. (Cited on pages ix, 33, and 34.)

Ruddy, E. (2017). London fatal fire sparks high-rise safety concerns. `https://www.reminetwork.com/articles/londons-fatal-fire-sparks-high-rise-safety-concerns/`. (Cited on pages ix, 1, 19, and 20.)

Rusthi, M., Keerthan, P., Ariyanayagam, A.D. and Mahendran, M. (2015). Numerical studies of gypsum plasterboard and mgo board lined lsf walls exposed to fire. In: *Proceedings of the Second International Conference on Performance-based and Life-cycle Structural Engineering (PLSE 2015)*, pp. 1077–1084. The University of Queensland. (Cited on page 68.)

SABS (2005). Fire testing of materials, components and elements used in buildings – part 2: Fire resistance test for building elements. Standard, SABS Standards Division, Pretoria. (Cited on pages 35 and 41.)

SABS (2011). The application of the national building regulations. Standard, SABS Standards Division, Pretoria. (Cited on pages xiii, 12, 41, 53, 95, 107, 132, and 133.)

Safety and Risk Management Office (2017). Fire extinguisher training. SlidePlayer, published by Alison Mussey. Slide 2.
Available at: `http://slideplayer.com/slide/2599198/` (Cited on page 17.)

Schaumann, P. and Hothan, S. (2002). Fire design of a new slim floor beam system using fem-analysis. In: *2nd International Workshop "Structures in Fire", Christchurch*, pp. 291–302. (Cited on pages xi, 33, 72, 73, 74, 75, 87, and 127.)

Shahbazian, A. and Wang, Y.C. (2013). A simplified approach for calculating temperatures in axially loaded cold-formed thin-walled steel studs in wall panel assemblies exposed to fire from one side. *Thin-Walled Structures*, vol. 64, pp. 60–72. (Cited on pages 70 and 79.)

Sultan, M.A. (2006). Fire resistance furnace temperature measurements: Plate thermometers vs shielded thermocouples. *Fire technology*, vol. 42, no. 3, pp. 253–267. (Cited on page 45.)

Swift Heat (2017). Temperature sensors.
Available at: `http://www.swiftheat.com/products-2/temperature-sensors-2/` (Cited on page 44.)

The Engineering ToolBox (2017). Specific heat of solids.
Available at: `http://www.engineeringtoolbox.com/specific-heat-solids-d_154.html` (Cited on page 77.)

Thomas, G.C., Buchanan, A. and Fleischmann, C.M. (1997). Structural fire design: the role of time equivalence. *Fire Safety Science*, vol. 5, pp. 607–618. (Cited on pages 79 and 80.)

Vassart, O., Zhao, B., Cajot, L., Robert, F., Meyer, U., Frangi, A., Poljanšek, M., Nikolova, B., Sousa, L., Dimova, S. *et al.* (2014). Eurocodes: Background & applications structural fire design. *Luxembourg. doi*, vol. 10. (Cited on page 12.)

Voidcon (2014*a*). *Design Tables*. Voidcon Group.
Available at: `https://www.voidcon.co.za/images/Design%20Tables_2014.pdf` (Cited on pages 76 and 116.)

Voidcon (2014*b*). *Voidcon Advantages*. Voidcon Group.
Available at: `https://www.voidcon.co.za/index.php/advantages` (Cited on pages 40 and 116.)

Wald, F. (2016). *Fire Engineering of Steel Structures*. Published on Researchgate, Czech Technical University in Prague, Czech Republic.
Available at: `https://www.researchgate.net/publication/267429001_FIRE_ENGINEERING_OF_STEEL_STRUCTURES` (Cited on page 12.)

Walls, R.S. (2016). *A beam finite element for the analysis of structures in fire*. Ph.D. thesis, Stellenbosch: Stellenbosch University. (Cited on page 32.)

Wang, H.-B. *et al.* (1995). *Heat transfer analysis of components of construction exposed to fire*. Ph.D. thesis, University of Salford. (Cited on page 79.)

Wang, Y., Burgess, I., Wald, F. and Gillie, M. (2013). *Performance-based fire engineering of structures*. CRC Press. (Cited on pages 11, 24, and 25.)

Weber, B. (2012). Heat transfer mechanisms and models for a gypsum board exposed to fire. *International Journal of Heat and Mass Transfer*, vol. 55, no. 5, pp. 1661–1678. (Cited on pages 30 and 31.)

Wickström, U. (2010). The plate thermometer for measuring fire exposure in terms of adiabatic surface temperature. *Fourth International Symposium on Tunnel Safety and Security, Frankfurt am Main, Germany*. (Cited on page 45.)

Wickström, U. and Palsson, J. (1999). A scheme for verification of computer codes for calculating temperature in fire exposed structures. *Fire Technology, SP Report*, vol. 36. (Cited on pages xi, xiii, 32, 65, 66, 67, 68, 70, and 77.)

Zaharia, R. (2014). Thermal response. European Erasmus Mundus Master Course (520121-1-2011-1-CZ-ERA MUNDUS-EMMC), Lecture 3. Sustainable Constructions under Natural Hazards and Catastrophic Events. (Cited on pages ix and 10.)